# MEASUREMENT OF THE ELECTRICAL PROPERTIES OF CONCRETE AT RADIO FREQUENCIES

GERARD STARRS

A Thesis Submitted for the Degree of Doctor of Philosophy

NAPIER UNIVERSITY

EDINBURGH

April 1994

# Abstract

This thesis is a presentation of research into the elecrical properties of concrete at radio frequencies (1-1000 MHz). The physical properties of concrete are examined and found to be profoundly influenced by water both at gauging and at later stages of development. The merits of currently used test methods for quality assessment of concrete are discussed.

The theory of polarization in dielectric materials is examined and a range of formulae suitable for frequency dispersion calculations in homogeneous and heterogeneous materials is presented.

A review of previous research into the electrical properties of concrete at frequencies in and below the RF range, including a brief description of Ground Probe Radar techniques, is presented and the results discussed. A distinct shortage of data is found in the 100-1000 MHz range.

The electrochemical properties of concrete are considered and their influence on the electrical properties is examined. A previous hypothesis in this area, based on the behaviour of ions in the mix water, is shown to be incorrect, but a new hypothesis relating the dielectric dispersion of fresh concrete to ionic effects at the surface of hydrating cement grains is proposed. The results from calculations based on the hypothesis are compared with available data at 1-1000 MHz and found to be in agreement. A geophysical explanation, previously derived for sedimentary rocks, is proposed as an influencing factor on the electrical properties of hardening concrete in the same frequency range.

Measurement techniques at radio frequencies are considered and the application of these to concrete measurements is discussed with reference to two particular electrode systems at 1-100 MHz and 100-1000 MHz. A technique for calibrating out the effects of connector distortion is described and the results of tests presented.

The results from a range of experiments on various concrete mixes in the 1-1000 MHz range are presented and discussed. The data obtained for fresh concrete agree very well with the hypothesis. The data for hardening concrete show a qualitative

agreement with the relevant hypothesis. The probable effects on Ground Probe Radar signals of the dispersion observed for hardening concrete in the 100-1000 MHz range are discussed. Suggestions for further research are given.

# Declaration

I declare that this thesis was written entirely by me and that all the work reported herein was carried out by me except where acknowledged otherwise in the text. The work was carried out at Napier University between July 1989 and January 1993.

Gerard Starrs

April 1994

# Acknowledgements

Funding for this research was provided by the Science and Engineering Research Council from July 1989 to July 1991 and by Napier University from July 1991 to July 1992. Receipt of this funding is gratefully acknowledged.

I would like to express my gratitude to the following members of staff at Napier University for their assistance at various stages :-

Mr Allister Hutton who constructed the moulds and the electrode parts; Mr Jim Clark who assisted in all the early experimental work and kept the laboratory in good order; Mr Gavin Wilson who was very helpful in providing instruction and facilities for the transfer of data between various operating systems; Dr Dave Roberts who provided advice on the Newton Raphson method and introduced me to the use of the bilinear transform method; Mr John Sharp for helpful discussions on RF techniques; the technical staff in the department of Biological Sciences for providing de-ionised water and sodium chloride; Mr Alan Barber of the Building Engineering department for carrying out the crushing tests on the sample cubes; and the Library staff at the Craiglockhart campus.

I wish to thank John Dorner and Steve Mowbray at RTT for their help with computing facilities and word/data processing.

I am very grateful to Dr John Wilson my director of studies for his guidance, supervision and patience throughout this research. Gratitude is also expressed to Professor H.W. Whittington of the University of Edinburgh for acting as second supervisor and for helpful suggestions at various stages.

I would especially like to thank my wife Lisa, to whom this thesis is dedicated, for all her support and care.

For Lisa, without whom it wouldn't have been possible.

# Table of Contents

# CHAPTER 1

# Introduction

The work presented in this thesis was carried out as part of the research effort involved in the **Measurement and Applications of the Electrical Properties of Concrete** project at Napier University in Edinburgh, the long term aim of which has been to establish the basis of a reliable, accurate, non-destructive and quick to implement method for the early quality assessment of concrete. Emphasis has been placed on developing a quantified correlation between the *fundamental* mechanical/physical and electrical properties of the material: an empirical approach has been rejected because these are often technique specific and of limited value (c.f. [1]). As a precursor to a test technique, this experimental and theoretical study of the properties of both fresh and set concrete as a dielectric material across a wide band of radio frequencies (up to 1000 MHz) was undertaken.

This investigation extends and assesses previous work reported by Wilson [2] and Wilson and Whittington [3][4][5].

Previous work had, in general, clarified aspects of the electrical behaviour of concrete, especially at lower frequencies. It was confirmed, for instance, that alterations in the physical state of the material as it developed subsequent to gauging were mirrored by changes in measured electrical impedance.

Differences in original mix proportions were similarly shown to be detectable but only where data could be obtained at high frequencies (>1 MHz). However, due to the approximate nature of the mathematical process employed in the analysis of experimental readings, the validity of the absolute values of the intrinsic dielectric parameters (dielectric constant and conductivity) de-imbedded from high frequency impedance measurements was not certain. The subsequent development of a more precise mathematical model of the then existing electrode/sample arrangement

allowed more accurate estimate of dielectric parameters to be made from impedance measurements. However, the results obtained demonstrated two areas where further investigation was deemed necessary :-

**(i)** For frequencies of investigation above 3 MHz *negative* values of dielectric constant were produced. This effect was particularly noticeable in fresh concrete across almost two decades of frequency (≈3-150 MHz).

**(ii)** The mathematical algorithm used in analysis failed to converge to any meaningful solutions for dielectric constant or conductivity at frequencies beyond 100 MHz, a frequency band considered necessary for mix proportion verification.

With respect to **(i)** above, a search of the literature has revealed no other reported occurrence of such values for concrete or similar materials. Also, while negative dielectric constants have been observed at very much higher frequencies ($>10^{15}$ MHz) [6][7], these are noted as occurring in ionised gases due to resonance processes inside atoms which do not manifest themselves at the much lower frequencies applied here to concrete.

For **(ii)**, the failure to converge was taken at the time as an indication of the need for further development of the mathematical model, and/or the de-imbedding process, on which data analysis was based, and also as a possible sign that the physical structure of the electrode system might require modification. It is a point of note that no published data charting the fundamental electrical behaviour of concrete or mortar in the 100-1000 MHz range as it changes state, other than that which had previously arisen from this project, was available during the course of the current research.

It was therefore considered essential to produce reliable data for the dielectric constant and conductivity of concrete/mortar across the 100-1000 MHz frequency range, and to verify or rectify the previous data and theory for the 1-100 MHz band, thereby filling a notable gap in the literature and providing the means for a deeper theoretical understanding of these materials. This should, in turn, allow the establishment of a scientific foundation for the development of a nondestructive assessment technique for concrete.

# CHAPTER 2

## Properties of Concrete and Constituents

The use of concrete as a building material has a long history. Calcareous cements, the basis of concrete, were used by many early civilisations to one extent or another with the Romans eventually developing a definite concrete technology which had remarkable similarities to that of the present time [8]. Today, the importance of concrete as a structural material can be gauged from its extensive use in many applications within the civil engineering and building industries. However, despite its long history and widespread use, concrete is conversely one of the least understood construction materials. For instance, due to its heterogeneous structure it is intrinsically more complex than homogeneous steel - another comparably widely used material - and this makes its behaviour more difficult to assess. Neville, comparing the use of concrete with that of steel in the preface of his book "Properties of Concrete" [9], points out that the variability which often occurs between *specified* concrete and the material which actually ends up being placed, is due to the fact that concrete, in contrast to steel, is usually made *in situ* where quality control is accordingly more difficult. This further adds to the difficulty encountered in predicting its behaviour.

The following definition of concrete was given by one correspondent in a letter to "The Quantity Surveyor" :

> "Concrete is a heterogeneous system of solid discrete, gradiently sized, inorganic mineral aggregates, usually plutonic (feldspathosilicaceous or ferro-magnesian) or sedimentary calcareous in origin, embedded in a matrix compounded of synthesized polybasic alkaline and alkaloidal silicates held in aqueous solution and coprecipitate dispersion with other amphoteric oxides, this matrix being originally capable of progressive dissolution, hydration, reprecipitation, gelatinization, and solidification through a continuous and co-existant series of crystalline, amorphous, colloidal and cryptocrystalline states and ultimately subject to thermoallotriomorphic alteration, the system when first conjoined being transiently plastic during which stage it is impressed to a predetermined form into which it finally consolidates, thus providing a structure relatively impermeable and with useful capacity to transmit tensile, compressive and shear stresses."

While somewhat overstated, the above does serve to illustrate something of the complex nature of concrete.

More simply put, basic concrete is made by combining a mixture of aggregates (particles of rock), cement, and water. Chemical reactions occur between the cement and the water, resulting in a matrix of various compounds which eventually consolidate, binding the aggregates together in a solid mass which is able to withstand considerable compressive load.

The aggregates can be subclassified as fine aggregate and coarse aggregate. The fine aggregates are usually called sand, with the word aggregate often (though mistakenly) referring only to the coarse types. Sand is defined as particles in the size range 0.07 mm to 5.0 mm and coarse aggregate consists of particles greater than 5.0 mm. Particles in the range 0.002 mm to 0.07 mm are called silt and anything smaller is referred to as clay. Ideally, the aggregates in concrete can be regarded as inert fillers with any chemical activity being restricted to the cement and water.

Cement, in the building industry context, is a bonding material used to amalgamate other materials (stones, bricks, building blocks etc) together. Its principal constituents are compounds of lime which have the property of setting and hardening in water as a result of chemically reacting with it. It is therefore classified as calcareous hydraulic cement. In Scotland, and the rest of the U.K., the cement most commonly used in the making of concrete is Ordinary Portland Cement (OPC). This material is one of a range of Portland cements which, though broadly similar in basic composition, are each designed with specific behavioural properties in view (e.g. sulphate resistance, rapid and extra-rapid hardening, low heat evolution during hydration, and colour variations). Portland cement, first mentioned in a patent as far back as 1824 by Joseph Aspdin, was so named for its resemblance, once set, to Portland stone, a limestone quarried in Dorset. It is manufactured from a mixture of calcareous and argillaceous (or other silica, alumina, and iron oxide bearing) materials, which are burned at extremely high temperatures and the resultant clinker ground into the familiar cement powder.

A concrete mix is defined by the ratios of the original constituents. These can be in terms of volume but are normally specified in terms of mass. The two ratios usually considered are :

**i)** The Water/Cement ratio (w/c)

**ii)** The Cement/Aggregate, or Cement/Sand/Aggregate ratio (c/a or c/s/a).

These ratios are specified at the design stage with a view to promoting the required concrete properties. However, it is worth pointing out that concrete itself is defined in terms of those properties which it is designed to possess (e.g. strength), and not the mix ratios as such.

The quality of concrete for its use in construction is traditionally inferred from its compressive strength, this parameter providing engineers with information on load bearing capacity, tensile strength and also durability. The strength of concrete is predominantly dependent, as will be shown, on the cement matrix, which in turn depends on the water/cement ratio of the original mix. The role of water, at mixing and at later stages, is particularly important to concrete development and to its properties. This point is demonstrated by the relationship :

$$S = \frac{A}{B^{w/c}}$$

where $S$ is the compressive strength, $A$ and $B$ are constants (which depend on environment, age of concrete, cement type and test method), and $w/c$ is the water/cement ratio.

This empirically derived relationship is sometimes known as Abrams law, after Duff Abrams who formulated it in 1919 [9].

While concrete is a strong material under compression, it is relatively brittle and its tensile strength is therefore comparatively low (as little as one tenth of its compressive strength, according to Neville [9]). For this reason concrete is usually reinforced in some way when it is required to bear tensile or shear stress. The reinforcement can be in the form of steel rods or bars embedded in the concrete, or

carbon or glass fibres inter-mixed with the aggregates. The resultant composite is a material capable of resisting high compressive, tensile or shear stresses. Another way of strengthening concrete is to reinforce it using prestressed steel bars or wires. Embedded high carbon steel bars or wires are held in tension before the concrete hardens. When the tension is released the resultant concrete is effectively held in horizontal compression which allows it to transmit considerably more tensile stress. As a result a much stronger material is obtained.

## 2.1 Properties of OPC and Cement Paste

Since OPC accounts for approximately 90 percent of the total cement used in construction projects in both the UK and the USA, it is with this cement that the present work is concerned.

### 2.1.1 Manufacture of OPC

In the brief description already given, it was noted that the principal raw materials used in OPC manufacture are calcareous (calcium carbonate, in the form of limestone or chalk) and argillaceous (iron oxide and silicates of alumina, in the form of clays and shales). Also used is a material called Marl which is a mixture of both types.

These materials are mixed in the approximate ratio of 2 parts calcereous to 1 part argillaceous, with limestones and shales being first crushed to manageable sized particles. There are two processes which are used to produce a thorough mixture of the materials before they are burnt. These are the "wet" process and the "dry" process.

Detailed summaries of these processes, are given by Neville [9] and Lea [10].

In the wet process, the raw materials are mixed separately in washmills with water to reduce the particle size of the solids, and then combined to produce a liquid of creamy consistance called slurry, which has a water content of approximately 35 to 50 percent and a maximum particle diameter of about 90 μm. The slurry is stored in tanks before being passed into a rotary kiln to be burned at a temperature of between 1400°C and 1500°C, using pulverised coal, oil or gas as fuel.

In the dry process, the raw materials are fed, in a crushed condition and in the correct proportions, into a grinding mill where they are dried and reduced to a fine powder called raw meal. The raw meal is then pumped to a blending silo where final adjustments can be made to the mix proportions, and from there it is pre-heated to 800°C before being fed to a rotary kiln for burning at 1400°C to 1500°C.

There are relative advantages and disadvantages associated with both processes. In the UK during the 1970's the wet process was more commonly used as it allowed more accurate control of the ultimate composition of the cement, due to the ease with which the chemical composition of the slurry could be checked, and if necessary corrected, before it was passed to the kiln. The dry process has been the more usual method since the 1980's as less fuel and a smaller kiln size are required at the burning stage for the production of a comparable amount of cement.

The result of the high temperature burning in the kiln is a sintered material called clinker. Once the clinker has cooled, by which time it is characteristically black, glossy and hard, it is intermixed with a quantity of gypsum (calcium sulphate hydrate), not usually exceeding 2-3 percent of the total weight. The gypsum is added to control the rate of setting of the cement. The mixing is carried out in a ball mill where the clinker/gypsum blend is ground into a fine powder producing Ordinary Portland Cement.

The materials used in cement manufacture are impure, but consist mainly of lime ($CaCO_3$), silica ($SiO_2$), alumina ($Al_2O_3$) and iron oxide ($Fe_2O_3$). These react in the high temperatures of the rotary kiln to form more complex compounds which exist, before cooling, in a state of chemical equilibrium. However, a complication arises during the cooling of the clinker in that both crystalline and amorphous forms of the material are produced. Although the compounds which constitute these forms have nominally the same chemical composition, the properties of the amorphous material (known as glass) differ considerably from those of the crystalline type. Another complication which can arise is the reaction of the emerging crystalline compounds with the still liquid part of the cooling clinker. Despite these complications, the cooled cement products are assumed to be in the state of equilibrium which existed before cooling commenced.

All the processes involved in cement production require intimate mixing of the raw materials, because a part of the chemical reactions in the kiln take place by diffusion in solids, thus necessitating a uniform, "homogenised", distribution of the constituents to ensure a uniform final product.

The acceptability of a particular batch of cement is normally determined by direct physical (not chemical) testing of those properties which are considered to be of most practical significance, among these being the fineness of the largest cement grains and the distribution of grain size. Both of these properties have consequences for the ease of water penetration into the cement powder and the rate of cement hydration, especially early hydration.

## 2.1.2 Chemical Composition of OPC

The chemistry of Portland cement has been studied extensively (see the reference list for chapter 1 of [9]), and over many years (for instance the mineralogic composition of cement is often calculated from the results of chemical analysis by means of a method which was developed by Bogue [11] as far back as 1929). Brief summaries are given by Orchard [12] and Chong [13], and more detailed surveys by Neville [9] and Lea [10].

Of the compounds produced by the manufacturing process, the four which are generally regarded as being the main constituents of cement are :

**i)** Tricalcium silicate (Alite) ($3CaO.SiO_2$)
**ii)** Dicalcium silicate (Belite) ($2CaO.SiO_2$)
**iii)** Tricalcium aluminate ($3CaO.Al_2O_3$)
**iv)** Tetracalcium alumino-ferrite ($4CaO.Al_2O_3.Fe_2O_3$)

Cement chemists denote each of the oxides by one letter, viz. : Lime (CaO)=**C**, alumina ($Al_2O_3$)=**A**, silica ($SiO_2$)=**S**, ferrite ($Fe_2O_3$)=**F**. Similarly, water is ($H_2O$)=**H**.

Thus, the major constituents of OPC in shorthand form are :

**i)** $C_3S$ **ii)** $C_2S$ **iii)** $C_3A$ **iv)** $C_4AF$

In addition to these four compounds, there are a number of minor compounds present which usually account for no more than a few percent of the total cement weight. Examples of these are MgO, $TiO_2$, $Mn_2O_3$, $K_2O$ and $Na_2O$. Among these compounds, the oxides of sodium and potassium ($Na_2O$ and $K_2O$ - known as *the alkalis*) are of particular interest because they have been found to react with some aggregates, leading to deterioration of the concrete, and also to affect the rate of strength gain of cement. The description *minor* refers therefore to quantity and not to their significance.

Among the major compounds, $C_3S$ is normally present in the largest amounts and occurs as small, equidimensional, colourless grains. As the clinker cools below 1250°C in the kiln, the $C_3S$ slowly decomposes but provided the cooling rate is not too slow it remains unchanged, and is comparatively stable at ordinary temperatures.

$C_2S$ occurs in the clinker during cooling in any one of three (possibly four) known forms ($\alpha$, $\beta$, and $\gamma$), depending upon the temperature in the kiln. $\alpha$-$C_2S$ is present only at the highest temperatures and inversion to $\beta$-$C_2S$ (known as belite) takes place at approximately 1450°C. $\beta$-$C_2S$ inverts to $\gamma$-$C_2S$ on cooling to around 670°C, but due to the cooling rates applied to commercial cements it is $\beta$-$C_2S$ which is preserved in the clinker, where it forms rounded grains typically occurring in pairs.

In the crystalline form of the cement clinker, $C_3A$ occurs as rectangular crystals, but in frozen glass it takes the form of an amorphous interstitial phase.

$C_4AF$ is a convenient formula giving a simplified description of a range of compounds ($C_2F$ to $C_6A_2F$) which occur in solid solution. It is the iron oxide in this material which gives OPC its characteristic colour.

The relative quantities of the main compounds determine the behaviour of Portland cement, and correct proportioning of these materials permits the production of cements with the various properties mentioned previously (i.e. sulphate resistance, rapid and extra-rapid hardening, low heat evolution during hydration, and colour variations). Both Orchard [11] and Neville [9] demonstrate that, although the quantities of $C_3S$, $\beta$-$C_2S$, $C_3A$ and $C_4AF$ are directly dependent on, and calculable

from, the quantities of the constituent oxides (CaO, $Al_2O_3$, $SiO_2$, and $Fe_2O_3$), very small variations in the oxide proportions can result in comparatively large variations in the compound composition of the cement.

In recent years it has been realised that changes have occurred in the constituent proportions and the properties of OPC (and other Portland cements) [14][15]. The nature of these changes has consisted mainly in an increase in the amount of $C_3S$ accompanied by a corresponding decrease in the amount of $C_2S$. This has resulted in a significant increase in the reported strength of cement, which is due to the fact that most specifications are based on measurement of strength at 28 days after gauging, at which point $C_3S$ is the largest contributer. What was apparently not realised, however, is that using high-$C_3S$/low-$C_2S$ cement as a constituent in concrete or mortar can result in a reduction in the durability of these materials.

Recent changes notwithstanding, typical figures for the compound composition of OPC are :

| Constituent Compound | %age |
|---|---|
| **i)** Tricalcium silicate | 54.1 % |
| **ii)** Dicalcium silicate | 16.6 % |
| **iii)** Tricalcium aluminate | 10.8 % |
| **iv)** Tetracalcium alumino-ferrite | 9.1 % |

These figures are produced by Neville [9], and are derived, using the method of Bogue [16], from the defined oxide composition limits for Portland cements.

### 2.1.3 Hydration of OPC

OPC is a hydraulic cement which becomes a bonding agent when water makes contact with it and the resultant mixture chemically reacts. The silicates and aluminates form products of hydration, referred to collectively as *gel*, which in time produce a hardened mass. Although the term "hydration" is used to refer to the entire chemical process, there are actually two ways in which the cement and the

water react, viz : true hydration (in which whole molecules of water are combined with silicates and aluminates) and hydrolysis (in which water molecules are chemically broken down and recombined with other ions).

It has long been recognised that the products of cement hydration are, by and large, chemically the same as the products of hydration of the individual compounds (assuming similar conditions). In fact, the physical behaviour of OPC during hydration is comparable to that of the two calcium silicates ($C_3S$ and $C_2S$) alone, these being the main cementitious compounds in the cement.

Berner [10] has modelled the hydration reactions of Portland cement as a step towards modelling the porewater chemistry of the hardened material. The following equations are given as "main reactions", which always occur on hydration :

**Tricalcium silicate and water** :

$$C_3S + (2.5+n)H_2O \rightarrow C_{(1.5+m)}SH_{(1+m+n)} + (1.5-m)Ca(OH)_2 \qquad ...(2.1)$$

**Dicalcium silicate and water** :

$$C_2S + (1.5+p)H_2O \rightarrow C_{(1.5+q)}SH_{(1+q+p)} + (0.5-q)Ca(OH)_2 \qquad ...(2.2)$$

( where, $-0.1 \leq m$ ; $q \leq 0.3$ ; $n,p \geq 0.5$ )

On hydration, both $C_3S$ and $C_2S$ consume approximately the same amount of water and the colloidal calcium silicate hydrate (CSH) precipitates produced by each, sometimes referred to collectively as tobermorite gel, are more or less indistinguishable. However, the hydrolysis of $C_3S$ produces more than twice as much calcium hydroxide which, initially giving rise to a supersaturated solution, subsequently precipitates out in the hardening cement paste as large hexagonal plate-like crystals called portlandite. The calcium silicate hydrates have often been assumed to be amorphous in form but Neville [9] points out that the use of electron microscopy has revealed a degree of crystalline structure. Henderson and Bailey [17] have reported work in which the molecular structures of synthetic CSH's were examined by transmission electron microscopy (TEM). They found that at the

molecular level the CSH's formed 1nm thick sheets with an area of $10^2$ to $10^6$ $nm^2$, this basic structure being independent of composition, degree of order, and mode of formation. They also found that the degree of CSH amorphism is affected by the presence of calcium hydroxide in aqueous solution during hydration, with saturated solutions promoting typically amorphous hydrates, while solutions at lesser concentrations produce more ordered types. Thus, the proportion of $C_3S$ to $C_2S$ in OPC, determining as it does the amount of calcium hydroxide liberated during hydration, may well affect the eventual molecular structure of the hydrate gel. Since calcium silicate hydrates account for approximately 70 percent of the material in mature cement paste, their properties and structure have important consequences for the setting and hardening of concretes and mortars containing OPC.

The initial hydration of $C_3S$ in OPC does not proceed at a uniform rate, an effect which is most likely to be due to the deposition of a CSH coating on the outside of otherwise unhydrated cement grains which occurs as a result of the initial rapid release of calcium hydroxide into solution. This leads to a "dormant" period during which the rate of hydration, as indicated by gel formation, is greatly retarded [9]. It is postulated that the CSH coating is selectively permeable in character allowing inward diffussion of water molecules and outward diffusion of calcium and hydroxyl ions, but no outward diffussion of silicate ions. The dormant period persists until the coating on the grains ruptures under the osmotic pressure exerted by the build up of hydrous silicate products beneath which then precipitate as CSH gel in the bulk solution [18]. Despite this non-uniformity, the overall reaction rate of $C_3S$ (its "hydraulicity") is much higher than that of $C_2S$ so that most of the early compressive strength of hydrating cement is due to the contribution of $C_3S$ hydrates, which allow the cement to achieve about 85 percent of its final strength after 28 days. The strength contribution of $C_2S$ hydrates, increasing more gradually, eventually catches up, in relative proportional terms, after more than 300 days.

**Tricalcium aluminate and water** :

$$C_3A + 6H_2O \rightarrow C_3AH_6 \text{ ..... } (C_3AH_6 = 3CaO.Al_2O_3.6H_2O) \quad ...(2.3)$$

**Tricalcium aluminate, Calcium hydroxide and water** :

$$C_3AH_6 + Ca(OH)_2 + 12H_2O \rightarrow C_4AH_{19} \quad ...(2.4)$$

**Tricalcium aluminate, Gypsum and water :**

$$C_3A + x(CaSO_4.2H_2O) + (y\text{-}2)H_2O \rightarrow C_3A.xCaSO_4.yH_2O \quad ...(2.5)$$

( where, $1 \leq x \leq 3$ ; $12 \leq y \leq 32$ )

The reaction of pure $C_3A$ with water is very rapid, releasing considerable heat, and can cause immediate stiffening of the cement paste, a phenomenon known as *flash set*. It is to prevent the occurrence of flash set that gypsum ($CaSO_4.2H_2O$) is added to the cement clinker during manufacture. Equation (2.5) describes the reaction between $C_3A$, gypsum and water, and shows that the reaction products are distributed between two phases, ettringite ($x$=3, $y$=32) and calcium aluminate-monosulphate ($x$=1, $y$=12). These phases gradually give rise to the formation of a tricalcium aluminate hydrate ($C_3AH_6$). Thus, the presence of gypsum overcomes the problem of flash set by effectively slowing down the production of $C_3AH_6$ as described by equation (2.3).

The hydration rate of $C_3A$ is also retarded by the calcium hydroxide released during the hydrolysis of $C_3S$. This is shown in equation (2.4). The $C_4AH_{19}$ produced delays the reaction of $C_3A$ by forming a coating on the unhydrated grains, greatly curtailling the access of water. The $C_4AH_{19}$ then eventually changes to crystalline $C_3AH_6$, which is the stable form of the calcium aluminate hydrate ultimately existing in the hydrated cement paste. It occurs as cubic crystals. Thus, equation (2.3), while missing out the intermediate steps and therefore not truly stochiometric, is a realistic representation of the overall hydration reaction of $C_3A$.

$C_3A$ requires much more water than the silicates for hydration. However, the products of hydration contribute little or no cementitious value to hardened cement. In fact, its presence in cement is actually undesirable at the hydration stage, but it contributes to the manufacturing process by acting as a flux in the kiln reactions. Its presence in hardened cement renders the material liable to disruption by sulphate

attack because ettringite, the product in equation (2.5), is an expansive compound which swells as it imbibes water. Such swelling can lead to rupture of the hydrated cement paste structure.

**Tetracalcium alumino-ferrite, Calcium hydroxide, water and Tricalcium aluminate hydrate** :

$$"C_4AF" + 2Ca(OH)_2 + (2x\text{-}2)H_2O + zC_3AH_6 \rightarrow (z+2)C_3(A,F)H_x \qquad ...(2.6)$$

( both A and F = $z + 1$ ; $1 \leq x \leq 3$ )

$C_4AF$, like $C_3A$, has little or no cementitious properties but it also acts as a flux in the kiln reactions. It hydrates in a similar manner to $C_3A$. As shown in equation (2.6), $C_4AF$ reacts with calcium hydroxide and water to produce a solid solution of materials ranging in composition from tricalcium aluminate hydrate to tricalcium ferrite hydrate. $C_4AF$ also reacts with gypsum and water to form calcium sulphoaluminate and calcium sulphoferrite.

The hydration reactions of OPC are exothermic and the process of hydration can be monitored by the measurement of heat evolution within the material [9].

An high initial peak of heat generation is reached in the first few minutes subsequent to gauging. It is believed that this is a result of the heat of wetting of $C_3S$ (i.e. the adsorption of water onto cement grain surfaces and the formation of gelatinous coatings of hydration products around the grains) and possibly the hydration of any free lime in the cement [18]. The heat generated falls to a low value for the period between 1 and 3 hours after gauging (the induction period), this period corresponding to the "dormant" period described above, when reactions continue only on the inside of the cement grain coatings. The rate of heat generation then begins to rise again (the acceleration period), as the coatings are ruptured and hydration products begin to be formed between cement grains, and comes to a peak between 8 and 10 hours and thereafter gradually falls away. The time taken to reach the second peak is inversely proportional to the ambient temperature of the curing environment and this indicates that the rate of hydration is proportional to

temperature. Figure 2.1, after Double [18], shows the rate of heat evolution for hydrating tricalcium silicate at an ambient temperature of 25°C, plotted as a function of time since gauging.

The shape of the characteristic for $C_3S$ corresponds closely to that of hydrating cement, although it should be noted that, because the individual compounds in OPC hydrate at different rates, the overall rate of heat evolution is affected by the compound proportions (in particular by $C_3A$ at the early stages of hydration and by $C_2S$ at later stages). In a concrete mix, variation in the cement/aggregate ratio additionally has an effect. Another point of note is that, because concrete has a relatively low thermal conductivity which does not allow rapid dissipation of heat, the internal *temperature* of a large mass of concrete will remain elevated, or even continue to increase, after the rate of heat evolution has fallen away.

During hydration, especially in the early stages, the free water in the cement paste contains a high concentration of various ion species, primarily $Na^+$, $K^+$, $Ca^{2+}$, $SO_4^{2-}$ and $OH^-$, the relative concentrations of which vary with time. As with the rate of heat evolution, these changes in the aqueous solution chemistry are related to the stages of the hydration process. Figure 2.2, after Double [18], shows the typical variation of cement paste ionic concentration over the first 16 hours after gauging. Initially, the highest concentrations are of calcium and sulphate ions, which reach a peak within the first few minutes subsequent to gauging. This peak is associated with the dissolution of gypsum. After about two hours the concentration of sulphate ions falls to a relatively low level, this trend probably being related to the aluminate and aluminoferrite reactions with gypsum. The calcium ion concentration also falls, though not quite so rapidly, but it rises again and reaches a lower and broader peak after approximately two hours. The concentration of hydroxyl ions is initially low but it rises rapidly to a peak level at two hours at which point it is by far the most numerous species. This peak is associated with the end of the induction period and the onset of the acceleration stage. The concentration of potassium and sodium ions is relatively low throughout hydration, the more numerous of these two species being potassium. At all times the silicate, aluminate, and ferrite ion concentrations are very low.

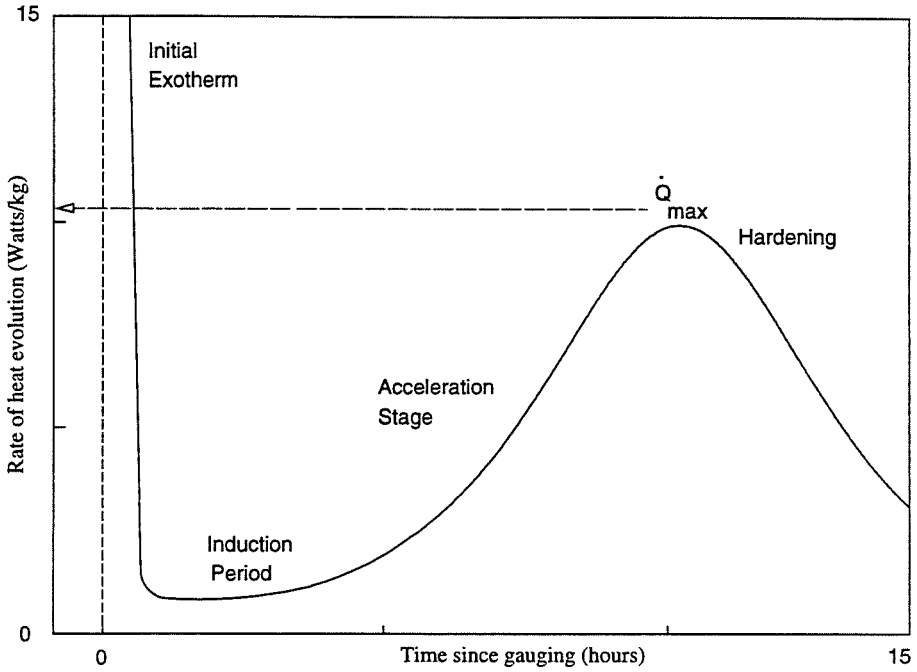


**Figure 2.1 Rate of Heat Evolution of $C_3S$ at 25°C**

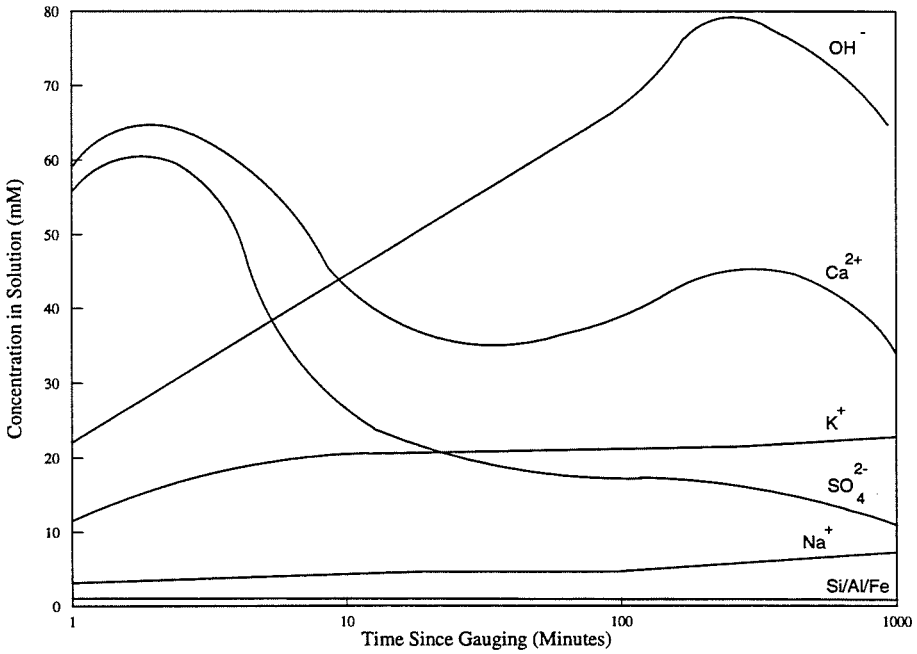


**Figure 2.2 Ionic Concentrations in Free Water of Cement Paste**

It has been found that the overall free water ionic concentration is still high after 16 days, which is probably indicative of the presence of unhydrated cement [2].

Thus, the aqueous solution chemistry of hydrating cement paste could also be used to monitor the hydration process.

### 2.1.4 Development of Hydrating OPC

According to Neville [9], the mechanical properties of hardened cement (and therefore mortar and concrete) are determined not so much by the chemical composition of hydrated cement as by the physical structure of the hydration products (see also section 2.1.3). The physical properties of hydrated cement paste are therefore of considerable importance to the quality of concrete or mortar.

At this point it is perhaps useful to define three terms which are associated with the development of hydrating cement paste, and which may at times overlap or be confused, viz. : Setting, Hardening, and Curing.

**i) Setting**

This term is used to describe the stiffening of the cement paste which occurs when the material changes from a fluid to a rigid state. Two stages of setting can be identified. The first is *initial set*, which coincides with the initial exotherm a few minutes after gauging. The second is *final set*, which occurs at the second thermal peak (for OPC this is about 7-8 hours after gauging at room temperature). Thus, setting is defined in terms of change of material state and specified in terms of temperature changes in the cement paste. Although some strength is gained by the material during setting, for practical purposes the term refers only to a change in state.

**ii) Hardening**

This term is used to describe the process of strength gain which is considered to commence once setting has taken place and the cement paste has become a rigid

structure. Hardening can continue for a long period of time as the cement continues to hydrate. The compressive strength of the material of which the cement paste is a part is taken as a measure of the degree of hardening achieved at any time.

### iii) Curing

This term refers to the procedures which are carried out in order to promote the hydration, and consequent hardening, of the cement paste. Curing involves the control of the temperature of the material and of the movement of moisture into and from it. The object of curing is to keep the material saturated, or nearly saturated, until the desired extent of hydration has been achieved. Curing at elevated temperatures can incease the rate of early hydration (and thereby the rate of strength gain), but beyond a certain temperature (depending on cement type) later strength and quality may be adversely affected [10]. Curing is therefore usually carried out at 'normal' temperatures (e.g. 20°C) if possible.

Thus, setting and hardening refer to stages in the hydration process, while curing refers to procedures which are implemented to promote hydration. Curing is made necessary by the fact that hydration of cement can only take place in water-filled spaces within the structure of the cement paste itself. Evaporation and consequent loss of water must therefore be prevented until sufficient hardening has occurred. Also, ingress of water to the structure of the material (cement, mortar or concrete) must be facilitated because of the internal drying effects of self-dessication caused by continuing hydration.

The structure of hydrating OPC has been investigated in detail by Double [18], Double et al. [19] and Birchall et al. [20]. Fresh cement paste is a network of cement grains (which can range in diameter from <10 μm up to 90 μm) dispersed in water. At later stages of hydration, the cement paste matrix consists of hydrates of the various compounds (i.e. cement gel), crystals of calcium hydroxide, unhydrated cement, some minor compounds, and the residue of water filled spaces in the fresh paste.

The structure of the gel has been described as consisting of irregular fibres of silicate growing from the surface of the hydrating cement grains and bridging the spaces between them, with calcium hydroxide also appearing in the structure in the form of plate-like crystals [18][19][20]. After initial wetting, the gelatinous coating on the surface of the cement grains is between 0.1 and 1.0 μm thick. The outgrowth of gel from the cement grain surfaces occurs after rupture of the gelatinous coating during the acceleration stage, and this corresponds to the setting of the cement paste. When the paste is fully mature the structure shows considerable infilling between the grains by the fine grained silicate hydrate gel and crystalline hydration products. On the inside of the cement grain coatings structures of a fine grained and compact texture are formed, differing in some respects from the outer products.

Due to the initial random distribution of cement grains and water, zones which are not filled with gel or cement powder arise in the matrix. These zones, which are reckoned to have a range of diameters from 8.0 nm up to 1.0 μm (with the vast majority in the range 8.0-80.0 nm) [22], are called capillary pores and they form an interconnected water-filled system randomly distributed throughout the paste structure [9]. Pores of diameter 1.0-4.0 μm, which are far fewer in number, are called mesopores [22]. It is in the water of the capillary pores (and mesopores) that the bulk of the hydration reactions continue to take place, the capillary network thus representing that part of the total volume of hydrating cement paste which has not yet been filled with hydration products. As hydration proceeds the volume of the network reduces due to the twofold increase in volume between unhydrated cement and the resultant gel [9].

The gel itself is not a continuous mass but consists of particles of various shapes separated by water-filled interstitial spaces. These spaces, which are between 1.5 and 2.0 nm in diameter (i.e. only one order of magnitude greater than a water molecule - 0.1571 nm [64]), are referred to as gel pores. There is very little spread in the diameters of the gel pores [22].

Thus, two distinct but interlinked classes of pore are present in hydrated cement paste. Figure 2.3 is a simplified diagrammatical representation of the hydrated cement paste showing the pores. The relative sizes of particles and pores are obviously not shown to scale.

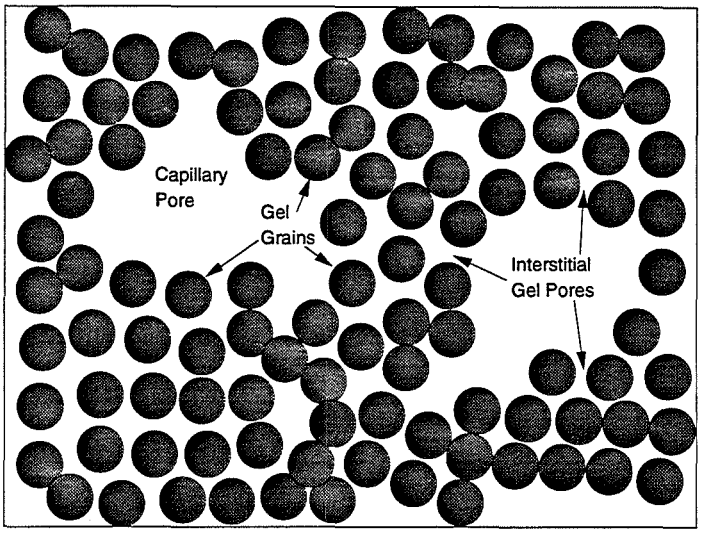


**Figure 2.3 Diagram of Cement Paste Pore Structure**

About 28 percent of the volume of the gel is accounted for by the gel pores, and it is interesting to note that the pore/solid ratio is not affected by the original water/cement ratio of the mix [9], or the degree of cement hydration (at least up to a time since gauging of many years, after which the gel pores can begin to fill with products of hydration [10]). This is not true, however, in the case of the capillary pore network which is influenced by both the mix water/cement ratio and the degree of hydration.

For water/cement ratios which are sufficiently low, and where the paste is allowed to undergo moist curing for long periods of time, part of the capillary pores may become blocked up with gel. This produces an overall paste pore network consisting of segmented capillary pores interconnected by much narrower gel pores. Neville [9] points out that for water/cement ratios greater than 0.7 segmentation of the capillary network is impossible. Lower water/cement ratios, which promote pore segmentation, therefore tend to produce more compact cement paste structures.

However, for values of w/c less than 0.38 complete hydration of the available cement becomes impossible, partly because the available water tends to get used up (self dessication), but also because the capillary spaces become entirely blocked, preventing further hydration even where moisture is available from outside. The capillary porosity of cement paste can range from 0-40 percent depending on water/cement ratio and degree of hydration. For water/cement ratios between 0.38 and 0.7 there will always be some degree of cement paste capillary porosity, even in fully hydrated cement, but the stage at which segmentation occurs will vary depending on the mix (e.g. 3 days for w/c=0.4, up to 1 year for w/c=0.7 [9]). Thus, for cement pastes used in normal construction the capillary pore network over the first day after gauging is always continuous.

The source of the strength of cement gel is still not fully understood [9], but it is believed to be due to two mechanisms of cohesion. The first of these is the physical attraction which exists between solid surfaces separated by very small distances. Such conditions exist between gel particles where the separation, as mentioned, is only 1.5-2.0 nm. This type of cohesion is one of the three types which make up the Van der Waals bond [21]. The second type of cohesion is thought to be due to some degree of chemical bonding between the gel particles. Evidence for this is inferred from the fact that the gel particles cannot be dispersed by the addition of water, which suggests the existence of cross-linking chemical forces between them. Both of these forces contribute to the high strength of the gel, but the relative contribution of each is not known [9].

Neville suggests that gel of similar properties is formed at all stages of hydration independent of mix proportions, which in turn implies that the strength of the cement gel is similarly independent of age and original mix water content. On the other hand, Double [18] states that the morphology of the CSH gel particles *is* dependent on both w/c ratio and the age of the hydrating cement, although it is not made clear whether such morphological factors are thought to affect the physical properties of the gel.

The strength of hydrated cement paste will depend on three main factors, viz :

**i)** The strength of the combined hydration products which constitute the gel, inclusive of tobermorite (i.e. CSH) and crystalline portlandite (i.e. CaOH).
**ii)** The porosity of the gel due to the interstitial spaces.
**iii)** The porosity of the paste due to the capillary pore network.

For a given cement, according to Neville [9], the first two factors, relating only to the gel itself, can probably be regarded as constants which in themselves are largely independent of original water content of the mix, whereas the third factor is known to be directly dependent on the water/cement ratio (although it is worth noting that Penttala [22] states that the relationship between capillary porosity and strength is not actually fundamental but that intrinsic gel strength is controlled by the same factors as the porosity, thus giving the appearance of the strength/porosity relation). Thus, at any given stage of hydration, variations in strength can be promoted by variations in water/cement ratio, with lower water/cement ratios tending to produce stronger hydrated cement pastes than higher water/cement ratios. For a given age of paste the curing regime will also affect the strength since it controls the access of moisture to the paste structure and so affects the rate of hydration.

Lea [10] states that, irrespective of initial water/cement ratio or curing regime, mature concrete which has dried out can lose 20-40 percent of its compressive strength on reabsorbing moisture. This is thought to be a result of the weakening of the forces between gel particles.

Obviously, the role of water at the time of gauging, and at subsequent stages, is of great importance to the quality, as indicated by strength, of hydrated cement paste.

Water is held in the paste structure in a number of ways, and the total amount held is dependent on the ambient humidity. If this falls to below 45 percent, the free water in the comparatively large capillary pores can evaporate, leaving them empty or with adsorbed water held only on the pore wall surfaces. However, the gel water is still found to be present at very low humidities.

The water held in the gel is bound in a number of ways. Firstly there is adsorbed water which is held in layers approximately four molecules thick in the interstitial pores by the surface forces of the gel. The second form of gel water is also adsorbed

but is trapped in one molecule thick layers between the surfaces of tobermorite sheets in the gel, and is known as zeolitic or interlayer water. Lattice water is held in the crystal lattices of the cement hydrates but is not chemically combined with them. Finally, there is chemically combined water which forms a part of the various hydrates in the gel. The energy of binding of water in the hydrates is, on average, higher than that of the interlayer water, which in turn is higher than than that of the surface adsorbed water. Figure 2.4, after Neville [9], shows the probable structure of hydrated silicates, including the surface adsorbed and zeolitic water.

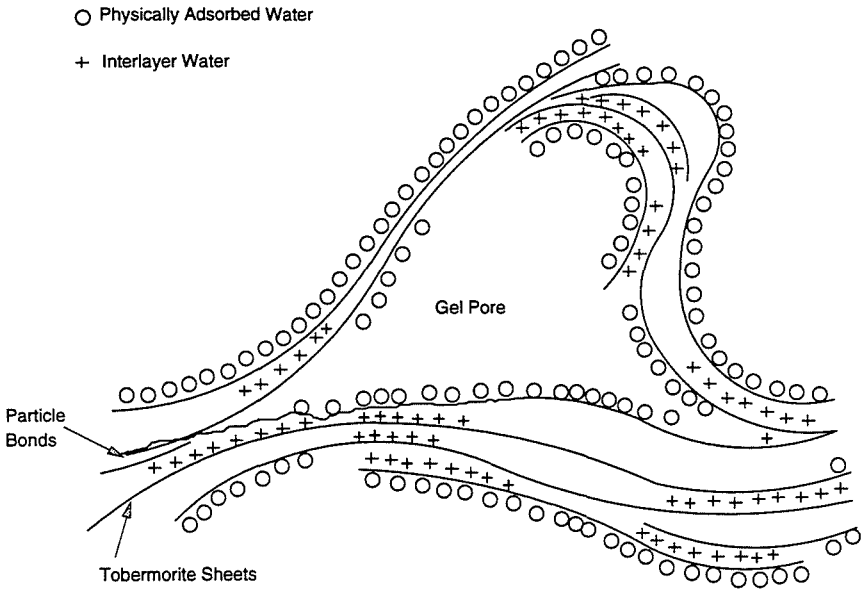


**Figure 2.4 Gel Particle Structure and Water Retention**

The properties of the variously bound paste water are dependent on the modes of retention [9], and the relative percentage volumes of the different forms change as hydration proceeds. A distinction is often made between evaporable water, which is usually assumed to be physically bound in gel (adsorption) and capillary pores (adsorption and condensation), and non-evaporable water, which is assumed to be chemically combined in the gel hydrates. However, while this distinction can be a useful one to make in practice (e.g. for the measurement of permeability and gel/capillary porosity) it is known that there is quite an overlap of firmness of bond

between adsorbed and combined water in hardened cement paste. This means that techniques which rely on evaporation for measuring paste porosity can give only an approximation of this parameter [10].

## 2.2 Properties of Aggregates

Since aggregates may occupy about 75 percent of the total volume of a concrete mass, some space is devoted here to examining their general properties.

One way of classifying aggregates is according to density. The three recognised ranges of density are :

**i)** Heavyweight aggregates - those having a specific gravity $\geq 4.0$

**ii)** Normal weight aggregates - those having a specific gravity = 2.5-3.0

**iii)** Lightweight aggregates - those having a specific gravity $\leq 2.5$

Structural concrete is generally made with normal weight aggregates and these are very often obtained - in the form of natural sands and gravels - from stream deposits, sand dunes and glacial deposits. Stream deposits generally prove to be the most satisfactory source, providing well rounded individual particles which have been cleaned by the naturally abrasive action of flowing water.

Among the criteria which are considered important with regard to the quality of aggregates are, freedom from organic and chemical contamination, porosity (or permeability - a function of porosity), particle shape and surface texture, and strength.

Organic and chemical contaminants can react with cement paste and interfere with the hydration process. The presence of salts in aggregates may later lead to corrosion problems in concrete reinforcement bars and may also promote sulphate attack on hardened concrete. Salts are usually washed out before the aggregates are used in concrete production.

The adherence of clay and silt particles to the surface of aggregates can be detrimental to the strength of the bond formed with cement paste, leading to less durable concrete. Again, washing the aggregates helps to minimize this problem.

The aggregates used in a concrete mix are not chemically reactive and do not demonstrate significant electrical conduction.

However, some types of aggregate are at risk of chemically reacting with hydrating cement paste, the most common reaction being between active silica in the aggregate and alkalis in the cement paste water ($Na_2O$ and $K_2O$ as mentioned in 2.1.2). This type of reaction results in the deposition of a gel on aggregate surfaces which swells on imbibing water, resulting in the possibility of rupture to the aggregate/cement-paste bond. This problem can be minimised by avoiding high alkali cements and reactive aggregates, although there are no reliable quick tests for detecting the latter. Fortunately, this problem is rare in Scotland, though it is widespread elsewhere [23].

For structural concrete it is preferrable to use coarse aggregates which are not highly porous, because high levels of porosity can lead to the problem of drying-shrinkage. This problem, as its name suggests, consists in the volume expansion and contraction of aggregate particles on wetting and drying. If such volume changes are large enough the concrete of which the aggregate is a part may be disrupted and crack, leading to substantial reduction in durability. There is particular risk of this where the material is subject to cyclic moisture changes. A similar potential problem associated with highly porous aggregates, is that of the expansion and contraction of rocks containing moisture on freezing and thawing, this again leading to possible disruption of concrete. However, in this case the problem only manifests itself where the pore diameters are about 4μm or smaller.

Another consequence of using highly porous aggregate is that if, on mixing the concrete, the aggregate is very dry, absorption of some of the gauging water will take place, thereby effectively altering the water to cement ratio of the mix. This can alter the properties of the concrete.

Some degree of porosity, on the other hand, is desirable as it helps to facilitate a strong bond between the cement paste and the surface of the aggregate particles, this in turn strengthening the concrete. Roughened surfaces and angular shaped aggregate particles are also of benefit in ensuring a firm bond.

The solution to the above problems is to test the aggregates and avoid using excessively shrinkable types in structural concrete. BS.812:Part 120 gives details of such testing [23].

At the point of gauging of a concrete mix, the ideal condition of an aggregate particle is moisture saturated and surface dry (i.e. the pore structure of the rock is filled with water but no moisture is adsorbed on any external surface). Such a condition assures that no further moisture will be absorbed from the gauging water into the aggregate pores, but also that no water will be added to the mix from the aggregate surface.

Normal density rocks which are of a close grained crystalline-type structure are usually sufficiently strong and resistant to impact, crushing, and abrasion, to be used in structural concrete. The strength of aggregates themselves, assuming they are of suitable quality as described, is usually well in excess of the strength of hardened cement paste and is therefore unlikely to be a limiting factor in the strength of concrete.

As a general rule, granite, basalt, hard crystalline limestone, quartzite and fresh felsite are strong, but not highly porous rocks and are therfore preferrable as aggregates.

## 2.3 Quality of Concrete

To determine the quality of concrete for use as a construction material two basic requirements need to be considered. First, the concrete must be *strong* enough to withstand the stresses applied to it *in situ*. Second, the concrete must be *durable* enough to withstand the conditions for which it is designed over a long period of time (many years), without deterioration. Thus, strength and durability are the two main quality parameters of concrete.

### 2.3.1 Strength and Durability

Durability can be adversely affected by external environmental factors and/or by internal factors operating within the concrete itself. The concrete may be affected externally by weathering, extreme temperatures, abrasion and chemical attack (natural or industrial), or internally by thermally induced volume changes, alkali-aggregate reaction, and above all by permeability (i.e. the rate at which a liquid will pass through the material). Permeability renders concrete vulnerable to invasion by external agencies and this is almost always a major factor in concrete deterioration [9]. Assuming that the aggregates used in the production of concrete are ideal (i.e. not chemically reactive with hydrating cement and of suitable particle shape and size) then it will be the permeability of the cement paste which will determine the resistance of the concrete to chemical attack by penetration of deleterious substances (e.g. sulphates). In reinforced concrete the most serious problem with associated durability is corrosion of the steel reinforcement (which can lead to structural weakening and disruption and cracking of the concrete) and a high value of permeability is one of the main factors in the promotion of corrosion. Since permeability is a measure of the ease with which water can penetrate the paste, it has an important bearing also on vulnerability to frost and to the effects of wetting-expansion and drying-shrinkage (as with porous aggregates). Permeability is determined to a very large degree by the capillary porosity, and the interconnectedness of the capillaries, of the cement paste and it is therefore directly related to initial water/cement ratio [9]. Thus, the durability of concrete is very much affected by water/cement ratio and the subsequent moisture content of the capillaries.

It has already been pointed out that compressive strength is an indicator of general concrete quality. This is because the strength of concrete is directly related to the structure of the hardened cement paste [9]. In section 2.1.4 it was shown that the structure and strength of hydrated cement paste are dependent on the paste porosity which, for a given cement type, depends on the water/cement ratio of the mix. Abrams Law, stated previously, shows that the strength of concrete is inversely proportional to the water/cement ratio. However, the Abrams formula is based on the assumption that the material has been fully compacted and therefore contains no

air voids resulting from the mixing process. In practice a certain amount of air tends to be entrapped during mixing due to the presence of aggregate, and this adds to the porosity of the hardened paste. Air can also become present in hardened cement paste when excess water has been used in the mixing process. The water collects in pools and subsequently evaporates, leaving large air filled voids in the material.

Feret's formula for the strength of concrete, which was empirically arrived at before Abrams Law, takes the amount of entrapped air into consideration :

$$S = K\left(\frac{C}{C+W+A}\right)^2$$

where $S$ is the compressive strength, $K$ is a constant and $C$, $W$, and $A$ are the volumes of cement, water and air respectively. This shows that the inclusion of air reduces the strength of cement paste.

The overall strength of concrete will be dependent on :

**i)** The strength of the cement paste.
**ii)** The strength of the bond developed between the paste and the aggregates.
**iii)** The strength of the aggregate particles.
**iv)** The degree of compaction.

For concrete containing suitable aggregates the factors limiting material strength will be the strength of the cement paste and the degree of compaction, both of which are related to the water/cement ratio of the mix. Ease of compaction of fresh concrete (known as workability - a measure of the amount of work required to overcome frictional forces within the material which resist compaction) is increased by adding water, but this reduces the strength of the hardened cement paste. On the other hand, poor compaction also leads to strength reduction so the water/cement ratio must be sufficiently high to allow the fresh concrete to be compacted but not so high as to significantly impair later strength.

It is clear from consideration of the factors which control both strength and durability that the quality of concrete, assuming the individual constituents (cement,

water and aggregates) to be of acceptable quality, is primarily determined by the water content of the original mix, the access to water during hydration, and the presence of water in the mature material.

### 2.3.2 Testing of Concrete Quality

Bate [8] discusses a number of major failures in concrete structures and concludes that such problems seldom, if ever, arise from a lack of scientific or technical knowledge. Instead, he attributes the occurrence of failures to improper application of knowledge, or to an absence of good engineering judgement. In particular, human error resulting from mismanagement (i.e. the acceptance of wrong priorities, misunderstanding, or lack of communication between those with different responsibilities in a given project) is cited as the most likely cause of subsequent failure.

Proper testing of the quality of concrete at various stages of manufacture and placement should expose the effects of errors thereby contributing to a reduction in the occurrence of subsequent failures.

A wide range of both in-situ and laboratory testing methods are currently available for the assessment of concrete. Neville [9] summarises a range of tests for fresh and hardened concrete and Bungey [24] provides a thorough survey of in-situ tests.

Wilson [2] has previously reviewed the various tests available when examining the justification for pursuing the current research towards the development of non-destructive testing based on the measurement of electrical parameters. It is therefore not the intention of the current author to re-examine the merits of individual non-electrical tests other than to briefly summarise the current situation.

At the present time the quality assurance tests most likely to be carried out in practice are basic tests on the suitability of the individual constituents, workability tests on fresh concrete (usually the well known slump test or other similar tests), crushing tests for the assessment of compressive strength carried out on standard cubes or cylinders, and surface hardness tests such as the Schmidt rebound hammer test. The tests on the pre-mixing quality of the individual constituents (whether

chemical, physical or simple inspection etc) can give no assessment of the actual concrete mixture. Workability testing of fresh concrete can require a high degree of practical experience on the part of the user since different mix proportions may produce similar results. Also, the workability of fresh concrete is not likely to be correlated to its quality in the hardened state [2]. The crushing of sample cubes or cylinders remains the single most important means of assessing concrete quality because other quality parameters are very much related to the compressive strength. However, crushing tests must be performed on hardened material, and this in practice means that they are normally carried out at 7 or 28 days after the mixing of the concrete in question. The usual delay is 28 days by which time concrete has achieved a great deal of its final strength and hardness (approximately 85 percent) which could result in great expense, difficulty and further delay should its quality be found to be inadequate. This may mean there is a temptation to leave poor quality material in place unless the case for its removal is overwhelming.

There are a number of more sophisticated tests available, such as ultrasonic methods of characterisation, laboratory chemical analysis of fresh and hardened concrete, radiation tests using gamma or X-ray sources and the use of on-site Rapid Analysis Machines (RAMs). These methods require highly trained personnel for operation and/or maintenance and can be expensive or even potentially dangerous (e.g. in the case of radiation tests).

Wilson's conclusion is that, in consideration of convenience and expense, the currently employed methods are realistic, but the time delay involved in establishing the quality of concrete is a definite weak link in the system. The development of a test which could be applied on-site, within one day of gauging and by personnel who do not require special skills or training, would be very worthwhile [2].

Investigations suggest that a technique based on the measurement of the electrical properties of concrete would have particular potential for development into a simple, quick to apply, nondestructive quality assessment method [25][2][3][4][5].

# CHAPTER 3

# Dielectric Theory

"Dielectrics" describes a class of materials which are not simply insulators (the usual electrical engineering interpretation of the term), but which includes any nonmetal when interaction with electric, electromagnetic, or magnetic fields is being considered. Comprehensive theoretical surveys of fundamental dielectric properties are provided by von Hippel [6][26] and Bottcher [27]. In this work the materials of interest (i.e. concrete and its constituents) are non-ferro-magnetic and their influence on magnetic fields is consequently assumed to be equivalent to that of free space. Attention is therefore focused on the effect of dielectrics on electric fields and propagating electromagnetic waves.

This chapter is concerned initially with the electrical properties of dielectrics when their behaviour is observed phenomenologically in terms of perturbation effects on an applied electric field (the Macroscopic approach), and subsequently with examination of the intrinsic material properties which give rise to the observed behaviour (the Molecular approach).

## 3.1 Macroscopic Approach

In this section the focus of attention is on the phenomenological aspects of dielectric behaviour. In particular, the external effects observed when dielectric material is placed in the electric field between the plates of an ideal parallel plate capacitor are considered and suitable parameters for describing such effects are derived. The presentation of dielectric data is also considered.

### 3.1.1 Parameters Describing Dielectrics

A capacitor consisting of two parallel plates of area A $m^2$, separated by a vacuum d m deep, has a value of capacitance :

$$C_0 = \varepsilon_0 \frac{A}{d} \qquad \cdots(3.1)$$

where, $C_0$ is the vacuum (or geometrical) capacitance (F), and $\varepsilon_0$ is the permittivity of free space (=$8.854\times10^{-12}$ $Fm^{-1}$).

A dielectric material placed between the plates of the vacuum filled capacitor increases its charge storage capacity such that :

$$C = \varepsilon_r C_0 \qquad \cdots(3.2)$$

where, C is the resultant capacitance (F).

The multiplying factor, $\varepsilon_r$, is the ratio of the permittivity of the dielectric material, $\varepsilon$, to the permittivity of free space, $\varepsilon_0$ (both $Fm^{-1}$), and is known as the *relative permittivity* :

$$\varepsilon_r = \frac{\varepsilon}{\varepsilon_0} \qquad \cdots(3.3)$$

For lossy materials, in which electrical energy is dissipated as well as stored, $\varepsilon_r$ is complex :

$$\hat{\varepsilon}_r = \varepsilon_r' - j\varepsilon_r'' \qquad \cdots(3.4)$$

In this work $\varepsilon_r'$, associated with energy *storage* effects, is referred to as the ***dielectric constant*** of the material and $\varepsilon_r''$, associated with energy *dissipation* effects, is referred to as the ***loss factor***. von Hippel [6] shows that the dielectric constant and the loss factor are not independent of each other but are both functions of frequency and are related by the Hilbert transforms (also known as the Kramers-Kronig relations).

When the capacitor containing the dielectric material is connected to a sinusoidal voltage source :

$$V = V_0 e^{j\omega t} \qquad \cdots(3.5)$$

then the product of angular frequency, $\omega$, loss factor, $\varepsilon_r''$, and free space permittivity, $\varepsilon_0$, is equivalent to a conductivity ($Sm^{-1}$) :

$$\sigma = \omega \varepsilon_r'' \varepsilon_0 \qquad \cdots(3.6)$$

Thus, the relative permittivity can be represented by the expression :

$$\hat{\varepsilon}_r = \varepsilon_r' - j\frac{\sigma}{\omega\varepsilon_0} \qquad \cdots(3.7)$$

This conductivity is the summed effect of all dissipative mechanisms in the dielectric material, and it may include losses associated with the movement of free charges as well as those associated with the polarization of bound charges.

Alternatively, if the dielectric material has a known value of D.C. conductivity, $\sigma_{DC}$, it may be desireable to express the effects of this separately from the purely dielectric effects in which case the relative permittivity can be represented by :

$$\hat{\varepsilon}_r = \varepsilon_r' - j\left(\varepsilon_r'' + \frac{\sigma_{DC}}{\omega\varepsilon_0}\right) \qquad \cdots(3.8)$$

The conductivity arising from $\varepsilon_r''$ is then known as the *dielectric conductivity*, $\sigma_d$, and it gives rise to an A.C. displacement current in the dielectric material. The overall conductivity of the dielectric material, $\sigma$, is the sum of this and the D.C. conductivity.

In this work the parameters primarily used to describe the dielectric properties of concrete, and associated materials, will be the ***dielectric constant***, $\varepsilon_r'$, and the ***conductivity***, $\sigma$.

### 3.1.2 Polarization and Polarizability

Dielectrics increase the charge storage capacity of a parallel plate capacitor by neutralizing some of the charges which build up on the plates, thus tending to reduce the electric field between them, necessitating the build up of more charge to maintain the field. This neutralizing of electrode charge is facilitated by the separation of bound charges within the structure of the dielectric material under the influence of the applied voltage. The electric field is sustained by free charges on the plates, supplied from the voltage source, which are not neutralized by the dielectric. Thus, only part of the total charge stored in the capacitor contributes to the externally observable electric field, the remainder being bound by the polarization of the dielectric material.

The total charge stored is distributed on the surface area of the capacitor electrodes and is represented as a charge density by the vector, $\vec{D}$, the electric *flux density* ($Cm^{-2}$) (this assumes that the direction of $\vec{D}$ is normal to the surfaces of the parallel plates of the capacitor).

The free charges on the plates of the capacitor give rise to an external electric field represented by the vector $\vec{E}$ ($Vm^{-1}$), again normal to the plate surfaces. These charges constitute a free charge density, $\varepsilon_0\vec{E}$ ($Cm^{-2}$).

The difference between the total charge and the free charge is represented by the vector $\vec{P}$ ($Cm^{-2}$), the polarization of the dielectric material. These vectors are related by the equation :

$$\vec{D} = \vec{P} + \varepsilon_0\vec{E} \qquad \cdots(3.9)$$

It is also known that :

$$\vec{D} = \varepsilon_r\varepsilon_0\vec{E} \qquad \cdots(3.10)$$

and by combining this with (3.9) the result is :

$$\varepsilon_r = 1 + \frac{\vec{P}}{\varepsilon_0 \vec{E}} \qquad \cdots(3.11)$$

Thus, the proportional relationship between the degree of polarization and the relative permittivity is direct and linear.

The polarization of the dielectric can be thought of as resulting from the setting up of a large number of electric dipoles, each consisting of two opposite charges, ±Q, displaced, in line with the electric field, by d m. Such a dipole will have a moment (Cm) :

$$\vec{\mu} = Q\vec{d} \qquad \cdots(3.12)$$

The total charge bound on the capacitor electrodes will be equal to the number of dipoles created in the volume of the dielectric so that the polarization, $\vec{P}$, is equal to the *total dipole moment per unit volume* of the material ($Cmm^{-3}$ or $Cm^{-2}$). From equation (3.11) the polarization can be shown to be :

$$\vec{P} = (\varepsilon_r - 1)\varepsilon_0 \vec{E} \qquad \cdots(3.13)$$

von Hippel [6] shows that the polarization can be thought of as resulting from the additive action of N elementary dipole moments (the number in a unit volume of dielectric) of average value $\vec{\mu}$ (Cm). The average dipole moment may be assumed to be proportional to *local electric field*, $\vec{E}'$, such that :

$$\vec{\mu} = \alpha \vec{E}' \qquad \cdots(3.14)$$

The factor $\alpha$ is a measure of the average dipole moment per unit field strength and is termed the *polarizability* of the dielectric material. The polarization is related to the polarizability thus :

$$\vec{P} = N\alpha \vec{E}' \qquad \cdots(3.15)$$

Comparison of (3.15) with (3.11) yields the relationship between relative permittivity and polarizability :

$$\varepsilon_r = 1 + \frac{N\alpha}{\varepsilon_0}\frac{\vec{E}'}{\vec{E}} \qquad \cdots(3.16)$$

In practice, because of the effects of molecular interaction, the local electric field, $\vec{E}'$, will not be equal to the externally applied field, $\vec{E}$, but the use of the external field value in equations (3.14) and (3.15) will often provide a good approximation for non-dense materials (i.e. gases). However, for denser materials such as liquids and solids a useful approximation for the local electric field can be obtained from the Mosotti equation [6] :

$$\vec{E}' = \vec{E} + \frac{\vec{P}}{3\varepsilon_0} \qquad \cdots(3.17)$$

This expression may then be substituted into equations (3.15) and (3.16) allowing calculations which do not require knowledge of local field.

### 3.1.3 Presentation of Dielectric Data

When dielectric materials are perturbed by alternating electric fields the effects observed are found to be frequency dependent. Thus dielectric constant and dielectric conductivity data (as well as related parameters such as loss factor, intrinsic impedance and admittance etc.) are ideally represented by plotting against frequency. This may be done on a standard graph such as the one shown in Figure 3.2 where the parameter axis is linear and the frequency axis is logarithmic.

Another type of graphical representation is the complex plane method, first used in relation to permittivities by Cole and Cole [28] (and often referred to as a Cole-Cole plot). In this method the imaginary part of the relative permittivity (loss factor) is plotted against the real part (dielectric constant) with frequency as a parameter. An example of a Cole-Cole plot is given in Figure 3.2. This method can be particularly instructive when considering the data obtained from relaxation processes (as described in section 3.2) since the shape of the graph obtained can provide immediately recognisable information on the nature of the observed dispersion.

Dielectrics can also be represented by equivalent circuits, generally of the RC type, which display relaxation behaviour. The value and arrangement of circuit elements (i.e. parallel and series combinations of resistors and capacitors) can be chosen to provide a two terminal network which has a frequency response equivalent to that of the dielectric material. However, it must be recognised that for any two terminal representation no single component arrangement is unique and an infinite number of circuits can be constructed to give the same overall response. Thus the elements of the equivalent circuit will not necessarily represent *directly* the physical properties of the dielectric.

## 3.2 Mechanisms of Polarization

From a microscopic viewpoint, polarization represents the superposed action of numerous elementary dipole moments which arise in a dielectric from separate mechanisms, depending on the structure of the material. These mechanisms, each contribute to the polarizability of the dielectric, and are responsible for the dispersion of its permittivity.

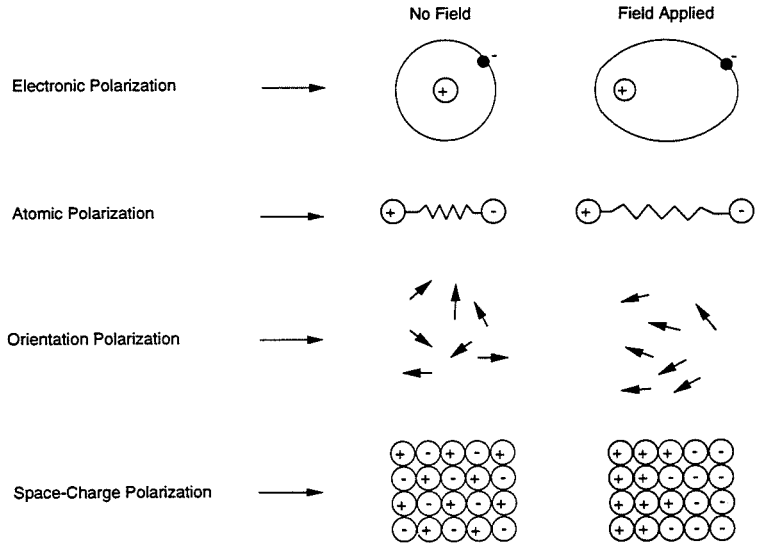


**Figure 3.1 Polarization Mechanisms**
(after von Hippel [26])

A number of fundamental mechanisms of polarization are known to operate in homogeneous materials , viz. *electronic*, *atomic* and *orientation* polarization. There are also a large number of mechanisms associated with mixtures and heterogeneous materials which can be grouped under the general heading of *space-charge* polarization (also called interfacial polarization). The following discussion of these phenomena is aided by the schematic diagram of Figure 3.1.

### 3.2.1 Electronic and Atomic Polarization

When an atom of any material is in a state of equilibrium, the centres of charge of the electron cloud and the nucleus which it surrounds will coincide. If the atom is then placed in an electric field these centres of charge will be displaced, the electron cloud towards the positive direction of the field and the nucleus towards the negative direction, resulting in an induced dipole moment. This effect is called electronic polarization and it is characterised for different elements by an *electronic polarizability*, $\alpha_e$.

Due to differences in electronegativity, the sharing of electrons between atoms in molecules may not be symmetrical, in which case the atoms acquire charges of opposite polarity. The effect of an electric field on such a molecule will be to change the equilibrium positions of the oppositely charged atoms (or groups of atoms) with respect to one another, resulting in a second type of induced dipole moment. This effect is is known as atomic polarization and it is characterised by an *atomic polarizability*, $\alpha_a$.

Both of these mechanisms are intra-molecular in operation and are therefore not temperature dependent [6]. They are characterised in frequency by a resonance dispersion which results from the restoring force which acts between the polarizing elements against the applied field. This produces an inability to respond to the electric field at frequencies above that of resonance. At such frequencies polarization is no longer observed because the finite time required for the induction of dipole moments is longer than the period of the alternating electric field and the contribution to dielectric constant consequently disappears. The resonance frequencies of electronic polarization mechanisms are found to lie above $10^{15}$ Hz and those of atomic polarization above $10^{12}$ Hz. These frequencies are far in excess

of the range of investigation in the present work and the contributions made by these mechanisms to the dielectric constant of concrete will therefore effectively constitute an apparent high frequency limiting value for other mechanisms.

### 3.2.2 Orientational Polarization

The molecules of some materials, such as water and hydrogen fluoride, are permanently polarized due to asymmetric charge distribution between unlike partners (atoms or groups of atoms). In the case of water, it is the physical structure of the $H_2O$ molecule which produces the displacement of the centres of charge equilibrium. The linking together of several water molecules by hydrogen bonding further increases the size of the permanent dipole moments. When an electric field is applied to water the permanent moments will tend to align with the field direction due to a torque action (see Figure 3.1 where the arrows represent permanent dipoles) giving rise to an orientational polarization, an effect which is characterised by an *orientation* or *dipole polarizability*, $\alpha_d$.

This mechanism has a *relaxation* dispersion in the frequency domain which results from the inability of the dipoles to maintain alignment with an alternating field when an increasing frequency reaches and exceeds some critical value. The loss factor associated with this mechanism reaches a maximum at the critical frequency. van Beek [29] explains the occurrence and dispersion of dielectric loss as follows : at very low frequencies the polarization easily follows the alternating field so that no loss occurs and the contribution to dielectic constant is maximal. At very high frequencies the field alternates too fast for polarization to occur so that no energy is lost and there is zero contribution to dielectric constant. Between these two extremes a lag develops between the field and the resultant polarization so that energy is dissipated and the contribution to dielectric constant begins to reduce. The critical, or relaxation, frequency, $f_R$, at which maximum loss occurs is related to a relaxation time constant, $\tau_R$, such that,

$$\tau_R = \frac{1}{2\pi f_R} = \frac{1}{\omega_R} \qquad \cdots(3.18)$$

Debye [30] developed expressions for the frequency dependent dielectric constant and loss factor of a liquid material consisting of polar molecules. He envisaged the dipoles as spheres with oppositely charged "ends" able to rotate in a viscous medium under the influence of an electric field. The equations he produced (the proofs for which are given by von Hippel [26] and Bottcher [27]) are :

Complex Relative Permittivity,

$$\hat{\varepsilon}_r = \varepsilon_{r\infty} + \frac{\varepsilon_{rs} - \varepsilon_{r\infty}}{1 + (j\omega\tau_R)} \qquad \cdots(3.19)$$

Dielectric Constant,

$$\varepsilon_r' = \varepsilon_{r\infty} + \frac{\varepsilon_{rs} - \varepsilon_{r\infty}}{1 + (\omega\tau_R)^2} \qquad \cdots(3.20)$$

Loss Factor,

$$\varepsilon_r'' = \frac{(\varepsilon_{rs} - \varepsilon_{r\infty})\omega\tau_R}{1 + (\omega\tau_R)^2} \qquad \cdots(3.21)$$

where, $\varepsilon_{rs}$ and $\varepsilon_{r\infty}$ are the low ("static") and high ("infinite") frequency limiting values of dielectric constant associated with the particular polarization dispersion, and $j = \sqrt{-1}$. Figure 3.2 presents graphical representation (both frequency and Cole-Cole plots) of the form of the dispersion curves for dielectric constant and loss factor.

It is evident from Figure 3.2 that the loss factor is at a maximum at the relaxation frequency, $f_R$, at which point $\omega\tau_R = 1$. From equation (3.21) the maximum value of $\varepsilon_r''$ is :

$$\varepsilon_{rM}'' = \frac{(\varepsilon_{rs} - \varepsilon_{r\infty})}{2} \qquad \cdots(3.22)$$

From equation (3.20) the value of dielectric constant at $f_R$ is :

$$\varepsilon_r' = \varepsilon_{r\infty} + \frac{(\varepsilon_{rs} - \varepsilon_{r\infty})}{2} \qquad \cdots(3.23)$$

$$\varepsilon_r' = \varepsilon_{r\infty} + \varepsilon_{rM}'' \qquad \cdots(3.24)$$

For a material in which the only mechanism of polarization operating is of the Debye dipolar type, the value of $\varepsilon_{r\infty}$ will be 1 (i.e. the dielectric constant of free space). In real physical cases, however, mechanisms of electronic and possibly atomic polarization, which have resonant frequencies much higher than the relaxation frequency of orientation mechanisms, will also be operating (for instance in water). Because of this the value of $\varepsilon_{r\infty}$ for the dipolar mechanism will actually result from the contribution made by the low frequency (static) electronic and atomic polarizabilities.

The conductivity arising from the dielectric losses will also be frequency dependent and can be obtained from the expression for loss factor (equation (3.21)) in accordance with equation (3.6) such that,

$$\sigma' = \sigma_s + \frac{(\sigma_\infty - \sigma_s)(\omega\tau_R)^2}{1 + (\omega\tau_R)^2} \qquad \cdots(3.25)$$

The dispersion of the dielectric conductivity is simply a mirror image of the dielectric constant (though on a different scale) reflected about the relaxation frequency. It therefore reaches a maximum value at frequencies above $\omega_R$.

The meaning of the term relaxation in the context of polarization is best explained by considering a volume of a material consisting of polar molecules, such as water, polarized by a static (i.e. D.C.) electric field. If the field is removed suddenly, random movement of the molecules due to thermal agitation will eventually cause the material to revert to its equilibrium state (which on average is non-polarized in any direction), and the polarization will "relax" as the average dipole moment per unit volume (i.e. considered in any single direction) returns to zero.

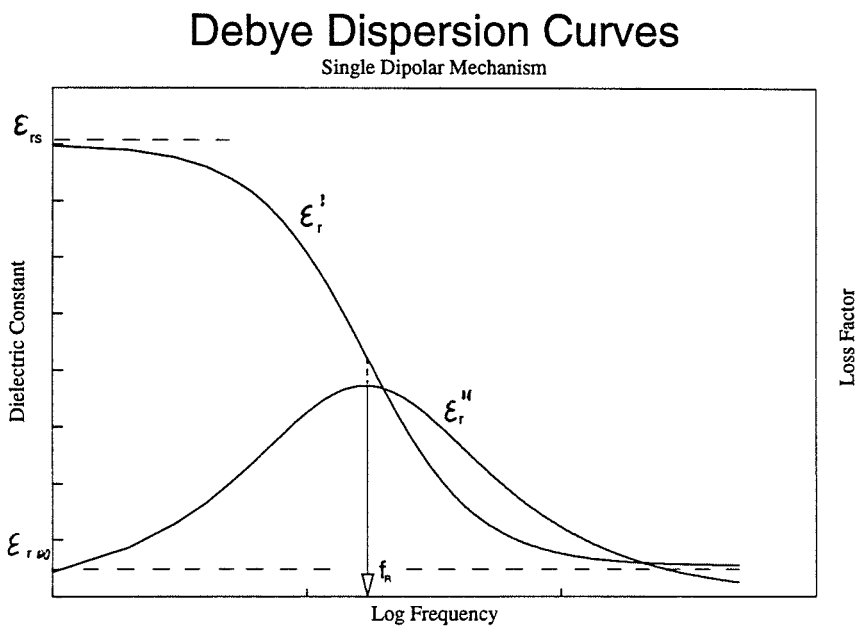


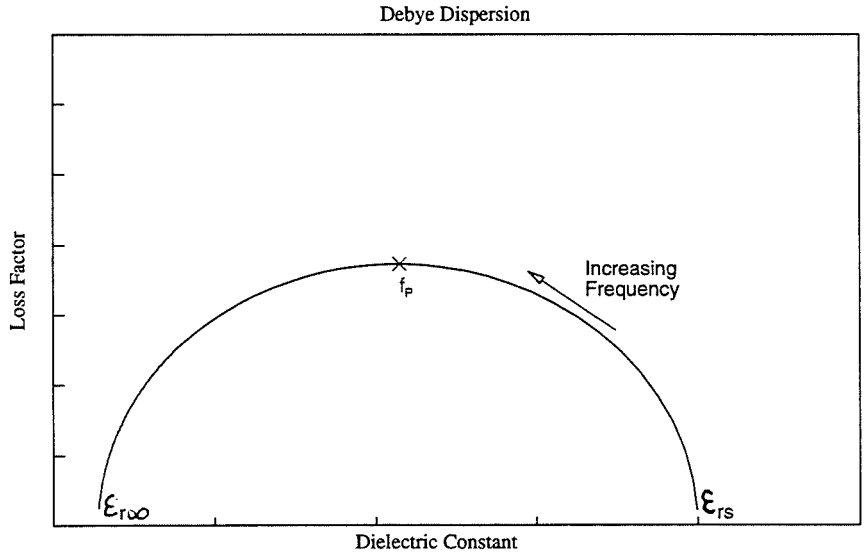


**Figure 3.2 Theoretical Debye Dispersion**

The time taken for this process is dependent on the extent of departure from equilibrium caused by the polarizing field and is governed by the exponential decay function, $\phi(t)$ :

$$\phi(t) = \left(1 - e^{t/\tau_R}\right) \qquad \cdots(3.26)$$

where, t is time and $\tau_R$ is the relaxation time constant [64]. The time constant associated with such a process is temperature dependent as are the dielectric constant and loss factor. Obviously, this time/temperature dependent behaviour is what determines the characteristic frequency dispersion of any particular polarization mechanism.

### 3.2.3 Space-Charge Polarization

This mechanism, unlike the above three, results from the presence of charges in a material which are not locally bound in atoms, molecules or the structures of liquids or solids, and are consequently free to migrate to some extent through the dielectric. It operates in heterogeneous materials placed in an electric field, where the presence of regions of different electrical properties (primarily conductivity [6]) can promote charge accumulation at spaces around region interfaces, where barriers to charge carrier migration exist. This is represented schematically in Figure 3.1. Such charge accumulation can lead to large polarizations and consequent macroscopic field distortions which are indistinguishable to an outside observer from a real rise in dielectric constant. Interfacial polarization has a relaxation dispersion in the frequency domain and is characterised by an *interfacial* or *space-charge polarizability*, $\alpha_s$. van Beek [29] has provided an extensive review of the fundamentals of this polarization mechanism.

The basic idea of interfacial polarization effects may be understood from a simple two layer capacitor example. This is the method originally used by both Maxwell [31] and Wagner [32] to explain what are now referred to as *Maxwell-Wagner* effects, viz. an enhancement of dielectric constant below, and of conductivity above, a relaxation frequency in heterogeneous materials containing regions of different conductivity; the "static" dielectric constant of the composite being often

considerably higher than that of any of the individual constituents. The two layer capacitor consists of two parallel plates both of surface area, S, and separation d, containing sheets of dielectric materials, (1) and (2), and characterised by dielectric constant, conductivity and thickness ($\varepsilon_{r1}'$, $\sigma_1$ and $d_1$) and ($\varepsilon_{r2}'$, $\sigma_2$ and $d_2$) respectively. It is shown with its equivalent circuit in Figure 3.3.

The relaxation time constant of the circuit in Figure 3.3 is shown by von Hippel [6] to be :

$$\tau_R = \frac{R_1 R_2 (C_1 + C_2)}{R_1 + R_2} = \frac{\varepsilon_0 (\varepsilon_{r1}' d_2 + \varepsilon_{r2}' d_1)}{\sigma_1 d_2 + \sigma_2 d_1} \qquad \cdots(3.27)$$

where, $R_1=d_1/(S\sigma_1)$, $R_2=d_2/(S\sigma_2)$, $C_1=(S\varepsilon_0\varepsilon_{r1}')/d_1$ and $C_2=(S\varepsilon_0\varepsilon_{r2}')/d_2$.

From its equivalent circuit the simple two layer dielectric can be shown to have a frequency dependent effective dielectric constant and loss factor which display Debye-like dispersive behaviour, with "static" and "infinite" dielectric constants, DC conductivity, and relaxation time constant all determined by the electrical properties of the two dielectric materials and their relative thicknesses. van Beek [29] gives the following expressions for Figure 3.3 :

$$\varepsilon_{rs} = \frac{d(\varepsilon_{r1}' d_1 \sigma_{DC2}^2 + \varepsilon_{r2}' d_2 \sigma_{DC1}^2)}{(\sigma_{DC1} d_2 + \sigma_{DC2} d_1)^2} \qquad \cdots(3.28)$$

$$\varepsilon_{r\infty} = \frac{d\varepsilon_{r1}'\varepsilon_{r2}'}{(\varepsilon_{r1}' d_2 + \varepsilon_{r2}' d_1)} \qquad \cdots(3.29)$$

$$\sigma_{DC} = \frac{d\sigma_{DC1}\sigma_{DC2}}{(\sigma_{DC1} d_2 + \sigma_{DC2} d_1)} \qquad \cdots(3.30)$$

$$\tau_R = \frac{\varepsilon_0 (\varepsilon_{r1}' d_2 + \varepsilon_{r2}' d_1)}{(\sigma_{DC1} d_2 + \sigma_{DC2} d_1)} \qquad \cdots(3.31)$$

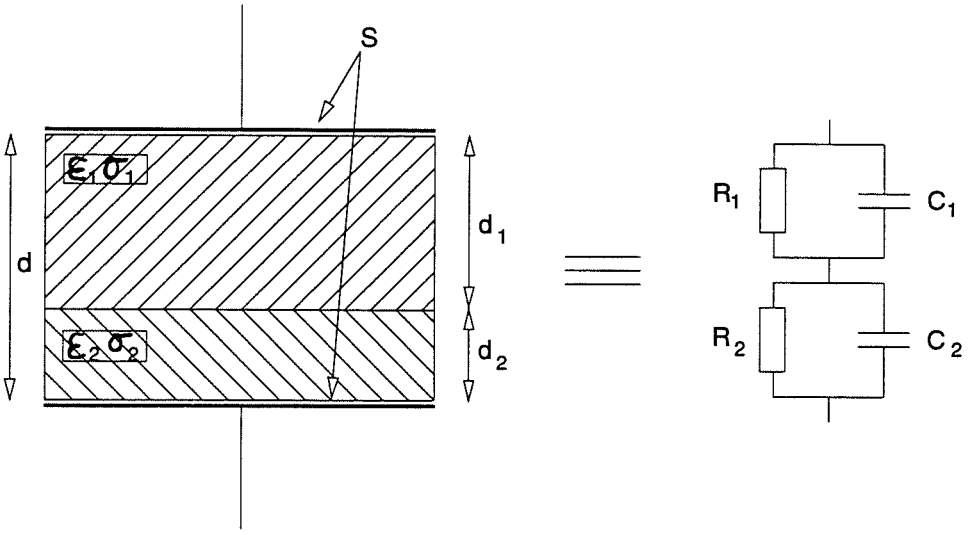


**Figure 3.3 Maxwell-Wagner Two Layer Capacitor**

The dispersion of the dielectric constant of the two layer material is directly analogous to the Debye case in accordance with equation (3.20), but the loss factor dispersion is modified by the DC conductivity, represented by the series resistance $R_1+R_2$, as per equation (3.8). The loss factor is therefore described by :

$$\varepsilon_r'' = \frac{(\varepsilon_{rs} - \varepsilon_{r\infty})\omega\tau_R}{1+(\omega\tau_R)^2} + \frac{\sigma_{DC}}{\varepsilon_0\omega} \qquad \cdots(3.32)$$

The form of this "modified Debye" behaviour is shown in Figure 3.4. At very low frequencies the loss factor of the heterogeneous material can become very large due to the conductivity term. However, if one of the dielectric layers is non-conducting at D.C. then the dispersion curves will be identical to those of a non-conducting dipolar mechanism.

von Hippel [6] shows for the above example that, provided the volume of the respective materials remains unaltered, the two layers may be subdivided and the different dielectrics interleaved without altering the results of the basic analysis.

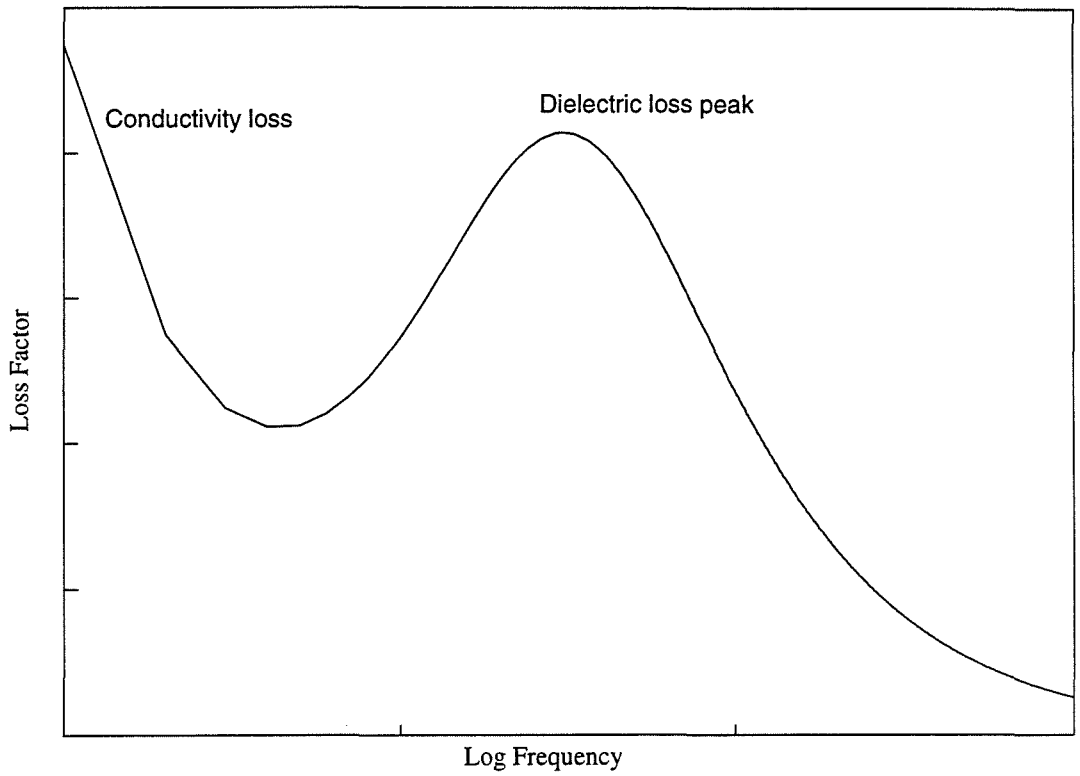


**Figure 3.4 Effect of D.C. Conductivity on Loss Factor**

van Beek [29] shows that a system containing i layers in series with the field direction, all of different individual dielectric properties, will still have an overall dielectric response described by the Debye equations but that the limiting dielectric constants will be :

$$\varepsilon_{rs} = d\frac{\left(\sum_i d_i \varepsilon_{ri}'/\sigma_{DCi}^2\right)}{\left(\sum_i d_i/\sigma_{DCi}\right)^2} \qquad \cdots(3.33)$$

$$\varepsilon_{r\infty} = \frac{d}{\left(\sum_i d_i/\varepsilon_{ri}'\right)} \qquad \cdots(3.34)$$

If, instead of layers, material (2) is distributed throughout material (1) in various geometrical shapes (such as spheres, ellipses or rods [6]), without altering the material mass ratio, the complex relative permittivity, $\hat{\varepsilon}_r$, is found to vary according

to the particular shape. Orientation of the shapes (other than spheres) also affects the overall dielectric behaviour, but the size of the distributed particles is not in itself a relevant factor.

van Beek [29] presents an analysis of a system consisting of spherical inclusions of radius, r, dielectric constant, $\varepsilon_{ri}'$, and conductivity, $\sigma_i$ ($Sm^{-1}$), dispersed in a host material of dielectric constant, $\varepsilon_{rh}'$, and conductivity, $\sigma_h$. The system is analysed in terms of its *admittivity* (i.e. complex conductivity - which van Beek terms specific admittance), $\Lambda = \sigma + j\omega\varepsilon_0\varepsilon_r'$, which is a function of the admittivities of the inclusions and host materials. The relationship is represented by the expression :

$$\Lambda = \Lambda_h \frac{2\Lambda_h + \Lambda_i + 2v_i(\Lambda_i - \Lambda_h)}{2\Lambda_h + \Lambda_i - v_i(\Lambda_i - \Lambda_h)} \qquad \cdots(3.35)$$

where $v_i$ is the volume fraction occupied by the inclusions.

Equation (3.35) describes a Debye process with relaxation time constant :

$$\tau_R = \varepsilon_0 \frac{2\varepsilon_{rh}' + \varepsilon_{ri}' - v_i(\varepsilon_{ri}' - \varepsilon_{rh}')}{2\sigma_h + \sigma_i - v_i(\sigma_i - \sigma_h)} \qquad \cdots(3.36)$$

and static and infinite frequency limiting dielectric constant and conductivity :

$$\varepsilon_{sr} = \varepsilon_{r\infty} + \frac{9v_i(1-v_i)(\varepsilon_{rh}'\sigma_i - \sigma_h\varepsilon_{ri}')^2}{[(\varepsilon_{ri}' + 2\varepsilon_{rh}') - v_i(\varepsilon_{ri}' - \varepsilon_{rh}')]\,[(\sigma_i + 2\sigma_h) - v_i(\sigma_i - \sigma_h)]^2} \qquad \cdots(3.36)$$

$$\varepsilon_{r\infty} = \varepsilon_{rh}' \frac{2\varepsilon_{rh}' + \varepsilon_{ri}' + 2v_i(\varepsilon_{ri}' - \varepsilon_{rh}')}{2\varepsilon_{rh}' + \varepsilon_{ri}' - v_i(\varepsilon_{ri}' - \varepsilon_{rh}')} \qquad \cdots(3.37)$$

$$\sigma_\infty = \sigma_s + \frac{9v_i(1-v_i)(\varepsilon_{rh}'\sigma_i - \sigma_h\varepsilon_{ri}')^2}{[(\varepsilon_{ri}' + 2\varepsilon_{rh}') - v_i(\varepsilon_{ri}' - \varepsilon_{rh}')]^2\,[(\sigma_i + 2\sigma_h) - v_i(\sigma_i - \sigma_h)]} \qquad \cdots(3.38)$$

$$\sigma_s = \sigma_h \frac{2\sigma_h + \sigma_i + 2v_i(\sigma_i - \sigma_h)}{2\sigma_h + \sigma_i - v_i(\sigma_i - \sigma_h)} \qquad \cdots(3.39)$$

Fricke [33] presents the results of a similar analysis for a heterogeneous material in which the inclusions are randomly oriented ellipsoids. In terms of the admittivities the relationship of composite material to component parts is given by :

$$\Lambda = \Lambda_h + \frac{1}{3} v_i \Lambda_h \sum_{k=1}^{\infty} \frac{1}{\Lambda_h + A_k(\Lambda_i - \Lambda_h)} \qquad \cdots(3.40)$$

for low values of fractional volume ($v_i \leq 0.1$), and by :

$$\Lambda = \Lambda_i + \frac{(\Lambda_h - \Lambda_i)(1 - v_i)}{1 + \frac{1}{3} v_i (\Lambda_h - \Lambda_i) \sum_{k=1}^{\infty} \frac{A_k}{\Lambda_h + A_k(\Lambda_i - \Lambda_h)}} \qquad \cdots(3.41)$$

for more concentrated fractional volumes. $A_1$, $A_2$, and $A_3$ are the depolarization factors of the ellipsoidal inclusions, which are defined for prolate geometries as :

$$A_1 = \frac{1}{1 - \left(\frac{a}{b}\right)^2} + \frac{\left(\frac{a}{b}\right)}{\left(\left(\frac{a}{b}\right)^2 - 1\right)^{1.5}} \ln\left(\frac{a}{b} + \left(\left(\frac{a}{b}\right)^2 - 1\right)^{0.5}\right) \qquad \cdots(3.42)$$

$$A_2 = \frac{1 - A_1}{2} \qquad \cdots(3.43)$$

$$A_3 = A_2 \qquad \cdots(3.44)$$

where a is the major axis length of the ellipsoids and, b is the maximum diameter.

Specific examples of interfacial relaxation mechanisms which are of direct relevance to the study of concrete are considered in chapter 5.

### 3.2.4 Electrode Polarization

Electrode polarization is associated with measurements employing metal electrodes on electrolytic materials, and occurs due to conditions and reactions which are present at the interface between the electrodes used and the electrolyte itself. It is not, therefore, a result of the material bulk properties as such, but because of the distortion caused to dielectric measurements this mechanism may have to be taken

into account when electrical characterisation of the electrolytic material is being considered. Concrete can, in many respects, be classified as an electrolyte [34], and is known to give rise to electrode polarization effects, particularly when measured at low frequencies.

Electrode polarization does not result from a single mechanism but from a combination of effects which each contribute a degree of polarizability to the sample/electrode arrangement in a dielectric measurement system.

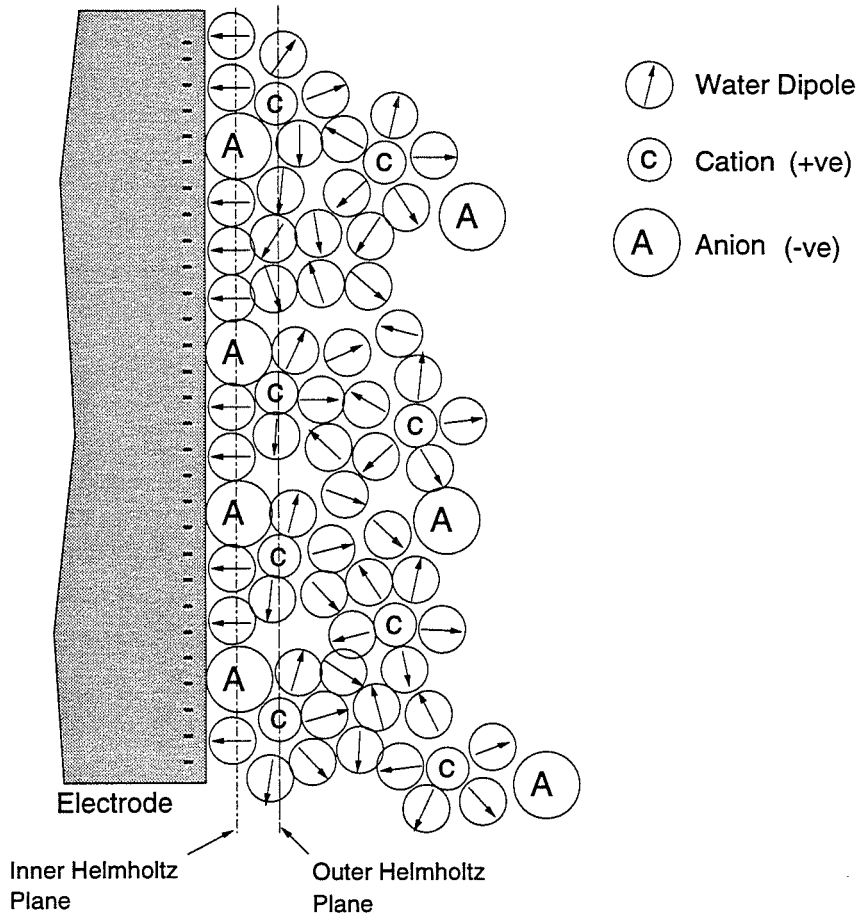


**Figure 3.5 Schematic Representation of Electrode Charge Double Layer**

The mechanisms which contribute to electrode polarization phenomena are :

**i)** An electrical double layer surface capacitance on the electrodes themselves. This is shown in Figure 3.5 and it takes the form of a 2-dimensional concentration of charge on the metal side of the interface (due to an excess or deficit of electrons) and an adsorbed "Helmholtz" layer of solvent molecules and ions on the solution side.

The Helmholtz layer is in two parts, comprising an inner Helmholtz plane of solvent molecules (water) adsorbed to the electrode surface plus unsolvated ions which are *always* anions (these being far more easily desolvated), and an outer Helmholtz region of solvated cations; beyond the outer surface (the outer Helmholtz plane ) of the outer region is a diffuse layer of solvated ions [35][65]. The potential difference between the the outer Helmholtz plane and the bulk solution is known as the *zeta potential*, $\zeta$ [69].

The inner electrical double layer has a typical value of capacitance, according to Sylvan [36], of about 10 $\mu Fcm^{-2}$ and is around 0.1 nm thick (although the thickness, and hence capacitance, is affected by the potential applied to the electrode, and also by the electrolyte concentration, with lower concentrations giving rise to thicker diffuse layers).

**ii)** A charge transfer resistance at the interface between electrolyte and electrode. This resistance represents the energy dissipated in the transfer of charge across the interface (i.e. from the electrolyte to the metal or vice versa).

**iii)** A Warburg impedance element (sometimes called a Faradaic impedance), accounting for the movement, by diffusion, of reacting ionic species in the vicinity of the electrolyte/electrode interface. The effect of this is particularly prevalent at very low frequencies. The Warburg element is notable for the fact that both the resistive and capacitive parts are frequency dependent (both decreasing proportionally with the square root of increasing frequency) and that the phase angle between the resistance and reactance is constant with frequency at a value of 45° [37].

The above mechanisms can be represented as an equivalent circuit as shown in Figure 3.6. For the purpose of analysis this equivalent circuit would be placed in series with the equivalent circuit of the electrolyte.

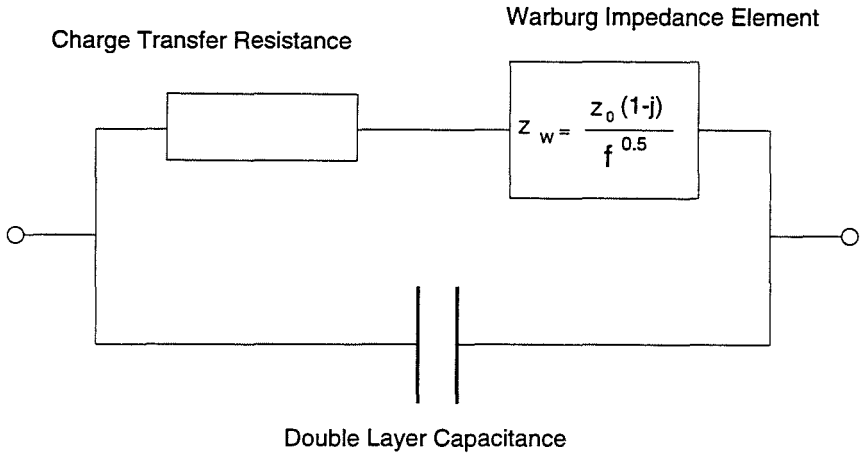


**Figure 3.6 Equivalent Circuit of Electrode/Electrolyte Interface**

The charge transfer resistance and Warburg element appear in parallel with the double-layer capacitance because the transfer of charge from reacting ion species to electrode can only occur when an ion penetrates the Helmholtz layer from the bulk electrolytic solution by a process of diffusion. Thus, the serial combination of transfer resistance and diffusion impedance effectively constitute a "leakage impedance" across the double layer capacitance as shown.

Terry [38] has suggested that A.C. electrode polarization may be modelled by a large series capacitance element attributable to a very thin layer of gas between electrode and electrolyte. Wilson and Whittington [4][5] attribute the low frequency dielectric behaviour of concrete to a similar thin gas layer. While it is true that gas will be generated at the electrodes to some extent, thus enabling the setting up of the necessary conditions for bi-directional charge transfer, the gas molecules will remain adsorbed to the electrode surface and will not bubble out unless the concentration reaches sufficient levels to equal or exceed atmospheric pressure. In an A.C. situation the build up of gas will be reversed over each alternate half cycle and the required concentrations are therefore not likely to be achieved, particularly

as frequency is increased. Onaral and Schwan [36], working on the problem of electrode polarization with platinum electrodes, found that a polarization resistance, $R_p$ (the real part of polarization impedance), tends towards a constant at very low frequencies (<1 Hz) and at D.C. has a value of about 200 kΩ. This finite value of resistance suggests that the existence of a gas layer, which would not permit D.C. conduction, is not a viable explanation for electrode polarization effects. However, their results were obtained using platinum electrodes coated with platinum black, which acts as a catalyst for the recombination of any gas produced. The situation for stainless steel electrodes (as used in the work of the author) is likely to be quite different and at *very low* frequencies (as $\omega \rightarrow 0$) gas bubbles will possibly be in evidence.

Electrode polarization effects are known to diminish rapidly with increasing frequency, although the cutoff point is thought to vary in proportion to the conductivity of the electrolyte. McCarter and Brousseau [39] state that the cutoff frequency is about 10 kHz in 1 day old cement paste while Wilson and Whittington [5] assume that electrode polarization is still effective above 1 MHz in concrete less than 1 day after gauging. Onaral and Schwan [37] produced data on the electrode polarization impedance of platinum electrodes in physiological saline of concentration 0.9% (which suggests a theoretical conductivity of 1.345 $Sm^{-1}$) which show that it becomes negligible somewhere between 1 kHz and 100 kHz. The conductivity of this saline is similar to the value for the water in fresh cement paste calculated in section 5.1.3 (1.3552 $Sm^{-1}$), suggesting that electrode polarization effects with respect to the cement paste water would become insignificant at similar frequencies (certainly below 100 kHz). However, as part of a study on highly conductive microemulsions, Giri et al. [40] investigated the electrode polarization effects associated with gold plated electrodes and saline solutions of 10% and 5% NaCl (12.67 $Sm^{-1}$ and 6.96 $Sm^{-1}$ respectively), and their findings suggest that at frequencies up to 20 MHz results are possibly still affected. They also propose that the cutoff frequency for electrode polarization is inversely proportional to ionic concentration.

Scott et al. [41] investigated the electrical properties of moist porous rocks and soils at frequencies from 100 Hz up to 1 MHz, and studied the effects of electrode polarization for electrodes of various materials, including stainless steel as used in this work on concrete. Measurements were made of the electrical properties at 100 Hz of samples of two different lengths (i.e. gap between electrodes), and the difference between apparent dielectric constant for the otherwise identical samples was taken as an indication of the effects of electrode polarization. By this method the authors were able to find which electrode materials were least prone to polarization. The amount of polarization depended on which material was being measured and its water content, but it was found that platinised platinum electrodes (as used by Onaral and Schwan [37] above) were non-polarizing for all samples and that stainless steel electrodes were always polarizing. The extent of the distorting effect of electrode polarization on the measured dielectric constant was found to depend on sample length, with longer samples (i.e. greater electrode separation) providing less distorted measurements. This is due to the increased impedance of longer samples, as pointed out by Schwan et al. [77]. However, the results of a comparison between polarizing and non-polarizing electrodes, when used to measure the dielectric constant and conductivity of shale with 3.8% water content over the frequency range 100 Hz to 1 MHz, show that at the higher frequencies polarization effects are no longer operative so that at 1 MHz no advantage is gained from the use of non-polarizing electrodes. At the lower frequencies the error in dielectric constant for the polarizing electrodes was found to be an order of magnitude. Thus, at 100 Hz moist shale with a true dielectric constant of $\approx 10^4$ had an apparent dielectric constant, when measured with polarizing electrodes, of $\approx 10^5$. In similar fasion, the conductivity was found to be reduced to $\approx 0.002$ $Sm^{-1}$ from $\approx 0.005$ $Sm^{-1}$.

The conclusion of the author is that while fresh and hardened cement paste, whether neat or present in concrete or mortar, will undoubtedly give rise to electrode polarization effects when investigated using metal electrodes, it is unlikely that such effects will play any significant part at the frequencies used in this work (1-1000 MHz).

### 3.2.5 Multiple Relaxation

The Debye equations, whether applied to orientation or interfacial polarization mechanisms, are characterised by a single time constant which assumes that the dipoles or equivalent entities are unrestricted in their movement. In practice, however, many liquids and solids, even those manifesting only a single relaxation dispersion, are found to be characterised by a statistical distribution of relaxation frequencies, grouped around a single "most probable" frequency, suggesting that the dipoles (or polarizing elements) are in some way coupled to their surroundings [26]. The reasons for the distribution may therefore be located in the material physical structure. For instance, in the example, quoted in 3.2.3, of ellipses of one material distributed throughout a host material, a random orientation of the ellipsoidal particles would produce a distribution of relaxation frequencies. This effect manifests itself in a frequency domain plot as a reduction in the maximum value of the loss factor and a widening of its "bell" shaped characteristic. Also, the relaxation characteristic of the dielectric constant is less steep, occurring over a wider frequency band.

In a Cole-Cole plot a spread of relaxation frequencies shows up as a tilting of the characteristic semi-circle below the real axis. The spread of relaxation frequencies is represented by a modified Debye equation as :

$$\hat{\varepsilon}_r = \varepsilon_{r\infty} + \frac{\varepsilon_{rs} - \varepsilon_{r\infty}}{1 + (j\omega\tau)^{(1-\beta)}} \qquad \cdots(3.45)$$

The value of $\beta$ can range between 0 and 1 depending on the extent of "spread" inherent in the polarization mechanism. Figure 3.7 shows the effect of a spread of relaxation times characterised by a $\beta$ value of 0.2.

The spread parameter, $\beta$, may be obtained from the angle of tilt displayed by a Cole-Cole plot of the dielectric response as shown in Figure 3.8.

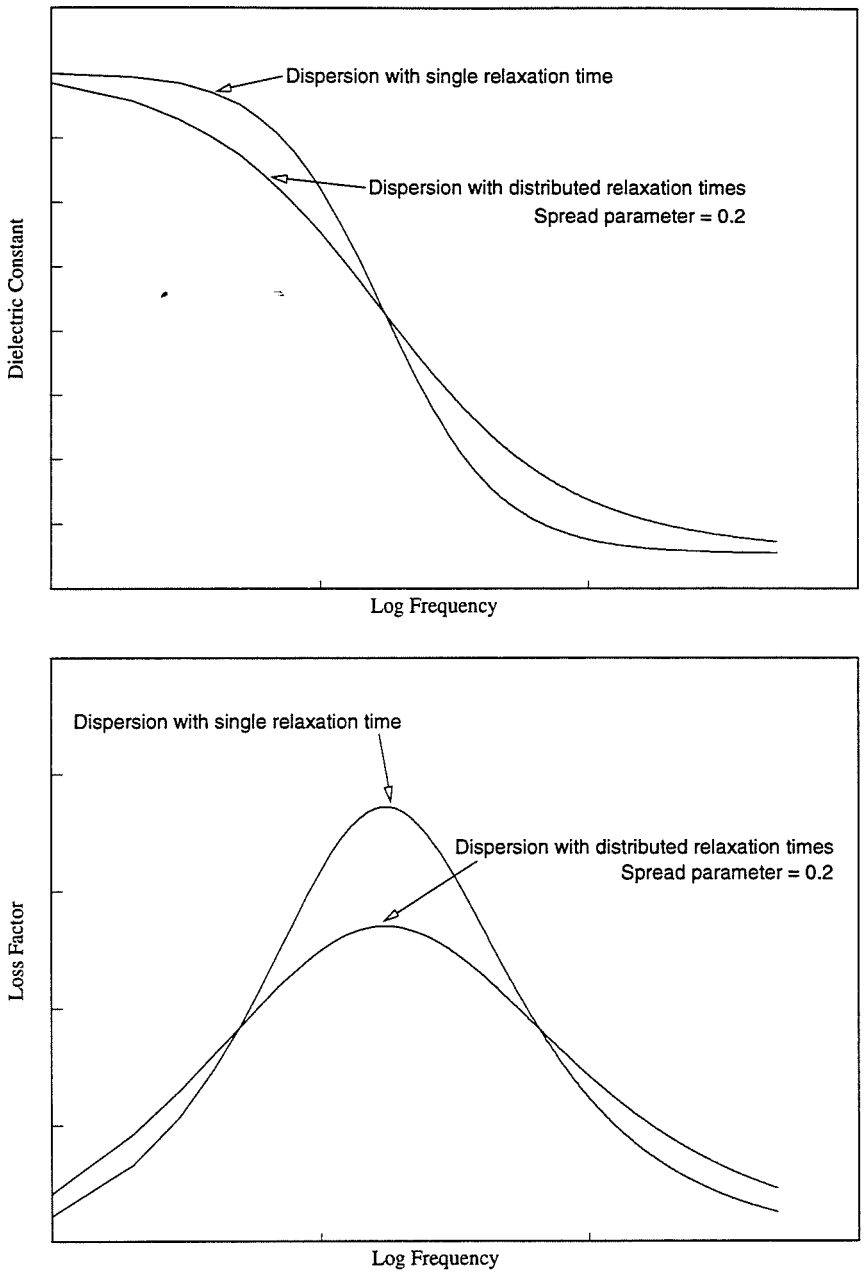


**Figure 3.7 Effect of Spread of Relaxation Times**

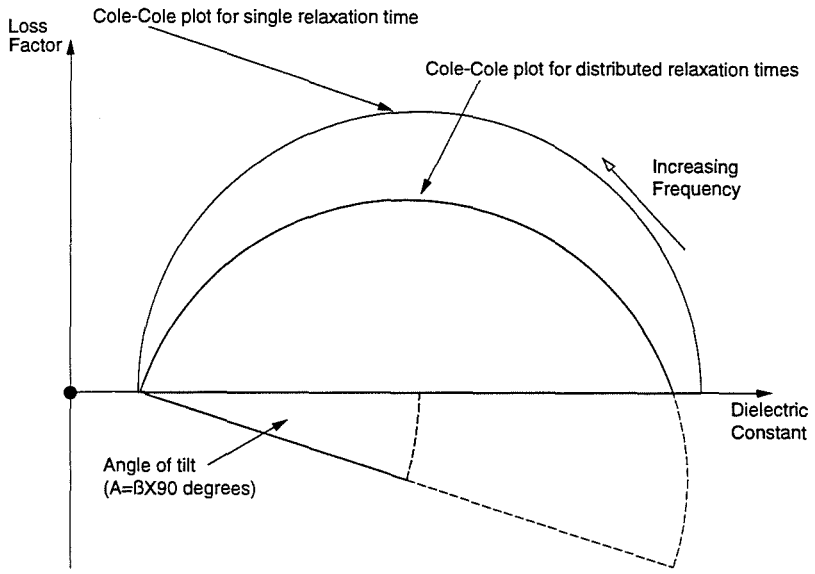


**Figure 3.8 Cole Cole Plot of Distributed Relaxation Dispersion**

The angle, A, of tilt in degrees is :

$$A = \beta \times 90 \qquad \cdots(3.46)$$

Thus, the value of β may be easily calculated from measurement of A.

Multiple relaxation may also be observed in heterogeneous dielectrics in which more than one relaxation mechanism is operating (e.g. the multi layer capacitor described in 3.2.3 or a variety of shapes of one material distributed throughout a host material as also mentioned in 3.2.3), this resulting, if the relaxation time constants of the respective mechanisms are sufficiently far apart, in a series of relaxation "steps" in the dielectric constant frequency characteristic, and a series of peaks in the loss factor frequency characteristic. If the time constants are too close together, however, the resulting superposed frequency plots may merge into one another obscuring the individual dispersions. An example of a typical multiple relaxation spectrum comprising three regions of dispersion, A, B, and C, is shown in Figure 3.9.

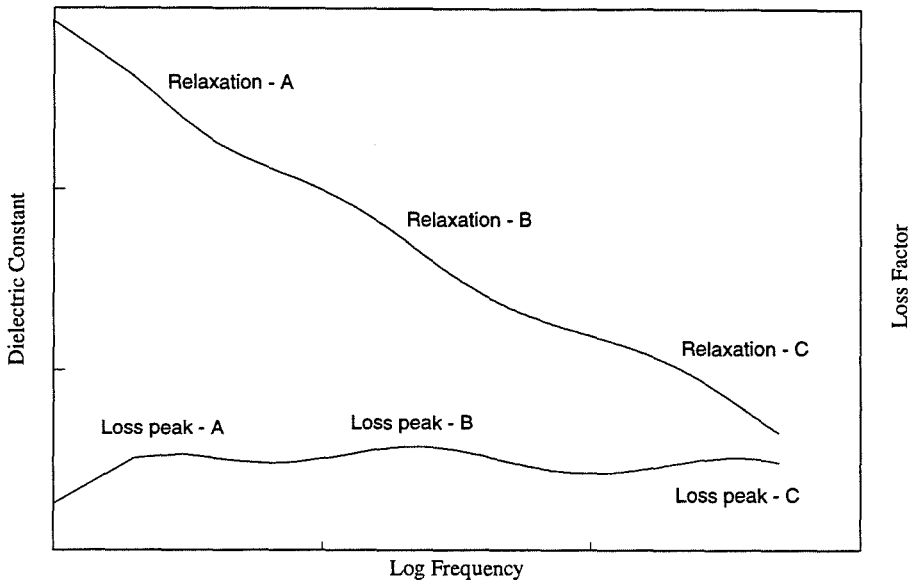


**Figure 3.9 Typical Multiple Relaxation Dispersion**

In a complex heterogeneous material like concrete both types of multiple relaxation are likely to occur, allowing dielectric characterisation of the material to be realised.

## 3.3 Dielectric Mixture Formulae

Section 3.2.3 dealt with the effect of polarization at the dielectric interfaces of a heterogeneous material; interfacial polarisation being a relaxation mechanism which enhances the overall dielectric constant of the material beyond the "true" mixture value.

This section is not so much concerned with relaxation phenomena as with the relative permittivities which result from the mixing of two or more materials of differing permittivity. van Beek [29] points out that with respect to Maxwell-Wagner effects it must be understood that it is the value of $\varepsilon_{r\infty}$ which is of importance in the calculation of mixture permittivities, i.e. dielectric mixture formulae can only be applied at frequencies above that of the relaxation of any interfacial mechanism associated with the heterogenous material.

One problem encountered in deriving dielectric mixture formulae is that the permittivity of the host medium immediately surrounding the inclusions cannot necessarily be assumed to be that of the bulk host. For very low volumes of dispersed medium, such an assumption is acceptable, but for more concentrated mixtures a value much closer to the effective permittivity of the heterogeneous material must be used. This complicates the derivation of mixture formulae.

van Beek [29] lists a large number of formulae for dielectric materials containing a range of inclusions of various shapes. Of particular interest is a formula for the case of dispersed spherical inclusions in a host medium :

$$1 - v_i = \frac{\varepsilon_{ri} - \varepsilon_{re}}{\varepsilon_{ri} - \varepsilon_{rh}} \left( \frac{\varepsilon_{rh}}{\varepsilon_{re}} \right)^{\frac{1}{3}} \qquad \cdots(3.47)$$

where the subscripts e, i, and h denote effective, inclusion and host parameters respectively. This formula is not convenient for the calculation of $\varepsilon_{re}$, however, due to the need to solve a cubic equation. Sen et al. [122] have derived a two-phase mixture formula, for a conducting host with nonconducting inclusions, identical in form to equation (3.47) in which the dielectric constant quantities are replaced by complex relative permittivity. They show that in the low frequency limit the general expression yields Archie's Law [44] for conductivity :

$$\sigma_e = \sigma_h (1 - v_i)^{1.5} \qquad \cdots(3.48)$$

Another pair of derived formulae [29] relating to similar materials and which has been shown experimentally to be more accurate for higher concentrations of inclusions are presented in equations (3.49a) and (3.49b).

$$v_i = \frac{\varepsilon_{re}^{\frac{1}{3}} - \varepsilon_{rh}^{\frac{1}{3}}}{\varepsilon_{ri}^{\frac{1}{3}} - \varepsilon_{rh}^{\frac{1}{3}}} \qquad \cdots(3.49a)$$

$$\varepsilon_{re} = \left[ \varepsilon_{rh}^{\frac{1}{3}} + v_i \left( \varepsilon_{ri}^{\frac{1}{3}} - \varepsilon_{rh}^{\frac{1}{3}} \right) \right]^3 \qquad \cdots(3.49b)$$

These expressions are accurate when the inclusions are spherical but may become less so for indeterminate shapes and would therefore find more limited use in the investigation of materials like concrete (e.g. fresh concrete with rounded aggregate particles). An empirical formula which is applicable to random mixtures and has been successfully applied to asphalt-aggregate-moisture-air mixtures (i.e. four components) is presented by Subedi and Chatterjee [42] :

$$\varepsilon_{re}' = \sum_{p=1}^{n} v_p \varepsilon_{rp}' + \begin{Bmatrix} \sum_{p=1}^{n-1} \sum_{q=p+1}^{n} v_p v_q (\varepsilon_{rp}' - \varepsilon_{rq}') & \text{for } \varepsilon_{rp}' > \varepsilon_{rq}' \\ \sum_{p=1}^{n-1} \sum_{q=p+1}^{n} v_p v_q (\varepsilon_{rq}' - \varepsilon_{rp}') & \text{for } \varepsilon_{rp}' < \varepsilon_{rq}' \end{Bmatrix} \quad \cdots(3.50)$$

This formula was tested by Subedi and Chatterjee for a two component mixture (moist aggregate) against a range of other formulae from the literature, including equation (3.49b), and found to perform far more accurately when compared to measured results. It might therefore be more suitable for application to concrete and mortar. Since equaton (3.50) for dielectric constant is not dependent on the loss factor of any component, a similar expression should hold for effective loss factor, and hence conductivity.

# CHAPTER 4

# Review of Previous Research

## 4.1 Low Frequency Electrical Properties of Concrete (<100 kHz)

Previous work at low frequencies has only indirect relevance to the present work. However, for the purpose of establishing the likely low frequency limits to the RF electrical properties of concrete, as well as providing a starting point for investigations at higher frequencies, some previous L.F. research is examined here.

### 4.1.1 Whittington et al.

In this paper Whittington et al. [43] have presented the results of an investigation into the D.C. resistivity characteristics of concrete and cement pastes from gauging up to 90 days. The purpose of the investigation was to assess the dependence of resistivity on mix-proportions, water/cement ratio (W/C), and temperature with a view to developing a theoretical model for the conduction of current in concrete for later application to the quality control of structural concrete.

The authors note that the characteristics of cement paste vary considerably throughout the setting process with consequent age dependence for such factors as polarization and capacitive effects. They also note the possibility of variations in the electrical properties throughout the bulk of concrete and cement paste samples, due to stratification during placing, and moisture gradients caused by preferential evaporation from exposed surfaces.

From their review of previous work Whittington et al. take a number of assumptions as the basis for their work, viz. air dried hardened concrete is a very good insulator (resistivity $\approx$ 10 k$\Omega$m), the response of concrete to an A.C. source is dominated by its resistive impedance *at all ages* (capacitive reactance being so large it can be ignored), the resistivity of concrete increases with time but decreases for increasing salinity of mixing water, and the resistivity has a negative temperature coefficient.

A theoretical model of electrical conduction in concrete is developed, based on the assumption that three conduction paths through the material are possible. These are, the cement paste itself, the aggregate particles in contact with one another, and the aggregate and cement paste in series. Of these, the cement paste itself is considered to be by far the major contributer to electrical conduction and although it is recognised that both ionic and electronic mechanisms, attributable to ions in pore water and cement compounds respectively, will operate in the paste these are not considered separable for the purposes of analysis.

A modified version of Archie's law [44] (c.f. equation (3.48)), with porosity replaced by the fractional volume of the cement paste and a modifying constant of proportionality included, is developed for relating the resistivity of concrete to mix proportions, based on the above model. Thus :

$$\rho_c = \rho_p A \phi^{-m}$$

where, $\rho_c$ is the resistivity of concrete, $\rho_p$ is the resistivity of cement paste, $\phi$ is the fractional volume of the paste within the concrete, and A and m are constants.

A range of experiments was performed on 100 mm cubes of various cement pastes, mortars and concretes, with water/cement ratios in the range 0.4-0.8, and cement aggregate ratios of 1/1-1/2 for mortars and 1/3-1/6 for concretes. 100 mm square external brass electrodes were interfaced to opposite faces of the cubes either before setting, by placing in moulds with fresh material, or after demoulding at 24 hours by means of a thin layer of low resistivity cement paste. After 24 hours the samples were cured under water at 23°C, but were surface dried for measurements to prevent surface conduction. After curing for 13 days, some of the samples were stored outdoors under 200mm of sand.

To prevent electrode polarization effects, which would occur at DC for a material like concrete, a low frequency square voltage wave (actual frequency not stated) was used to monitor the resistive response. Resistivity tests were obtained from 10

minutes up to 128 days for all the samples. Graphs of resistivity against time for the cement pastes and the 1/2/4 concrete, for different water/cement ratios, are presented for the periods 10-1500 minutes (i.e. up to 1 day) and 1-128 days.

The results demonstrate various trends in the resistivity characteristics of concrete. Changes in resistivity are minimal for pastes and concretes over the first 6 hours, then the resistivity climbs steeply up to about 18 days and thereafter increases only very gradually with time. Differences between the characteristic shapes of the graphs for pastes and concretes in the early stages (up to 6 hours) are explained on the basis of heat loss in the materials. The pastes show little variation in resistivity for different water/cement ratios before setting, although such differences are notable for both concretes and pastes after the onset of hardening.

The samples stored outdoors show fluctuations in resistivity/time which are temperature related. From these results a temperature coefficient of resistivity of -0.022/°C is calculated (this compares with a value of -0.025/°C from Spencer [45] and Buenfeld and Newman [46]).

By application of the modified Archie's law to the results obtained, the constants A and m were found to have values of 1.04 and 1.20 respectively, although these figures are averages and only apply to the moist cured samples, not those stored outdoors. The ratio of concrete resistivity to paste resistivity, called the formation factor, is found to be constant with time for a particular mix and water/cement ratio.

Whittington et al. conclude by showing that the resistivity against time characteristic of concrete is related strongly to the degree of hydration of the cement paste and in particular has a strong similarity to the strength versus time characteristic. This, coupled with the sensitivity of resistivity to the water/cement ratio and the fractional volume of cement paste, is taken as confirmation that electrical testing of concrete has a place in the non-destructive quality testing of the material.

Detailed information on the variation of resistivity with time, for cement pastes, mortars and concretes is provided and a plausible theoretical explanation of the these variations with accompanying electrical model is presented. The electrical model, however is limited in that it considers only resistive effects, whereas fresh concrete

is known to have approximately equal resistive and reactive components of impedance at low frequencies. This oversight is a consequence of the initial assumptions based on the results of previous workers for *hardening* concrete and may cast some doubt on the accuracy of the results for fresh materials. Also, the authors do not give much consideration to the effects of electrode polarization which again may have consequences, depending on the frequency of square wave used, for the accuracy of the results for fresh materials. This paper may be considered a definitive work on the D.C. resistivity characteristics of concrete, producing more detailed data than its predecessors.

### 4.1.2 McCarter and Curran

McCarter and Curran [47] investigated the low frequency A.C. electrical properties of cement pastes and mortars over the first 24 hours after gauging. This paper is essentially an extension of the work of Whittington et al. (section 4.1.1), with additional account being taken of capacitive effects in the A.C. response of fresh cement paste. An electrical model of a cement paste sample, consisting of a resistance element in parallel with a capacitance element, is presented and the capacitance and resistance are further related to the fundamental electrical parameters $\varepsilon$ and $\rho$, the dielectric constant and resistivity, of the cement paste ($\varepsilon$ being equivalent to $\varepsilon_r'$ in this thesis). A summary of the various mechanisms of polarization likely to be operating in fresh cement paste is also presented, as is a summary of the chemical and physical changes which occur in the material as it sets.

The materials of investigation were cement pastes of water/cement ratios 0.3, 0.4 and 0.5, and mortars of cement/sand ratio 1/2, and water/cement ratios 0.6 and 0.8.

An 80 mm long coaxial electrode system was used as a test cell, with the radius of the central conductor being 2.5 mm and that of the outer 50 mm. The cell was calibrated for fringe field capacitance errors using measurements obtained with cyclohexane ($\varepsilon_r$=2.0025 at 20°C) and butanol ($\varepsilon_r$=17.8 at 20°C) as standard dielectrics to calculate a correction factor, $k$. The material used for the electrodes is not specified.

The test samples were stored in a cabinet at 20°C and 50% humidity, with internal sample temperature monitored by means of a thermistor imbedded in a 100 mm cube of equivalent material.

Measurements of impedance were carried out at 1000 Hz (sine wave) using a commercial A.C. bridge, and acquired at intervals of 300 seconds. The resistance and reactance measurements were converted to values of resistivity and dielectric constant by a data processing program implemented on a HP85 computer.

The results for the pastes reveal some interesting features. The values obtained for dielectric constant, especially in the first two hours, are very high, some being in excess of $1.1\times10^6$. These are explained as being due to the very large polarizabilities produced by the double charge layer which forms around particles suspended in an aqueous electrolyte, in this case the hydrating cement particles in the ion saturated mix water. The dielectric constant versus time characteristic shows an average fall over the full period which is rapid in the inital stages (a full order of magnitude in the first hour) and much more gradual in the later stages. However, there is an abrupt discontinuity at approximately 250 minutes where the characteristic peaks sharply for a short period as well as a more gradual rise at approximately 500 minutes. These peaks, the exact times of which vary for different mix proportions, correspond to the period of initial and final set of the pastes as determined by testing with a Vicat needle and they are also shown to correlate well to the internal temperature characteristic of the samples. The resistivity graphs for each sample show a reciprocal characteristic to that of the corresponding dielectric constant. The values of resistivity range between 2 Ωm at the point of gauging (for all pastes) and >80 Ωm at 24 hours for the paste with water/cement ratio 0.3. The graphs of dielectric constant and resistivity for the mortar samples are very similar in form to those obtained for the pastes, although the actual values of these parameters are generally lower for the mortars.

Graphs of tan δ versus time for the cement pastes are also presented ($\tan\delta = \varepsilon_r''/\varepsilon_r'$). However, calculations by the author reveal a discrepancy between values of tan δ and the corresponding values of resistivity and dielectric constant. For instance, from the graph showing resistivity and dielectric constant for the cement paste with

water/cement ratio 0.4, the values of $\rho$ and $\varepsilon_r$ at 750 minutes indicate that a $\tan\delta$ value of 3.6 should be expected whereas the corresponding graph of $\tan\delta$ shows a value of 2.0 at this time. This could be a reflection of errors in the values of either or both of these parameters (i.e. $\rho$ and $\varepsilon_r$) but it seems more likely that, since the resistivities are calculated *directly* from resistance measurements using a reliable formula, the calibration method for capacitance is the source of this discrepancy. If the resistance and reactance data which correspond to the published resistivity and dielectric constant values were available, along with the calibration data, it might be possible to ascertain the source of error.

McCarter and Curran make no mention of electrode polarization effects in their theory or their results analysis. However, in a reply to comments on this paper published by Wilson and Whittington [48], they indicate that consideration was given to the possibility of such effects with the conclusion that they were negligible at the frequency of investigation. Wilson and Whittington had proposed electrode polarization as the cause of the very large dielectric constants observed by the authors. In view of later work by McCarter and Brousseau [39] and also Scott et al. [41] (see section 3.2.4) it seems likely that electrode polarization was at least partly responsible for the large $\varepsilon$ values of the authors, but work on double layer polarization in polystyrene colloidal suspensions by Schwan et al. [77] suggests that such effects have also played a part.

McCarter and Curran have demonstrated successfully that changes in the A.C. electrical properties of cement based materials during the process of hydration do reflect the chemical and structural changes which are occurring in the cement paste, particularly during the period when the paste acquires its rigidity. This correlation is notably connected to changes in the water/cement ratio.

## 4.2 Radio Frequency Electrical Properties of Concrete (>100 kHz)

Since the work of the author is concerned with the R.F. properties of concrete, attention is focused in this section on previous published work at similar frequencies.

### 4.2.1 Taylor and Arulanandan

In this paper Taylor and Arulanandan [49] report on a preliminary investigation into the relationship between the physical and electrical properties of cement pastes.

The authors give a brief review of the current techniques available for the quality testing of cement based materials (primarily concrete), dividing the methods into those which are fundamental in approach and those which are phenomenological. The disadvantages associated with the respective approaches are considered (e.g. difficulty of sample preparation, unrepresentativeness of samples/conditions, and general expense associated with scientific methods, and lack of fundamental understanding associated with empirical techniques). In particular, two common practical disadvantages are noted, viz., the time delay incurred while concrete hardens, and the fact that most tests are destructive in nature.

By contrast, R.F. electrical techniques are envisaged as having the following five major advantages :

**(i)** They bridge the gap between sophisticated fundamental examination and traditional empirical testing.

**ii)** They are non-destructive.

**iii)** They are able to monitor cement gel properties which cannot be measured any other way (e.g. permeability).

**iv)** They are readily adaptable to field use.

**v)** They are possibly capable of assessing quality early (i.e. less than 1 day) in the life of a concrete structure.

At the time of the publication of this paper no other investigators, to the best of the present author's knowledge, had produced data on the dielectric constant and conductivity dispersion of concrete either at lower frequencies or at radio frequencies.

The authors base their investigation on the assumption that the properties of materials like concrete and mortar are determined exclusively by the properties of the component cement paste, and they list a number of characteristics of concrete and relate them to the microstructural features of the paste. Reference is made to a number of investigations into the electrical properties of materials with similar microstructures to cement paste [50][51](e.g. clays, soils and ion exchange resins), which used the same measurement technique as the authors.

The authors propose an equivalent circuit model of hydrating cement gel based on three main microstructural components :

**i)** Solid particles surrounded by an ion atmosphere double layer.

**ii)** Solid particles in contact with each other.

**iii)** Pore spaces filled mostly with water, though often containing dissolved compounds.

These components are assumed to give rise to three conduction paths :

**i)** Through the solution and conducting particles in series.

**ii)** Through particles in contact with each other

**iii)** Through the solution

Each of these paths is represented in the equivalent circuit as a parallel combination of resistance and capacitance, the relative values of which are assumed to be determined by their physical properties which in turn determine the cross-section presented by each to the flow of current through a unit sample. These cross-sections are denoted by three parameters, a, b, and c. Path **(i)** is further represented by two parallel combinations in series, with a fourth parameter, d, representing the proportion of the current in the solid particles (inclusive of ion atmospheres).

Expressions which relate the conductivity and dielectric constant of each physical component (solid or solution) and the parameters a, b, c and d to the measured values of sample conductivity and dielectric constant are given.

The measurement system used (essentially a R.F. impedance meter connected to a lumped element parallel plate electrode cell with adjustable plate spacing) is described elsewhere [51]. The R.F. effects of the leads which connect the electrodes to the impedance meter, as well as stray capacitance associated with the cell, are calibrated out by computation from measurments of different sample lengths of materials with known electrical properties. Measurements were made at frequencies between 1 MHz and 100 MHz.

Cylindrical cement paste samples of diameter 12.7 mm and length 38.1 mm were used in this investigation. The water/cement ratios were 0.30 and 0.35 (by weight) for measurements obtained at intervals up to 1 week after gauging. Further measurements were obtained at approximately 24 hours for pastes with water/cement ratios of 0.3, 0.35, and 0.4. Companion cylinders of diameter 50.8 mm and length 101.6 mm were cast to allow compressive strength crushing tests to be carried out at 3, 7, and 10 days.

The dielectric dispersion data obtained were fitted to the theoretical expressions using computer based optimisation techniques which provided values for parameters a, b, c, and d.

Graphs showing the dispersion of conductivity and dielectric constant over 10-50 MHz are presented for cement paste of water/cement ratio 0.35 at 23, 35 and 52 hours. These graphs appear to indicate the presence of a relaxation process centered at approximately 30 MHz but the frequency range of the presented data is too narrow to be certain of the true dispersion characteristics. The absolute values of dielectric constant (e.g. $\approx$104 at 10 MHz dropping to $\approx$70 at 50 MHz for 23 hour cement paste) are similar to those obtained by Olp et al. [57].

Graphs which show the changes in the values of a, b and c (and hence changes in the cross-sectional area of the samples occupied by the three conduction paths) with time are also presented. These results are compared to the changes which are known to occur in the structure of hydrating cement paste. Excellent agreement between current understanding of cement chemistry and what the authors results purport to show is claimed. In particular, it appears that the characteristic of the parameter indicating conduction through particle-particle contact (i.e. b) plotted against

water/cement ratio correlates with the value of 7-day strength when plotted against water/cement ratio, and the parameter which indicates conduction through the pore solution (i.e. c) is indicative of permeability.

The authors conclude by acknowledging that many other factors (primarily chemical) may affect the findings which they have presented. Also, they accept that their model could be developed further. They point out, however, that their results do indicate that R.F. electrical measurements can provide useful information on the microstructure of cement paste and that the development of a test method based on such measurements should be feasible.

Taylor and Arulanandan have provided useful information on the dielectric properties of cement paste in part of the frequency band which is of interest to the current author. Their interpretation of the results, in light of the 3-path model, is, however, in some doubt. The model itself seems arbitrary, especially the assumption that all solid particles are surrounded by an ionic double layer. To support a double layer the particles would have to be in aqueous suspension, a suggestion which may be viable in the case of fresh cement paste but which invalidates the solid-solid contact aspect of the model for hardening paste. A number of anomalies are also apparent in the computed model parameters. For instance, for water/cement ratio 0.3 the solid-solid contacts appear to decrease over the first 24 hours while the liquid path increases, and the solid-liquid path increases dramatically over the same period. These trends are opposite to what should be expected as cement hydrates. These anomalies and others are probably attributable to the inadequacy of the model.

The authors give no attention to consideration of the likely mechanisms of dielectric relaxation operating in cement paste at these frequencies.

### 4.2.2 Wilson and Whittington

In this paper Wilson and Whittington [4] present work concerned with both low and high frequency measurements on concrete. Mechanisms of conduction are discussed with the conclusion that ionic charge transport is the dominant mode. For low frequencies a lumped element circuit model of concrete/electrode system is

proposed and discussed. A series capacitance element due to electrode polarization (actually due to a layer of gas) is a feature of the model but this is assumed to disappear as a short circuit at higher frequencies. An RC parallel circuit represents the bulk properties of concrete. Variations in the properties (mechanical and electrical) of concrete are primarily viewed as changes in the pore network in the hardening material, with greater porosity equating to lesser strength and vice versa. The developing pore structure is presumed to reduce the cross-section of the sample available for conduction, this effect being especially noticeable at the point of setting. Pore segmentation is believed to produce an enhanced dielectric constant due to increased space charge polarization effects.

The low frequency measurement system is described and results for resistivity are presented graphically. The graphs show that resistivity is sensitive to water/cement ratio and to the age of concrete. Mix proportion differences can be detected but batch to batch variations for the same nominal mix are not yet explained.

The original version of the high frequency measurement system is described. It was based on a HP4191A impedance analyser under the control of a HP85 computer. Initial investigations were limited to the measurement of the magnitude of impedance of 150 mm cubes of concrete sandwiched between two 150 mm square stainless steel electrodes (14 s.w.g.). These electrodes are interfaced to the coaxial connector of the analyser via a transition network. Differences in additional amounts of aggregate and entrapped air are shown to produce variations in electrical impedance. These results are presented graphically for the frequency ranges 1-100 MHz and 500-700 MHz. It is claimed that high frequency measurements provide more information on mix proportion variations than those made at low frequencies. However, the mix proportions of the concrete measured are not stated.

A developed high frequency system, based on a more powerful HP9816 computer and including a purpose built electronics unit which allows measurements to be carried out on four samples housed in an environmental control system, is described. The electrode system is modelled as an open circuit loaded parallel plate transmission line containing concrete as a dielectric, and values of dielectric constant and conductivity are de-imbedded from measurements of complex

impedance on the basis of the model. The effect of the connection between the electrodes and the analyser coaxial cable is calibrated out by using measurements from different lengths of transmission line containing correspondingly different lengths of sample.

This system formed the basis for the present work.

Graphs are presented showing the variations of conductivity and dielectric constant with frequency as the material changes state over a period from 1 hour to 6 days. The mix proportions of the concrete mix used are not given. Further results for concretes of water/cement ratios 0.4, 0.5, and 0.6 are also presented graphically for 1 hour and 1 day. In all these results the frequency range of measurement was 1-100 MHz.

The results for conductivity up to ≈20 MHz show little variation with frequency at any stage for a given mix but the values drop with the age of the concrete (from ≈0.2 S/m at 1 hour to ≈0.025 S/m at 6 days). Above 20 MHz the value of conductivity drops steadily for ages up to ≈0.4 days, whereas for older concrete a rise is evident but only up to ≈55 MHz. Beyond this frequency the value falls again. The rise in conductivity for concrete older than 0.4 days is said to be due to the Maxwell-Wagner effect, which becomes more evident after the change in material state at the point of setting. This does not, however, explain the fall in conductivity above 40-50 MHz. The conductivity is seen to be sensitive to the water/cement ratio, with higher ratios resulting in higher conductivities and vice versa.

The results for apparent dielectric constant are very unusual in that *negative* values are obtained above 3 MHz for fresh concrete (1 hour) and above 40 MHz for hardening concrete (>1 day). This remarkable phenomenon is not explained by the authors in their analysis of results.

The dielectric constant increases in value as hydration proceeds and this is taken by the authors as indicative of an increase in interfacial polarization effects, especially after the material has set and has developed a definite pore structure. A steep fall in the value for fresh concrete between 1 and 5 MHz (where it crosses the zero axis) is explained as being due to the residual high frequency effects of electrode

polarization. The values of dielectric constant for all ages of concrete converge together to a negative value at frequencies above 60 MHz and the negative effect itself is seen to be decreasing in this same range. This effect is not explained. Water/cement ratio differences are shown to be discernable from differences in dielectric constant at frequencies below 40 MHz.

Wilson and Whittington have shown that high frequency impedance measurements on concrete do reveal variations in mix proportions especially above 100 MHz, and also that variations in the intrinsic parameters, conductivity and dielectric constant, appear to reflect changes in the state of concrete as the cement hydrates. An interfacial polarization mechanism, due to the developing pore structure, is suggested as the cause of this correlation. However, inconsistences in their results above 20 MHz remain unexplained as do the occurrence of negative dielectric constants, especially in fresh concrete, between 3 MHz and 100 MHz. These anomalies may be a reflection of a faulty calibration procedure.

### 4.2.3 Kim and Yoon

Kim and Yoon [52] investigated the dielectric response of cement paste over the first 2 days of hydration in the frequency range 10 kHz up to 1 MHz. They also included in their investigation measurement of the heat evolution in cement paste during hydration. The paper is introduced by a brief description of cement chemistry and a cursory review of some previous research on cement paste electrical properties. A description of the test equipment used in this work is given, as well as details of the experimental materials. Cement pastes made from Korean standard OPC were gauged with water/cement ratios of 0.4, 0.5 and 0.6. These were cast into prisms measuring 4×4×2 $cm^3$ in moulds which contained parallel aluminium electrodes of area 4×4 $cm^2$. The electrodes were covered with teflon to insulate them electrically from the cement paste samples. A Hewlett Packard 4277A LCZ meter, controlled by a personal computer, was used to obtain conductance, capacitance and dissipation factor (i.e. $\tan\delta = \varepsilon''/\varepsilon'$) for the samples. The effects of sample configuration, analyser connectors, electrodes and teflon insulation were calibrated out by zero-setting (although it is not explained what this actually

entailed). Thus the dielectric constant and loss factor of the samples are obtained directly from capacitance and conductance measurements and the geometry of the samples.

The authors present a short summary of general dielectric theory and the dielectric properties of cement paste. It is stated that the permittivity of a material manifesting several polarization mechanisms can be calculated simply from the sum of the permittivities due to each individual mechanism. Thus they present the equation :

$$\varepsilon = \varepsilon_s + \varepsilon_d + \varepsilon_i + \varepsilon_e$$

which they attribute to von Hippel [6], with the subscripts s, d, i and e referring to space-charge, dipolar, ionic and electronic mechanisms. Strictly speaking, however, von Hippel presents the above equation for the *polarizabilities* due to the respective mechanisms, from which may be derived an equation for the total electric susceptibility ($\chi_e = \varepsilon_r - 1$) as the sum of individual susceptibility contributions, thus the permittivity of free space should also be added to the right hand side of the above equation.

The authors state that the relaxation times of space-charge polarization mechanisms are in the range a few seconds up to several minutes, and are therefore outside their frequency range of interest. It is also stated that dipolar relaxation times, especially for highly viscous liquids, are in the range $10^{-6}$ s to $10^{-4}$ s which puts them directly in the authors' range of investigation. It is suggested that cement paste is a viscous liquid and will therefore display low frequency dipolar relaxation.

On the basis of the above assumptions the authors model the dielectric response of cement paste as a simple Debye process displaying a single relaxation time which increases as the paste hydrates from $10^{-6}$ s to $10^{-3}$ s. The values of static and infinite frequency permittivity are assumed to remain constant throughout hydration.

It is difficult to see the justification for the above assumptions. For instance with respect to space-charge polarization van Beek [29] and others [68][6] have shown that the relaxation times for heterogeneous materials can range from minutes down to nanoseconds which includes the whole range investigated in this paper. While

fresh cement paste can be regarded as homogeneous in some respects, it is essentially heterogeneous as soon as the pore structure begins to form and the dielectric effects of this are therefore likely to influence electrical measurements in the frequency range of the authors. Also, although fresh cement paste may appear physically similar to a viscous liquid, it is in fact a colloidal suspension and it is possible that colloidal double layer polarization will play a substantial role in determining its dielectric response in the 1-1000 kHz range which will have implications for the validity of the authors' model.

The constancy of static and infinite frequency permittivities is not a justifiable assumption since these are both likely to be affected by the changes in state of the hydrating paste as the results of other workers have shown [4][43].

The results of real and imaginary permittivity measurements on a paste of w/c ratio 0.4 at 10, 50 and 100 kHz are presented graphically. The data are plotted as functions of time up to 48 hours and the upper and lower limits of measured dielectric constant are obtained from the plots as 163 and 83 respectively. Other similar profiles for pastes of w/c ratios of 0.5 and 0.6 are also presented. These appear to show upper and lower dielectric constant limits of very similar value to the w/c 0.4 paste and the authors apply these values to their Debye model for the pastes. However, it is not easy to understand why values of permittivity apparently demonstrated by the pastes before and after setting (i.e. functions of time) should be related to the static and infinite frequency permittivities of a frequency dependent Debye model. The authors claim that the plots demonstrate a single relaxation time for the pastes which varies as hydration proceeds, and they attribute this to the operation of a dipolar polarization mechanism in the pastes in accordance with the assumptions made at the modelling stage.

In conclusion, it is stated that the frequency dependence of the permittivity of cement paste in the 10 kHz to 1 MHz range can be explained on the basis of a dipolar mechanism of polarization showing Debye characteristics and a single relaxation time. The authors further conclude that the static and infinite frequency permittivities of the pastes measured are invariant with w/c ratio at values of 160

and 80 respectively. They therefore infer that the w/c ratio dependency of measured permittivity values is due only to relaxation time variations caused by paste viscosities.

This is a confusing paper, both in terms of the theoretical approach taken by the authors and the method of results presentation and interpretation. The author feels that the experimental results presented may have been distorted by the teflon insulation used in the sample moulds, but without details of the calibration procedure used by the authors it is not possible specify the nature of any such distortion.

### 4.2.4 McCarter and Garvin

In this paper McCarter and Garvin [53] present the results of an A.C. electrical impedance investigation into the moisture condition of cement paste and mortar specimens in the frequency range 20 Hz-110 MHz. The purpose of the investigation was to demonstrate the feasibility of employing cement based materials in novel applications such as humidity/moisture sensors, as opposed to the more usual construction uses.

The theory of cement hydration is considered with particular reference to the part played by various modes of water retention in the structural development of the cement gel and pores. The electrical response of hardened cement paste (HCP) samples placed between a pair of electrodes is considered to be dominated by the moisture distribution and the pore development. The authors model this sample/electrode configuration as a complex impedance of resistance (resulting from ionic conduction in water) in parallel with capacitive reactance (resulting largely from Maxwell-Wagner effects associated with charge build-up in segmented pores). They also consider that electrode polarization can affect results at very low frequencies.

Measurements were carried out over the specified range using a Wayne-Kerr 6425 component bridge and a Hewlett-Packard 4193A impedance analyser, both under the control of a Hewlett-Packard 9836U microcomputer. The measurements were corrected for stray and residual circuit impedance (due to the electrode/analyser

interface) by software, although no details are given of the technique used. The mortar and cement specimens, batched using OPC and Leighton Buzzard sand, were 50 mm cubes into which were embedded pairs of stainless steel electrodes, measuring 50×20×5 mm, placed 20 mm apart. Water/cement ratio was 0.35 for cement paste and mortar, and sand/cement ratio for mortar was 2/1. The cubes were cured under water at 20°C and measurements were performed periodically during hydration. After 100 days some cubes were oven dried at 70°C and then, after cooling, were immersed under 200 mm of water with all but the top faces sealed, and the impedance was monitored as permeation of water occurred.

Results are presented in the form of complex impedance plots (reactance against resistance with frequency as a parameter). On one graph the results for cement paste at 28 and 100 days are shown along with those for mortar at 100 days. On another graph results for mortar are shown at three stages of moisture permeation (after drying at 70°C and cooling in laboratory, after 10 minutes immersion in water, and after 24 hours immersion in water).

The basic form of all the complex impedance plots is a semicircular arc above the real axis with centre depressed below the axis, and a low frequency "tail" at the high resistance end of the curves inclined at ≈45° or greater from the real axis. The authors note that the tail is an indication of electrode polarization phenomena and it is interesting that the highest frequency at which these effects are noticable is about 4 kHz for 28 day old cement paste. This frequency decreases as hydration proceeds. The authors comment that the semicircular arc portion of their impedance curves is indicative of a relaxation process with time constant derived from the frequency at which maximum reactance occurs. This is deceptive, however, because for a material like cement paste, in which conduction and polarization operate effectively in parallel, a semicircular complex *impedance* plot (as distinct from complex *relative permittivity*) indicates a capacitance value which is constant with frequency, which in turn implies that there is no relaxation of polarization over the frequency range displayed. Instead, it is the depression of the arc centre below the real axis which is indicative of dielectric relaxation, and not the arc as such. Thus, the interpretation of relaxation time from the plots is less certain than the authors suggest. Nevertheless a value of ≈12 MHz is claimed for cement paste at 28 days

and this is attributed to Maxwell-Wagner effects in the pore structure of the HCP. The bulk resistance of the material is obtained from the plots at the low frequency point of intercept with the real axis and this is found to increase with age. The authors attribute this trend to the gradual segmentation of the HCP pore structure and the consequent increasing tortuosity of ionic conduction paths.

The capacitance of the samples is found to decrease with age and this is also consistent with the pattern of HCP development. It is also found that both capacitive reactance and resistance are greater for mortar than for cement paste, and this is seen as a reflection of the mixing laws for heterogeneous dielectrics.

The results for the permeation of water tests show a low frequency tail still in evidence for oven dried (70°C) mortar, suggesting that ionic conduction is still occurring. The authors attribute this to adsorbed gel water. Resistance and reactance are seen to decrease markedly as water permeates the dry mortar, and the cutoff frequency for electrode polarization increases during this process, eventually exceeding the pre-drying value. The overall shape of the curve is seen to be flatter after the drying and rehydration of the mortar sample. The trend observed for apparent relaxation time on moisture permeation (decreasing) is counter to what should be expected, which is perhaps related to the problem of interpretation mentioned above.

A final graph showing the increase of both sample conductance and moisture absorption with time shows strong correlation between these two parameters. This graph also suggests two separate stages to the moisture permeation process. These are a phase dominated by capillary suction, and a subsequent phase where slower diffusion processes dominate.

This work has demonstrated the decisive part played by water in the electrical properties of cement based materials, but the interpretation of results with respect to relaxation processes operating in HCP is not certain. The fact that the authors treated the electrode/sample arrangement as a lumped impedance may also cast some doubt on the results at the high frequency end because a distributed parameter model may be more appropriate towards 110 MHz.

### 4.2.5 McCarter and Brousseau

McCarter and Brousseau [39] have investigated the A.C. electrical properties of cement paste in the frequency range 10 mHz up to 15 MHz. While this range is largely low frequency there is some frequency overlap with the work of the author and interest is shown here in the model developed by the authors for explaining their experimental results. This paper is also a follow on work from the investigations carried out by McCarter and Garvin described in section 4.2.4.

The purpose of the investigation was to demonstrate the need for monitoring the electrical behaviour of cement based materials over a wide frequency range in order to produce a more complete characterisation, and also to develop a general electrical model explaining the observed behaviour. This approach is compared to the more limited approach used in the past at very low frequencies or D.C. which tended to focus only on resistivity/conductivity measurements for electrical characterisation.

The authors point out that one of the prime reasons for using A.C. techniques in the electrical testing of cement paste is the minimization of interference produced by electrochemical processes at the electrodes. These effects are considered to disappear somewhere in the 100 Hz to 10 kHz range.

A complex plane representation for the electrical impedance measurements of cement paste is opted for, with capacitive reactance plotted against resistance using frequency as a parameter. The authors feel that this approach best enables the development of an equivalent circuit representation of the material. A set of rules for the correct modelling of the impedance response is given and an example of how a dielectric relaxation response may be synthesized by plotting the complex impedance response of a resistor and capacitor connected in parallel. Thus, a Debye type relaxation is produced if the resistance of the RC circuit is taken as analogous to dielectric constant, and the reactance as analogous to loss factor. The relaxation time is then simply R×C. The concept of a "non-Debye" frequency dependent capacitance is introduced for the purpose of modelling the statistical spread of relaxation times often observed in real polarization processes, and the complex impedance plot of this in parallel to a resistor is shown to be a semicircular arc with its centre inclined below the real axis by an angle related to the spread parameter.

The A.C. equivalent circuit representation of cement paste at low frequencies is given first. This is shown to consist of a series resistor, representing the bulk conductivity of the paste, in series with a resistor and capacitor in parallel, representing the electrode polarization effects. These effects are shown to be frequency dependent and to disappear at some cutoff point, considered to be no higher than ≈10 kHz. The authors point out that this model is defective since it implies that beyond the disappearance of electrode effects the paste impedance would be frequency invariant, which is known not to be the case. A frequency dependent capacitive element is therefore connected in parallel with the bulk conductivity resistor in order to account for dispersive polarization effects in the cement paste. Also added to the circuit is a Faradaic impedance element to represent ionic diffusion processes which occur at the electrodes. This is connected in series with the electrode charge transfer resistance already included. A complex impedance plot of the model is presented and is shown to consist of a low frequency tail at 45° to the real axis produced by the Faradaic element, a following low frequency arc produced by the electrode polarization circuit which intercepts the real axis at the value of resistance of the paste circuit, and a higher frequency arc following on from this which represents the response of the bulk material. Three significant frequencies are identified, viz. the relaxation frequency of the electrode polarization effects (found at the "crown" of the low frequency arc), the frequency at which electrode polarization is no longer effective (the point of intersection of the respective arc with the axis), and the relaxation frequency of the bulk paste response (the crown of the higher frequency arc).

The authors describe the measurement system used to obtain complex impedance data on cement paste samples made from OPC. A Solatron 1260 frequency response analyser, under the control of a HP9836U computer was used to obtain data at 150 points over the frequency range 10 mHz to 15 Mhz in a logarithmic sweep mode. Stainless steel electrodes of unspecified dimensions were connected to the analyser. An internal calibration routine was used to correct incoming data but no correction for any distortion due to the connection between analyser and electrodes was made. The electrodes were embedded in cement paste samples of water/cement ratio 0.27 measuring 50×50×50 mm.

Data are presented on a single complex impedance diagram for impedance measurements obtained at 1, 10 and 100 days after gauging. The basic form of the complex impedance plots remains fairly constant as the cement paste ages, comprising a dominant low frequency arc due to effects at the electrode/paste interface, and a much smaller arc due to cement paste bulk effects, but the impedance values measured and the consequent radii of the arcs increase markedly with the age of the paste. The smaller high frequency arcs are also presented on separate charts with enlarged scales.

A number of parameters are obtained from the plots and presented in tabular form. The relaxation frequency of the electrode polarization effect is shown to be very low and to decrease with the age of the paste (31.1 mHz at 1 day down to less than 10 mHz at 100 days), as does the frequency at which this effect drops out completely (8.17 kHz at 1 day down to 1.49 kHz at 100 days). The apparent relaxation frequency of the bulk polarization mechanism also decreases with time (5.55 MHz at 1 day, 2.73 MHz at 100 days) and the authors attribute this to a reduction in charge mobility due to gel development and pore constriction. However, this appears to be the opposite of what could be expected since the constriction of the pores containing the polarizable charges would be more likely to promote polarization effects at increasingly higher frequencies. The angles of depression of the arcs below the real axis are also tabulated and these show that while the spread parameter for the electrode polarization effects does not vary with hydration of the paste, the value for the bulk paste increases by ≈70% between 1 and 100 days.

The authors make comment on the increasing degradation suffered by the data as frequency is increased but give no details of their method of overcoming such problems. They point out that 15 MHz represented the upper limit of data reliability.

The paper is concluded by the assertion that the frequency dependence of the electrical properties, as demonstrated by the experimental results, necessitates the use of wide-band scans for the proper characterisation of cement paste and related materials.

The present author would make the comment that care must be taken over the interpretation of complex impedance measurements of a material like cement paste (or related materials such as mortar and concrete). Especially, it should be pointed out that while the impedance of an equivalent circuit can be used to *represent* the electrical response of the material, it does not follow that impedance measurements on an actual sample can be *directly* related to such a model. As pointed out in section 4.2.4 a sample of material with a *fixed* value of dielectric constant and conductivity positioned between two parallel plate electrodes would produce a semicircular arc on a complex impedance plot despite there being no relaxation process in operation. This is because the reactance *is* frequency dependent while the capacitance is not and it can therefore be a mistake to attribute the apparent relaxation time on an impedance plot to the supposed relaxation of a dielectric mechanism.

### 4.2.6 Wilson and Whittington

In this paper Wilson and Whittington [5] propose a number of theoretical mechanisms to account for the conductivity and dielectric constant of concrete in the frequency range 1-100 MHz, as it changes state over the period of 1 day since gauging. These mechanisms are suggested as an explanation for results arising from earlier work by the same authors [4][54].

A description of the automatic measurement system, based on a HP4191A complex impedance analyser under the control of a HP9816 computer, is given. The system is capable of carrying out measurements on up to four 150 mm cubic concrete samples sandwiched between 150 mm square steel electrodes. These electrodes are interfaced to coaxial connectors via a transition network and each individual coaxial line is connected to the analyser terminal through a R.F. switch network. Due to the fact that there are four different signal paths into the switch network, the analyser internal calibration routine cannot be used to refer measurements to the sample electrodes as it would normally. Instead, the routine is carried out using the standard Hewlett-Packard test pieces (s/c, o/c and 50Ω matched load) for each individual path, and the results stored on floppy-disk, rather than in the analyser internal memory, for subsequent calibration.

The coaxial to parallel plate transition network is modelled as a single complex impedance element. The effects of this element are calibrated out by taking complex impedance measurements on two different lengths of sample/electrodes (the material used being mortar), which provides a total of four numbers. These numbers are used to compute the four unknowns of the electrode system, viz., the real and imaginary parts of the transition and the conductivity and dielectric constant of the mortar. The electrode/mortar system is modelled as a parallel plate transmission line, assumed to be terminated in a perfect open circuit. This model, rather than a lumped element circuit model, is used because of the likelihood of the sample dimensions occupying a significant fraction of a wavelength at frequencies towards 100 MHz. The basis of the calibration computation is a four dimensional version of the Newton-Raphson iterative method.

The authors carried out measurements over 1-100 MHz on concrete samples of water/cement ratio 0.5 and cement/sand/aggregate ratio 1/1.5/3. Results are presented graphically, showing conductivity and dielectric constant against frequency for four samples at 1 hour and 1 day. The averages of the four samples for these two parameters, as the material develops over the period of 1 day (a total of nine plots for each), are also presented graphically. These results are identical in characteristic form to those presented by the same authors in reference [4] (section 4.2.2).

Wilson and Whittington propose three characteristic mechanisms which they suggest to be the cause of the unusual observed dispersion phenomena. These are :

**i)** Electrode polarization, resulting in the build up of a "significant" layer of gas at the electrodes due to the electrolytic nature of cement paste. This effect is thought to be responsible for the steep negative gradient in dielectric constant, especially just after gauging, in the frequency range 1-40 MHz.

**ii)** A change from homogeneous to heterogeneous conduction mechanisms as the structure of the concrete develops, especially at the point of setting, heterogeneous conduction being characterised by the Maxwell-Wagner effect. This effect is

thought to explain the characteristic of the conductivity dispersion in the frequency range 7-40 MHz, and the increase in dielectric constant with time at frequencies below ≈60 MHz.

**iii)** Effects, due to a viscous conduction mechanism, which limit the ability of an ion to respond to an alternating electric field above some cutoff frequency. This mechanism is believed to be responsible for the apparent negative values of dielectric constant and its relaxation is postulated as a possible explanation for the observed increase in dielectric constant with frequency above 35 MHz and particularly 60 MHz.

The authors consider each of the above effects in turn with the aim of explaining the overall dielectric behaviour of concrete which they have observed in the 1-100 MHz frequency range.

Electrode polarization effects are modelled by an equivalent circuit approach which consists of a resistor and capacitor in parallel, representing the bulk electrical properties of the concrete, in series with a capacitor, representing the layer of gas which builds up on the electrode surfaces due to electrolysis. The authors suggest that the presence of the gas layer, as represented by the series capacitance, could lead to very high values of apparent dielectric constant being measured at low frequencies, a typical figure being $3.7\times10^{9}$ at less than 1 Hz for concrete with a conductivity of 0.206 $Sm^{-1}$ at 1 MHz (taken from their own results). This remarkably high value for dielectric constant is based upon an assumed relaxation frequency of 1 Hz for the electrode polarization mechanism which the authors obtain from their own previous low frequency work. Due to this very high contribution to static dielectric constant the authors consider that electrode polarization will still affect results up to 10 MHz, despite the relaxation frequency of the mechanism being so low.

The Maxwell-Wagner effects, to which the authors attribute the changes with time of the conductivity and dielectric constant characteristics in the 7-40 MHz band, are thought to be caused largely by the physical changes in the cement paste which occur during hydration. Initially, the paste is thought to display homogeneous conduction but at the onset of hardening the pore structure which develops leads to

the presence of polarizable conducting volumes (the electrolyte filled pores) contained in an essentially non-conducting matrix (the hardened cement and aggregate). This heterogeneous system is assumed to increasingly display Maxwell-Wagner effects as the pore structure becomes segmented, and the effect is thought to be particularly enhanced by the geometry of the pores, which the authors propose as taking the form of long thin needles (i.e. ellipsoids of an extremely prolate geometry). However, Neville [9] states that for w/c ratios greater than 0.4 pore segmentation does not occur until at least 3 days after gauging, and that the capillary pore structure for w/c=0.5 (as in this paper) is *continuous* throughout the material for up to 14 days after gauging. This suggests that the changes monitored by the authors over the first day are not due to this particular aspect of hydration in the simple terms described. Also, the long thin conducting needle model, which is obtained from the survey by van Beek [29], is valid only for the condition that the conducting regions do not reach from one face of the dielectric to the other (i.e. between electrodes). For cement paste less than one day old this is not likely to be the case.

The mechanism proposed in (iii) is an attempt to explain the most striking and unusual feature of this work. Expressions are developed for the time constant, and the frequency dependent dielectric constant and conductivity of a conduction mechanism which operates by means of ions moving in a viscous medium. The notable point is that the contribution made by such a mechanism to the dielectric constant of the material in which it operates is shown to be negative. The developed expressions are then incorporated into equations for a material which demonstrates viscous conduction in parallel with a more conventional mechanism and the authors suggest that, depending on the relative level of contribution made by the two mechanisms, it is theoretically possible for such a material to have a negative value of dielectric constant. No actual calculations based on these equations are carried out by the authors but a graph is presented which shows the form of dispersion curves to be expected from this mechanism. Dielectric constant is seen to be negative at lower frequencies and to increase to a positive value above a relaxation frequency. Conductivity on the other hand is enhanced at lower frequencies and decreases above the relaxation frequency. The relaxation frequency of a typical viscous conduction mechanism had been calculated by Wilson previously [2] and

was reckoned to have a value of about 40 GHz, considerably above the frequencies of interest. However, as a consequence of the results presented in this paper they believe a reassessment of this value is necessary and have used 50 MHz in their current analysis.

A model of the dielectric and conductivity dispersions in concrete is synthesised by combining the expressions developed for the three above effects, and the results obtained from the model for conductivity and dielectric constant in the 1-100 MHz band are compared to the experimental results for concrete at 1 hour and 1 day.

To justify the model Wilson and Whittington make a number of assumptions which deserve comment.

Firstly, the authors state that the bulk dielectric constant and conductivity of concrete are relatively constant up to frequencies around 10 MHz. While the low frequency conductivity of concrete is probably constant with increasing frequency (because it is due predominantly to direct conduction in the mix water), it is not certain that this is the case in the MHz range. The dielectric constant is claimed by other workers (on the basis of experiment) to vary considerably with frequency below 1 MHz [55][56] and it would appear that Wilson and Whittington are assuming, for the purposes of their model, that all such variations are attributable to electrode polarization, and not bulk material properties. The authors have not fully validated this assumption. The findings of Scott et al. [41], presented in section 3.2.4, for work on moist porous rocks (which are similar to hardened concrete), show that while electrode effects are in evidence at frequencies less than 1 MHz other polarization mechanisms also substantially contribute to the dielectric properties. Scott et al. also found that electrode polarization was not a factor in measured dielectric properties at frequencies of 1 MHz or greater. The considerations presented in section 3.2.4 also cast doubt on the proposed electrode gas layer of Wilson and Whittington.

Secondly, it is stated that the electrical behaviour of the bulk material is controlled by ionic conduction mechanisms and that, as a consequence, the viscous conduction expressions developed for conductivity and dielectric constant will have a multiplicative effect on the material characteristics. This is not specifically justified

by the authors and is difficult to appreciate because elsewhere viscous conduction is envisaged as acting in parallel with other "conventional" mechanisms which suggests that these effects should be superposed (i.e. *added* in parallel) on the other characteristics which comprise the model.

The performance of the model is compared to actual experimental results and is shown to be good, though some inconsistencies are examined by the authors. The favourable result is not surprising, however, since appropriate values for the parameters were chosen to produce the conformation. Nevertheless, the authors have demonstrated that if their hypotheses as to which electrical mechanisms are operating in concrete are correct then their proposed model could be a valid explanation for their experimental results. No other other such analysis of the electrical behaviour of concrete at radio frequencies was available in the literature at the time of publication of this paper.

### 4.2.7 Olp et al.

Olp et al. [57] measured the dielectric constant and conductivity of various cement pastes and mortars over the frequency range 1 MHz to 3 GHz. This is more or less the same range of inquiry as that investigated by the author and the results presented in this paper, being very recent, were therefore of particular interest.

The authors point out that, while low frequency ($\ll$1 MHz) conductivity and microwave (>1 GHz) dielectric constant measurements on concrete have been well reported, the electromagnetic properties (i.e. both parameters) at radio frequencies have received scant attention. They state that their aim in measuring the R.F. electromagnetic properties of cement based materials is to identify useful frequencies of investigation and provide a body of data to help in the development of a suitable sensor for the on-site monitoring of concrete quality.

The authors used a coaxial dielectric measurement cell for acquiring their data, a schematic diagram of which is presented. The cell, constructed of brass, has a volume of 54 ml which is described as large in comparison to those available commercially. This is seen as a necessary feature of the cell because of the relatively large scale heterogeneities of cement mortar. The electromagnetic

properties of the sample are determined from the measurement of the scattering parameters (s-parameters) of the cell. The equipment used to obtain these measurements is not described. The cell is calibrated over the range of operation by measuring materials with known dielectric properties such as water, teflon and air.

A range of mortars with water/cement ratios of 0.45-0.6 and sand/cement ratios of 1.25-2.75, and a cement paste of water/cement ratio 0.5 were prepared for measurement. Two mortars incorporating calcium chloride and gluconic acid to modify setting times were also prepared.

Results are presented for the plain cement paste. The graphs of dielectric constant and conductivity show the variation of these parameters with time at various frequencies. Also presented are frequency dispersion graphs for the same sample at 12 hours after gauging, and a temperature versus time chart. The results show that dielectric constant varies with time but does so very much more markedly at frequencies below 30 MHz, where it rises steeply over the period 2-12 hours. The point of most rapid increase in dielectric constant corresponds to the peak in sample temperature. The results for conductivity demonstrate that changes with time are similar for all frequencies, this parameter peaking at 2 hours and then falling away relatively steeply as time progresses (although the value is still substantial after 24 hours). The authors state that the increasing value of dielectric constant may be attributable to the formation of electrical double layers around hydrating cement grains, but this is probably no more than speculation since colloidal double layer polarization would normally be expected to relax in the kHz frequency range or lower and such a mechanism is more likely to be influential before rather than after setting in contrast to what the authors suggest. The dielectric constant above 300 MHz decreases over the first 24 hours and it is suggested that this is due to the binding of water molecules in the hydrating cement paste, with a consequent hindering of the rotation of $H_2O$ molecules leading to a suppressed polarizability.

The frequency dispersion charts for the paste show that dielectric constant is high at lower freqencies (a peak value at 1 MHz of 359) but decreases as frequency increases, and that conductivity is lower at 1 MHz but increases with frequency. The high dielectric constant values are thought to be due either to electrochemical or

geometric effects which are not effective at higher frequencies, and the increasing conductivity is due to microwave absorption becoming increasingly dominant, which is the same as saying that dipolar relaxation of water molecules is responsible.

The results for the mortars are very similar in form, but the overall values of dielectric constant and conductivity are reduced. This reduction is related to variations in water/cement ratio and sand/cement ratio. The results for the mortars containing the admixtures confirmed that the characteristics in time of both conductivity and dielectric constant are correlated to the setting and hardening of the cement paste.

This paper is the only source of data on the electrical properties of concrete or mortar at radio frequencies available in the literature, other than the work of Wilson and Whittington, and provides a very useful source of data with which to compare results.

## 4.3 Radar Investigations (Ground Probe Radar)

The use of radar as a means of testing the quality and integrity of concrete structures is gaining in popularity. The idea of using radar in this capacity originally developed out of work done by the United States Army on equipment for the detection of non-metalic mines [58]. The current sub-surface radar equipment (or ground probe radar - abbreviated to GPR) used in the civil engineering industry was developed from geophysical applications. An extensive review of sub-surface radar technology is given by Daniels [59].

Radar is used both for quality testing and for the specific detection of sub-surface features in concrete structures. The frequencies of operation of GPR equipment are in the range 100-1000 MHz [60], rather than the microwave frequencies of more conventional radar systems. Frequencies at the lower end of this range are used when depth penetration of 4-5 m is required, while 1000 MHz permits the sharper resolving of specific features such as mesh, rebars, fractures and voids. It is because of this frequency range of operation that interest in GPR is shown by the author since, clearly, the electrical properties of concrete in the range 100-1000 MHz will affect such radar performance.

Radar operates on the basis of transmitted signals and received echos of such transmissions. Echos are produced when the transmitted signal encounters a discontinuity in the dielectric properties of the transmission medium, for instance when the signal meets an air filled void in a concrete structure. The relative differences in dielectric constant and conductivity at the boundary between two regions is what determines how much of the signal is transmitted across the boundary and how much is reflected back from the boundary. Two basic types of transmission signal are used in GPR investigations; Continuous-wave swept-frequency (CWFM) radar employs a continuous signal which is swept up and down in frequency, either linearly or sinusoidally. The echo which is received back from such a signal is compared in magnitude and phase to the original transmission. Pulsed radar employs a high voltage narrow pulse about 1 ns wide which is fed directly to a resonant antenna which in turn produces a transmission signal in the form of a damped oscillation. The time delay between transmitted and received pulses, as well as signal attenuation and phase inversion provide the relevant information in this case.

Techniques of investigation may also be grouped into Transmission and Reflection types [61]. Transmission techniques on concrete structures employ surface contacting antennae (often hand held) and the time taken for a transmitted pulse to travel through the structure to the other side and then return is the measured parameter. In the Reflection techniques a horn antenna held at some distance from the surface of a concrete structure is used to focus a beam onto the surface and the time taken for a reflected pulse to return from the structure surface is the measured parameter. Both of these parameters will be dependent on the dielectric constant and conductivity of the concrete in the structure under investigation but the reflection technique will be more influenced by dielectric conditions at the surface of the structure while the transmission technique could be expected to be more influenced by the "average" dielectric conditions of the material throughout the structure.

One problem that might be encountered with the use of GPR for the investigation of concrete structures is the occurrence of dielectric dispersion in the frequency band of GPR operation. For instance, if a CWFM signal sweeping in the 1-1000 MHz range

(say between 200 and 400 MHz or 400 and 800 MHz) is propagated in concrete which has a fall in dielectric constant (and consequent rise in conductivity) in the relevant frequency band, signal frequency components at the lower end of the spectrum will travel more slowly than those at the higher end because propagation velocity is inversely proportional to the square root of the dielectric constant. Similarly, higher frequency components will be attenuated more than lower frequency components due to conductivity dispersion. Thus, a reflected signal would arrive back at the receiver in a dispersed condition with the more highly attenuated high frequency components leading and the less attenuated lower frequency components lagging.

It has often been the case that engineers using GPR to investigate the presence of voids or defects, or the position of rebars, in a concrete structure will use an assumed fixed value of dielectric constant and conductivity of concrete [58] and base calculations of target position on such. In the case of the above hypothesis such an assumption would obviously lead to errors appearing as a result of the dielectric dispersion.

It is therefore the concern of engineers using GPR and other similar electromagnetic propagation techniques for the investigation of concrete structures that the results of studies on the fundamental electrical properties of concrete be made available [61][62] so that regions of dielectric dispersion in the frequency profile of the material may be better understood.

# CHAPTER 5

# Dielectric Properties of Concrete and its Constituents

This chapter presents a consideration of the theoretical dielectric properties of concrete and its constituents in the setting phase and the hardening phase. Particular attention is given to the dielectric properties of aqueous systems.

## 5.1 Dielectric Properties of Aqueous Systems

It was shown in chapter 2 (see especially sections 2.1.4 and 2.3.1) that the physical properties of cement paste, and hence concrete, are greatly influenced by the presence of water at all stages of development. In turn, the properties of the water held in the cement paste are determined by the mode of retention (whether absorbed or adsorbed in capillary pores and gel pores, or bound in the crystalline structure of the gel) and are consequently dependent on the paste structure. Clearly, therefore, the dielectric properties of water will have a strong influence on the electrical properties of cement based materials such as concrete. Those properties are considered in this section.

### 5.1.1 Pure Liquid Water

The macroscopic dielectric behaviour of water is both frequency and temperature dependent and is well understood in the frequency range of interest to this work. Many measurements have been carried out over the years and an accurate picture of the relaxation spectrum of water has emerged, although no fully valid theory of the molecular reasons for the observed behaviour yet exists [63]. Hastead [64] has produced an in-depth study of the dielectric properties of water and aqueous dielectric materials.

The dielectric behaviour of pure free water is dominated by an orientational polarization mechanism which has a relaxation spectrum described, to a very close approximation, by a simple Debye process with a single time constant. This

mechanism results from the permanently dipolar structure of the water molecule. The static dielectric constant and relaxation time are both temperature dependent and the following equations, derived empirically from published data by Malmberg and Maryott [65] and Grant et al. [66], can be used to calculate the value of each for any given temperature between 0°C and 99°C.

Static dielectric constant,

$$\varepsilon_{rs} = 87.740 - 0.40008 \cdot T + 9.398 \times 10^{-4} \cdot T^2 - 1.410 \times 10^{-6} \cdot T^3 \qquad \cdots(5.1)$$

Relaxation time constant,

$$2\pi\tau_R = 1.1109 \times 10^{-10} - 3.824 \times 10^{-12} \cdot T + 6.938 \times 10^{-14} \cdot T^2 - 5.096 \times 10^{-16} \cdot T^3 \cdots(5.2)$$

where $\varepsilon_{rs}$ and $\tau_R$ are identified as previously, and T is the temperature in °C.

The high frequency limit of the dielectric constant, $\varepsilon_{r\infty}$, is generally accepted to be constant (i.e independent of temperature) and has a reported measured value ranging from 4.8 to 6.1. A value of 5.5 is therefore reasonable and is the one assumed in this work [67]. From Denaro [68], the D.C. conductivity of water at 25°C is $4 \times 10^{-6}$ $Sm^{-1}$ which, according to Davies [69] (who states a temperature dependent increment of +2%(°C)$^{-1}$), gives a value of $3.623 \times 10^{-6}$ $Sm^{-1}$ at 20°C. This is very low, and results from the partial ionisation of the water molecules.

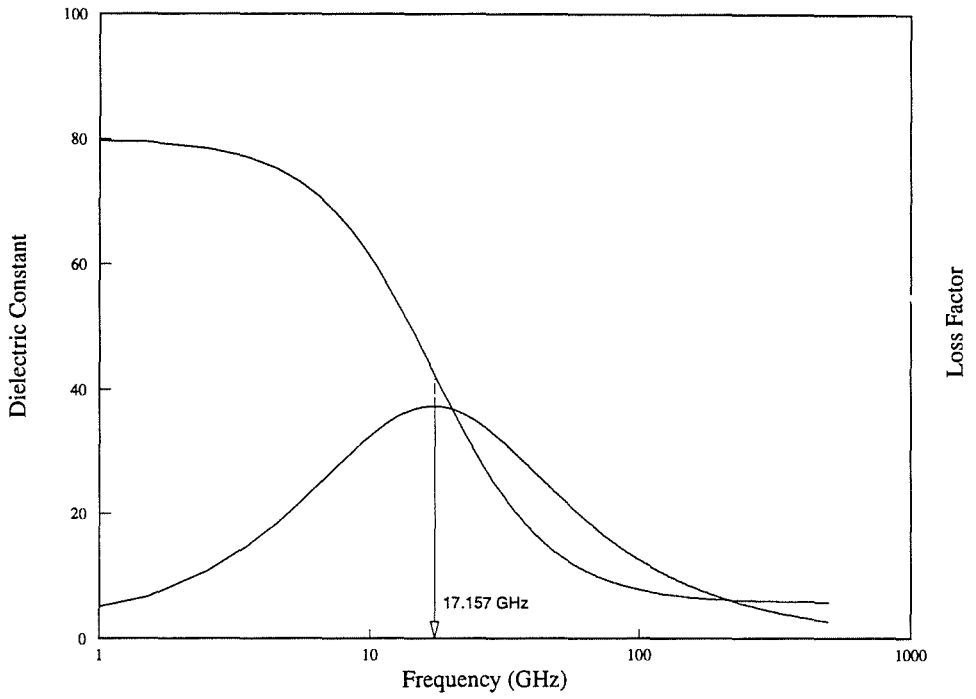


**Figure 5.1 Dielectric Dispersion of Pure Water at 20°C**

Figure 5.1 shows dispersion curves for pure water between 1 and 1000 GHz, produced from equations (5.1) and (5.2) in conjunction with equations (3.20) and (3.21) for a temperature of 20°C, at which $\varepsilon_{rs}$ and $\tau_R$ have values of 80.103 and $9.2764\times10^{-12}$ s respectively.

From Figure 5.1 it is evident that the relaxation frequency (17.157 GHz) is significantly higher than the maximum frequency of investigation in this work (1000 MHz), suggesting that the main dispersion characteristics of pure free water will not be a major influencing factor in the dispersions observed for the dielectric constant of concrete. Table 5.1 presents dielectric data for water at a temperature of 20°C at decade intervals between 1 MHz and 1000 MHz, as calculated from equations (3.20), (3.21) and (5.1).

| | 1 MHz | 10 MHz | 100 MHz | 1000 MHz |
|---|---|---|---|---|
| $\varepsilon_r'$ | 80.103 | 80.103 | 80.101 | 79.850 |
| $\varepsilon_r''$ | $4.348\times10^{-3}$ | $4.348\times10^{-2}$ | $4.348\times10^{-1}$ | 4.334 |
| $\sigma_d$ ($Sm^{-1}$) | $2.419\times10^{-7}$ | $2.419\times10^{-5}$ | $2.419\times10^{-3}$ | $2.411\times10^{-1}$ |
| $\sigma_{DC}$ ($Sm^{-1}$) | $3.623\times10^{-6}$ | $3.623\times10^{-6}$ | $3.623\times10^{-6}$ | $3.623\times10^{-6}$ |
| $\sigma$ ($Sm^{-1}$) | $3.865\times10^{-6}$ | $2.781\times10^{-5}$ | $2.423\times10^{-3}$ | $2.411\times10^{-1}$ |

**Table 5.1 Dielectric Parameters of Water at Decade Intervals (1-1000 MHz)**

It can be seen from Table 5.1 that the percentage increment in dielectric constant over the frequency range of interest is fairly small ($\Delta\varepsilon_r' = -0.316\%$) though not totally insignificant, and that it occurs predominantly in the upper part of the 100-1000 MHz range. By contrast, the percentage increment in conductivity is very large ($\Delta\sigma = 6.238 \times 10^6\%$). At lower frequencies the conductivity is determined primarily by the D.C. contribution but above 10 MHz the displacement conductivity of the dielectric loss factor is the major contributer and above 100 MHz the D.C. contribution is comparatively negligible. Thus, at 1 MHz *pure* (de-ionised) water is highly resistive and could be approximately represented by an equivalent circuit consisting of a single capacitive element, while at 1000 MHz its conductivity is similar to that of semiconducting materials (e.g. for germanium $\sigma \approx 2$ $Sm^{-1}$ and for silicon $\sigma \approx 2\times10^{-3}$ $Sm^{-1}$, both at room temperature), and an equivalent circuit representation would require an additional resistive element in parallel with the capacitance.

## 5.1.2 Aqueous Ionic Solutions

The general theory of electrolyte behaviour is given by Denaro [68] and is summarised here.

When an ionic substance is dissolved in water a gain in entropy occurs, indicating that the structure of the solution has become less ordered than that of the original solvent. This effect is due to the orientation of the polar water molecules around the dissolved ions which is a consequence of the local electric field generated by the ion charge. The result is the disruption of hydrogen bonds in the structure of the water and in the acquiring of a "sheath" of bound water molecules by each ion. The extension of the bound water sheath into the surrounding solvent increases, for monatomic ions, with increasing valence number [21][35]. The degree of solvation is also inversely proportional to ion radius [68]. An outer, more loosely bound, atmosphere of water molecules is associated with the sheath.

The water incorporated in the ion sheath has a dielectric constant of only ≈5.5 [36], the high frequency limit, $\varepsilon'_{r\infty}$, of water quoted in 5.1.1. This results from the irrotational binding of the dipolar molecules which prevents alignment with an applied electric field. This means that a decrement in dielectric constant from that of pure water is observed for electrolytic solutions which is proportional to ionic concentration. Hastead [64], quoting data from Collie et al. [70], shows that the effect of ions on the static dielectric constant of water is approximated, for concentrations of ≤0.2 mol.litre$^{-1}$, by the linear expression :

$$\varepsilon_{ss}' = \varepsilon_{sw}' + \delta c \qquad \cdots(5.3)$$

where,

$\varepsilon_{ss}'$ is solution static dielectric constant

$\varepsilon_{sw}'$ is water static dielectric constant

c is the concentration of electrolyte (mol.litre$^{-1}$)

$\delta$ is the dielectric decrement

For concentrations stronger than 0.2 the relationship between $\varepsilon_{ss}'$ and c is not linear, although the departure from linearity depends on ion species. Solutions of NaCl, for instance, still show almost linear behaviour at concentrations approaching 3.0 mol.litre$^{-1}$ [67], while KCl solutions are markedly non-linear beyond 0.5 mol.litre$^{-1}$.

The relaxation frequency of an aqueous solution is also affected by the presence of ions. The trend at lower concentrations (≤5 mol.litre$^{-1}$ for chloride salts according to Pottel [67]) is for an increase in relaxation frequency as concentration increases, and this trend is apparently linear at concentrations below ≈1.5 mol.litre$^{-1}$. The mechanism of relaxation frequency increment is not fully understood but it is suggested that the breaking of hydrogen bonds by the formation solvation sheath around the ions allows a faster response to an applied field by the free water molecules (a similar effect is produced by a rise in temperature). Hastead gives the following expression for the relationship between concentration and relaxation wavelength :

$$\lambda_s = \lambda_{sw} + 2\delta\lambda_s c \qquad \cdots(5.4)$$

where,

$\lambda_s$ is solution relaxation wavelength (m)

$\lambda_{sw}$ is water relaxation wavelength (m)

c is the concentration of electrolyte (mol.litre$^{-1}$)

$\delta\lambda_s$ is the relaxation wavelength decrement (m)

Hastead [64] gives a summary of relaxation wavelength decrements for various ions which is listed in Table 5.2, along with a summary of dielectric decrement values, also from Hastead, for the same ions.

| Ion | $\delta_+, \delta_-$ | $\delta\lambda_s^+, \delta\lambda_s^-$ ($m\times10^{-4}$) |
|---|---|---|
| $H^+$ | -17 | +4 |
| $Li^+$ | -11 | -3 |
| $Na^+$ | -8 | -4 |
| $K^+$ | -8 | -4 |
| $Rb^+$ | -7 | -5 |
| $Mg^{2+}$ | -24 | -4 |
| $Ca^{2+}$ | -23 | -7 |
| $Ba^{2+}$ | -22 | -9 |
| $La^{3+}$ | -35 | -15 |
| $F^-$ | -5 | -4 |
| $Cl^-$ | -3 | -4 |
| $I^-$ | -7 | -15 |
| $OH^-$ | -13 | -2 |
| $SO_4^{2-}$ | -7 | -11 |

**Table 5.2 Ionic Dielectric and Relaxation Wavelength Decrement Values**
(after Hastead)

In estimating the mean dielectric decrement, $\bar{\delta}$, from Table 5.2 of, for example, NaCl the values $\delta_+$ (-8) and $\delta_-$ (-3) are added together and divided by 2. Thus, $\bar{\delta}$(NaCl)=-5.5. In the case of the relaxation wavelength decrement the same procedure is followed. Thus, $\delta\lambda_s$(NaCl)=-4. The figures given above for calcium, $Ca^{2+}$, are estimated from those of barium and magnesium.

The conductivity, $\sigma$, of an aqueous ionic solution depends on a number of factors which include ion species, ion charge, ionic concentration, viscous retardation, and temperature. An electric field applied to an aqueous electrolyte will exert a force on the solute ions which will tend to accelerate them in line with the field. However, the viscosity, $\eta_v$, of the aqueous medium exerts a counter force which is proportional to ion velocity. As a consequence of the viscosity the ion is kept moving at an optimum constant velocity determined by the balance of electric field and viscosity forces. According to Stokes' law [69] the velocity of an ion under the above conditions can be obtained from equation (5.5) :

$$v = \frac{qE}{6\pi\eta_v r} \qquad \cdots(5.5)$$

where,

v is velocity ($ms^{-1}$)
q is particle charge (C)
E is electric field strength ($Vm^{-1}$)
$\eta_v$ is medium viscosity ($kgm^{-1}s^{-1}$)
r is particle radius (m)

The radius in expression (5.5) will not be the true ionic radius but will also include the effect of the solvation sheath of water molecules which apparently move with the ion. Also, because the ion/sheath complex will not be truly spherical at the molecular level Stokes' law cannot be applied in the strict sense, but it does provide a good approximation [36][69].

To take account of concentration variations different electrolytes may be considered in terms of their *molar conductivity*, $\Lambda$ ($Sm^{-1}mol^{-1}litre$), such that :

$$\Lambda = \sigma V = \frac{\sigma}{c} \qquad \cdots(5.6)$$

where V is the volume of solution (litres) containing 1 mol of electrolyte and c is the concentration ($mol.litre^{-1}$). An *equivalent conductivity* may also be specified by dividing $\Lambda$ by the valence number, z, of the particular ions, thereby providing a comparison of conductivities based on an equivalence of charge. Thus, the molar conductivity of a 1 $mol.litre^{-1}$ solution of $Na^+Cl^-(aq)$ would be compared directly to that of a 1 $mol.litre^{-1}$ solution of $0.5Zn^{2+}SO_4^{2-}(aq)$. The molar conductivity of a strong electrolyte (i.e. one which is always completely dissociated in solution) is known to increase linearly with dilution towards a limiting value, $\Lambda^\infty$ at infinite dilution. This parameter expresses the "true" conducting ability of a given electrolyte under conditions where charge carriers of opposite sign move independently of each other.

For dilutions less than infinity the interaction of oppositely charged ions reduces the conductivity by effectively increasing the viscous drag experienced by each ion. This increased viscosity is the result of two phenomena [36][68].

Firstly, the *asymmetry effect* results from the electrical retarding force exerted by the atmosphere of counter ions which continually forms around an ion as it migrates through the solution.

Secondly, the *electrophoretic effect* is an enhanced viscous drag exerted against an ion by the counter current of loosely bound water molecules associated with the counter ion current.

The retardation caused by the asymmetry effect disappears at higher frequencies when the ion atmosphere cannot respond to the rapidly changing direction of the ion, and an enhanced conductivity results. This is known as Debye-Falkenhagen relaxation. The frequency at which this relaxation takes effect is, according to Sylvan [36], 10c GHz (where c is molar concentration). Hastead [64] states that for concentrations of 0.1 mol.litre$^{-1}$ the rise in conductivity will be <3%. Cooper [71] has pointed out that the Debye-Falkenhagen effect becomes effective in the same frequency range as the dielectric relaxation of water and is therefore largely obscured by it. For instance, a 0.1 mol.litre$^{-1}$ solution of NaCl, of nominal D.C. conductivity at 20°C of 0.834 Sm$^{-1}$, would have a Debye-Falkenhagen relaxation frequency of ≈1 GHz and a maximum rise in conductivity of 0.0125 Sm$^{-1}$. At this frequency a much greater rise in conductivity of 0.2411 Sm$^{-1}$, resulting from the dielectric relaxation of water, would already be apparent (see Table 5.1).

Expression (5.7) relates the equivalent conductivity to the infinite dilution equivalent conductivity in terms of c, the molar concentration.

$$\Lambda = \Lambda^{\infty} - (b\Lambda^{\infty} + d)\sqrt{c} \qquad \cdots(5.7)$$

The constants b and d represent respectively the influence of the asymmetric and electrophoretic effects and it can be seen that the asymmetric effect is dependent on $\Lambda^{\infty}$ and concentration, while the electrophoretic effect depends only on concentration.

The ratio of actual equivalent conductivity to infinite dilution equivalent conductivity is known as the conductance ratio, κ. According to Glasstone [72] the conductance ratio is fairly independent of particular ion species but is controlled by valence number relationships. This is shown in Table 5.4 (after Wilson [2]).

| | Concentration of Solution (mol.litre$^{-1}$) | | |
|---|---|---|---|
| Valence Ratio | 0.1 | 0.01 | 0.001 |
| uni-uni | 0.83 | 0.93 | 0.98 |
| uni-bi | 0.75 | 0.87 | 0.95 |
| bi-uni | 0.75 | 0.87 | 0.95 |
| bi-bi | 0.4 | 0.65 | 0.85 |

**Table 5.3 Conductance Ratio and Relationship to Valence Number**
(after Wilson)

To account for the effect of solution temperature on ionic conductivity, Wilson [2] gives the following expression (valid between 15°C and 35°C) after Glasstone [72] :

$$\Lambda_T^{\infty} = \Lambda_{25}^{\infty} \cdot (1 + \alpha[T - 25]) \qquad \cdots(5.8)$$

where,

$\Lambda_T^{\infty}$, $\Lambda_{25}^{\infty}$ are the equivalent infinite dilution molar conductivities at T°C and 25°C

$\alpha$ is the temperature coefficient of conductivivty

The mobility, μ, of an ion species in solution is defined as the average velocity (ms$^{-1}$) at infinite dilution, in an electric field of 1 Vm$^{-1}$. It is a more fundamental quantity than equivalent conductivity, attributed as it is to the motion of a single ion, rather than a solution containing ions. The mobility is related to $\Lambda^{\infty}$ by expression 5.9, given by Denaro [68] :

$$\mu = \frac{\Lambda^{\infty}}{zF} \qquad \cdots(5.9)$$

F is the Faraday constant, which is quoted by Denaro as 96487 $C.mol^{-1}$ (this should be multiplied by $10^3$ if conductivities are in $Sm^{-1}mol^{-1}.litre$), and z is valence number. The velocity, v, of an ion in a solution at finite dilution is related to $\mu$ by the conductance ratio, $\kappa$, such that :

$$v = \mu\kappa \qquad \cdots(5.10)$$

The temperature dependence of ionic mobility will be identical to that of the infinite dilution equivalent conductivity and may be obtained by substituting $\mu$ for $\Lambda^{\infty}$ in equation (5.8).

### 5.1.3 Cement Paste Mix Water

As discussed in section 2.1.3, the water in cement paste contains ions at all stages of hydration, the type and concentration of which are shown in Figure 2.2 to vary with time. Since the ions in an aqueous solution modify the electrical behaviour of the water as described in section 5.1.2, it is necessary that the ionic content of cement paste water be taken into account when considering the effect of such on the electrical properties of the paste.

Table 5.4 gives infinite dilution equivalent conductivities, mobilities and temperature coefficients for the predominant ions (from Figure 2.2) which appear in OPC mix water after gauging. The values presented are corrected from standard values at 25°C (obtained from Denaro [68]) using equation (5.8). The temperature coefficients are from Wilson [2] after Glasstone [72].

| Ion | $\Lambda^{\infty}$ | $\mu \times 10^8$ | $\alpha \times 10^2$ |
|---|---|---|---|
| $OH^-$ | 18.179 | 18.841 | 1.60 |
| $Ca^{2+}$ | 10.644 | 5.516 | 2.11 |
| $K^+$ | 6.638 | 6.880 | 1.89 |
| $SO_4^{2-}$ | 14.431 | 7.478 | 1.96 |
| $Na^+$ | 4.475 | 4.638 | 2.09 |

**Table 5.4 Corrected Equivalent Conductivities and Mobilities in Mix Water**

The units of $\Lambda^{\infty}$ are $Sm^{-1}mol^{-1}.litre$, those of mobility are $ms^{-1}$, and those of $\alpha$ are $^{o}C^{-1}$.

The analysis of Appendix A shows the development of expressions for the conductivity and dielectric constant contribution to the same parameters of a liquid in which charged particles are moving under an electric field. The results of the analysis may be applied to a solvent in which dissolved ions are the moving charged particles. The expressions produced are :

$$\varepsilon_r' = -\frac{\mu\eta q\tau}{\varepsilon_0} \cdot \frac{1}{1+(\omega\tau)^2} \qquad \cdots(A.11)$$

$$\sigma_d = \mu\eta q \cdot \frac{1}{1+(\omega\tau)^2} \qquad \cdots(A.12)$$

The dielectric constant contribution described by equation (A.11) results only from the movement of the ions, and does not take account of the structure breaking effects of solvation described in 5.1.2. This *ionic conduction* contribution to dielectric constant was cited by Wilson and Whittington [5] as a possible explanation for negative dielectric constants observed in their experiments on concrete (sections 4.2.2 and 4.2.6).

Based on figures obtained from Double [18] (see Figure 2.2) for ionic concentration, c (mol.litre$^{-1}$), in cement paste water at 100 minutes, equations (A.11) and (A.12) were used to produce the following data for increments in the conductivity and dielectric constant ($\Delta\sigma$ and $\Delta\varepsilon_r'$) of mix water at 40 MHz :

| Ion | c | $\eta\times10^{-25}$ | $m\times10^{26}$ | $\mu\times10^{8}$ | $f_R$ | $\Delta\sigma$ | $\Delta\varepsilon_r'\times10^{4}$ |
|---|---|---|---|---|---|---|---|
| $OH^-$ | 0.0681 | 4.1029 | 2.824 | 18.841 | 4791.4 | 1.2383 | -46.456 |
| $Ca^{2+}$ | 0.0394 | 2.3699 | 6.655 | 5.516 | 13926.5 | 0.2094 | -2.704 |
| $K^+$ | 0.0206 | 1.2422 | 6.493 | 6.880 | 5707.6 | 0.1369 | -4.311 |
| $SO_4^{2-}$ | 0.0181 | 1.0901 | 7.980 | 7.478 | 8566.4 | 0.1304 | -2.737 |
| $Na^+$ | 0.0050 | 0.3011 | 3.817 | 4.638 | 14399.6 | 0.0224 | -0.279 |
| | | | | | Totals→ | 1.7374 | -56.487 |

**Table 5.5 Dielectric Constant and Conductivity Increments in Mix Water**

where,

c is molar concentration (mol.litre$^{-1}$)
$\eta$ is ion density (m$^{-3}$)
m is ion mass (kg)
$\mu$ is ionic mobility (m$^2$V$^{-1}$s$^{-1}$)
$f_R$ is ion relaxation frequency (GHz) (calculated from relaxation time, $\tau_R$ (s) - equation (A.6))

The frequency of calculation (40 MHz) was chosen to allow direct comparison with the work of Wilson and Whittington [4][5]. The values for ionic mass, m, were obtained from Gross and Wiseall [21] and those for ionic mobility, $\mu$, were calculated from equivalent ionic molar conductivities obtained from Denaro [65] with the temperature assumed to be 20°C.

The reference from which the above ionic concentrations were taken [18] lists the water/cement ratio of the paste in question as 2.0. This seems very high if mass ratios are being considered since structural concrete normally contains cement paste with water/cement ratio in the approximate range 0.35-0.70. It could be that the author was quoting a *volume* water/cement ratio of 2.0 (neither volume nor mass were specified), in which case, for a specific gravity for OPC of 3.15 ($g.ml^{-1}$) [9], a more plausible mass ratio of 0.635 is indicated.

| Ion | $\Lambda^{\infty}$ | c | $\Delta\sigma$ |
|---|---|---|---|
| $OH^-$ | 18.179 | 0.0681 | 1.238 |
| $0.5Ca^{2+}$ | 5.322 | 0.0394 | 0.2097 |
| $K^+$ | 6.638 | 0.0206 | 0.1367 |
| $0.5SO_4^{2-}$ | 7.216 | 0.0181 | 0.1306 |
| $Na^+$ | 4.475 | 0.0050 | 0.0224 |
| | | Total→ | 1.7374 |

**Table 5.6 Conductivity Contributions to Mix Water**

($\Lambda^{\infty}$ and c as before, $\Delta\sigma$ in $Sm^{-1}$)

To account for the ionic interaction at the finite dilution of the mix water solution a value for the conductance ratio, $\kappa$, was calculated based on the assumption that the ions in the mix water were present in cation/anion groups. These groups were taken to be the ionised compounds $Ca(OH)_2$, $CaSO_4$, $K_2SO_4$, and $Na_2SO_4$. The effective concentration of each electrolyte was calculated from the individual concentrations weighted by a relative volume assumed to be occupied in the solution by each. The relative volumes were obtained by assuming that each individual ion occupied the same volume of water irrespective of type. An average value of conductance ratio was then estimated by proportioning figures obtained from Table 5.3 in accordance

with the relative volumes. A resultant $\kappa$ of 0.78 was applied to the conductivity total of Table 5.5. The result is a conductivity of 1.3552 $Sm^{-1}$. This value accords reasonably well with figures quoted by other workers [2].

Table 5.6 gives the conductivities calculated, using equation (5.6), from the equivalent conductivities in Table 5.4 and the molar concentrations in Table 5.5.

Using the conductance ratio ($\kappa$=0.78) to correct the total conductance in Table 5.6 gives a resultant value of 1.3552 $Sm^{-1}$. This compares very well with the conductivity calculated using equation (A.12) and serves as a verification of the analysis of Appendix A.

From Table 5.5 it can be seen that the relaxation frequencies, $f_R$, for the major ions in OPC paste water range from 4791.4 GHz up to 14399.6 GHz. Wilson [2] calculates a relaxation frequency for the $OH^-$ ion of ≈40 GHz by assuming that the ion mass is effectively increased by the additional mass of 100 solvation molecules (thereby increasing the value of $\tau$ calculated from equation (A.6) by a factor of $>10^2$). This seems rather a large mass increase since the molecules in such a large solvation sheath are not necessarily all immobilised in the ion vicinity and are therefore not actually part of the accelerated mass [70]. In the case of the hydroxyl ion, for instance, the effective mass increase due to solvation would result from the addition of about four water molecules [34] (the rest of the solvation sheath being only loosely bound), which would reduce the relaxation frequency from ≈4.8 THz to ≈0.9 THz (the mass of a water molecule being $3.012\times10^{-26}$ kg [21]). The relaxation frequencies of the other ions in Table 5.5 might be similarly reduced but will still remain far higher than the frequencies of interest to this work (the $OH^-$ ion having the lowest relaxation frequency of the group). However, there is good reason to suppose that the solvation sheath size may be effectively neglected due to the mode of transfer of the hydroxyl ion through the solution. The large value of mobility attributed to the hydroxyl ion (Table 5.4) results from the fact that the propagation of this ion is by proton transfer along chains of water molecules (the "Grotthus chain" mechanism [69][21]) rather than from direct transfer of the ion itself. Thus, the hydration sheath of a hydroxyl ion will play very little part in its apparent movement under an electric field. From Table 5.5 it can be seen that the hydroxyl

ion contribution to the conductivity is around 70% of the total and that for dielectric constant it is around 80%. This means that the bulk of the conduction mechanism contribution to the dielectric constant of the mix water will be unaffected by hydration sheath mass increase. Even allowing for the mass increase proposed by Wilson, the lowest resultant frequency of relaxation (44.5 GHz for the $OH^-$ ion with the others all $\gg$100 GHz) still suggests the conclusion that no dielectric *dispersion* attributable to electrophoretic-type ionic effects need be considered here.

The main interest for this work is in the negative contribution to dielectric constant and the likelihood of ionic movement producing negative dielectric constants in fresh concrete (c.f. chapter 1). From table 5.5 a value of $-5.649\times10^{-3}$ is seen to be the total contribution to the dielectric constant of the paste water. This should also be corrected for the ionic interactive effects which occur at finite dilutions by use of the conductance ratio, $\kappa$. Since $\Delta\varepsilon_r'$ is proportional to $\mu^2$ (see equation (A.11)), the above figure is multiplied by $\kappa^2$ (=0.6084). From Malmberg and Maryott [62] the dielectric constant of water, $\varepsilon_{rw}'$, at 20.0°C is 80.103, and this value will be reduced by the electrophoretic movement of ions in cement paste water to :

$$\begin{aligned}\varepsilon_{rpw}' &= \varepsilon_{rw}' + \Delta\varepsilon_{re}' \\ &= 80.103 - (0.6084 \times 5.649 \times 10^{-3}) \\ &= 80.100\end{aligned}$$

Equation (A.11) shows, however, that $\Delta\varepsilon_r'$ is proportional to the mass of the particles, which may be increased due to the ionic solvation sheath as described above. If an extreme mass increase of a factor of 100 is applied to all the ions then the overall value of $\Delta\varepsilon_r'$ will be increased proportionately to -0.344, resulting in a dielectric constant for the mix water of 79.759. This is still a very small value of increment and could in no way account for the occurrence of a negative dielectric constant for concrete.

The contribution of the electrophoretic movement of ions to the dielectric constant of cement paste water is therefore minimal in comparison to other mechanisms and may be ignored for practical purposes.

One further qualitative argument can be raised against the validity of the electrophoretic conduction explanation of negative dielectric constant. Water promotes the ionisation of ionic compounds by virtue of its relatively high dielectric constant, which reduces the force acting between oppositely charged ions according to Coulombs law [21]:

$$F = \frac{z_+ z_- e^2}{\varepsilon_r \varepsilon_0 d^2}$$

where,

F is the force acting between the two ions (N)
$z_+$ is the charge number of the positive ion
$z_-$ is the charge number of the negative ion
e is the charge on an electron ($1.6021 \times 10^{-19}$ C)
$\varepsilon_0, \varepsilon_r$ are defined as before

If the electrophoretic movement of ions in the mix water of concrete were to cause the dielectric constant of the resulting solution to drop below a certain threshold no further ionisation of the solute would be possible, thus any further drop in dielectric constant would be prevented. In practice the electrophoretic reduction to dielectric constant is too small to promote this effect, but even if it was large enough to reach the threshold of ionisation the dielectric constant could certainly never be forced below zero.

Table 5.7 lists the effect on the dielectric constant and relaxation wavelength of cement paste water caused by the ions according to the increment values given in Table 5.2 after Hastead [61], and calculated using equations (5.3) and (5.4). These are the effects caused by the disruption of hydrogen bonds in the water structure as described in section 5.1.2.

| Ion | c | $\Delta\varepsilon_r'$ | $\Delta\lambda_r$ |
|---|---|---|---|
| $OH^-$ | 0.0681 | -0.885 | -27.24 |
| $0.5Ca^{2+}$ | 0.0394 | -0.906 | -55.16 |
| $K^+$ | 0.0206 | -0.165 | -16.48 |
| $0.5SO_4^{2-}$ | 0.0181 | -0.127 | -39.82 |
| $Na^+$ | 0.0050 | -0.040 | -4.00 |
| | Totals→ | -1.578 | -118.84 |

**Table 5.7 Effect of Ions on Dielectric Properties of Mix Water**

where, $\Delta\lambda_r$ is in μm.

The total values given in Table 5.7 are not simply the sums of the individual increments but are calculated as described in the footnote to Table 5.2.

The resulting static dielectric constant, $\varepsilon_{rs}'$, and relaxation frequency, $f_R$, of the mix water are 78.525 and 17.274 GHz respectively (compared to 80.103 and 17.157 GHz for de-ionised water). It is notable that the increment in the dielectric constant of the water is larger for the destructuring effects of the ions than for the predicted effects of ionic electrophoretic movement. Since the dielectric increments given in Table 5.2 are the result of experimental observation [70] it must be assumed that they include the electrophoretic effects, which further corroborates the conclusion that such effects do not cause the dielectric constant of concrete to become negative.

Table 5.8 shows the predicted dielectric and conductivity parameters for mix water at decade intervals over 1-1000 MHz at 20°C. These values include the dielectric and D.C. conductivity of pure water modified from Table 1 in accordance with the change in relaxation frequency calculated above.

| | 1 MHz | 10 MHz | 100 MHz | 1000 MHz |
|---|---|---|---|---|
| $\varepsilon_r'$ | 78.525 | 78.525 | 78.523 | 78.281 |
| $\sigma$ ($Sm^{-1}$) | 1.3552 | 1.3552 | 1.3576 | 1.5896 |

**Table 5.8 Dielectric Parameters of Mix Water at Decade Intervals (1-1000 MHz)**

### 5.1.4 Bound and Interfacial Water

The properties of water are changed when it is bound either physically or chemically, as is the case in hydrating cement paste. Neville [9] gives figures of 12% and 24% for the gel water content of 0.475 w/c ratio cement paste at 50% and 100% hydration respectively. The corresponding capillary water contents are given as 33.5% and 7.0%. It is to be expected that the dielectric properties of this bound water, and the relative volume changes with time, will influence the electrical properties of the cement paste.

Hastead [64] points out that the dielectric properties of bound water are not fully understood but assumes that they lie somewhere between those of ice and those of liquid water. Hastead gives the activation energy of water molecule reorientation in the liquid state as ≈4.5 $kcal.mol^{-1}$ (the energy required for the breaking of one hydrogen bond), while that of the same process in a single ice crystal is ≈13 $kcal.mol^{-1}$ (the energy required for the breaking of three hydrogen bonds). The reorientation energy of bound water has been found to lie between these two values in two loose groupings which each give evidence of a spread of relaxation times.

Palmer et al. [73] presented the results of preliminary experiments in which the dielectric properties of layers of water trapped between thin mica plates were investigated. At frequencies of 2 and 3 MHz they found that the dielectric constant decreased with the thinness of the film from >20 at 5 μm to <10 for thickness <2

μm. In very wet composite materials of similar structure the dielectric constant of the water never exceeded 60. The relaxation frequency of this interlayer water was found to lie somewhere in the kHz/MHz region.

Thompson [74], de Loor [75] and Hastead [64] each present graphical evidence that in a moist heterogeneous material the dipolar relaxation of some forms of bound water occurs in the 1-1000 MHz range and most likely in the 100-1000 MHz range, with dielectric loss for bound water at 100 MHz being significantly higher than that of free water, as well as of both ionic conductivity loss and Maxwell-Wagner loss. This is represented in Figure 5.2. The water of crystallization in inorganic crystalline hydrates (e.g. some forms of CSH gel) usually undergoes a relaxation process in the kHz region, indicating that its properties are perhaps much closer to ice than bulk water. Another significant loss mechanism in aqueous heterogeneous materials is surface conductivity, which operates at interfaces where thin layers of bound (i.e. adsorbed) water containing ions are present. This mechanism is generally thought to be operative at 1 kHz up to 10 MHz but could be significant between 10 and 1000 MHz.

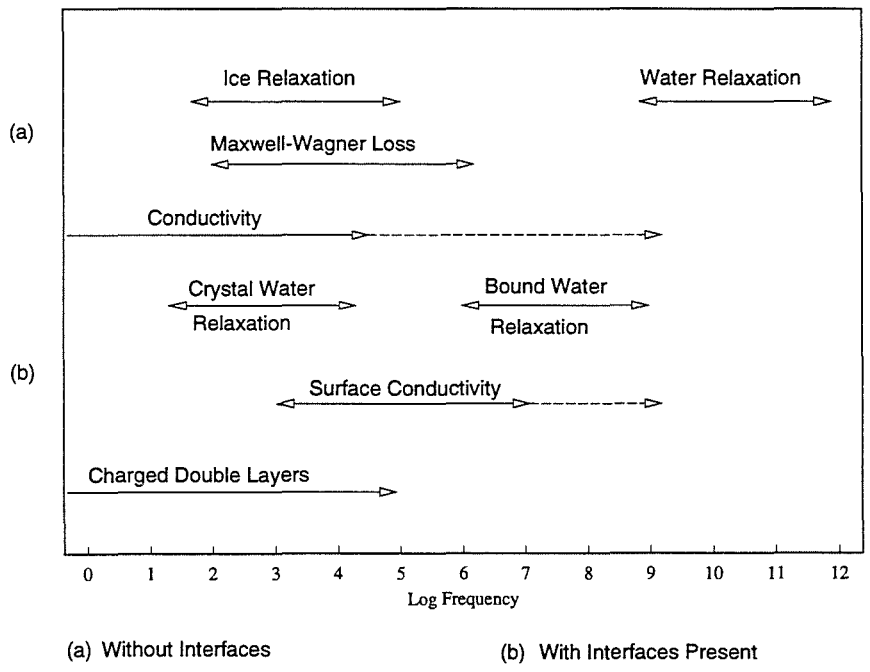


**Figure 5.2 Loss Mechanisms in Aqueous Heterogeneous Materials**

Clifford [76] has surveyed the available literature on previous experimental and theoretical investigations into the general properties of water in thin films and capillaries. His conclusion is that current understanding of water in such circumstances is far from complete. However, with respect to the electrical properties, a number of findings are of interest here. The viscosity of water in quartz capillaries of diameter 0.1 - 2.0 μm was found to be greater than the normal bulk viscosity. For a diameter of 0.1 μm the increase was by a factor of 1.5. This could indicate an altered structure in the water adsorbed to the capillary surface. Other workers have reported no increased viscosity for pores as small as 4.5 - 30 nm, but the same investigators did find reduced diffusion rates for small uncharged molecules in the same pores. While viscosity is not itself an electrical property, the fact that water adsorbed onto a capillary surface is found to be more viscous than the bulk material suggests that the orientation of such molecules in an alternating electric field will be partly curbed with a consequent reduction in dielectric constant and relaxation frequency. However, another investigation reported that in pores of 3 nm diameter etched in mica sheets the ionic conductivity of a 0.1 mol.litre$^{-1}$ solution of potassium chloride was not affected. All of these pore systems are of similar dimensions to the gel and capillary pores found in cement paste.

Clifford states that in thin films and pores the dimensions of the film or pore may affect the properties of water directly by not allowing sufficient space for the bulk structure to develop. However, it is still not clearly known what constitutes sufficient space. Estimates vary between 0.6 and 6 nm, with more recent investigations supporting the smaller figures. It can be definitely stated that where films are less than 50 nm thick electrostatic double layer effects will alter the properties of water. Also, for films of water less than three molecules or so thick, the behaviour at a surface or in a pore will be determined by interactions with the surface and will differ considerably from bulk water. Water layers thicker than 1 μm can be assumed to posses bulk properties, but the properties in layers/pores of 1 nm to 1 μm thickness are not yet established although recent evidence suggests that the influence of a surface does not extend much more than ≈10 nm. These dimensions include all the gel pores and a large number of the capillary pores in a typical cement paste which suggests the possibility that much of the water retained in a paste, even of the evaporable type, could exist in an altered structural form.

This is especially likely because, as Clifford also points out, water has a tendency to create pores and indentations on the surfaces of many materials by small scale chemical attack and dissolution with the result that even in relatively large pores (>1 μm) much of the surface water can effectively be constrained in small molecule sized spaces created by surface imperfections and macromolecular chains. The true surface area in such cases may be many times the superficial area. It is very possible that such surface conditions may be found in the randomly formed capillary network of cement paste.

Clifford also considers investigations which have been made into the properties of "anomalous" water (also known as polywater). The existence of this form of water is still very much a subject of debate but it appears that water condensed into narrow capillaries (<2 μm in diameter) often posseses properties very different to that of the bulk form. Greatly enhanced viscosity (up to a factor of 20) which disappears on movement of the sample and reappears after settling is one such property. The electrical conductivity of anomolous water in glass capillaries was found to be ≈0.1 $Sm^{-1}$ which is very high (c.f. ≈$4\times10^{-6}$ $Sm^{-1}$ from Table 5.1). At present it is not clear whether the observed anomalous properties are the result of contaminants from the silica surfaces of the capillaries or of the presence of a polymeric form of water. The anomalous effects have not been observed when water is drawn into the capillaries from a bulk source or when the capillaries are open into water having bulk properties, only when they are isolated. Nevertheless, the fact that such alterations to the properties of water in small quartz and glass capillaries have been observed is of some interest when considering the likely properties of water in the pore structure of cement paste. Such absorbed water may be structurally altered and yet remain "free" in the sense of being readily evaporable.

Hastead [64] has contrasted the qualitative differences between the frequency dependence of the dielectric properties of moist brick and moistened hydrated OPC paste at low temperatures. His conclusion is that the brick properties are dominated by Maxwell-Wagner effects arising from absorbed capillary water, while the cement paste properties are dominated by bound water relaxation which maximizes at ≈10 kHz. Evidence for this is inferred from the fact that there is no freezing point discontinuity in the dielectric properties of cement paste, while in moist brick a

temperature discontinuity is observed at 2°C. Hastead also states that the dielectric loss of hydrating cement changes exponentially with temperature, yielding an energy of activation of 13 kcal.mol$^{-1}$, which, being close to that of ice, is an acceptable indicator of bound water. These results suggest that it is the effects of tightly bound water (water of crystallisation in cement paste gel) which have been observed, hence the low frequency relaxation process (c.f. Figure 5.2). Water which is more loosely bound would show dipolar relaxation in the RF range (100-1000 MHz).

### 5.1.5 Colloidal and Surface Double Charge Layers

Fresh cement paste is essentially a colloidal suspension of cement grains in aqueous solution. Various workers [47][49][55][57] have cited colloidal properties as being at least partly responsible for the observed dielectric properties at various frequencies. Such properties are therefore considered here.

The surface of a solid becomes electrically charged when placed in contact with an ionic aqueous medium; the potential acquired at the interface thus attracts oppositely charged ions to the surface vicinity and establishes an electrical double layer at the solid/liquid interface. For colloidal particles the double charge layer is essentially the spherical analogue of the double charge layer formed at the surface of electrodes in an electrolytic solution as described in 3.2.4. Under the influence of an electric field the double layer can be highly polarizable, leading to a large enhancement of dielectric constant for the overall suspension.

Schwan et al. [77] investigated this effect for a suspension of polystyrene particles in potassium chloride solution. Solutions of ionic conductivity 0.05 to 0.2 Sm$^{-1}$ were used with four different diameters of particle ranging from 0.0878 to 1.17 μm suspended at various volume fractions. Particle diameter for each individual experiment was kept very uniform. Very large static dielectric constants were obtained for the suspensions. For instance, for particles of diameter 1.17 μm at a volume fraction of 0.22 in a KCl solution of conductivity 0.081 Sm$^{-1}$, a value of $37\times10^4$ was obtained for static dielectric constant and 560 Hz for relaxation frequency. At higher volume fractions and solution conductivities this figure fell but still remained very high. Dielectric constant was found to increase with particle

radius, while relaxation frequency fell with the square of particle radius. To explain the experimental results of Schwan et al., Schwarz [78] developed expressions for the enhanced static dielectric constant and relaxation time constant of colloidal particles based on the concept of a frequency dependent particle surface admittance. This included a frequency dependent capacitance resulting from the effects of ionic diffusion in the double charge layer. Schwarz assumed that the double layer was of negligible thickness in comparison to particle radius and that the ions in the double layer had mobility along the particle surface but not in any other direction. Expression (5.11) describes the enhancement of particle relative permittivity according to Schwarz :

$$\Delta\hat{\varepsilon}_{rp} = \frac{2q\mu_s\delta_q\tau_R}{r\varepsilon_0} \cdot \frac{1}{1+j\omega\tau} \qquad \cdots(5.11)$$

where,

q is electron charge (C)
$\mu_s$ is ionic surface mobility ($m^2s^{-1}V^{-1}$)
$\delta_q$ is surface charge density ($m^{-2}$)
$\tau_R$ is relaxation time constant (s)
r is particle radius (m)

The time constant, $\tau_R$, is determined by diffusion processes in the double layer and is found from equation (5.12).

$$\tau_R = \frac{qr^2}{2\mu_s kT} \qquad \cdots(5.12)$$

where k is the Boltzmann constant and T is absolute temperature (°K).

From other results given by Schwan et al. the relaxation frequency for polystyrene spheres of radius 0.094 $\mu m$ in KCl solution was 15 kHz, which gives a time constant of $1.061\times10^{-5}$ s. Substitution of this value into equation (5.12) gives a surface ionic mobility for potassium ions of $1.649\times10^{-8}$ $m^2s^{-1}V^{-1}$ at 25°C ($1.493\times10^{-8}$ at 20°C) which is significantly reduced from the bulk solution value (c.f. table 5.4). Surface

charge density ($\delta_q q$) for colloidal particles has a maximum value of 1.6021 $Cm^{-2}$ (Schwan et al. quote a figure of ≤10 elementary charges per $nm^2$ of surface), howevever Bolt [79] suggests a value of 0.24 $Cm^{-2}$ for amorphous silica grains in an alkaline electrolyte which is perhaps more applicable to cement paste. Fresh OPC paste will contain a range of particle radii from 5 to 45 μm (section 2.1.1) which according to equation (5.12) gives a range of relaxation frequencies of 0.05 to 3.9 Hz with a value of 0.15 Hz for particles of mean radius (25 μm). Equation (5.11) yields static dielectric constant increments in the range $5.363\times10^6$ to $4.831\times10^7$, with a value of $2.681\times10^7$ for particles of mean radius. It should be noted that these are for the colloidal (i.e. cement) particles and not the overall suspension (i.e. cement paste). These dielectric constant contributions are huge but the relaxation frequencies are very low indeed and seem to suggest that, despite very large *static* dielectric constant contributions, colloidal double charge layer polarisation, as interpreted by the Schwarz model, will not contribute significantly to cement paste polarization at frequencies above ≈1000 Hz.

However, the model proposed by Schwarz has been criticised for being somewhat ad hoc, particularly with respect to the assumed tightly bound double layer. Chew and Sen [80][81] have analysed the surface admittance of colloidal particles in terms of a diffuse double layer, similar to the system described in 3.2.4, and have produced the expression given in equation (5.13) to describe the static dielectric increment, $\varepsilon_{ss}$, in the dielectric constant of colloidal particles.

$$\varepsilon_{ss} = 36 v_i \varepsilon_{sw}' \frac{t^2}{(1-t^2)^2} \qquad \cdots(5.13)$$

where,

$v_i$ is the volume fraction of particles in suspension
$\varepsilon_{sw}'$ is the static dielectric constant of the solution
t is a numerical calculation factor

The value of t is found from equation (5.14), which is given by Chew and Sen. This expression is based on the Boltzmann distribution in terms of the double layer potential :

$$t = \tanh\left(\frac{zq\zeta}{kT}\right) \qquad \cdots(5.14)$$

where, k and T are identified as for equation (5.12), q is electron charge, z is the valence of the ions and $\zeta$ is the zeta potential of the double layer, as defined in section 3.2.4.

In the analysis by Chew and Sen [81] the dielectric constant enhancement of the particles is not due to induced interfacial charges as is the case in the Schwarz model and with Maxwell-Wagner enhancement (see 3.2.3), but depends on an induced diffusion cloud of ions which extends far beyond the boundary of the unperturbed double layer. Chew and Sen describe the process of polarization enhancement as follows : in the presence of an external electric field a large counter ion current flows in the double layer region, causing charges to pile up at tne ends of the particle. These excess charges discharge into the bulk solution by a process of diffusion as well as by conduction. The process sets up a diffusion cloud of size $\sqrt{2D/\omega}$ which at low frequencies ($\omega \rightarrow 0$) can become very large. D is the diffusion coefficient ($m^2s^{-1}$). Since the cloud will reach its maximum size at the turn around point of the alternating field, the diffusion current is out of phase with the field, which in turn causes the circumferential current in the double layer to be out of phase. This situation creates an out of phase dipole moment on the particle which greatly enhances the dielectric constant of the particle. At high enough frequencies there is insufficient time for the diffusion cloud to build up so that the induced out of phase dipole moment becomes negligible and the dielectric enhancement disappears.

Chew and Sen have also found that the relaxation response of the diffusion polarization mechanism has a broader frequency characteristic than the classic Debye response such that the factor :

$$\frac{1}{1 + j\omega\tau_R} \qquad \cdots(5.15)$$

of the standard Debye equation is replaced by the more gradual relaxation of :

$$\frac{1}{1+\sqrt{j2\omega\tau_R}+j\omega\tau_R} \qquad \cdots(5.16)$$

The relaxation time constant, $\tau_R$, is found from equation (5.12) as for Schwarz [77]. An alternative expression from Chew and Sen is :

$$\tau_R = \frac{r^2}{2D} \qquad \cdots(5.17)$$

where, r is particle radius, and D is diffusion coefficient. Comparison of (5.17) with the expression for diffusion cloud size above shows that the diffusion cloud size is equal to the particle radius at the relaxation frequency. By comparison of equation (5.17) with equation (5.12) an expression for the diffusion coefficient is found :

$$D = \frac{\mu_s kT}{q} \qquad \cdots(5.18)$$

Thus, the relative permittivity of a colloidal inclusion particle suspended in an ionic solution is :

$$\hat{\varepsilon}_{ri} = \varepsilon_{rp} + 36 v_i \varepsilon_{sw}' \frac{t^2}{(1-t^2)^2} \cdot \frac{1}{1+\sqrt{j2\omega\frac{r^2}{2D}}+j\omega\frac{r^2}{2D}} \qquad \cdots(5.19)$$

where, $\varepsilon_{rp}$ is the unenhanced dielectric constant of the particle material.

This model was developed by Chew and Sen [81] to explain the part played by double layer ionic polarization at the rock/water interfaces found in the pore structure of sedimentary rocks [80]. In fact, it has not yet been applied quantitatively in such situations because rock pore structures are not amenable to simple mathematical treatment in the same way as spherical colloidal particles. Nevertheless, application to ionic solution filled pores is still of obvious interest in the study of concrete because of the pore structure in the hardening material which is likely to have similarities to that of sedimentary rocks. If the solution filled pores could be considered as "inside out" colloidal particles then some form of treatment

on simplified geometries might be possible. The simple point to be made is that while hardened cement paste is not a colloidal suspension the mechanism of double layer polarization considered above may still contribute to an enhanced low frequency dielectric constant due to the polarization of charges at gel/water interfaces.

To calculate the actual dielectric response of an aqueous colloidal suspension for the above effect, expression (5.18) should be substituted into expression (3.35), which describes the Maxwell-Wagner effect for a suspension of spherical inclusions in a host medium. The dispersion of the host medium should also be included, if appropriate to the frequency range of interest. This produces a frequency dispersion which depends on a combination of Maxwell-Wagner and double layer diffusion effects as well as possibly dipolar dispersion. The application of this theory to fresh cement paste is considered in section 5.2.

Sen and Chew [80] suggest that the hydration and silanation of dangling oxygen atoms on the surface, and hydration of counterions near the surface, of quartz (sand) affects the rotation of water molecules, giving rise to a relaxation phenomena in the upper megahertz range. This mechanism could well be operative in the pore structure of hardening cement paste. They do not quantify this effect, however.

## 5.2 Dielectric Properties of Cement Paste

The dielectric constant of dry OPC is not expected to show any dispersion in the frequency range of interest. Wilson [2] assumes a value of 7.0 for both OPC and dry cement paste based on consideration of the dielectric constant of a range of dry rocks and minerals. This is the value assumed in this work. This section is concerned with an examination of the possible polarization mechanisms operating in cement paste both in the fresh (unset) state and the hardening state.

### 5.2.1 Setting Cement Paste

As pointed out in section 5.1.5, *fresh* cement paste may be regarded as a colloidal-like suspension of cement grains in aqueous electrolytic solution. This situation comes about because of the initial reaction of $C_3S$ with water which

promotes the rapid leaching from grain surfaces of (primarily) $Ca^{2+}$ and $OH^-$ ions, leaving behind surface layers rich in hydrosilicate ions which consequently acquire a net negative charge [55]. The grain surfaces very quickly become coated with CSH gel and are surrounded by a diffuse electrical double layer of ions. This is shown schematically in Figure 5.3.

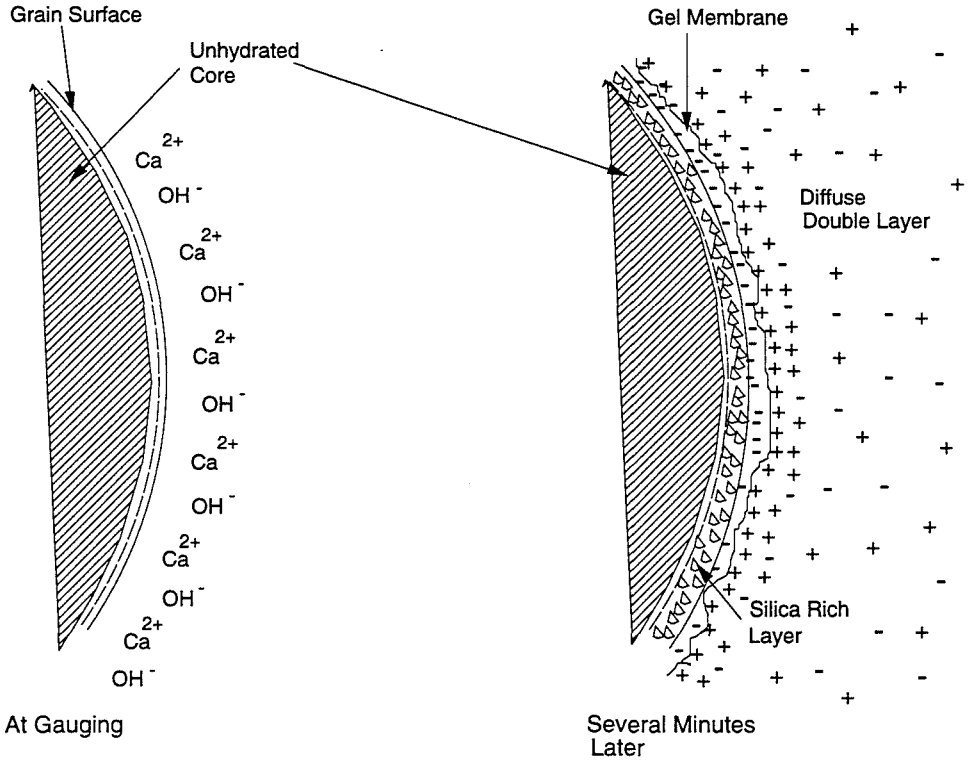


**Figure 5.3 Schematic Representation of Hydrating Cement Grain**
(after McCarter and Afshar [55])

The grain surfaces remain in the condition represented in Figure 5.3 during the induction period (approximately the first 3 hours - section 2.1.3), although the ionic concentration of the mix water gradually increases during this time as reactions continue beneath the semi-permeable gel membrane. For an ambient temperature of 20°C the ionic content of the mix water will be as described in section 5.1.3 at around 2 hours, resulting in a conductivity of 1.3552 $Sm^{-1}$, a static dielectric constant

of 78.525 and a dipolar relaxation time of $9.2136\times10^{-12}$ s. Assuming the grains are spherical (a reasonable assumption considering the grinding process during manufacture - section 2.1.1), with a radius of 25 μm (the average for OPC), then the frequency dependent conductivivty and dielectric constant for the cement paste at this time may be calculated from equation (3.35) by including a relative permittivity for the inclusions calculated from equation (5.19), and for the host material (mix water) from equation (3.19) plus an additional term ($\sigma_{DC}/(j\omega\varepsilon_0)$) to account for the D.C conductivity.

The value of $v_i$ in equation (3.35) can be calculated from the water/cement ratio of the paste by using a specific gravity, $sg_c$, for OPC of 3.15 $g.ml^{-1}$ [9]. The conversion equation is :

$$v_i = \frac{1}{1+(w/c)sg_c} \qquad \cdots(5.20)$$

No available figures were found for the zeta potential, ζ, of cement or cement gel, but Sen and Chew [80] give a value of 80 mV for quartz in contact with aqueous electrolyte. It is assumed that a similar figure can be used for cement particles. A value of 82.0 mV was used in the calculations for Figure 5.4.

The cations in the double layer around the grains are primarily calcium ($Ca^{2+}$) with a valence number z of 2. However, there are also univalent (z=1) sodium ($Na^+$) and potassium ($K^+$) ions in lower concentrations. The author decided, therefore, that an average value of z, obtained from a consideration of the ionic concentrations given in Table 5.5, should be estimated for use in equation (5.14). A value of 1.606 was calculated.

The diffusion coefficient can be calculated from equation (5.18), which requires a value for ionic mobility in the double layer. Due to the presence of the $Ca^{2+}$, $K^+$ and $Na^+$ ions, it was decided that an equivalent mobility calculated from a weighted average of the individual mobilities of should be used. From section 5.1.5 the value for potassium at 20°C is $1.493\times10^{-8}$ $m^2s^{-1}V^{-1}$, and the values for calcium and sodium have been calculated from Table 5.4 by assuming that they are reduced from their bulk solution values by the same factor as that of potassium.

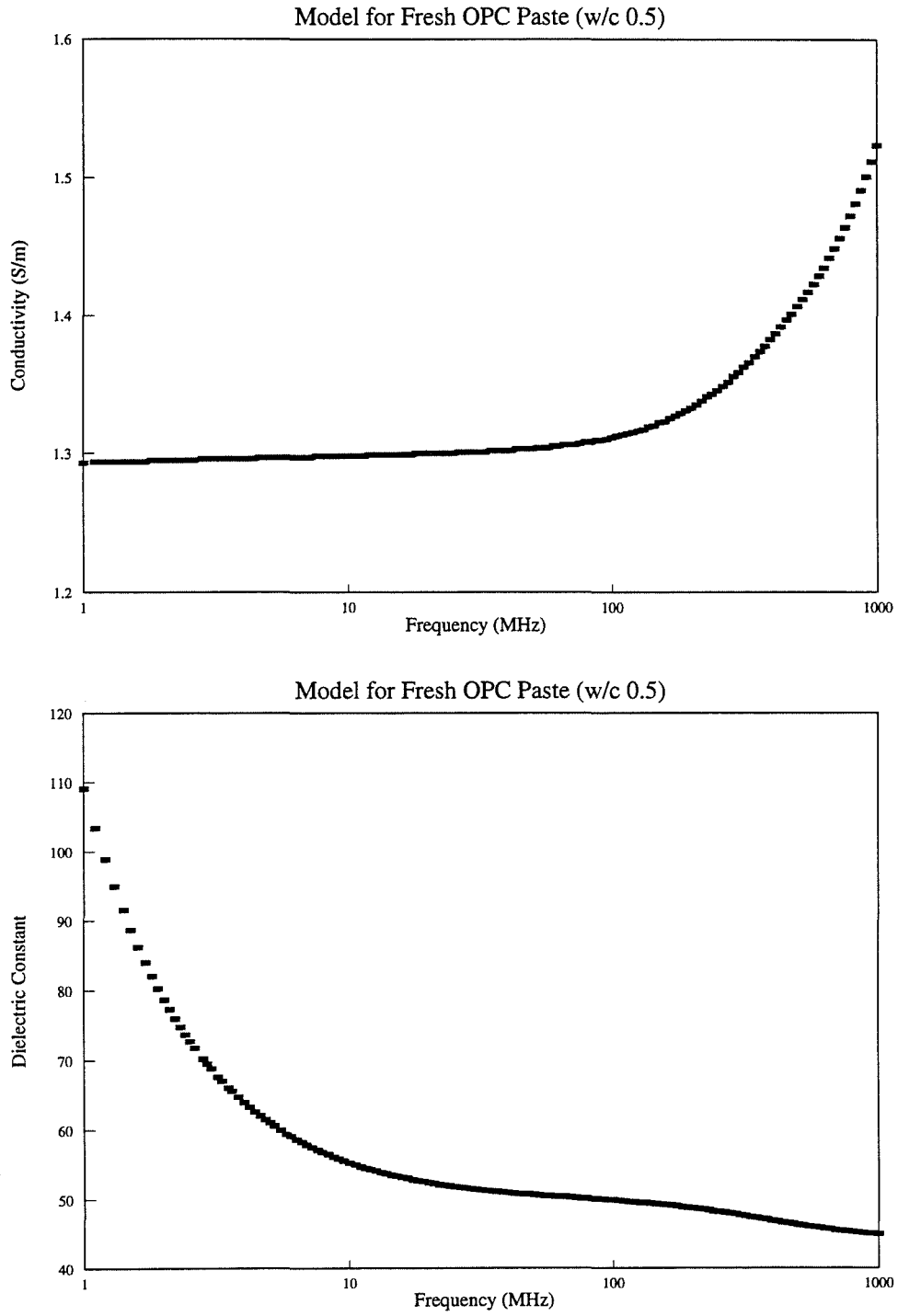


**Figure 5.4 Electrical Parameters for Fresh OPC Paste Model (w/c 0.5)**

This gives $1.197\times10^{-8}$ for calcium and $1.007\times10^{-8}$ for sodium. From these an effective surface ionic mobility for cement paste ions is calculated to be $1.246\times10^{-8}$ $m^2s^{-1}V^{-1}$. This in turn gives a diffusion coefficient of $D=3.146\times10^{-10}$ $m^2s^{-1}$.

The above figures give a static dielectric constant increment for the cement grain double layer of $\varepsilon_{ss}$ =1.0178149×10$^{11}$, and a relaxation time constant of $\tau_R$=0.9933 s ($f_R$=0.16 Hz).

A water/cement ratio of 0.5, giving cement volume fraction $v_i$=0.388, was assumed, and the above parameter values were used to model the complex relative permittivity of cement paste in accordance with equation (5.19). A relaxation time constant spread parameter ($\beta$=0.002) was used in equation (5.19) in accordance with equation (3.45) to account for the distribution of particle size likely to be found in OPC. The results for conductivity and dielectric constant over the frequency range 1-1000 MHz are shown in Figures 5.4a and 5.4b.

The conductivity dispersion agrees very well with results presented by Olp et al. [57] (section 4.2.7) for OPC paste of w/c 0.5 over the range 1-300 MHz. Olp et al. give a conductivity of ≈1.45 $Sm^{-1}$ increasing to ≈1.5 $Sm^{-1}$ over this range at 2 hours after gauging compared to 1.293 increasing to 1.360 for the model. Their results were obtained for an ambient temperature of 25°C (T=298°K), however, which would tend to increase the conductivity in comparison to the model. Using the temperature coefficient of resistivity given by Whittington et al. [43] for hardened cement paste (-0.022(°C)$^{-1}$) to convert the model values to 25°C equivalents gives 1.453 $Sm^{-1}$ at 1 MHz increasing to 1.528 $Sm^{-1}$ at 300 MHz. In view of the temperature difference, plus the various approximations involved in the calculation of the model parameters, the predicted conductivity is remarkably close to the measured results. The increase in conductivity shown by the model between 200 and 1000 MHz is due to dipolar relaxation in the mix water. Olp et al. [57] came to the same conclusion for their conductivity measurements obtained in the in the same range.

The dielectric constant dispersion for the model also agrees well over the 1-300 MHz range with the results of Olp et al., who give a value of≈62 at 1 MHz

decreasing to ≈44 at 300 MHz. The 1 MHz value of the model is higher than the measurement, perhaps indicating a slightly different relaxation time for the double layer polarization, but it may also be because the assumed spread of relaxation times used for the model differed from the practical case. The value at 300 MHz is in good agreement. It is interesting to note the predicted relaxation evident in the 100-1000 MHz range. No other source of data for fresh cement paste at these frequencies was found in the literature by the author at the time of writing.

The model was also used to calculate dielectric constant values for fresh cement paste of w/c 0.3 at low frequencies ($10^2$-$10^5$ Hz). This was done to allow comparison of the predicted values with those measured by McCarter and Afshar [55][56] and McCarter and Curran [47] for similar cement paste, which had suggested that cement paste was highly polarizable at lower frequencies. The results are presented in Figure 5.5.

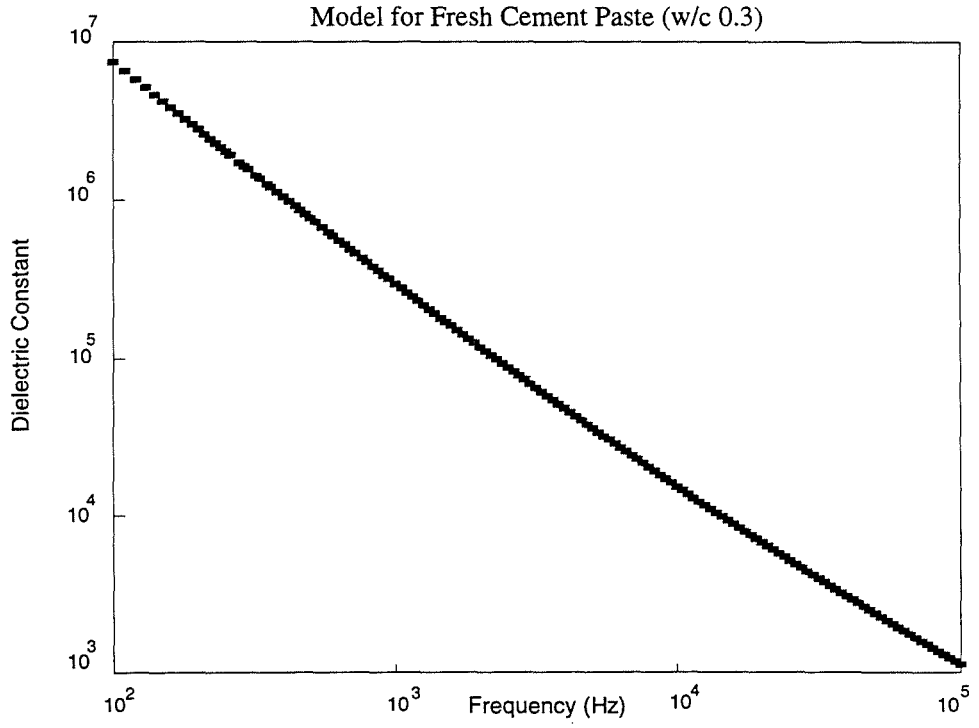


**Figure 5.5 Model Dielectric Constant for w/c 0.3 at $10^2$-$10^5$ Hz**

The model predicts extremely large values for dielectric constant at low frequencies, which is in fair agreement with the findings of McCarter (section 4.1.2) [47][55][56] although the values suggested by Figure 5.5 are almost one order of magnitude lower than McCarter's at 1000 Hz ($\approx 3\times10^5$ as compared to $\approx 10^6$). This may be due to the effects of electrode polarization which McCarter and Curran [47], and McCarter and Afshar [55][56], did not take into account, and would be consistent with the findings of Scott et al. [41] as considered in section 3.2.4.

On the whole the model performs reasonably well at low frequencies and very well in comparison to known data at radio frequencies. This suggests that colloidal double layer effects and dipolar relaxation are the dominant polarization mechanisms in fresh cement paste.

A Mathcad version (see section 6.2.2) of the model algorithm is presented in Appendix B.

### 5.2.2 Hardening Cement Paste

The properties of hardened cement paste are likely to be more difficult to model than those of fresh paste because of the more complicated structure which develops as hydration proceeds.

After the induction phase is over the semi-permeable gel coating on the grain surfaces is ruptured by the osmotic pressure of hydration products which have built up inside due to the imbibing of water. At this stage fibrillar outgrowths of fine grained CSH gel are formed from the grain surface and begin to extend towards other grains [18][19][20]. Also, platey crystalline calcium hydroxide (portlandite), which begins to form by precipitation during the induction phase, becomes more evident in the mix water. In this way the interstitial spaces between grains are gradually filled in (section 2.1.3). This is shown schematically in Figure 5.6 (after Birchall et al. [20]).

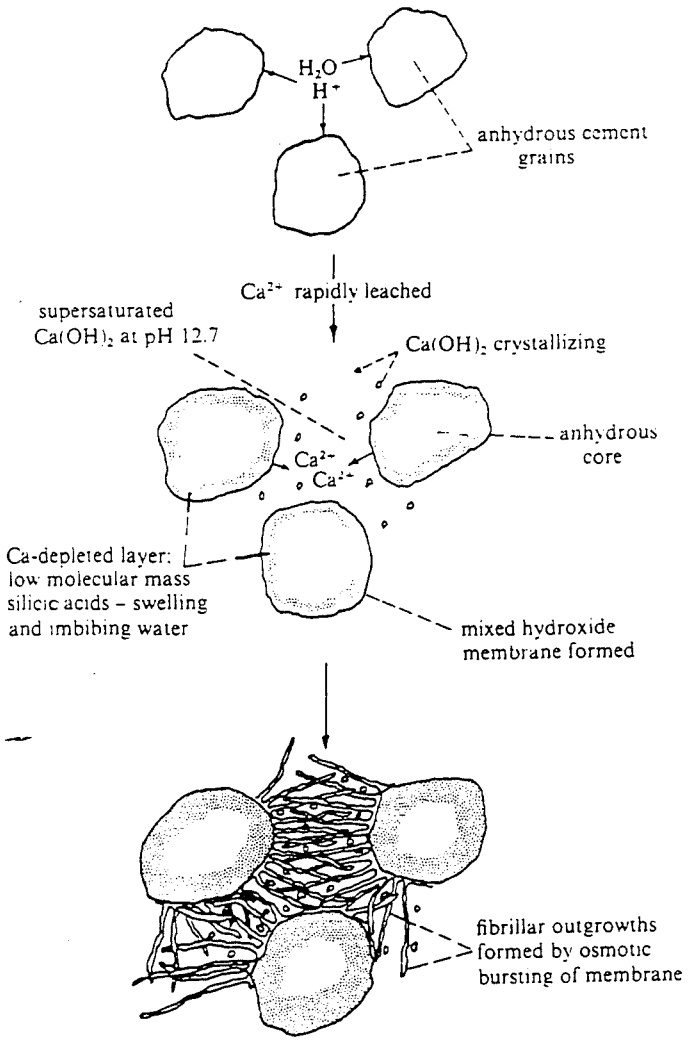


**Figure 5.6 Development of Gel in Hardening Cement Paste**

The rupture of the gel coating will inhibit the effects of double layer polarization on the surface of the cement grains, thereby reducing the contribution of this mechanism to the dielectric constant of the paste. Also, the infilling of the interstitial spaces by CSH and CaOH will reduce the effective cross-sectional area of the conducting electrolytic solution, leading to a reduction of paste D.C. conductivity, an effect which is compounded by the increasing tortuosity of the conduction paths. This aspect of conductivity will also decrease due to reduction in the ionic content of the water as hydration progresses (Figure 2.2).

The free water content of the mix will decrease as water is used up in the reactions of hydration and becomes bound in various ways in the hardening paste matrix. Thus, the direct contribution of dipolar polarization in free water to the overall paste polarization can also be expected to decrease as hydration proceeds and the dipoles become irrotationaly bound to varying extents.

The model for fresh cement paste proposed in section 5.2.1 will therefore become inappropriate from the point of setting onwards.

Hardened cement paste is a matrix of solid material (CSH gel) permeated by a random network of interconnected capillary pores. Wilson [2], and Wilson and Whittington [5] have envisaged the pore network as a random distribution of high aspect ratio prolate ellipsoids filled with conducting electrolyte. Based on this model they have used Fricke's equations [33] (section 3.2.3) to model the effective dielectric constant of concrete at one day after gauging. However, Wilson's model [2] assumes a segmented network of straight pores of diameter 1.3 μm and length 40 mm in paste of 12% porosity (assuming the cement paste to be 50% hydrated [9]). According to calculations by the present author, this results in static and infinite frequency dielectric constants of 155 and 11.31 respectively, and a relaxation frequency of ≈300 kHz. These results in turn mean that no appreciable dispersion will be apparent over the 1-1000 MHz range, the dielectric constant staying constant at ≈11.3. This is not consistent with the findings of Olp et al. [54] who found a dielectric constant for cement paste at 24 hours after gauging of ≈350 at 1 MHz falling to ≈40 at 300 MHz.

The capillary network is unlikely to conform to the Fricke model for two primary reasons. Firstly, for 24 hour old cement paste of water/cement ratio 0.5, the capillaries will form a continuous network rather than a segmented distribution of ellipsoids. This will remain the case even up to 14 days, according to Neville [9]. Thus, charge build up at the ends of segmented pores is not possible. Secondly, it is questionable whether the random nature of the capillary network will give rise to pores which are straight over any appreciable distance. This is likely to exclude the use of formulae based on simple geometries such as the 40 mm long ellipsoids proposed by Wilson and Whittington [5]. Another point is that, instead of being fixed at 1.3 μm, the capillary diameters range, according to Pentalla [22], from 8.0 nm up to 1.0 μm (with the vast majority in the range 8.0-80.0 nm), further complicating the application of the Fricke equations.

Nevertheless, it is reasonable to expect that some contribution from Maxwell-Wagner type polarization due to the ions in the pore solution will be present in hardening paste, but to what extent this will contribute to the overall polarization, and at what frequency it will relax, is not certain. The diagram of Figure 5.2 suggests that Maxwell-Wagner losses mostly occur just below the MHz frequency range so it is possible that residual effects may be present in the 1-1000 MHz range.

It is known that moist granular rocks containing clay particles can have very large dielectric constants ($>10^4$) at low frequencies [41][80][82] which cannot be dismissed as artefacts caused by measurment error. It is believed that at very low frequencies some contribution to these large dielectric constants comes from the polarization of electrical double layers as discussed in section 5.1.5. However, this mechanism is not held to be responsible for enhanced dielectric constants which relax in the MHz frequency range and which are also observed in porous rocks. Also, Poley et al. [80] have studied dielectric dispersions for two rocks of very similar known porosity (≈12.8%) over the frequency range 1-1000 MHz and have noted that, despite apparently equivalent structures and pore water conductivities, the dielectric constant of one sample was greatly enhanced over the other at 1 MHz but was virtually equal at 1000 MHz. This discrepancy in behaviour suggests that effects other than double-layer or pore related Maxwell-Wagner polarization are

responsible for the dielectric behaviour in the MHz range. Sen [83] has proposed a geometrical explanation for dielectric constant enhancement at the lower radio frequencies which appears capable of explaining this anomalous electrical behaviour.

Sen's suggestion is that high aspect platey grains, typical of clay particles, imbedded in the pore structure of moist porous rocks can act, at low frequencies, like small capacitors connected in parallel with the bulk material of the rock. This can give rise to a very large capacitance value depending on the concentration and aspect ratio of the platey grains. This effect allows for the continuous porosity of the rock to give rise to a D.C. conductivity while at the same time producing a large dielectric polarizability. The ionic conductivity of the pore water is responsible, with the effective value of capacitance resulting from the platey grains, for the relaxation frequency of this mechanism. Equations (5.21a) and (5.21b) are presented for the effective static dielectric constant, $\varepsilon_{se}'$, and D.C. conductivity, $\sigma_{DC}$, of a porous rock of conductivity $\sigma_R$, containing a concentration, $\eta$, of platey grains of aspect ratio $\delta$ and dielectric constant $\varepsilon_{rg}'$ :

$$\varepsilon_{se}' = \frac{\varepsilon_{rg}'}{\delta - \eta}\frac{\eta}{\delta} \qquad \cdots(5.21a)$$

$$\sigma_{DC} = \frac{\delta - \eta}{\delta}\sigma_R \qquad \cdots(5.21b)$$

where,

$$\delta = \frac{\pi a}{2b} \qquad \cdots(5.22)$$

with a and b the minor and major axes respectively of the platey grains.

The relaxation time constant is found from the expression :

$$\tau_R = \frac{\varepsilon_{se}'\varepsilon_0}{\sigma_R} \qquad \cdots(5.23)$$

It is proposed that the above model may provide at least a partial explanation for the dielectric behaviour of cement paste at frequencies above $\approx 10^5$ Hz. This suggestion is based on the fibrous structure of cement gel as it grows out from the cement grains after setting, as illustrated in figure 5.6. The gel fibres growing between the hydrating cement grains may be thought of as high aspect platelets imbedded in the conducting capillary pore structure in a similar fashion to clay particles in sedimentary rock pores. The dielectric response for hardening cement paste has been modelled by the author as follows :

From Double et al. [19], the gel fibre lengths at ≈24 hours are shown by high voltage electron microscope to be ≈1.5 μm in length. If an arbtrary width of 10 nm is assumed (apparent gel particle size according to Neville [9]) this results in an aspect ratio, $\delta$, of 0.010472. Sen and Chew quote a platey grain concentration, $\eta$, for a typical sedimentary rock of $10^{-4}$. However, the concentration of gel fibres in cement paste is likely to be much higher than this so a nominal value of $3\times10^{-3}$ has been assumed. A value of 7 (the approximate dielectric constant of CSH gel [2]) is assumed for the dielectric constant of the fibres, and from Olp et al. [57] a conductivity of 0.2 $Sm^{-1}$ for the low frequency conductivity of the paste.

From equations (5.21) to (5.23), the above assumed parameter values give an effective static dielectric constant, $\varepsilon_{se}'$, of 268.4 and a relaxation frequency, $f_R$, of 13.4 MHz. A non-enhanced dielectric constant of 40 was assumed for the cement paste [57]. Figures 5.7a and 5.7b show the dispersion of dielectric constant and conductivity over the frequency range 1-1000 MHz obtained from equation 3.19 for the above parameter values. A spread parameter, $\beta$, of 0.2 was applied to the Debye equation to take account of any inherent spread in the relaxation process (section 3.2.5).

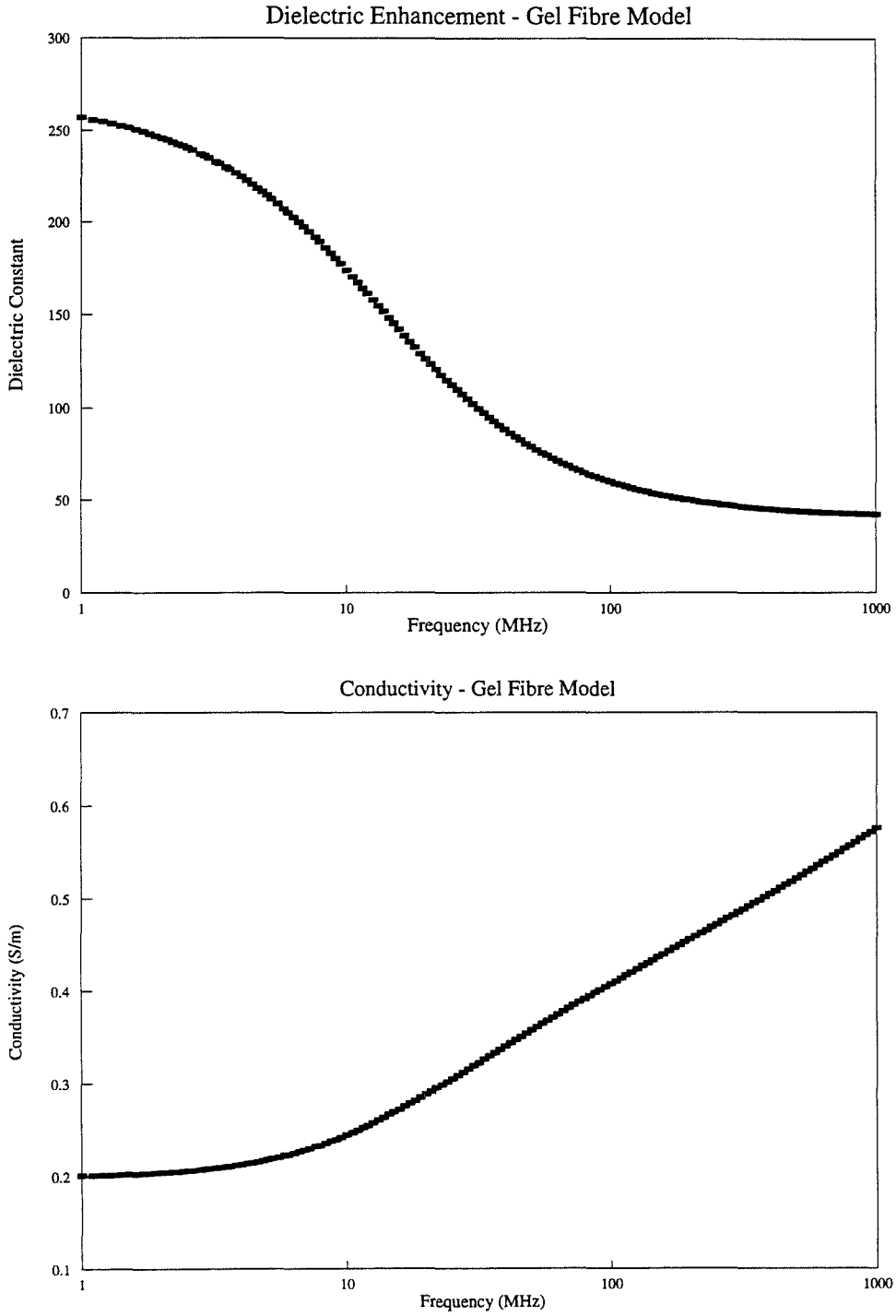


**Figure 5.7 Electrical Parameters - Gel Fibre Model**

The conductivity shown in Figure 5.7b is the sum of the D.C. value and the value arising from the polarization mechanism. These graphs fit well with the results of Olp et al. [57] (cement paste of w/c 0.5 at 24 hours) both in characteristic shape and actual parameter values, although at 1 MHz both parameters are about 65% short of the measured results. Some of the model parameters have been assigned values somewhat arbitrarily (though not entirely without justification) but the results demonstrate that polarization associated with the presence of CSH gel fibres (and possibly CH crystals) in the paste pore structure could be responsible for an enhanced dielectric constant in the radio frequency range.

A Mathcad version (see section 6.2.2) of the model algorithm is presented in Appendix C.

At lower frequencies double layer polarization will contribute to the polarization of hardening cement paste. The gel fibres and particles will have associated charged surface double layers in similar fashion to the cement grains in fresh OPC paste. The much smaller gel particles are likely to give this mechanism a considerably higher relaxation frequency in comparison to that of fresh cement paste in accordance with the particle radius dependence of equation (5.14). However, the irregularity of gel and capillary pore surface shape, and the possible modifications to the behaviour of water and associated ions in the small spaces of the interstitial pores (c.f. section 5.1.4), plus the fact that the polarizing double layers will be on the inside of the pores rather than the outside of solid particle surfaces, all make this effect very difficult to analyse mathematically. Attempts by the author to resolve the difficulties have so far proved unsuccessful. Nevertheless, this effect will be responsible for some of the shortfall at 1 MHz between the parameter values predicted by the geometrical model and the reported measured results [57].

The properties of bound water were considered in section 5.1.4 and it was concluded that relaxation was likely to be observed in the radio frequency range, especially between 100 and 1000 MHz (see Figure 5.2). An increased dielectric decrement can therefore be expected in this frequency range for hardening cement paste in comparison to fresh cement paste. This effect could be more pronounced than might at first be expected due to the possible alteration to the structure of the free

(evaporable) water held in the gel pores and some of the capillary pores (section 5.1.4). Surface conductivity in the zeolitic, and inter-layer water of CSH gel (see Figure 2.4) may also contribute to polarization in hardening cement paste; ionic activity in these thin layers of water causing them to act as highly polarizable capacitive elements (similar to the gel fibre capacitances). This effect could conceivably be as large as the geometrical effect considered above. Relaxation of this mechanism will probably occur in the MHz range, but it may be spread over a very wide frequency range depending on the range of areas and thicknesses of the trapped water layers.

## 5.3 Dielectric Properties of Aggregate

As a general rule, granite, basalt, hard crystalline limestone, quartzite and fresh felsite are strong, but not highly porous rocks and are therfore preferred for use as aggregates.

The electrical properties of rocks have been extensively reviewed by Parkhomenko [84], and summarised, for rocks used as aggregates, by Wilson [2]. Wilson states that for the aggregates used in the U.K. the predominant mechanism of conduction will be ionic charge transfer in water filled pores, i.e. the actual material of the aggregates may be regarded as purely insulating.

Parkhomenko [82] presents graphical dielectric dispersion data from various workers on a number of rock types. Porous sedimentary rocks are shown to have very high values of static dielectric constant which Parkhomenko attributes, possibly mistakenly, to electrode polarization. As pointed out in section 3.2.4, Scott et al. [41] demonstrated that, even after correcting for electrode polarization, saline saturated porous rocks were found to have dielectric constants in excess of $10^4$ at 100 Hz. Possible reasons for this are discussed in section 5.2.2 in relation to the work of Sen and Chew [80].

While very porous rocks such as large grain, loosely compacted sandstones can absorb significant amounts of moisture, and may carry clay particles in their pore

structures, the aggregates preferred for concrete production (e.g. granite, basalt, quartzite etc.) are not very porous and do not generally demonstrate the significantly dispersive interfacial dielectric behaviour of very moist heterogeneous materials.

Parkhomenko [82] lists dielectric constant values for dry rocks among which are quartzite/feldspar sandstones, granite, quartzite and basalt. For the sandstones the dielectric constant is measured in the range 3.96 - 5.1, for granite 4.5 - 5.42, for quartzite 4.36 - 7.0 and for basalt 10.3 - 15.6. Conductivivty values for the quartzite rocks and granite are extremely low to the point of being negligible. These results were obtained for a measurement frequency of 200 kHz.

Coarse aggregates such as chips of granite, feldspar or basalt may, on absorption of water, show some degree of low frequency dispersion, but not to anything like the extent of cement paste, and not at frequencies above 1 MHz. Also, Monfore [85] has shown that the conductivity of typical aggregates, when soaked in saturated calcium hydroxide, is considerably lower than that of cement paste.

In the experimental work of the author only quartz sand and granite chips have been used for producing concrete, and the results presented in this thesis are obtained from measurements carried out on sand mortars (these being regarded as "idealised" concrete). For the builders sand used a value of 4.5 has been assumed for dielectric constant and the conductivity has been assumed to be zero.

While the aggregates themselves are here considered inert and nondispersive, their presence in concrete does apparently still have an effect on the properties of cement paste. Xie Ping et al. [86] state that the results of scanning electron microscope (SEM) investigations suggest that the transition region in the cement paste around the surface of low porosity aggregates is of lower density than the bulk paste. Xie Ping et al. have confirmed this using conductivity measurements on Portland cement concrete containing flat limestone and silica glass aggregate particles. Their results show an enhanced conductance for the transition region. The effect appears to be independent of aggregate type and w/c ratio. These results suggest the possibility that the dielectric behaviour of concrete could be influenced by dispersive effects associated with the regions of different conductivity in the cement paste structure resulting from the presence of aggregate.

## 5.4 Dielectric Properties of Concrete

The properties of concrete will be largely the same as those of cement paste modified by the presence of aggregate, the particles of which are considered to be spherical inclusions of sand dispersed uniformly throughout the cement paste matrix. This allows use of Equations (3.35) to (3.39) (i.e. Wagner's equations for the calculation of the electrical properties of a mixture consisting of dispersed spherical inclusions in a host material) for the calculation of the dielectric properties of the concrete. In this case the inclusions are non-dispersive pure dielectrics as described in section 5.3, while the host is a highly dispersive conducting dielectric (either fresh or hardening cement paste) in accordance with section 5.2.

### 5.4.1 Fresh Concrete

The electrical properties of fresh concrete may be modelled by a three stage process. The procedure outlined in section 5.2.1 for the calculation of the dielectric properties of cement paste is followed first. This requires a knowledge of the water/cement ratio of the mix. The double layer effects at the surface of the cement grains are calculated from equation (5.19) and added to the inherent dielectric properties of the cement. The cement grains are then treated as spherical inclusions suspended, with a volume fraction obtained from the w/c ratio via equation (5.20), in a conducting aqueous host medium. The dielectric properties of the suspension are obtained from equation (5.19). Having thus calculated the dielectric properties of the cement paste these are then substituted for the admittivity of the host medium, $\Lambda_h$, in equation (3.35). To calculate the volume fraction of the aggregate inclusions requires knowledge of the cement/aggregate ratio (c/a) of the mix and the specific gravity of both the cement and the aggregate particles (3.15 $g.ml^{-1}$ and 2.62 $g.ml^{-1}$ for OPC and quartzite respectively [9]). The volume fraction of the inclusions is thus found from the expression :

$$v_i = \frac{sg_c}{sg_c + sg_a c/a(sg_c w/c + 1)} \qquad \cdots(5.24)$$

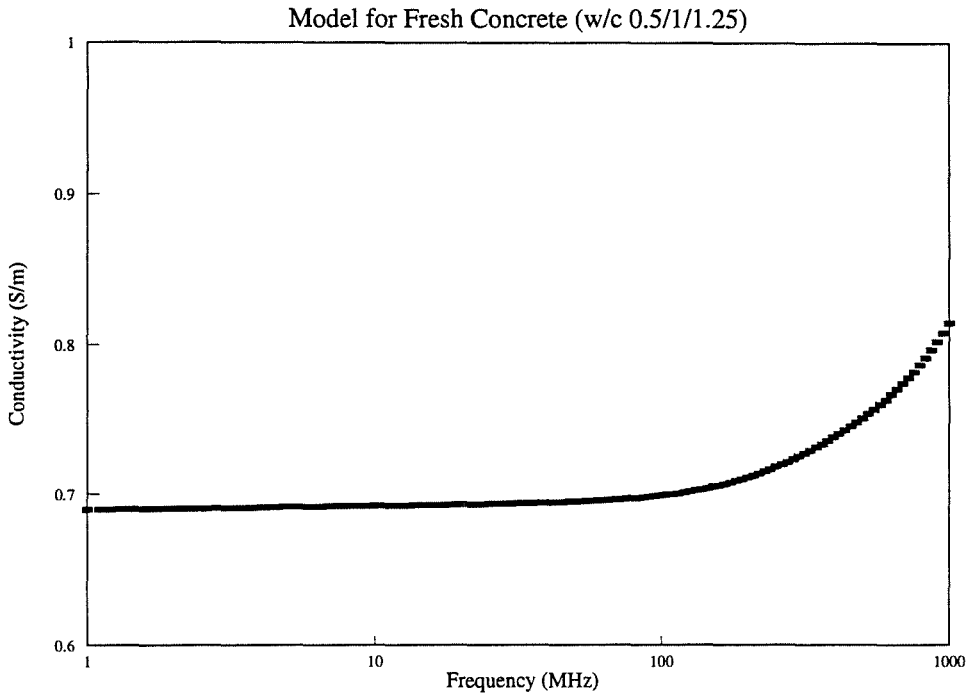


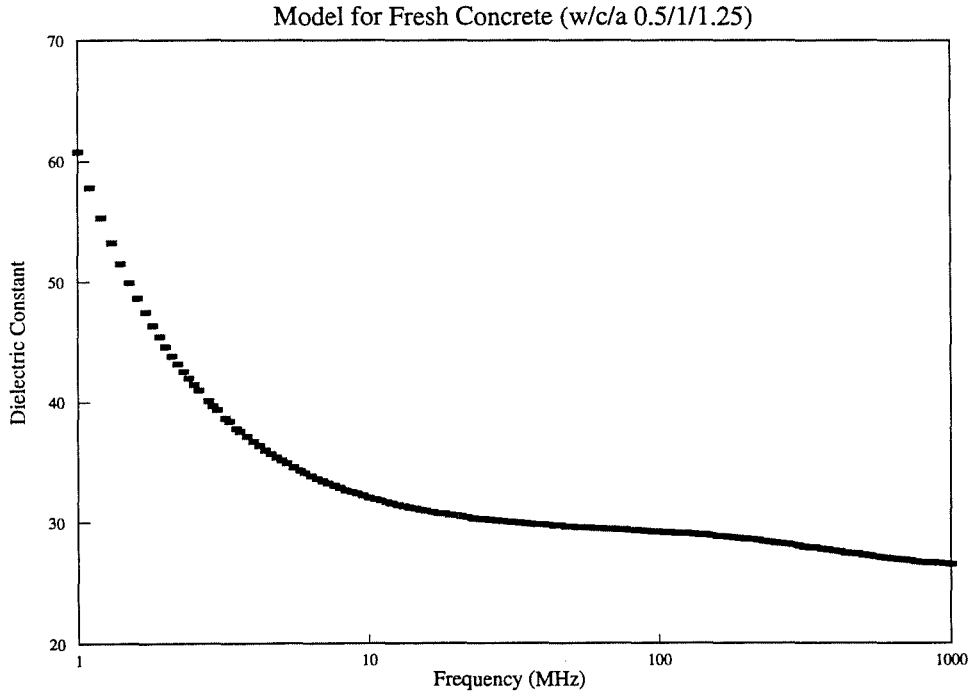


**Figure 5.8 Electrical Parameters for Fresh Concrete Model (w/c/a 0.5/1/1.25)**

The cement paste electrical properties modelled for w/c ratio 0.5 in section 5.2.1 were substituted for the host medium in equation (3.35) and those of sand (quartz), with dielectric constant 4.5 and zero conductivity, for the spherical inclusions. To allow comparison with the results of Olp et al. [57], the c/a ratio was assumed to be 0.8, giving an aggregate volume fraction of 0.369. The results obtained for this model are presented in Figures 5.8a and 5.8b.

As expected, the characteristics of the plots presented in Figure 5.8 are similar to those of Figure 5.4 for cement paste. The conductivity at 1 MHz is 0.690 $Sm^{-1}$ and this rises to 0.725 $Sm^{-1}$ at 300 MHz. This compares well with the results given by Olp et al. [57] who obtained a conductivity of ≈0.77 $Sm^{-1}$ at 1 MHz rising to ≈0.79 $Sm^{-1}$ at 300 MHz (although the different plots are somewhat obscured by each other). Using the temperature coefficient of resistivity given by Whittington et al. [43] ($-0.022(°C)^{-1}$) to convert the model values to 25°C gives 0.775 $Sm^{-1}$ at 1 MHz rising to 0.815 $Sm^{-1}$ at 300 MHz. Thus, as for the cement paste results, there is a very favourable comparison between the model conductivity characteristics and the measurements available in the literature for concrete.

The model results for dielectric constant also compare well with the measurements of Olp et al. The model gives a value of ≈61 at 1 MHz dropping to 28 at 300 MHz. The equivalent measurements are ≈50 at 1 MHz dropping to ≈26 at 300 MHz. The model/measurement comparison for concrete is therefore closer than for cement paste.

The predicted relaxation evident for both conductivity and dielectric constant in the 100-1000 MHz range is again due to the dipolar relaxation of water, as for cement paste.

## 5.4.2 Hardening Concrete

The RF electrical properties of hardening concrete will probably be almost identical in characteristic to those of hardening cement paste. The aggregate is likely to act only as an inert filler which has a "diluting" effect on the magnitude of the dielectric constant and the conductivity. There may, in addition, be some effect from the

enhanced conductance of the cement paste adjacent to the surface of the aggregate particles as discussed in section 5.3, but it is impossible to predict how evident this would be.

For concrete containing porous coarse aggregates there may also be a contribution to relaxation effects due to accumulation of ions in the aggregate pores and also the presence of platey grains as discussed in section 5.2.2. However, it is possible that these potential aggregate effects could be so similar to those of the cement paste as to be indistinguishable.

In summary, the radio frequency dielectric properties of hardening concrete will be determined by a combination of a number of relaxation-type polarization mechanisms, the most significant being :

**i)** Maxwell-Wagner interfacial polarization caused by charge build up in parts of the developing capillary pore system

**ii)** Geometrical effects caused by the growth of CSH gel fibres and CH crystals

**iii)** Residual RF effects from surface double layer polarization

**iv)** Relaxation of bound water, and associated ionic effects, in the 100-1000 MHz frequency range

In addition, enhanced conductivity in cement paste near aggregate surfaces, as well as relaxation processes in aggregate pores may also contribute. All of these effects will be profoundly influenced by the presence of water in its various states.

# CHAPTER 6

## Electrode Modelling and Algorithm Development

As frequency is increased in the RF range signal wavelength begins to decrease to the point where the dimensions of an electrode system used to obtain electrical measurements can occupy a substantial fraction of a wavelength. Under such conditions electrodes and connectors can no longer be accurately regarded as lumped circuit elements and simple circuit analysis must give way to the distributed parameter analysis of transmission line theory. Radiation and fringing field effects also become increasingly important and have to be accounted for in any accurate analysis.

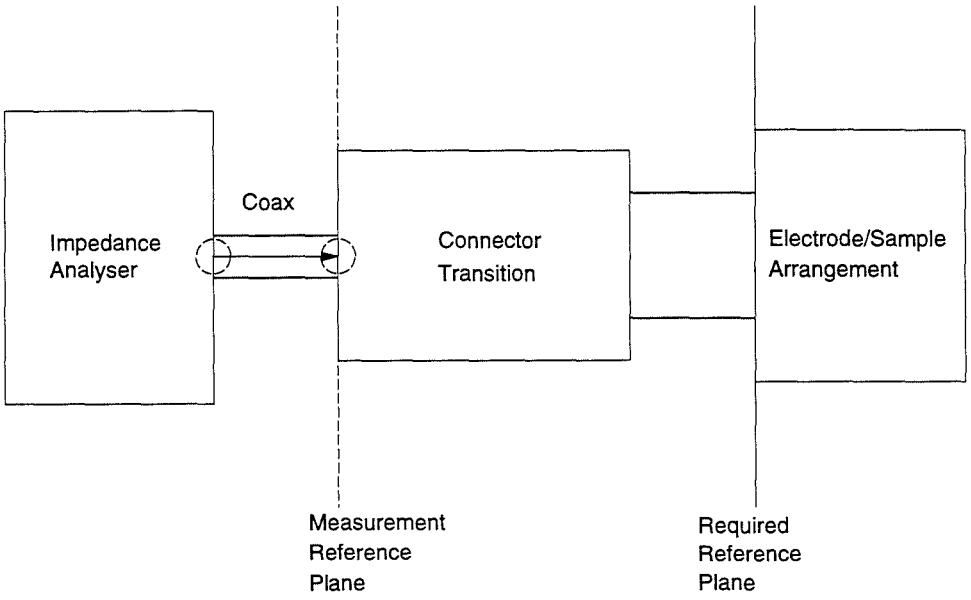


**Figure 6.1 RF Measurement System**

The general electrical scheme used to represent the measurement system in this work is shown in Figure 6.1. The RF impedance analyser has a single input/output port accessed by a coaxial connector to which a suitably matched coaxial line may be coupled. The coaxial line is then mated to an electrode/sample arrangement, as yet unspecified, via some form of transition connection which depends on the

specific geometry of the electrodes. The electrode geometry is designed to allow the driving point impedance at the arrangement input to be modelled mathematically, thereby facilitating the de-imbedding of the required electrical parameters of the sample.

The analyser itself is initially calibrated for the required measurement frequencies using standard test pieces, supplied by the manufacturer, which are fixed to the end of the coaxial line, thus establishing the measurement reference plane as shown in Figure 6.1. However, the electrical properties of the sample material are to be calculated from the impedance which is "seen" at the required reference plane located at the input to the electrode system, also shown in Figure 6.1. A discrepancy between the required impedance, $Z_r$, and the actual measured impedance, $Z_m$, will therefore exist which is dependent on the electrical properties of the transition, and which must be accounted for before the true electrical properties of the sample material can be obtained.

In this work the transition is modelled as a linear passive two-port network described in terms of its transmission parameters [87]. This leads to the relationship between $Z_r$ and $Z_m$ presented in equation (6.1), the derivation of which is given in Appendix D.

$$Z_r = \frac{aZ_m + b}{cZ_m + 1} \qquad \cdots(6.1)$$

where, $Z_r$ and $Z_m$ are the required and measured complex impedances respectively, and *a, b,* and *c* are the complex transition parameters.

Equation (6.1) shows that the required impedance may be obtained easily from the measured impedance if the transition parameters are known. However, if the transition parameters are unknown their effects can still be calibrated out provided that measurement data from samples with known electrical properties are available. To fully specify the three complex transition parameters requires complex impedance measurements from at least three different samples with known electrical properties. The methods considered and subsequently developed for the calibration of the transition are described in section 6.2.

## 6.1 Electrode systems

This section presents a brief description of the electrode system used in the work of Wilson and Whittington, from which this work continues.

Wilson [2], and Wilson and Whittington [4][5] used standard 150 mm cubes of concrete and mortar as the basic sample on which to perform electrical measurements. These sample dimensions comply with the BS1881 stipulations for 7 and 28 day compressive strength crushing tests [88], and were chosen to provide an element of continuity between standardised physical destructive testing and electrical nondestructive measurements. For resistivity and capacitance measurements at very low frequencies the sample cubes were sandwiched between two 150 mm square stainless steel electrodes which were connected to the measuring equipment by separate leads. The resultant sample/electrode configuration could be regarded as a lumped impedance element at the measurement frequencies used (2 kHz [2]).

Wilson and Whittington retained the sample dimensions and the same basic electrode structure for their measurements at higher frequencies (>1 MHz) [2][4][5][54], but, in order to facilitate a good connection to the coaxial connector input of the HP4191A RF impedance analyser used, a parallel-plate to coaxial-line transition element was mounted on the electode/sample configuration. The resulting arrangement is illustrated in Figure 6.2. The N-type coaxial connector to which the analyser cable was coupled was fixed, as shown, on the ground electrode, and the live central conductor was continued across the upper face of the concrete sample to the live electrode.

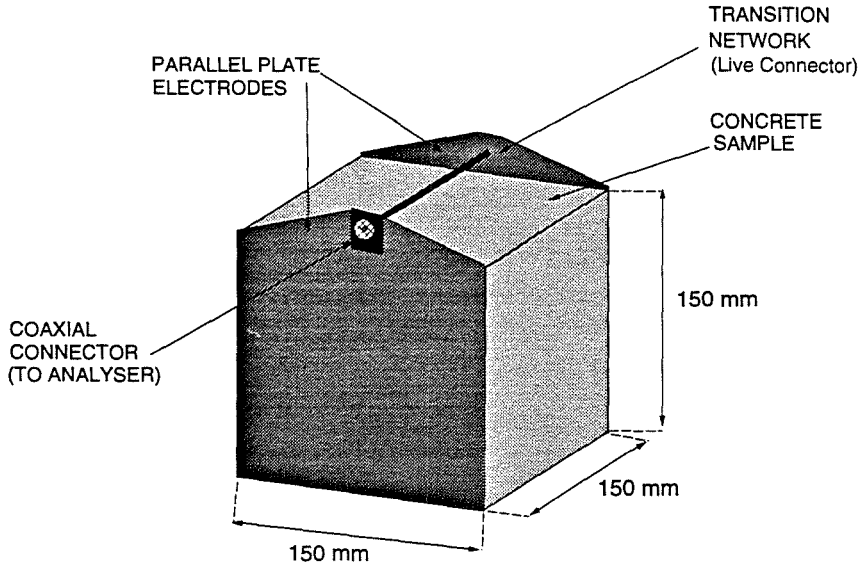


**Figure 6.2 Parallel Plate to Coaxial Line Transition of Wilson and Whittington**

It was realised that as the frequency of measurement increased the electromagnetic properties of the transition network would progressively obscure the true impedance of the parallel plate electrode/sample arrangement, and that the true impedance itself would begin to reflect the *distributed* electrical parameters of a parallel plate transmission line rather than a lumped circuit element [4]. Wilson and Whittington therefore modelled the transition/electrode/sample arrangement as a single complex impedance (the transition) connected in series with a parallel plate transmission line containing concrete as a dielectric material between the plates (the electrodes). In the diagram of Figure 6.2 direction of propagation of the TEM mode (Transverse Electro-Magnetic i.e. electric and magnetic field vectors normal to the plates) was expected to be downwards, parallel to the plate electrodes. Higher order modes were not considered at this stage because it was assumed that these would not become activated until the frequency was greater than 1 GHz.

This was the electrode structure initially used in this work to acquire RF impedance data in the frequency range 1-1000 MHz. However, for following reasons it was deemed necessary to modify the transition network represented in Figure 6.2.

The proximity of the live connector to the sample material meant that the electrical properties of the transition were likely to be coupled to those of the sample, making accurate calibration of the transition network virtually impossible since calibration parameters would vary as hydration of the sample material proceeded and from mix to mix. This was confirmed experimentally and it found that, especially in the 100-1000 MHz range, the transition electrical properties were actually more sensitive to the properties of the sample (especially concrete in the fresh state) than were those of the parallel plate electrode system. The calibration method is discussed in section 6.2.

The first attempt to overcome these problems involved two changes to the transition network. First, the naked conductor was shielded by a brass sheath, the dimensions of which were designed to give a characteristic impedance of 50Ω (the same as the analyser cable). Secondly, the transition was raised away from the sample surface by a further 50 mm in an attempt to additionally reduce the influence of the sample properties on the electrical properties of the network. The adapted arrangement is shown in Figure 6.3.

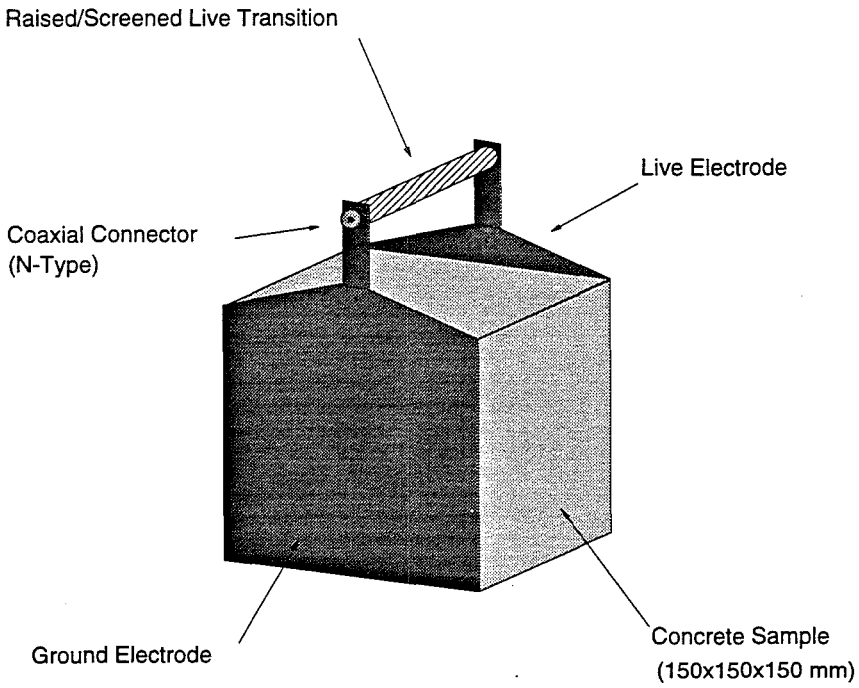


**Figure 6.3 Modified Wilson and Whittington Electrode System**

The electrode system of Figure 6.3 was used to conduct a wide range of experiments on concrete and mortar over the frequency range 1-1000 MHz. However, it was concluded that the results were unacceptable for several reasons. These were :

**i)** The electrical properties of the transition network were still found to be coupled to those of the sample material

**ii)** In the 100-1000 MHz range, the impedance measurements and the de-imbedded electrical parameters were found to remain virtually constant irrespective of the sample material. This was the case for different concrete mixes, the same mix at different stages of hydration, and for other materials such as saline solutions.

**iii)** In the 1-100 MHz range negative dielectric constant values were obtained for concrete mixes *and* for saline solutions. While these were still the subject of consideration for concrete samples, no such values should have been obtained for saline. Subsequent theoretical investigations (presented in chapter 5) uncovered no reasons why negative dielectric constants should be obtained from measurements on concrete either. The negative dielectric constants therefore cast doubt on the validity of both the electrode structure and the de-imbedding process used to obtain the results.

**iv)** The previous assumption that higher order propagation modes were insignificant in the measurement frequency range was reasoned to be incorrect for two reasons.

The first of these is best explained with reference to Figure 6.4 which shows the electric field lines for the electrostatic case (f=0 Hz) at the signal launch plane, located at the junction between the transition network and the parallel plate transmission line, for the electrode system of Figure 6.3. It is assumed for simplicity that the dielectric in the transmission line is air.

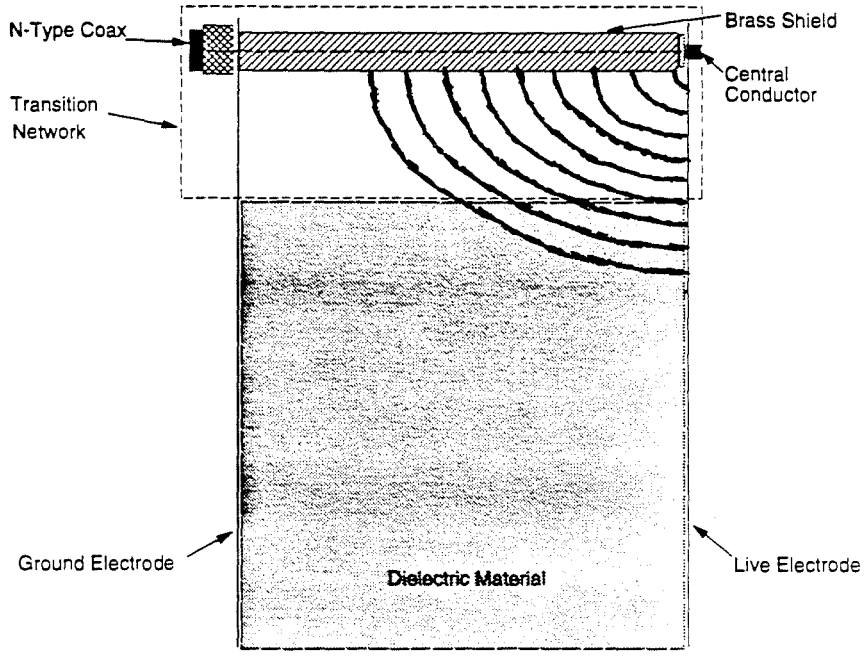


**Figure 6.4 Electrostatic Field Lines for Modified Wilson Transition**

Figure 6.4 shows that the wave incident on the input plane of the transmission line will not be normal to it, but will have a component pointing from one electrode to the other. Thus the propagated wave will not be truly TEM. This means that calculation of the input impedance of the transmission line will not be accessible to standard transmission line theory based on a distributed circuit element approach [89]. Thus, as the frequency of the signal is increased the transmission line model will become progressively inaccurate. Since this appearance of a non-transverse electric field at the transmission line feed point is a result of the transition network structure, it was decided that a complete redesign was necessary.

The second point concerns the dimensions of the transmission line itself. For a parallel plate transmission line with an air or vacuum dielectric the cut-off frequency for the lowest TM mode (Transverse Magnetic i.e. an *electric* field component parallel to the plates) occurs when the wavelength of the excitation signal becomes equal to or less than twice the gap between the plates. At such wavelengths the discontinuity at the transition/transmission-line junction will therefore promote the propagation of nontransverse electric or magnetic modes (depending on frequency) [90]. For the electrode system of Figure 6.3 the plate gap is 0.15 m which gives a

minimum wavelength for TEM operation of 0.3 m, resulting in a maximum frequency of ≈1000 MHz. However, the wavelength of the signal in the transmission line is also inversely proportional to the square root of the dielectric constant of the material between the plates [89]. Thus, for a dielectric constant of 10 the cut-off frequency of the $TM_{01}$ mode is ≈316 MHz, and for a saline solution (as eventually used for calibration purposes in this work) of dielectric constant ≈80 the cut-off frequency is reduced to ≈111 MHz. The parallel plate electrode system of Figure 6.4 is therefore inappropriate for electrical measurements required for this work in the 100-1000 MHz band due to the transition/parallel-plate discontinuity, irrespective of the design of the connecting transition.

In view of the frequency constraints placed on the parallel-plate electrode system for the given sample dimensions, it was decided that the 1-1000 MHz range should be considered as two separate bands and that a different electrode design should be implemented at higher frequencies. This decision was confirmed when it was discovered that measurements from the Hewlett-Packard 4191A impedance analyser, around which the measurement system was based, could be acquired more accurately by internally calibrating the analyser separately over the two frequency bands 1-100 MHz and 100-1000 MHz.

The analyser internal calibration routine is based on the measurement of reflection coefficient for standard 0 Ω, 0 S, and 50 Ω matched load test pieces. This procedure allows calibration to the measurement plane shown in Figure 6.1. Measurements are made at 51 spot frequencies across the entire range of interest, which in this case is 1-1000 MHz. However, during normal operation the analyser takes measurements at 51 spot frequencies *per decade* (46 over 1-10 MHz), which gives a total of 148 measurements over 1-1000 MHz. An internal interpolation routine is therefore used to achieve calibration for those measurement frequencies which lie between the specifically calibrated points. By conducting test measurements on the 50 Ω standard load after calibrating over the 1-1000 MHz range, it was discovered that the impedances for the interpolated points in the 100-1000 MHz range were not as accurately measured as the specifically calibrated points. The errors for some of these points were up to ≈7%. In the 1-100 MHz range the errors in the interpolated points were less than ≈0.05% which is virtually as accurate as those specifically

calibrated. It was therefore decided that a separate full 51 point calibration in the 100-1000 MHz range was required to guarantee maximum accuracy in the measurement data.

These considerations led to the design and construction of the electrode systems which were used in the experimental investigations of the present work, the details of which are given in sections 6.1.1 and 6.1.2

### 6.1.1 1-100 MHz

The purpose of investigation in this frequency range was to verify or rectify the data produced for the electrical properties of concrete by Wilson and Whittington (see chapter 1). The same basic parallel-plate electrode structure was therefore maintained for subsequent measurements, but the transition network enabling interface with the coaxial connector of the impedance analyser output was redesigned. The new electrode/transition design is as shown in Figures 6.5 and 6.6. The electrodes are extended by tapered sections which allow an N-type coaxial connector to be fixed to the ground electrode and connected to the live electrode by a threaded extension to the central conductor (M3 screw size ≈10 mm long), to which it is secured by a compatible nut. The transition sections are bent towards one another as shown, so that the gap between them at the coaxial connector end is 3.5 mm (maintained by a circular teflon spacer).

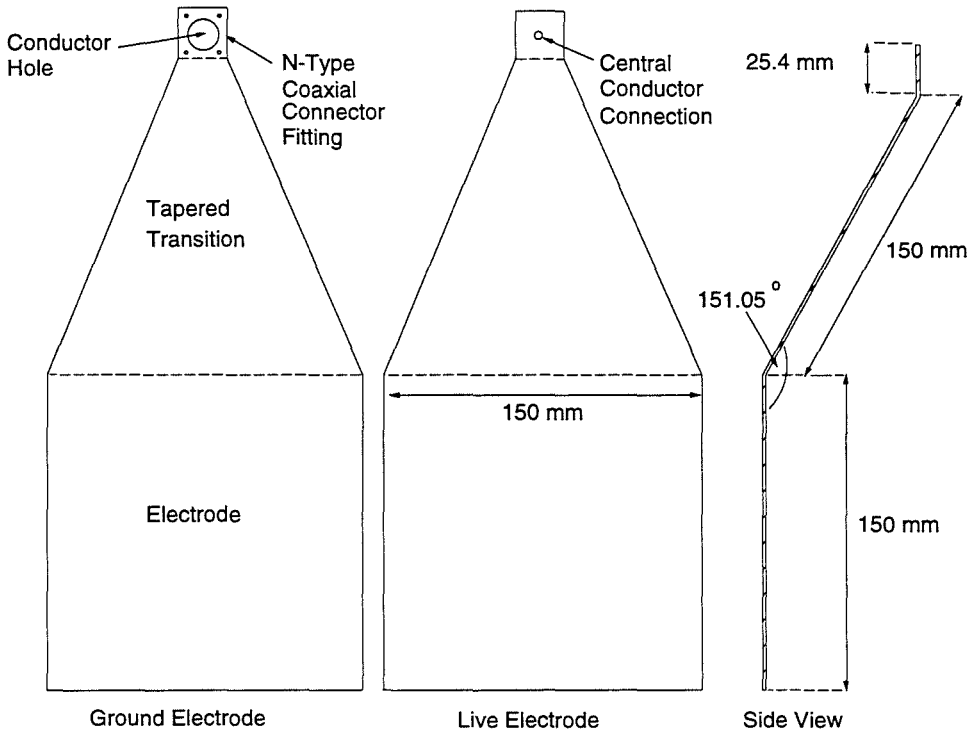


**Figure 6.5 Parallel Plate Electrodes - Redesigned Transition**

The tapered geometry of the new transition is designed to promote TEM propagation at both the coaxial interface with the analyser cable and the parallel plate interface with the transmission line, thereby justifying the use of two-port network theory for point frequency calibration. The field distribution in the transition network is not amenable to calculation by closed form expressions, but it was decided after consultation [90] that the dimensions shown would ensure that the above requirements were met.

This point is illustrated in Figure 6.6, which shows an approximate side view representation of the assumed field line distribution for the electrostatic (f=0 Hz) case. As can be seen, there will be TEM propagation at the input to the N-type coaxial connector (assuming this to be the case in the coaxial line) where measurements are obtained, and also at the input to the parallel plate transmission line, where measurements are required. The impedances at these points will correspond respectively to $Z_m$ and $Z_t$ in equation (6.1).

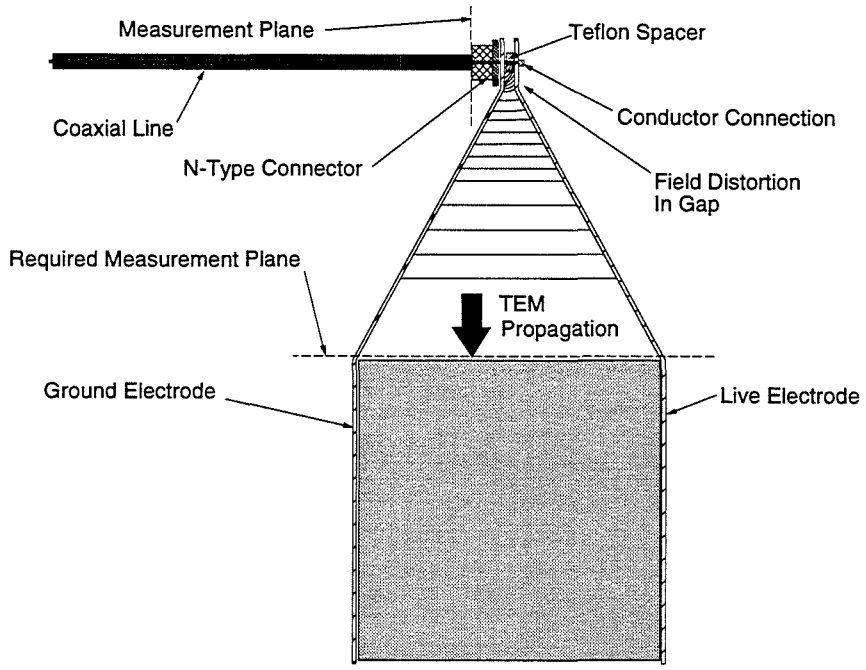


**Figure 6.6 Electric Field Distribution in New Transition**

The conversion from coaxial to parallel plate propagation will occur mostly in the small gap (3.5 mm), created by the teflon spacer, through which the central conductor of the coaxial line reaches the live side of the transition network. Thus, the 150 mm conductor exposed to the sample surface at close range in Figure 6.2 has been reduced to a 3.5 mm section located 131 mm clear of the sample. The electric field lines are shown closely spaced in the gap in order to illustrate the asymmetrical field "warping" at that point of the system. At the wide end of the transition network the field lines will be symmetrical with respect to the input face of the sample material, any distortion having become minimal.

The transmission line containing the sample is assumed to be terminated in an open circuit which allows the input impedance to be represented by equation (6.2) [89].

$$Z_l = \frac{Z_0}{\tanh(\gamma d)} \qquad \cdots(6.2)$$

where,

$Z_0$ is the line characteristic impedance ($\Omega$)
$\gamma$ is the line propagation coefficient
$d$ is the line length (m)

The characteristic impedance and the propagation coefficient are further represented in terms of the line parameters by equations (6.3) and (6.4).

$$Z_0 = \sqrt{(R + j\omega L)/(G + j\omega C)} \qquad \cdots(6.3)$$

$$\gamma = \sqrt{(R + j\omega L)(G + j\omega C)} \qquad \cdots(6.4)$$

where,

$R$ is electrode resistance per unit length ($\Omega m^{-1}$)
$L$ is electrode inductance per unit length ($Hm^{-1}$)
G is sample conductance per unit length ($Sm^{-1}$)
C is sample capacitance per unit length ($Fm^{-1}$)
$\omega$ is angular frequency ($rad.s^{-1}$)
j is the complex operator

For the stainless steel electrodes used, the value of $R$ was obtained from a consideration of penetration depth and conductivity at the frequencies of interest [91]. For the given electrode dimensions, $R$ was found to have the frequency dependent form shown by equation (6.5a).

The numerical value of $L$, given in equation (6.5b), was obtained from Wheeler [92], who presents equations and tabulated parameters derived from a conformal mapping approximation approach for a transmission line in which the plate separation is equal to plate width (as is the case in this work).

$$R = 6.5359 \times 10^{-5} \sqrt{f} \qquad \cdots(6.5a)$$

$$L = 5.94 \times 10^{-7} \qquad \cdots(6.5b)$$

where $f$ is the frequency in Hz.

The values of $G$ and $C$ are directly related to the intrinsic electrical parameters of the sample ($\sigma$ and $\varepsilon_r'$) and the line geometry in this work makes the relationship particularly simple, as shown in equations (6.6a) and (6.6b).

$$G = \sigma \qquad \cdots(6.6a)$$

$$C = \varepsilon_r' \varepsilon_0 \qquad \cdots(6.6b)$$

Equation (6.2) can be transformed to a simpler form to ease computational analysis for the deimbedding of the sample electrical parameters. The procedure of simplification is given in Appendix E, and the resulting expression is :

$$z \tan(z) - c = 0 \qquad \cdots(E.9)$$

where c and z are complex parameters related by simple linear transforms to the input impedance of the transmission line and the electrical parameters of the sample material respectively. The exact relationships are presented in Appendix E.

The above transmission line analysis does not take account of fringe field effects in the space outside the sample material. These were ignored because it was reasoned that the expected high dielectric constant of the sample material (whether saline at the calibration stage or concrete at the measurement stage) will cause most of the electric field to be concentrated between the electrodes, minimising the amount of energy in the field outside the sample. This point is also made by Schwan et al. [77] with respect to the investigation of saline based biological materials.

### 6.1.2 100-1000 MHz

#### General Electrode Considerations

As previously discussed, the parallel plate transmission line electrode system of section 6.1.1 is inappropriate for measurements above 100 MHz, such frequencies being too high for TEM propagation in high dielectric materials for the specified geometry. On the other hand, microwave waveguide systems of the hollow rectangular tube type, which rely on the propagation of modes of higher order than TEM, are generally used only at frequencies above 1000 MHz. This is especially the case for concrete and related materials measured in this work because of the large sample dimensions and dielectric constants involved.

Open ended coaxial probes of various types have been used for dielectric investigation of liquids [93][94] and biological materials [95][96][97], and such techniques are extensively reviewed by Stuchly and Stuchly [98]. A basic fringe (induction) field coaxial probe is shown in Figure 6.7. The probe is simply a piece of coaxial transmission line (of dimensions much smaller than signal wavelength [97]), the open circuit end of which is pressed onto the surface of the sample material. The admittance measured at the end of the probe is determined by the sample electrical properties because the fringe field at the aperture is contained in the material. The admittance of the probe in free space will therefore be purely susceptive (capacitive), but will be complex for a lossy material.

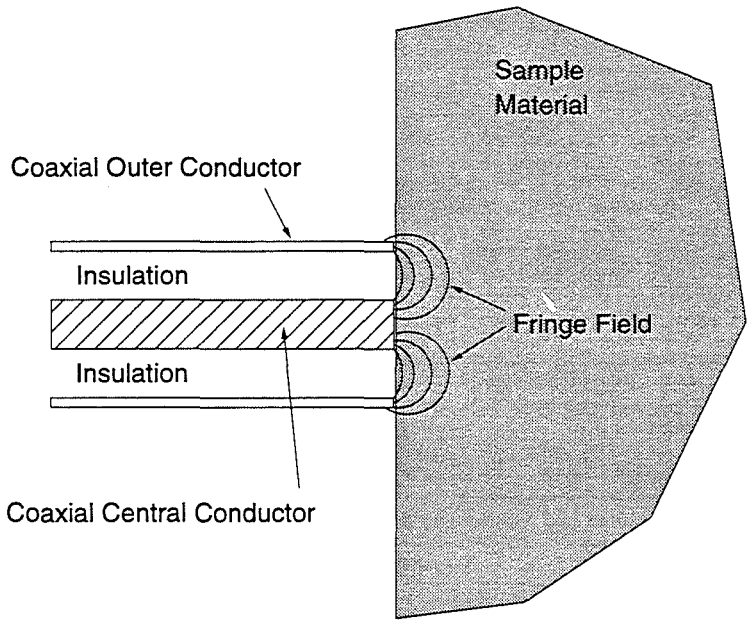


**Figure 6.7 Open-Ended Coaxial Fringe Field Probe**

The fringe field does not extend very far into the sample which makes this type of probe suitable only for very homogeneous materials, such as liquids, or in situations where surface effects are to be measured, or for measurements on thin samples. It is not ideal for use on concrete or mortar (or comparable materials such as soil), which on a small local scale are heterogeneous, because localised electrical properties may vary throughout the sample. Deeper field penetration, which produces a field perturbation resulting from more average sample properties, is therefore required for these materials.

A variation on the fringe field probe, which comprises a similar coaxial probe with the central conductor extended into the sample material, is described by Stuchly and Stuchly [98] and illustrated in Figure 6.8. Extending the central conductor, usually by a very small amount [96], leads to more extensive fringing, and, more importantly, also gives rise to a radiation field penetrating into the sample bulk as shown. The radiation adds a conductance term to the aperture admittance of the coaxial probe, even when in free space.

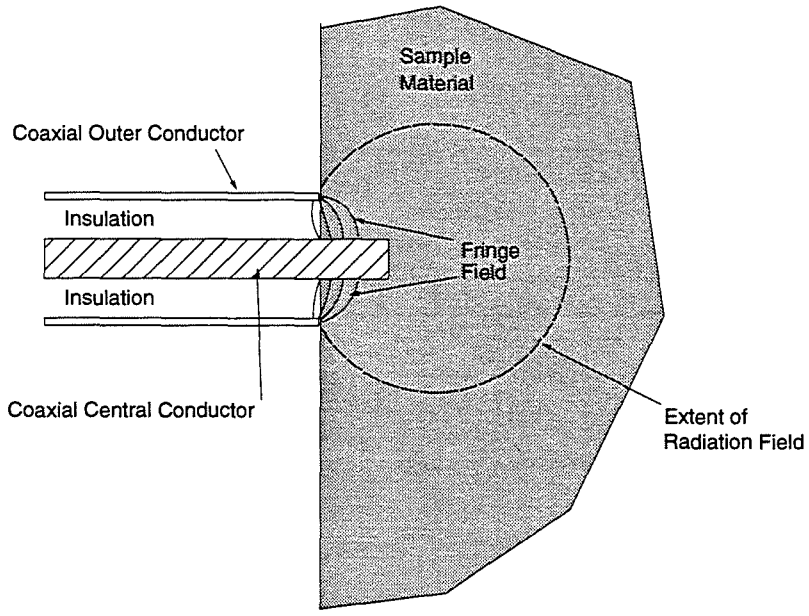


**Figure 6.8 Open-Ended Coaxial Probe with Extended Conductor**

The radiation field encompasses more of the sample material than the fringe field of the probe in Figure 6.7, which makes the probe of Figure 6.8 more suitable for materials with relatively large grain heterogeneities like concrete. The size of the extended conductor directly affects the extent of radiation into the surrounding material and, since it is considered necessary for analytical purposes that the sample should wholly enclose the field (not just the probe) [98], there will be a trade-off between sample size and conductor extension. Such a probe, with extended conductor lengths of 1.7 cm and 2.05 cm, has been used with reasonable accuracy for measurement of the *in situ* electrical properties of oil bearing rocks in the frequency range 150-1000 MHz [99].

When the length of the extended probe is no longer infinitessimal it may actually be regarded as a monopole antenna [95] and modelled as such in terms of the driving point admittance at the aperture of the coaxial line. However, for such analysis to be accurate the sheath of the coaxial line must be extended out from the aperture as a ground plane over which the antenna can radiate. Theoretically this should be infinite in radius but in practice a finite ground plane can be modelled as infinite if it is sufficiently large in comparison to both the longest wavelength of the radiation

and the length of the monopole antenna [98][100]. King et al. [101] have produced an excellent detailed text on the properties of various types of antenna radiating in matter.

**Radiating Probe Model**

For a probe radiating in a nonmagnetic material the antenna modelling theorem of Deschamps [102] relates the driving point impedance, $Z$, to that of the probe in free space and has the mathematical form given by equation (6.7).

$$\frac{Z(\omega,\hat{\varepsilon})}{\eta}=\frac{Z(\sqrt{\hat{\varepsilon}_r}\,\omega,\varepsilon_0)}{\eta_0} \qquad \cdots(6.7)$$

where,

$\eta_0$ is the intrinsic impedance of free space ($\Omega$)

$\eta$ is the intrinsic impedance of the material ($\Omega$)
$\hat{\varepsilon}$ is the complex permittivity of the material ($Fm^{-1}$)
$\hat{\varepsilon}_r$ is the relative permittivity of the material
$\varepsilon_0$ is the permittivity of free space ($Fm^{-1}$)
$\omega$ is angular frequency ($rad.s^{-1}$)

Multiplying both sides of equation (6.7) by $\eta$ leads to equation (6.8).

$$Z(\omega,\hat{\varepsilon})=\frac{Z(\sqrt{\hat{\varepsilon}_r}\,\omega,\varepsilon_0)}{\sqrt{\hat{\varepsilon}_r}} \qquad \cdots(6.8)$$

The equivalent expression in terms of admittances is simply :

$$Y(\omega,\hat{\varepsilon})=\sqrt{\hat{\varepsilon}_r}\,Y(\sqrt{\hat{\varepsilon}_r}\,\omega,\varepsilon_0) \qquad \cdots(6.9)$$

These are the general expressions for an antenna which may be used for analysis provided that a suitable analytic model is available for the driving point admittance or impedance of the probe.

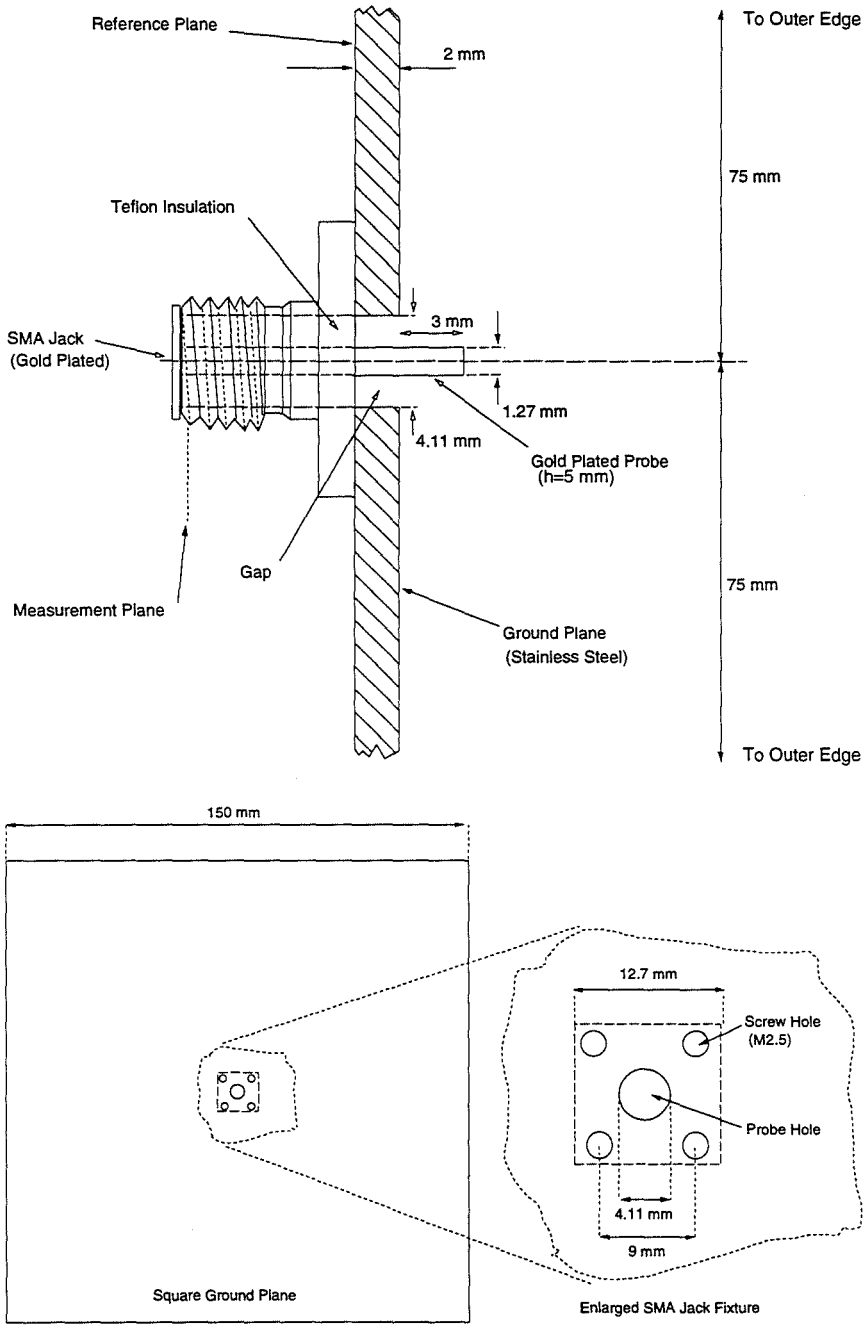


**Figure 6.9 Hybrid Electrode System for Measurements at 100-1000 MHz**

**Electrode Design**

An electrode system has been designed for use in the 100-1000 MHz frequency band which is essentially a hybrid combination of open-ended coaxial line and electrically short monopole antenna over a finite square ground plane. The design is illustrated in Figure 6.9, which presents a plan view of the ground plane dimensions and a cut-away side view of the probe aperture dimensions.

The dimensions of the probe result from the following constraints which are imposed by a combination of the frequency requirements and the geometry of the measurement samples:

**i) Antenna Length**

In order to be able to model the driving point admittance of the antenna by an analytic closed form expression, the antenna must be *electrically short*. The electrical length, which is defined in terms of signal wavelength, is inversely proportional, for a given frequency, to the square root of the dielectric constant of the sample medium. In this frequency range, the highest dielectric constant expected to be measured is a value of ≈80 for saline solution used for calibration, which implies a nine-fold increase in electrical length over the free space value (i.e. $\sqrt{80} \approx 9$). King et al. [101] show that the antenna may be considered electrically short when the length, h, corresponds to the inequality of expression (6.10).

$$h < \frac{c}{\omega\sqrt{\varepsilon_r}} \qquad \cdots(6.10)$$

where, $c=2.997925\times10^8$ $ms^{-1}$ [21] is the velocity of light *in vacuo*.

The shortest wavelength will occur at 1000 MHz, therefore it was for this frequency that the length of the antenna was determined. For the case of the probe immersed in saline, application of equation (6.10) gives an antenna length of 5.3 mm or less.

Alternatively, Burdette et al. [95] state that the antenna is electrically short when the length is approximately $\lambda/10$ or less, $\lambda$ being the wavelength in the sample medium. For this criterion applied to a saline solution, the required length at 1000 MHz is 3.3 mm or less.

**ii) Antenna Resonance Frequency**

Smith and Nordgard [103] also recommend that the antenna should operate below its resonance frequency (defined as the lowest frequency at which the driving point *reactance* goes to zero), which is determined by the length (shorter length for higher resonance frequency) and the permittivity of the sample medium. Smith and King [104] show that for fresh water the resonant length at 1000 MHz will be about 8 mm, and for salt water may be slightly shorter. This is longer than the electrically short antenna for the same medium, indicating that such an antenna will not resonate in the frequency range of interest.

**iii) Ground Plane Radius**

For accurate modelling of impedance or admittance to be facilitated, the ground plane radius must be chosen within constraints imposed by both the largest operating wavelength and the antenna length. However, since it was intended that the sample dimensions be kept the same as for the 1-100 MHz frequency range (i.e. a 150 mm cube in accordance with the stipulations of BS1881 [88]) the ground plane of the probe was limited to a maximum radius of 75 mm. Bahl and Stuchly [100] have investigated the effects of ground plane size on the input impedance of a monopole antenna immersed in lossy materials. Graphs were produced which show the difference between monopole input impedance calculated for an infinite ground plane, and impedances for various finite radii, assuming the antenna to be immersed in water. Plots for radius divided by free space wavelength versus real and imaginary impedance are presented separately. The results demonstrate that, for a probe of length less than 10 mm, a 75 mm restriction on ground plane radius has negligible effect at 100 MHz, where the longest wavelength in this work occurs, and no discernable effect at 1000 MHz. Thus, for the electrically short probe of Figure 6.9, which extends 3 mm above the ground plane, the 75 mm limit imposed by the sample geometry is perfectly adequate for the frequency range of interest.

### iv) Probe/Sample Interface

Smith and Nordgard [103] have shown that the interface between the dielectric insulation of the coaxial feed line to the antenna, and the material in which the probe is immersed, can give rise to higher order wave modes propagating across the gap between the inner and outer conductors. If the interface is flush with the ground plane, such as in Figure 6.8, then the electromagnetic field at the aperture will not be purely transverse, invalidating any TEM based impedance model.

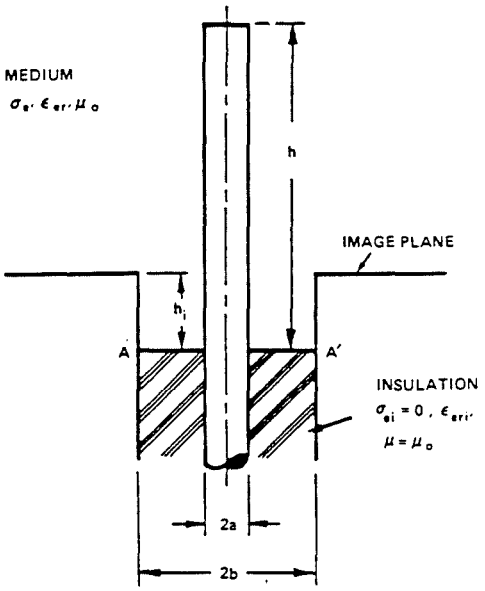


Monopole antenna fed by coaxial transmission line.

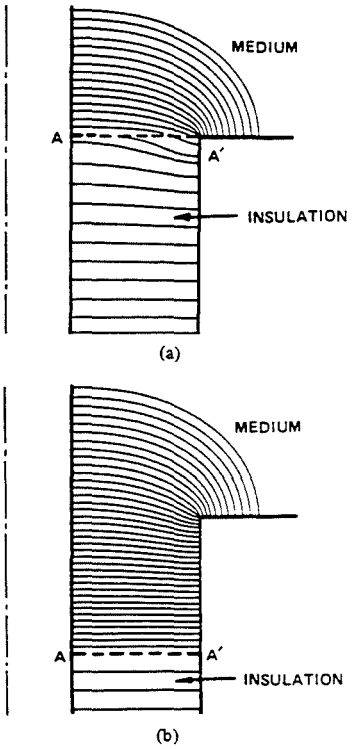


Electric field lines at feed point of a monopole. $b/a = 3.0$; $\sigma_e = 0$, $\epsilon_{er} = 3.0$; $\epsilon_{em} = 1.0$. (a) Flush insulation, $h_i = 0$. (b) Recessed insulation, $h_i = b - a$.

**Figure 6.10 Field Lines at Monopole Feed Point (Recessed and Unrecessed)**

However, recessing the interface into the coaxial line can substantially reduce this problem. Smith and Nordgard state that when the recess depth, $h_i$, is greater than the difference between the outer and inner conductor radii, a and b, of the feed line then the field at the interface will be very close to TEM. This is illustrated for the electrostatic case (f=0 Hz) in Figure 6.10, after Smith and Nordgard.

### v) Reflected Waves

Propagating electromagnetic waves are partially reflected at dielectric boundaries. The waves propagating through the sample will therefore produce reflections at the sample face opposite the antenna probe which will travel back towards the aperture. If these reach the aperture with sufficient power they will interfere with the electromagnetic conditions at the feed point, invalidating the impedance measurements. The amplitude of the propagating wave, as a function of distance travelled, is governed by the attenuation coefficient, $\alpha$, of the sample material. This in turn is dependent on the electrical properties of the sample, particularly the loss factor, and the signal frequency. The relationship is given by equation (6.11) [105].

$$\alpha = \frac{\sqrt{2}\pi}{\lambda_0}\sqrt{\left(\sqrt{(\varepsilon_r'^2 + \varepsilon_r''^2)} - \varepsilon_r'\right)} \qquad \cdots(6.11)$$

The penetration depth (or skin depth), $\delta$, of the sample material is the reciprocal of $\alpha$. In the case of the reflected waves the distance travelled (i.e. twice the sample depth) should be approximately equal to or greater than the value of $\delta$ [106] in order to sufficiently reduce interference. The penetration depth is greater for lower frequencies (i.e. longer wavelengths) and lower conductivity (loss factor) of sample material. Thus, it is for hardening concrete at 100 MHz that the penetration depth is most crucial as a limiting factor in this study. For a lower conductivity limit of 0.1 $Sm^{-1}$ ($\varepsilon_r'' \approx 18$), and a dielectric constant of 30 (see Figure 5.8) the penetration depth at 100 MHz is 300 mm, which is the upper limit for $\delta$, being exactly twice the sample depth. At these and higher frequencies and conductivities, therefore, there will be negligible interference from reflected waves.

### Probe Design Details

The design of Figure 6.9 conforms to all of the above constraints. The probe was constructed from a gold plated, flange mounted, SMA stub contact (jack receptacle) with extended conductor and dielectric insulation. The inner conductor radius, a, is 0.635 mm and the outer radius, b, is 2.057 mm. The SMA jack is mated to the N-type connector of the HP4191A analyser by an N-type/SMA adaptor. The central

conductor extension was cut back to a length of 5 mm and the dielectric insulation was cut right back to the coaxial aperture of the flange. The stub contact is fixed by counter sunk M2.5 screws to a 150 mm square stainless steel ground plane of thickness 2 mm. The central hole of the ground plane provides the coaxial recess discussed in **(iv)** above. This has a depth of 2 mm (the thickness of the ground plane), which is greater than b-a (=1.42 mm), as required. The antenna length (5 mm from the coaxial aperture and 3 mm above the ground plane surface) fits the requirements discussed in **(i)** for the electrically short antenna across the whole 100-1000 MHz frequency range. The square ground plane has a minimum edge to centre distance of 75 mm and conforms, as described in **(iii)**, to the reqirements for an approximately infinite radius ground plane. The ground plane is assumed to be perfectly conducting.

The length of the antenna should mean that the resonance frequency of the probe lies above the 100-1000 MHz range. This was verified by measuring the reactance across this range, using the HP4191A analyser, with the probe in a 0.1889 mol.litre$^{-1}$ sodium chloride solution and also in a fresh mortar sample of w/c/a ratio of 0.45/1/2. The conductivity of the saline solution was measured using a Wayne-Kerr Bridge Analyser at low frequencies (<300 kHz) to be 1.71 Sm$^{-1}$, which is in excess of any likely measurement for concrete or related materials. The results are presented in Figure 6.11.

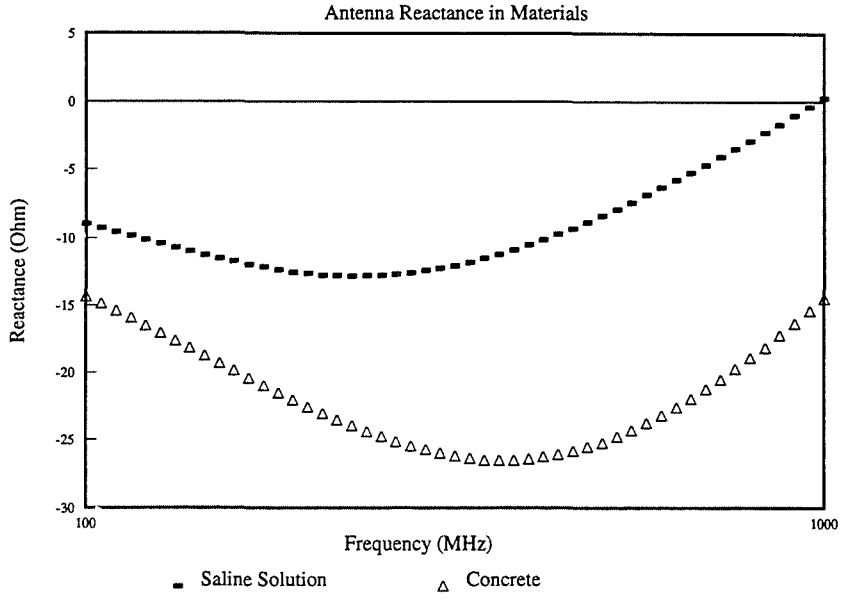


**Figure 6.11 Reactance of Probe Immersed in Saline and Fresh Mortar**

Figure 6.11 shows that for the mortar sample case the antenna reactance is capacitive (i.e. less than zero) across the 100-1000 MHz range. The saline sample case also remains capacitive across most of the range, but the resonance frequency appears to be very close to 1000 MHz. However, it should be mentioned that these reactance plots are not corrected for the effects of the transition between the coaxial cable and the required measurement plane of the probe, which are expected to be predominantly inductive. This means that the true resonance frequencies are likely to be even higher than suggested by Figure 6.11. Thus, the requirements of **(ii)** are satisfied by the probe geometry.

### Aperture Impedance/Admittance Models

Various models are available in the literature for the driving point admittance and impedance of the electrically short monopole antenna and the radiating open ended coaxial probe. All are approximations since no unique closed form expression exists [96]. To find the most appropriate model for the hybrid electrode system of Figure

6.9, six different models, each of which are dependent on the dielectric properties of the medium in which the probe is immersed, were investigated. Where appropriate, the models are identified by the names of the authors from which they were obtained. These are :

**i) Model I - Burdette et al.**

Burdette et al. [95] give the following frequency dependent expression for the impedance of an electrically short antenna radiating in free space :

$$Z(\omega,\varepsilon_0) = A\omega^2 + \frac{1}{jC\omega} \qquad \cdots(6.12)$$

where A and C are constants determined by the antenna geometry. Comparison of equation (6.12) with equation (6.8) yields the following expression for the antenna in sample material with complex permittivity $\hat{\varepsilon}$ :

$$Z(\omega,\hat{\varepsilon}) = A\sqrt{\hat{\varepsilon}_r}\,\omega^2 + \frac{\hat{\varepsilon}_r^{-1}}{\omega C} \qquad \cdots(6.13)$$

Thus, the driving point impedance is determined by the relative permittivity of the sample material and the geometrical parameters A and C.

**ii) Model II - Marsland and Evans**

Marsland and Evans [96] give the following frequency dependent expression for the admittance of a coaxial aperture radiating into free space :

$$Y(\omega,\varepsilon_0) = a_4\omega^4 + ja_1\omega \qquad \cdots(6.14)$$

where $a_1$ and $a_4$ are functions dependent on probe geometry. When equation (6.14) is applied to equation (6.9) for the probe in a material of permittivity $\hat{\varepsilon}$, the result is :

$$Y(\omega,\hat{\varepsilon}) = G_0(\omega)\hat{\varepsilon}_r^{5/2} + j\omega C_0\hat{\varepsilon}_r \qquad \cdots(6.15)$$

where $G_0(\omega)$ is the free space radiation conductance, and $C_0$ is the capacitance representing the fringe field in the material. Marsland and Evans present a correction to expression (6.15) which takes account of fringing in the insulation of the coaxial jack receptacle. The resulting expression is :

$$Y(\omega,\hat{\varepsilon}) = G_0(\omega)\hat{\varepsilon}_r^{5/2} + j\omega(C_0\hat{\varepsilon}_r + C_f) \qquad \cdots(6.16)$$

where $C_f$ is the fringing capacitance in the insulation.

### iii) Model III - Staebell and Misra

Staebell and Misra [94] present the following model for the admittance of an open ended coaxial line probe in material of permittivity $\hat{\varepsilon}$ :

$$Y(\omega,\hat{\varepsilon}) = \frac{j2\omega I_1}{(\ln(b/a))^2}\hat{\varepsilon} - \frac{j\omega^3\mu_0 I_2}{(\ln(b/a))^2}\hat{\varepsilon}^2 + \frac{\pi\omega^4\mu_0^{3/2}}{12}\left(\frac{b^2-a^2}{\ln(b/a)}\right)\hat{\varepsilon}^{5/2} \qquad \cdots(6.17)$$

where,

$\mu_0$ is the permeability of free space ($Hm^{-1}$)

$I_1$ and $I_2$ are triple integrals dependent on radii

$a$ and $b$ are the inner and outer radii of the coaxial line

Values for $I_1$ and $I_2$ can be interpolated from tables published by Misra [107], and for the dimensions of the probe of Figure 6.9 are :

$$I_1 = 2.414022937 \times 10^{-3}$$

$$I_2 = -4.012192037 \times 10^{-9}$$

### iv) Model IV - Staebell and Misra

Staebell and Misra [94] also present a simplified version of the model in equation (6.17) in which the third term (representing radiation conductance separately) is neglected, giving :

$$Y(\omega,\hat{\varepsilon}) = \frac{j2\omega I_1}{(\ln(b/a))^2}\hat{\varepsilon} - \frac{j\omega^3\mu_0 I_2}{(\ln(b/a))^2}\hat{\varepsilon}^2 \qquad \cdots(6.18)$$

The integrals $I_1$ and $I_2$ are the same as for Model III.

**v) Model V**

The simplified model of Staebell and Misra was adapted so that instead of using direct calculation for the coefficients of the permittivity terms in equation (6.18), unknown coefficients are used. These can then be derived from measurements on materials with known dielectric properties. The model is :

$$Y(\omega,\hat{\varepsilon}) = G_1\hat{\varepsilon}_r + G_2\hat{\varepsilon}_r^2 \qquad \cdots(6.19)$$

where, $G_1$ and $G_2$ are the unknown frequency dependent probe parameters.

**vi) Model VI**

A simple model, which treats the driving point admittance of the probe as a single complex number which is dependent on frequency and on the dielectric constant of the material in which the probe is immersed, was developed. The aperture admittance for this model is :

$$Y(\omega,\hat{\varepsilon}) = \hat{\Lambda}_p\hat{\varepsilon} \qquad \cdots(6.20)$$

where $\hat{\Lambda}_p$ is the admittance in free space.

This model lumps the fringe field capacitance and the radiation conductance into a single complex parameter, thereby assuming that the dependence of these effects on the dielectric constant of the sample material is the same.

The justification for this simplification is found in the work of Wei and Sridhar [93][108]. They showed, for open-ended coaxial probe investigations on the dielectric properties of liquids at frequencies up to 20 GHz, that the radiation

conductance dependence on the dielectric constant of the sample material *was* different to that of the fringing field, but that at low microwave frequencies (less than 2 GHz) the difference became negligible.

Models V and VI do not explicitly take account of the fringing field in the insulation of the SMA jack receptacle (c.f. model II), this effect being lumped in with the coefficients of the dielectric constant terms.

## 6.2 Measurement and Calibration Algorithms

Wilson and Whittington used an iterative method to calculate the transition parameter values from impedance measurements [4][5]. These were then used in subsequent calculations to refer impedance measurements to the required measurement plane shown in Figure 6.1 (i.e. the input of the parallel plate transmission line). As briefly described in section 4.2.6, they performed calibration measurements on different lengths of transmission line, containing mortar as a dielectric, with the transition design of Figure 6.2.

Their model of the transition comprised a single impedance element specified by one complex parameter, requiring one complex impedance measurement for calculation. However, because the electrical parameters of the mortar dielectric were unknown these also needed to be calculated as a by-product of the process, thus requiring two complex impedance measurements to specify the transmission line input impedance (dependent on the mortar conductivity and dielectric constant in accordance with equations (6.2), (6.3) and (6.4)) and the transition parameter. Wilson and Whittington therefore performed measurements on two lengths of transmission line and stored the complex transition parameter obtained at each frequency point on floppy disc for calibration of subsequent measurements.

The iterative procedure used by Wilson and Whittington was a multivariate version of the Newton-Raphson method. The basic Newton-Raphson method is a root finding technique described by the general expression given in equation (6.21) [109].

$$x_{n+1} = x_n - \frac{f(x_n)}{f'(x_n)} \qquad \cdots(6.21)$$

where,

$x$ is the independent variable
$f(x)$ is the function of $x$ of which the root is required
$f'(x)$ is the derivative of the function
$x_n$ is the current estimate of the root
$x_{n+1}$ the next (iterated) root estimate

The process works by calculating a "next estimate" of the required root from a "current estimate", and will converge rapidly to the required root provided that the function is relatively simple or that the initial estimate, $x_0$, of the required root is sufficiently accurate. Convergence is achieved when the difference between the current estimate and the previous estimate is acceptably small according to the desired accuracy.

The multivariate version of the Newton-Raphson method works on exactly the same principle as the basic method and is defined by equation (6.22) [110].

$$X_{n+1}^{\langle k \rangle} = X_n^{\langle k \rangle} - \lambda J(X_n^{\langle k \rangle})^{-1} F_n^{\langle k \rangle} \qquad \cdots(6.22)$$

where,

$X_n^{\langle k \rangle}$ is a column matrix of the $k$ current root estimates
$F_n^{\langle k \rangle}$ is a column matrix of the $k$ current function values
$X_{n+1}^{\langle k \rangle}$ is a column matrix of the $k$ next root estimates
$\lambda$ is a scaling factor between 0 and 1
$J(X_n^{\langle k \rangle})$ is the *Jacobian* matrix of $k^2$ partial differentials computed from the $k$ current root estimates

The scaling factor $\lambda$ is normally set to 1, but may be reduced if the process is iterating in a region where the function is steeply sloped.

As a later development of the work of Wilson and Whittington, the present author initially used the multivariate Newton-Raphson method to calculate all three of the complex transition parameters [111]. However, instead of using mortar as the transmission line dielectric, which would have required the calculation of four unknown complex numbers, measurements were carried out on three lengths with saline solution of known electrical properties as the dielectric between the plates. An error impedance, $Z_e$, was defined as the difference between the transition output impedance and the transmission line input impedance. The transition output impedance is given in terms of the measured impedance by equation (6.1) (c.f. Figure 6.1) and the transmission line input impedance by equation (6.2). Thus, the error impedance is :

$$Z_e = \left(\frac{aZ_m + b}{cZ_m + 1}\right) - \left(\frac{Z_0}{\tanh(\gamma d)}\right) \qquad \cdots(6.23)$$

Provided that the transmission line input impedance is known, and that a measurement of transition input impedance is available, the roots of this expression are the complex transition parameters $a$, $b$ and $c$. In order to solve this problem on the HP9816 computer used in this work it was necessary to split equation (6.23) into separate real and imaginary expressions. Thus, for the three lengths of transmission line six simultaneous equations needed to be solved. The multivariate Newton-Raphson expression of the problem is given by equation (6.24).

As can be seen, the solution of the problem involved a Jacobian matrix comprising 36 partial derivatives of the error impedance functions. These were each worked out analytically and the resulting expressions then programmed. The programming effort involved in developing and testing this method was considerable. Problems of non-convergence were encountered for various frequency points in the range of interest and while some of these may have been associated with steep impedance/frequency gradients the reasons for the problems were not always apparent. There were also problems in selecting suitable starting values for the transition parameters.

$$\begin{bmatrix} a_r \\ a_i \\ b_r \\ b_i \\ c_r \\ c_i \end{bmatrix}_{n+1} = \begin{bmatrix} a_r \\ a_i \\ b_r \\ b_i \\ c_r \\ c_i \end{bmatrix}_n - \lambda \cdot \begin{bmatrix} \frac{\partial Z_{er1}}{\partial a_r} & \frac{\partial Z_{er1}}{\partial a_i} & \frac{\partial Z_{er1}}{\partial b_r} & \frac{\partial Z_{er1}}{\partial b_i} & \frac{\partial Z_{er1}}{\partial c_r} & \frac{\partial Z_{er1}}{\partial c_i} \\ \frac{\partial Z_{ei1}}{\partial a_r} & \frac{\partial Z_{ei1}}{\partial a_i} & \frac{\partial Z_{ei1}}{\partial b_r} & \frac{\partial Z_{ei1}}{\partial b_i} & \frac{\partial Z_{ei1}}{\partial c_r} & \frac{\partial Z_{ei1}}{\partial c_i} \\ \frac{\partial Z_{er2}}{\partial a_r} & \frac{\partial Z_{er2}}{\partial a_i} & \frac{\partial Z_{er2}}{\partial b_r} & \frac{\partial Z_{er2}}{\partial b_i} & \frac{\partial Z_{er2}}{\partial c_r} & \frac{\partial Z_{er2}}{\partial c_i} \\ \frac{\partial Z_{ei2}}{\partial a_r} & \frac{\partial Z_{ei2}}{\partial a_i} & \frac{\partial Z_{ei2}}{\partial b_r} & \frac{\partial Z_{ei2}}{\partial b_i} & \frac{\partial Z_{ei2}}{\partial c_r} & \frac{\partial Z_{ei2}}{\partial c_i} \\ \frac{\partial Z_{er3}}{\partial a_r} & \frac{\partial Z_{er3}}{\partial a_i} & \frac{\partial Z_{er3}}{\partial b_r} & \frac{\partial Z_{er3}}{\partial b_i} & \frac{\partial Z_{er3}}{\partial c_r} & \frac{\partial Z_{er3}}{\partial c_i} \\ \frac{\partial Z_{ei3}}{\partial a_r} & \frac{\partial Z_{ei3}}{\partial a_i} & \frac{\partial Z_{ei3}}{\partial b_r} & \frac{\partial Z_{ei3}}{\partial b_i} & \frac{\partial Z_{ei3}}{\partial c_r} & \frac{\partial Z_{ei3}}{\partial c_i} \end{bmatrix}^{-1} \cdot \begin{bmatrix} Z_{er1} \\ Z_{ei1} \\ Z_{er2} \\ Z_{ei2} \\ Z_{er3} \\ Z_{ei3} \end{bmatrix} \quad \cdots(6.24)$$

Tanguay and Vaillancourt [112] have examined the problems of convergence and choice of starting values associated with the Newton Raphson method. They divide the possible iterative cyles which the process may enter into three classes, viz. : attractive cycles, repulsive cycles and indifferent cycles.

Repulsive cycles are characterised by rapid divergence away from required roots and can be easily identified in a practical iterative scheme. Indifferent cycles are characterised by very slow convergence or divergence and in practice would be discarded because of eventual nonconvergence, but the authors state that these have not been observed to cause any problems in the iteration of equation (6.21). Attractive cycles occur in different orders, and cycles of order 1 will lead to the roots of $f(x)$ in equation (6.21). Higher order attractive cycles can trap the process indefinitely and are therefore to be avoided by the choice of appropriate starting values. Tanguay and Vaillancourt have produced formulae for the selection of starting values which always guarantee convergence to the required roots. These formulae are for the trancendental function of equation (E.9) which may be related to the model for the input impedance of a parallel plate transmission line (see Appendix E). Application of this is considered in section 6.2.2.

Hofstadter [113] describes the characteristics of attractive cycles and relates their occurrence to the steepness of the iterating function.

The main difficulty with respect to testing and modifying the algorithm of equation (6.24) was that the process is essentially six dimensional which makes visualization of its progress and potential problems impossible. Trial and error therefore seemed the only available investigative method and this was confirmed after consultation with an authority on numerical analysis [114]. The process was found to be highly sensitive to the starting values but no general criterion governing the choice of such for all frequencies was found. The author did observe the occurrence of a number of attractive cycles which led to indefinite recurring loops. Adjustment of the scaling factor $\lambda$ (see equation (6.24)) sometimes prevented the onset of such loops but, as with the starting values, no discernable pattern was evident concerning the amount of adjustment needed.

Because of the difficulties encountered with this method of calibration it was eventually abandoned in favour of a much more rapid and mathematically accurate method which is described in section 6.2.1. However, the Newton-Raphson method was retained, where necessary, for the de-imbedding of the electrical properties of the samples once calibration of the transition effects was achieved.

### 6.2.1 Calibration Procedure

Examination of equation (6.1) shows that it has the form of a bilinear transformation which maps points in the measurement plane (i.e. values of $Z_m$) onto points in the required reference plane (i.e. values of $Z_r$). The coefficients of the mapping are the transition parameters $a$, $b$, and $c$. The properties of the general bilinear transformation are presented in Appendix F.

If the general system of Figure 6.1 were used to obtain measurements on three materials ($Z_{m1}$, $Z_{m2}$ and $Z_{m3}$) with known electrical properties (i.e. such that three known values of $Z_r - Z_{r1}$, $Z_{r2}$ and $Z_{r3}$ – were available) then it would be possible to produce a system of three simultaneous equations in $a$, $b$, and $c$ and hence obtain the transition parameter values. These could then be used to calibrate subsequent impedance measurements. However, equation (F.7) shows that, as a result of the anharmonic invariance principle (which states that if two planes are related by a bilinear transform then the anharmonic ratio of four points in the original plane is equal to the same ratio of four image points in the image plane), a fourth

measurement on a material with unknown electrical properties may be calibrated without direct knowledge of the transition parameter values simply by using the measurements obtained from the known materials.

For impedance measurements obtained from four different materials (i.e. with four different sets of electrical properties) the anharmonic ratio value, $K$, of the transition transformation can be obtained from equation (F.5) which, when applied to the transition equation (6.1), gives :

$$K = \frac{(Z_{m1} - Z_{m2})(Z_{m3} - Z_{m4})}{(Z_{m1} - Z_{m4})(Z_{m3} - Z_{m2})} \qquad \cdots(6.25)$$

Having obtained $K$ by measurement it may substituted into equation (F.7) which, when applied to equation (6.1), leads to :

$$Z_{r1} = \frac{KZ_{r4}(Z_{r2} - Z_{r3}) - Z_{r2}(Z_{r4} - Z_{r3})}{(Z_{r3} - Z_{r4}) - K(Z_{r3} - Z_{r2})} \qquad \cdots(6.26)$$

Where $Z_{r1}$ is the input impedance of the electrode system in the material with unknown electrical properties. Having obtained $Z_{r1}$ thus, the unknown properties (dielectric constant and conductivity) can then be derived from the analytic impedance model representing the particular electrode system.

The above calibration method has a number of important advantages over the iterative technique (and other similar procedures) discussed previously. Among these are :

**i)** Calibration is performed as a single step process rather than a series of steps and is therefore faster.

**ii)** The calculation is exact, rather than approximate within a given tolerance band, and is therefore more accurate.

**iii)** The problem of finding suitable starting values for iterates is eliminated, which removes the risk of convergence to physically meaningless solutions or the problem of indefinite attractive cycles.

**iv)** The problems associated with divergence or very slow convergence are eliminated.

**v)** There is no need to calculate the analytical solutions to the derivatives of a Jacobian matrix such as in equation (6.24), so the technique is mathematically simpler and easier to program.

**vi)** The method is also error correcting in that errors present in the electrode system model have been shown by Misra et al. [115] to be reduced by this method, especially at frequencies below ≈2 GHz.

**vii)** The anharmonic invariance property allows simplification of impedance models for $Z_r$ by linear transformation without altering the validity of the technique.

For the three known material measurements in this work it was decided to use a short circuit, an open circuit and a sodium chloride solution of known concentration (and hence electrical properties). These standards were chosen in order calibrate to a material of similar electrical properties to concrete (the saline solution), as well as over a wide range of conductivity (the open and short circuits) and dielectric constant (the open circuit and the saline solution).

Application of the calibration technique to measurements obtained employing the electrode systems of Figure 6.6 and Figure 6.9 is considered in sections 6.2.2 and 6.2.3.

## 6.2.2 De-imbedding of Electrical Parameters - 1-100 MHz

### Standard Impedance Measurements

To employ the procedure described in section 6.2.1 to calibrate the electrode system of Figure 6.5 it is necessary to be able to produce a short and open circuit at the reference plane. This was achieved by constructing a replica of the transition section of the electrode system without the attached parallel plate transmission line sections. The basic construction was an open circuit which could be placed in contact with a steel plate to create a short circuit. A side view of the transition, which corresponds with the illustration of Figure 6.6, is shown in Figure 6.12.

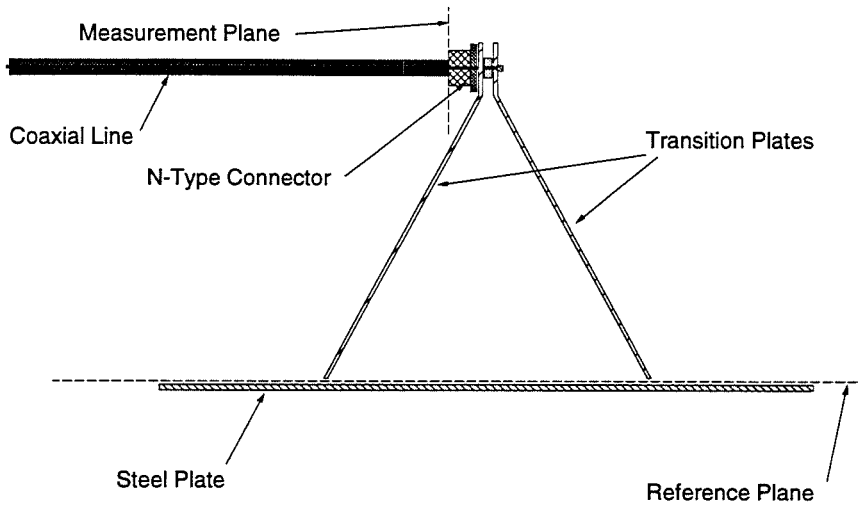


**Figure 6.12 Transition Section for Open and Short Circuit Measurements**

The steel plate measured ≈300 mm in length and ≈170 mm in width. To facilitate a better contact with the plate for short circuit measurements, several layers of aluminium foil were folded round the edges of the transition plates and the transition placed on top as shown. Mild pressure was used to make sure that the full edge of each plate made contact. Open circuit measurements were achieved by removing the steel plate and pointing the edges into free space. It was assumed that the short and open circuits were perfect (i.e. 0 Ω and 0 S respectively) but, in fact, a fringing field will be present during open circuit measurements at the transition output plane which means that the open circuit is an approximation. It was reasoned, however that this effect would not invalidate the method [96].

The measurements on saline solution were obtained by filling a clean unused plastic concrete mould (150 mm cube with extra space in one dimension to allow for the 2mm thickness of the parallel plate electrodes) with deionised water and adding 4.0 grammes of sodium chloride. This gave a concentration of 0.02028 mol.litre$^{-1}$. The conductivity of the solution was measured at low frequencies (less than 300 kHz) using a Wayne-Kerr impedance bridge connected to two 150 mm square parallel plate electrodes without the transition network. The conductivity was of the order of 0.209 Sm$^{-1}$, depending on the temperature of the solution which was recorded using a mercury thermometer.

The dielectric constant of the solution was calculated from the concentration for the relevant frequencies by application of equations (5.1), (5.3), (5.2), (5.4), and (3.20), with data for equations (5.3) and (5.4) obtained from table 5.2. The measured D.C. conductivity was then used in conjunction with equations (3.32) and (3.6) to calculate the overall conductivity at the relevant frequencies. The dielectric constant and conductivity thus obtained were then used with equations (6.2) to (6.6) to calculate the input impedance of the saline filled parallel plate transmission line.

The measured D.C. conductivity was found to correspond very closely to the value for sodium chloride which could be calculated from the theory presented in section 5.1.2. Dielectric constant could not be measured accurately at low frequencies using the Wayne-Kerr bridge because of the errors introduced by the large difference between resistive and reactive impedance for the saline solution at such frequencies (e.g. at 300 kHz $R \approx 32\ \Omega$ and $X \approx 5000\ \Omega$ assuming a parallel equivalent circuit, and at lower frequencies the difference is even greater). The Wayne-Kerr bridge measures impedance magnitude and phase angle and subsequently calculates real and imaginary parts (resistive and reactive components respectively). Very small errors in phase angle can lead to substantial errors in subsequently calculated capacitance (hence dielectric constant). For the same reasons, however, conductance or resistance measurements are very accurate.

**Impedance Measurement Calibration**

To calibrate the system the HP4191A analyser was first calibrated to the measurement plane at the N-type connector using HP standard test pieces (0 S, 0 Ω and 50 Ω). Then the electrode system calibration measurements were taken.

A problem was encountered when measuring the impedance of the open circuited transition. It was found that at a large number of the frequency points in the 1-10 MHz range, errors were obtained in the form of *negative* resistance values (all -50 Ω). The occurrence of these negative values invalidated the calibration procedure. On investigation it was found that the reflection coefficients measured by the analyser (from which impedance is internally calculated) for the transition open

circuit were so close to those measured during the analyser internal calibration routine for the HP standard open circuit that, due to the inherent measurement tolerance of the analyser ($\pm(0.0025 + j0.00025)$ [116]), reflection coefficients marginally greater than 1 were obtained at some frequencies. Such values for reflection coefficient are physically untenable in passive systems so the analyser returned impedance values of -50 Ω as defaults.

### Adapted Analyser Internal Calibration Routine

To overcome this problem a new calibration procedure was developed which combined the internal analyser calibration with the transition calibration.

This was achieved by using the analyser internal calibration routine with the Hewlett-Packard open and short circuit test pieces replaced by the transition open and short circuits, and the 50 Ω matched load test piece replaced by the saline filled transmission line electrode system of Figure 6.5. This effectively referred all subsequent measurements to the required reference plane at the input to the parallel plate transmission line. However, because the internal analyser calculation of impedance is based on a matched load standard of 50 Ω, it was necessary to transform the impedance measurements, $Z_m$, by dividing by 50 and multiplying by the calculated input impedance of the saline filled transmission line, $Z_s$, at each frequency.

Thus, the calculation of reference plane impedance for subsequent measurements on concrete is reduced to the simple operation of equation (6.27).

$$Z_r = \frac{Z_m}{50} Z_s \qquad \cdots(6.27)$$

The drawback with this method is that the accuracy of measurements obtained with the HP4191A analyser is normally determined by the accuracy of the calibration terminations used, particularly the 50 Ω matched load. In the case of the transition pieces and the saline filled transmission line no accuracy figures are known.

**De-imbedding of Sample Electrical Parameters**

Equation (E.9) gives the transformed input admittance of the parallel plate transmission line, which is derived from equation (6.2) by the procedure presented in Appendix E.

$$z\tan(z)-c=0 \qquad \cdots(E.9)$$

Where $z$ is the complex valued unknown to be solved for, and $c$ is the complex valued measured quantity.

Equation (E.9) can be solved for $z$ using the Newton-Raphson method described previously. Tanguay and Vaillancourt [112] have shown that for the condition $\Re(c) \leq 0$ (a physical requirement - c.f. equation (E.11)) then equation (6.28) will provide a starting value for $z$ which will always promote successful convergence of the Newton-Raphson procedure to the required lowest order root.

$$z_0=(0.3+0.7/\sqrt{|c|})\tan^{-1}(|c|)+j\left(\frac{b}{1+|c|^2}\right)\left(\frac{1+3b^2}{1+2|c|^2}\right) \qquad \cdots(6.28)$$

Application of equation (6.21) to equation (E.9) is particularly simple and leads to the iterative expression of equation (6.29) :

$$z_{n+1}=z_n-\frac{z_n\tan(z_n)-c}{[z_n/(\cos(z_n))^2]+\tan(z_n)} \qquad \cdots(6.29)$$

Once the root value of $z$ is obtained the admittivity may be derived via equation (E.8) such that :

$$\Lambda_s=\frac{-z^2d^2}{R+j\omega L} \qquad \cdots(6.30)$$

where R and L are given in equations (6.5a) and (6.5b) and d is transmission line length (=0.15 m). The conductivity and dielectric constant of the sample material are then obtained from :

$$\sigma = \Re(\Lambda_s) \qquad \cdots(6.31)$$

$$\varepsilon_r' = \frac{\Im(\Lambda_s)}{j\omega\varepsilon_0} \qquad \cdots(6.32)$$

Expression (6.29), however, contains complex variables and leads to the complex root $z$. To program the relevant expressions ((E.9), and (6.28) to (6.32)) in HP Basic on the HP9816 computer it is necessary to separate out real and imaginary components and deal with two simultaneous equations. This requires use of the multivariate version of the Newton-Raphson method. The simultaneous equations obtained are :

$$\frac{2x\sin(2x) - y(e^{2y} - e^{-2y})}{2\cos(2x) + (e^{2y} + e^{-2y})} - a = 0 \qquad \cdots(6.33)$$

$$\frac{2y\sin(2x) + x(e^{2y} - e^{-2y})}{2\cos(2x) + (e^{2y} + e^{-2y})} - b = 0 \qquad \cdots(6.34)$$

where $x$ and $y$ are the real and imaginary parts of $z$, and $a$ and $b$ are the real and imaginary parts of $c$. The values of $a$ and $b$ are obtained from the measured impedance, transformed by equation (6.27) (i.e. $Z_r$), and the transmission line constants $R$, $L$ and $d$, by equations (6.35) and (6.36) :

$$a = \frac{-d(R_r R + X_r \omega L)}{R_r^2 + X_r^2} \qquad \cdots(6.35)$$

$$b = \frac{d(X_r R + R_r \omega L)}{R_r^2 + X_r^2} \qquad \cdots(6.36)$$

where $R_r$ and $X_r$ are the real and imaginary parts of $Z_r$.

Equations (6.33) and (6.34) are then solved for $x$ and $y$ in accordance with the process of expression (6.22), and the conductivity and dielectric constant obtained from :

$$\sigma = \frac{(y^2 - x^2)R - 2xy\omega L}{d^2(R^2 + \omega^2 L^2)} \quad \cdots(6.37)$$

$$\varepsilon_r' = \frac{(x^2 - y^2)\omega L - 2xyR}{\varepsilon_0 \omega d^2(R^2 + \omega^2 L^2)} \quad \cdots(6.38)$$

Software was written in HP Basic to facilitate the above process which is made much more complicated by the need to separate complex variables. However, the process was also written into a routine on a personal computer using the **Mathcad** mathematics package. This package provides a mathematics environment which allows the user to input equations and processes in a format very similar to written form. The package also handles complex variables so that no preliminary analytical separation of real and imaginary components is necessary when solving problems such as equation (6.29). The Mathcad package provides a much faster and more flexible testing facility than HP Basic programming, so the author decided to use Mathcad for all subsequent results analysis and algorithm development.

The resulting algorithm written in Mathcad is presented in Appendix G.

### 6.2.3 De-imbedding of Electrical Parameters - 100-1000 MHz

To calibrate the electrode system of Figure 6.9 impedance measurements must be refered to the reference plane at the aperture of the coaxial SMA jack receptacle. For the calibration method discussed in section 6.2.1 this requires that a short and open circuit can be produced at the aperture.

**Standard Impedance Measurements**

An approximate open circuit can be achieved by simply pointing the probe into free space [96] and this was the method used in this work. The short circuit was achieved by crushing several layers of aluminium foil (conductivity of $3.72\times10^7$ $Sm^{-1}$) into the recess around the antenna (the central hole in the ground plane) so that it was filled and a small mound of aluminium covered the antenna tip. The aluminium foil was thoroughly compacted. A similar approach was adopted by Marsland and Evans [96] for creating a short circuit at the end of an open-ended coaxial probe.

As with the parallel plate electrode system, the third calibration standard was a sodium chloride solution. However, depending on the particular aperture admittance model used, it was sometimes necessary to have four measurements on known materials rather than three. For this reason two standard solution measurements were taken and the concentrations of these were chosen so that a relatively large difference in conductivity could be realised. The solutions eventually used had concentrations of 0.00507 mol.litre$^{-1}$ and 0.09126 mol.litre$^{-1}$. The low frequency conductivities of these were measured by the Wayne-Kerr bridge analyser at 0.05128 Sm$^{-1}$ and 0.834 Sm$^{-1}$ respectively.

As with the parallel plate electrode system, the dielectric constants of the solutions were calculated from the concentration for the relevant frequencies by application of equations (5.1), (5.3), (5.2), (5.4), and (3.20), with data for equations (5.3) and (5.4) obtained from table 5.2. The measured D.C. conductivities were then used in conjunction with equations (3.32) and (3.6) to calculate the overall conductivities at the relevant frequencies. The same limitations, as discussed in section 6.2.2, applied to the measurement of static dielectric constant using the Wayne-Kerr bridge.

**Probe Model Simplification**

The anharmonic ratio invariance principle demonstrated by equation (F.6) allows the simplification of admittance models I, II, IV, V and VI by linear transformation. The transformations and resultant expressions used in this work are :

**i) Model I**

Dividing equation (6.13) by $A\omega^2$ gives the modified impedance expression :

$$Z' = \hat{\varepsilon}_r^{0.5} + G\hat{\varepsilon}_r^{-1} \qquad \cdots(6.39)$$

where G is an unknown frequency dependent geometrical parameter.

**ii) Model II**

By applying the following linear transformation to equation (6.16) :

$$Y' = \frac{Y(\omega, \hat{\varepsilon})}{j\omega C_0} - \left(\frac{C_f}{C_0}\right) \qquad \cdots(6.40)$$

the following expression for modified admittance is obtained :

$$Y' = \hat{\varepsilon}_r + G\hat{\varepsilon}_r^{2.5} \qquad \cdots(6.41)$$

**iii) Model III**

Model III is unmodified and is therefore still described by equation (6.17) :

$$Y(\omega, \hat{\varepsilon}) = \frac{j2\omega I_1}{(\ln(b/a))^2}\hat{\varepsilon} - \frac{j\omega^3\mu_0 I_2}{(\ln(b/a))^2}\hat{\varepsilon}^2 + \frac{\pi\omega^4\mu_0^{3/2}}{12}\left(\frac{b^2 - a^2}{\ln(b/a)}\right)\hat{\varepsilon}^{5/2} \qquad \cdots(6.17)$$

**iv) Model IV**

Dividing equation (6.18) by the coefficient of the $\hat{\varepsilon}$ term gives the modified admittance expression of equation (6.42) :

$$Y' = \hat{\varepsilon}_r - I_3\omega^2\hat{\varepsilon}_r^2 \qquad \cdots(6.42)$$

where, $I_3$=1.04428776×10$^{-12}$.

**v) Model V**

Equation (6.19) may be modified by dividing throughout by $G_1$ to give :

$$Y' = \hat{\varepsilon}_r + G\hat{\varepsilon}_r^2 \qquad \cdots(6.43)$$

### vi) Model VI

This model can be greatly simplified by dividing equation (6.20) by $\Lambda_p \varepsilon_0$ to give the modified "admittance" of equation (6.44) :

$$Y' = \hat{\varepsilon}_r \qquad \cdots(6.44)$$

which is in fact the complex relative permittivity of the measured material.

Equation (6.44) shows, for Model VI, that the anharmonic ratio of relative permittivities in the reference plane may be equated with the anharmonic ratio of admittances in the measurement plane. In fact, the invariance principle means that *impedances* may be used in the measurement plane and transformed *admittances* (relative permittivities in the case of Model VI) in the reference plane. Thus, there is no need to transform measured impedance into admittance to calibrate the measurements using the above modified admittance models. For the same reason, the fact that Model I (i.e. equation (6.13)) is an impedance rather than an admittance is therefore unimportant.

The actual de-imbedding process differs in some respects for each of the six models. However, for the general case the following terms are defined :

*zmU* is the measured impedance of the unknown material
*zmA* is the measured impedance of aluminium
*zmF* is the measured impedance of free space
*zmL* is the measured impedance of 0.00507 mol.litre$^{-1}$ saline
*zmV* is the measured impedance of 0.09126 mol.litre$^{-1}$ saline

The above nomenclature allows the following *measurement difference parameters* to be defined :

*DUA=zmU-zmA*
*DUF=zmU-zmF*
*DUL=zmU-zmL*
*DUV=zmU-zmV*

Other difference parameters follow logically from the above format (e.g. *DFL=zmF-zmL* etc.).

Similarly, for model admittances :

*yA* is the modified model admittance for aluminium
*yF* is the modified model admittance for free space
*yL* is the modified model admittance for 0.00507 mol.litre$^{-1}$ saline
*yV* is the modified model admittance for 0.09126 mol.litre$^{-1}$ saline

This nomenclature leads to similarly defined *model difference parameters* (e.g. *DyFL=yF-yL* etc.).

**Impedance Measurement Calibration**

Thus, with reference to equations (6.25) and (6.26), and the difference parameters defined above, the anharmonic ratios resulting from measurements on the standard materials, and the required reference plane admittances for the unknown materials, are given, for Models II and VI, by the following expressions :

**Model II**

$$K_m = \frac{DUA}{DUL}\frac{DFL}{DAF} \qquad \cdots(6.45)$$

$$yU = \frac{K_m.yL.DyAF - yA.DyFL}{K_m.DyAF - DyFL} \qquad \cdots(6.46)$$

**Model VI**

$$K_m = \frac{DUA}{DUF}\frac{DVF}{DVA} \qquad \cdots(6.47)$$

$$\hat{\varepsilon}_{rU} = \frac{K_m.\hat{\varepsilon}_{rF}.DyVA - \hat{\varepsilon}_{rA}.DyVF}{K_m.DyVA - DyVF} \qquad \cdots(6.48)$$

where the dielectric constant subscripts *U, A, V* and *F* have the same meaning as in the difference parameters.

Similar expressions are easily obtained for the other models but II and VI are presented here as these models were subsequently found to give the most reliable results.

For models III and IV the geometrical coefficients are already known from the probe geometry, the frequency, and the values of the integrals $I_1$, $I_2$, and $I_3$, so that calibration of the impedance of the unknown material requires only three standards. However, the presence of the unknown geometrical parameter G in the modified versions of Models I, II and V means that measurements from two standard saline solutions, as well as the short and open circuit measurements, are required in order to de-imbed the unknown values of conductivity and dielectric constant. G is calculated as a first stage in the process for these models.

In the case of model II equation (6.46) may be re-written as :

$$G\hat{\varepsilon}_{rV}^{2.5} + \hat{\varepsilon}_{rV} = \frac{K_m.yL.DyAF - yA.DyFL}{K_m.DyAF - DyFL} \qquad \cdots(6.49)$$

where the unknown material has been replaced by the 0.09126 mol.litre$^{-1}$ saline solution. From this expression, in which G is the only unknown, a quadratic in G may be developed which can then be solved by the standard formula for the roots of a quadratic [117]. The actual calculation may be found in Appendix H.

### De-imbedding of Conductivity and Dielectric constant

In the case of Model VI the dielectric constant and conductivity may be obtained from the relative permittivity by simple direct calculation after equation (3.7). For Models I to V it is necessary to use the Newton-Raphson iterative method to de-imbed these parameters. By using the Mathcad package, however, the simple expression of equation (6.21) may be employed and the relative permittivity obtained as a single complex root. Taking Model II as an example, the expression for which the root is required will be :

$$\hat{\varepsilon}_r + G\hat{\varepsilon}_r^{2.5} - yU = 0 \qquad \cdots(6.50)$$

Applying equation (6.21) to this expression gives :

$$\hat{\varepsilon}_{r(n+1)} = \hat{\varepsilon}_{r(n)} + \frac{yU - \hat{\varepsilon}_{r(n)} - G\hat{\varepsilon}_{r(n)}^{2.5}}{1 + 2.5G\hat{\varepsilon}_{r(n)}^{1.5}} \qquad \cdots(6.51)$$

No formula is available for the calculation of an appropriate starting value. The author therefore used the theoretical relative permittivity value of a typical saline solution. This was found to always give successful convergence.

### Model Verification

The six models were used to calculate the dielectric constant and conductivity of various saline solutions (other than the calibration standards) from impedance measurements obtained for the electrode system of Figure 6.9. The results were compared to the expected theoretical values. Models II and VI were found to give the most acceptable results for the given electrode structure. The relative performances for these two were so close (identical over 45 of the 51 frequency points in the 100-1000 MHz range) that, due to the much simpler mathematical approach necessary to implement Model VI, all subsequent results for concrete and other measurements were obtained using this model.

The varied performances of the models is an indication of the semi-empirical nature of the formulae. Models III and IV gave the least acceptable results, perhaps because these incorporated specific values for the geometrical parameters of the probe which were calculated for open ended coaxial geometries with no extended central conductor [94][107]. Models I and V gave fair results but were not as accurate as II and VI. Again this is possibly a reflection of the semi-empirical approximations adopted by the relevant workers [95].

A comparison between the expected thoeretical value of dielectric constant and the values obtained by models II and VI for a 0.0608 mol.litre$^{-1}$ saline across the 100-1000 MHz frequency range is presented in Figure 6.13. Also, presented is the percentage difference between the theoretical and measured quantities. The standard solution used for these measurements was a 0.0913 mol.litre$^{-1}$ saline. It can be seen in this case that the measured values from the two models coincide exactly at each frequency point. The difference between theoretical and measured values is less than 2% at all frequency points. This is a very acceptable accuracy and compares very favourably with similar reported results in the available literature [94][96][103].

A similar comparison for the conductivity of a 0.0913 mol.litre$^{-1}$ saline is presented in Figure 6.14. The standard solution used in this case was a 0.00507 mol.litre$^{-1}$ saline. The precentage difference between theory and measurement is greater than for dielectric constant but is still $\approx$5% or less over most of the frequency range and it can be seen that the characteristic of the measurement follows that of the theoretical prediction very closely. This still compares well with the results of other workers [94][96][103]. The temperature of the saline solutions in each case was 18°C and the ambient temperature was 20°C.

The Mathcad de-imbedding procedures for Models II and VI are presented in Appendix H and Appendix I respectively.

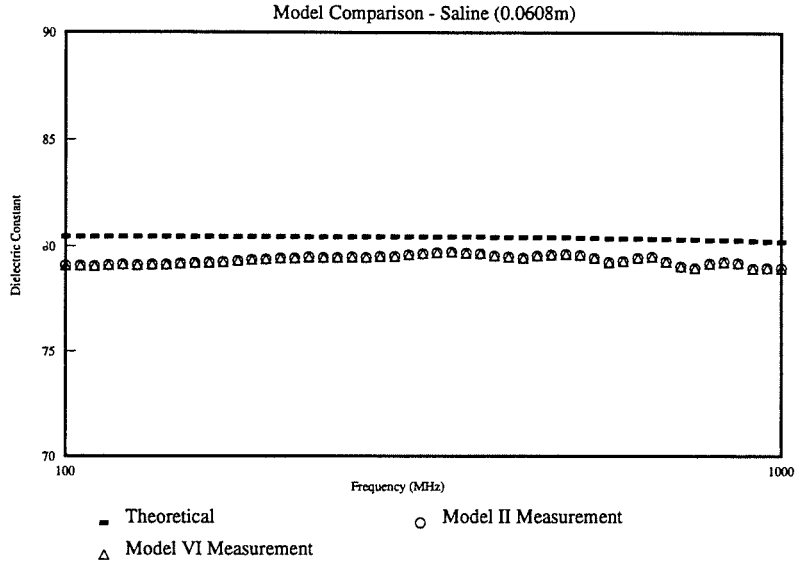


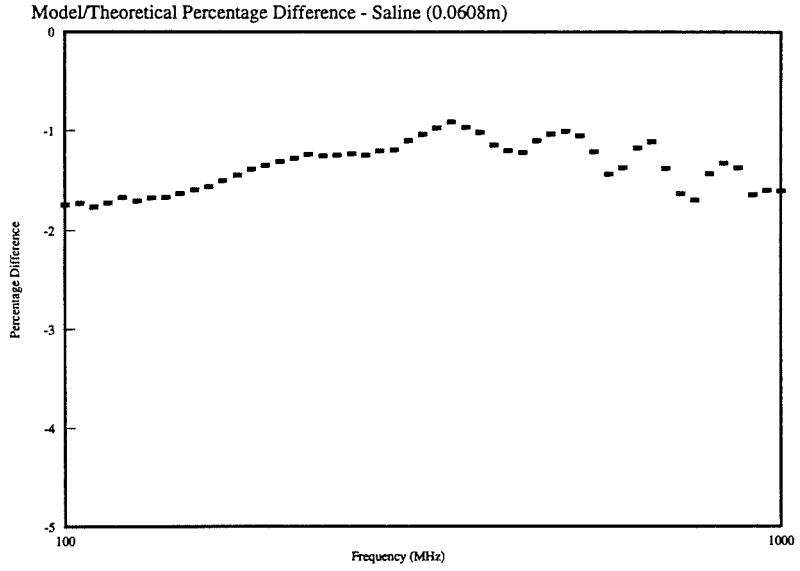


**Figure 6.13 Comparison of Theoretical and Measured Dielectric constant**

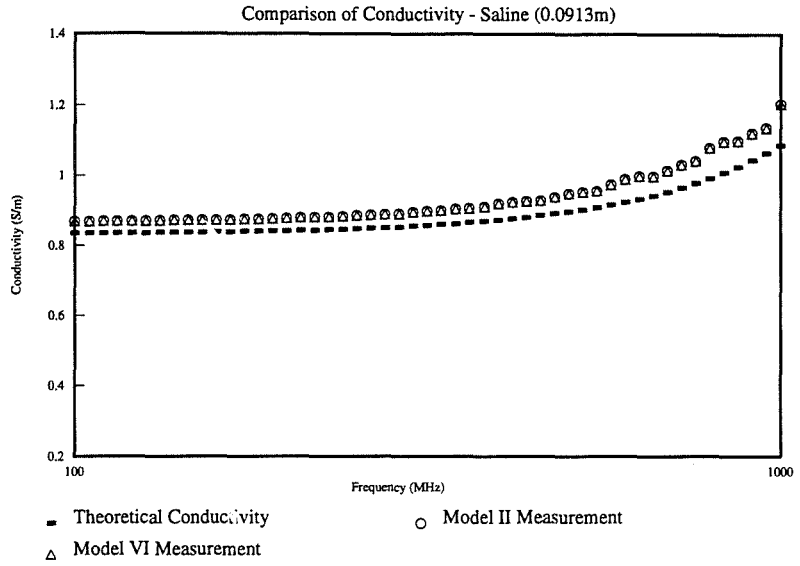


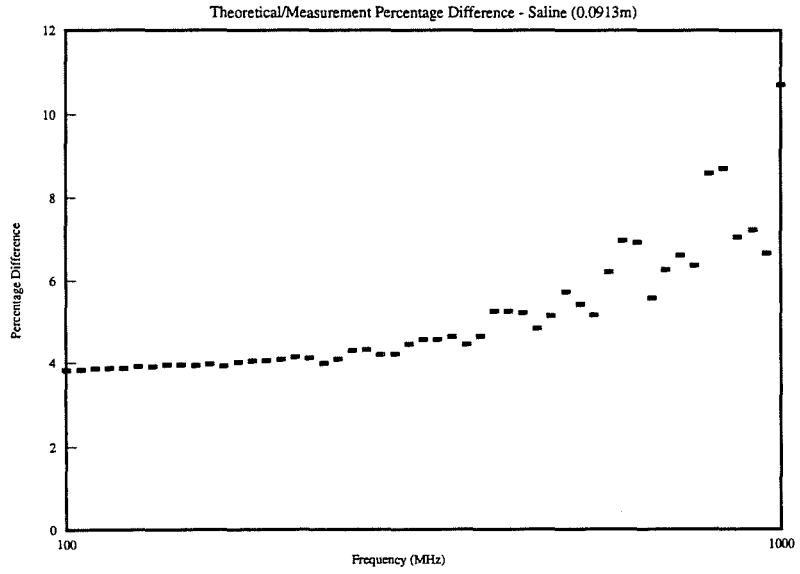


**Figure 6.14 Comparison of Theoretical and Measured Conductivity**

# CHAPTER 7

# Experimental Work

## 7.1 Measurement system

The measurement system used in this work was a simplified version of the one used by Wilson and Whittington [4][5] which is briefly summarised in sections 4.2.4 and 4.2.6. A block diagram of the overall system is presented in Figure 7.1.

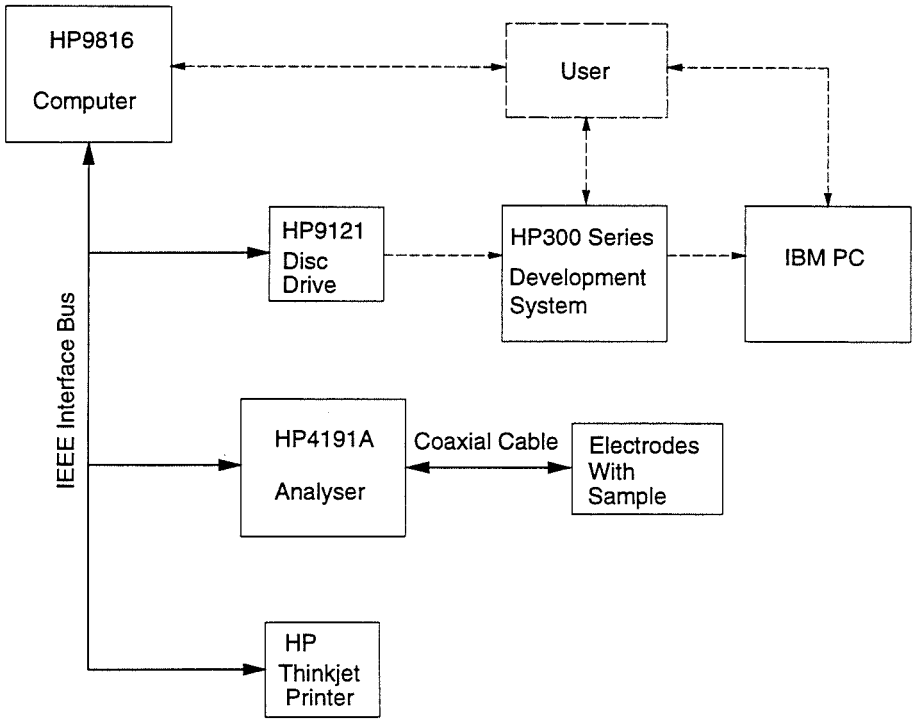


**Figure 7.1 Block Diagram of RF Measurement System**

The RF measurements are obtained using a HP4191A impedance analyser which is interfaced to the electrode/sample arrangement by a coaxial cable, as described in chapter 6. The analyser is controlled by means of a HP9816 microcomputer which communicates with it via an IEEE 488 interface bus. Impedance data are stored on 3.5 inch floppy disc carried by a HP9121 disc drive, and results are also printed out in tabular form on a HP Thinkjet printer. Both of these are also accessed via the IEEE bus. The timing of experiments is handled by software in the data acquisition

program run on the HP9816 computer which allows input of the mix details and gauging time at the start of each experiment, as analyser calibration is carried out. These details are also stored on floppy disc and printed out.

As mentioned in section 6.2.2, de-imbedding analyses of the fundamental electrical parameters from the impedance data was carried out using the **Mathcad** mathematics package. This package is run on an IBM compatible PC (personal computer) and will accept numerical data in the DOS operating system ASCII format. However, the HP9816 computer stores the arrays of acquired impedance data in binary form in an old Hewlett Packard format called LIF (Logical Interface Format), which means that they are not compatible with DOS or Mathcad. Software was therefore written to convert the binary files into LIF-ASCII. The LIF-ASCII files were then transferred to a HP series-300 computer, which was part of a development system in the Electrical Department at Napier University, where they could be converted in a two stage process, first into UNIX-ASCII and then into DOS-ASCII. The resulting files were then transferred to the IBM compatible PC on which all subsequent analysis, graph production, and word processing was carried out.

## 7.2 Experimental Procedure

### Materials and Mix Proportions

The cement used throughout the experimental work was from a single batch of Blue Circle OPC from Dunbar in East Lothian. Edinburgh tap water was used to gauge the cement. The aggregate used was medium concrete specification Tay sand [118], obtained locally. The sand was oven dried and allowed to cool to laboratory ambient temperature before each experiment. The use of the same batches of sand and cement for all the experiments was deliberate so as to ensure that any variability in results due to changes in material quality was minimised.

A total of five experiments were carried out at both frequency ranges (1-100 MHz and 100-1000 MHz) on different concrete mixes. The experiments carried out over the 1-100 MHz frequency range were designated PTM1 - PTM5, and those carried out over the 100-1000 MHz frequency range were designated ATM1 - ATM5. An extra experiment carried out at 20-200 MHz was designated TPM5 (see section 7.3.5).

The mix proportions used for each experiment, specified by water/cement (w/c) and cement/aggregate (c/a) ratio are presented in Table 7.1.

| Mix Proportions | | Frequency Range | | |
|---|---|---|---|---|
| w/c | c/a | 1-100 | 20-200 | 100-1000 |
| | | Experiment Title | | |
| 0.6 | 1/2 | PTM1 | * | ATM1 |
| 0.6 | 1/3 | PTM2 | * | ATM2 |
| 0.6 | 1/1.5 | PTM3 | * | ATM3 |
| 0.5 | 1/2 | PTM4 | * | ATM4 |
| 0.45 | 1/2 | PTM5 | TPM5 | ATM5 |

**Table 7.1 Experiment Titles and Mix Proportions Investigated**

These mix proportions were designed to allow comparison of three w/c ratios (0.6, 0.5 and 0.45) for a fixed c/a ratio (1/2), and three c/a ratios (1/2, 1/3 and 1/1.5) for a fixed w/c ratio (0.6).

In order to achieve a more homogeneous mix, no coarse aggregates were used in any of the experiments. It was reasoned that mortar could be considered an "idealised" concrete in which the aggregate has been spread more evenly throughout the material bulk. Neville [9] shows that the relationship between the compressive strength of mortar and concrete made with the same w/c ratio is linear up to at least 28 days after gauging, suggesting that their physical properties are linearly correlated. This is illustrated in Figure 7.2.

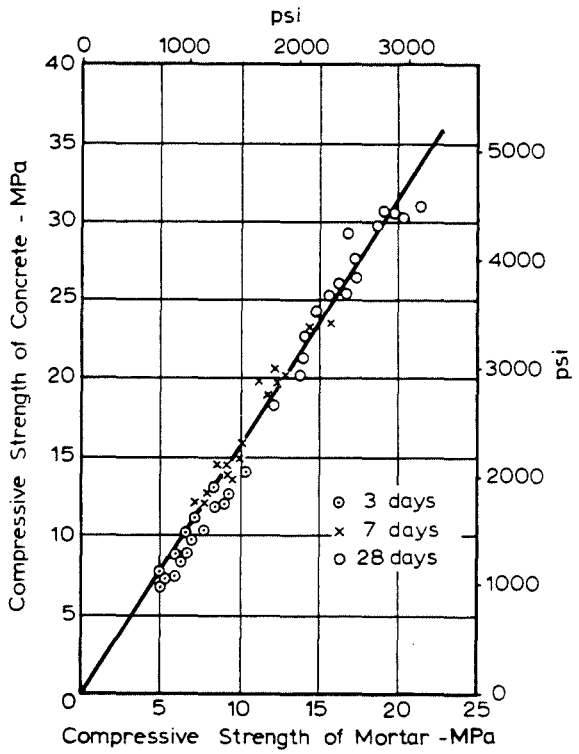


*Relation between the strengths of concrete and mortar of the same water/cement ratio*[1.37]

**Figure 7.2 Correlation Between Strengths of Concrete and Mortar**
(after Neville [9])

Also, the electrical behaviour of concrete and mortar will be predominantly determined by the cement paste (c.f. chapter 5) with the aggregate playing an essentially inert role. It was therefore assumed that the average RF electrical properties of mortar could be assumed to be closely representative of those of concrete containing coarse aggregate (in characteristic if not in absolute terms). The use of fine aggregates alone eased handling of the material at the mixing stage, and interfacing of the sample with the electrodes (especially with the hybrid antenna).

### Sample Manufacture

The 150 mm sample cubes were formed in PVC moulds, which were developed originally by Wilson [2]. The moulds were designed with a width of 154 mm so that two parallel plate electrodes of 2 mm thickness could be placed at opposite faces of the sample. For the parallel plate electrode system the electrodes were placed in the mould first then the concrete was poured in. For the hybrid antenna system the concrete was poured into the mould first then the measurement probe was placed on the top of the sample. This resulted in a sample width of 154 mm rather than the 150 mm of the true cubes. Figure 7.3 is a side view illustration of the sample/electrode arrangements for both frequency ranges in the moulds.

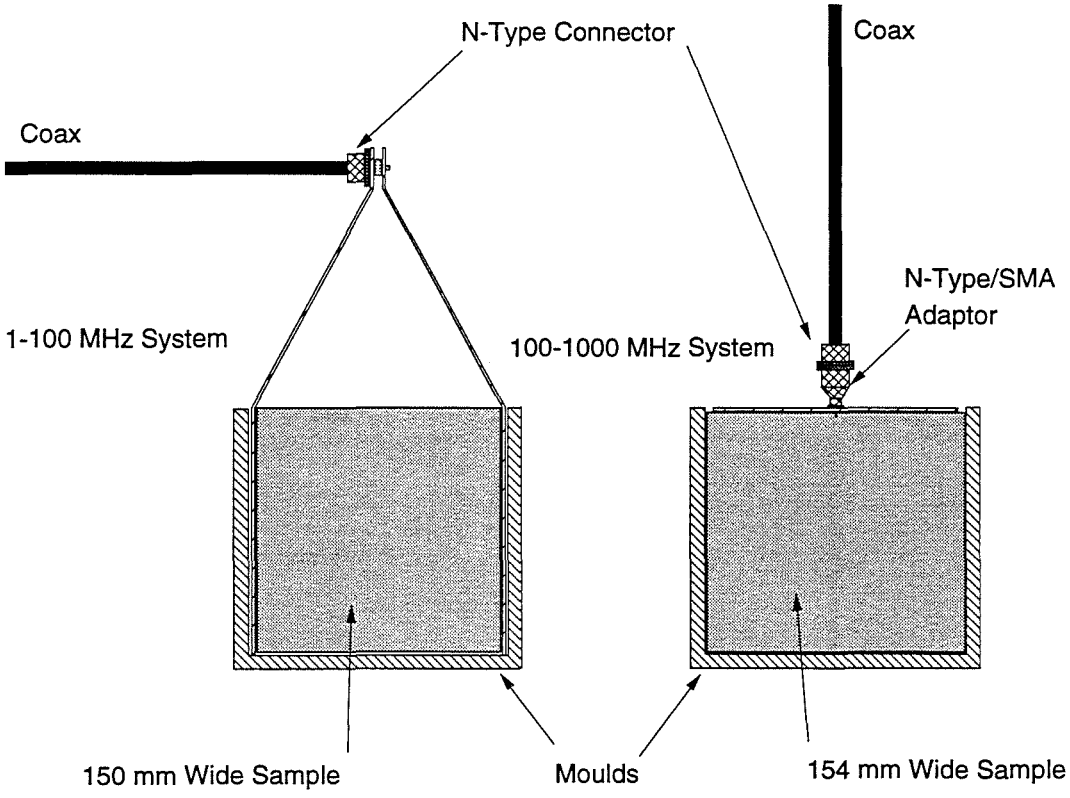


**Figure 7.3 Schematic of Sample/Electrode Arrangements in Moulds**

The concrete was made up in a small electrically powered mixer and mixed for a total of 6 minutes, stopping twice, after 2 and 4 minutes, to hand mix with a trowel. The mould, with electrodes fitted where appropriate, was placed on a vibrating table and the concrete was poured in in layers. Each layer was vibration compacted and the surface tamped down by hand. Once the mould was full the sample surface was

smoothed off and excess water removed by paper towelling. To fit the hybrid antenna a small spatula was used to first fill the coaxial recess with mortar from the sample then the probe was placed on top as shown in Figure 7.3. A small amount of vibration was used to ensure good contact between the sample and the probe.

**Period of Monitoring**

The monitoring period was limited to 1 day because of the need to assess different approaches (hardware and software) which necessitated the repetition of experiments. The previous results of Wilson and Whittington had suggested that changes between 1 and 6 days were much more gradual and did not show any dramatic variation in characteristic, whereas the period up to 1 day includes the change of state which occurs on setting. Also, it is the properties during the first 24 hours which are of most interest for the development of an early quality control test on concrete.

Measurements were carried out every hour from the first hour after gauging up to 6 hours. Therafter the measurements were carried out at logarithmically expanding time intervals, the changes in state of the material being expected to slow down after setting had occurred. Over each measurement range the frequency measurement points were spaced logarithmically. 96 points were covered in the 1-100 MHz range and 51 points in the 100-1000 MHz range. Nine measurement sweeps in total were taken across the 24 hour period, at 1-6 hours, and at 9.56, 15.15, and 24 hours.

When the measurement data was acquired the samples were demoulded and the surfaces inspected to check for voiding or faults, especially on the faces which had been adjacent to the electrodes. This was particularly important for verifying the validity of the 100-1000 MHz data because the process of fixing the hybrid antenna to the upper concrete surface was found to be awkward and it was crucial that no air voids or water pools were allowed to form in the vicinity of the aperture.

Because of the different analyser calibration requirements of the parallel plate electrode system (see section 6.2), the experiments using the two systems were carried out on different days. The actual concrete measured over 1-100 MHz was therefore not from the same batch as that measured over 100-1000 MHz or 20-200 MHz. However, care was taken to ensure as far as possible that the mix proportions were precisely adhered to, and that the mixing process was consistent.

When the cubes used with the parallel plate electrode system were demoulded they were stored under water at ≈20°C for a period of 28 days. After this they were allowed to dry at ≈20°C in the laboratory atmosphere for a further 12-14 days. They were then taken to the Building Engineering Department of Napier University and tested for compressive strength by crushing. The measurement of compressive strength thus obtained was subsequently used for comparison with the measured electrical properties of the sample. Although the crushing tests were not in strict accordance with BS1881 [88], which requires that they be carried out at 28 days, they were nevertheless applied consistently to the various cubes and so provided a good *relative* measure of compressive strength.

### Temperature Considerations

The ambient temperature in the laboratory was constant throughout all the experiments at ≈22°C, generally not varying by more than ±2°C.

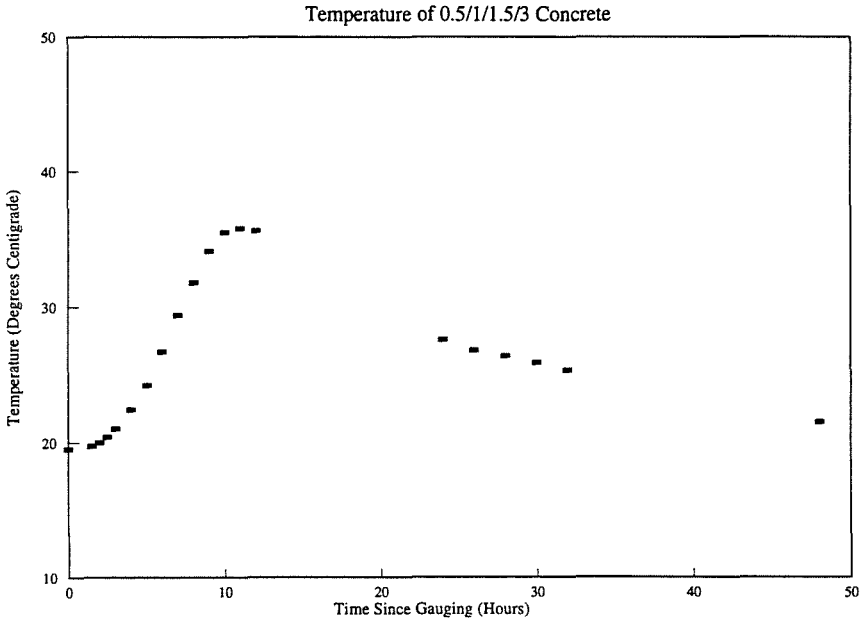


**Figure 7.4 Temperature Profile of 0.5/1/1.5/3 Concrete**

The internal temperature of the concrete samples was not monitored on an individual basis but Figure 7.4 shows the internal temperature profile of a typical concrete mix (w/c/s/a of 0.5/1/1.5/3) which was made in the same laboratory. The general characteristic of Figure 7.4 agrees with previously reported results [2][56][57], although actual temperature rise and time of peak will depend to some extent on mix

proportions, sample size, and sample insulation. For instance, Olp et al. [57] report a temperature peak of ≈64°C at approximately the same time as the peak of Figure 7.4 but their measurements were on cement paste in an enclosed brass cell at an ambient temperature of 25°C. McCarter and Afshar [56] found a peak temperature of ≈44°C for cement paste at an ambient temperature of ≈25°C (which suggests that the peak would be similar to Figure 7.4 at 20°C ambient), but their peak occurred ≈2 hours earlier. Wilson [2], on the other hand, found a temperature peak of only ≈30°C for a concrete of the same mix proportions and ambient temperature as that of Figure 7.4, but this occurred at ≈8 hours. In each case the characteristic shape was that of Figure 7.4 with the peak occurring after the cement had set.

**Measurement Accuracy**

The optimum operating temperature of the analyser is 23°C. Measurement accuracy is maximised by the use of good calibration standard terminations. The Hewlett Packard standard terminations (0 Ω, 0 S, and 50 Ω) are precision test pieces whose use at calibration will promote an accuracy for subsequent reflection coefficient measurements on the 50 Ω matched load of ±(0.0025+j0.00025) at any test frequency. The analyser itself is most accurate when measuring impedances which are close to the 50 Ω standard load. The impedance of the 20-200 MHz hybrid antenna electrode system in typical concrete (from the fresh to the hardening state) is between approximately 40 Ω and 450 Ω. For the 100-1000 MHz electrode system the equivalent figures are 20 Ω to 200 Ω. In both cases the accuracy of measurement will be lower at the high frequency end of the range where measurements have been found to be further from the 50 Ω standard, but for concrete both systems will provide better than 2% accuracy for all measurements and will be better than 1% for most. However, the impedance of the 100-1000 MHz electrode system in saline solution is much lower than 50Ω and decreases towards higher frequencies. In this case the measurement accuracy is about 2% at 100 MHz but decreases to 5% at ≈800 MHz, and at 1000 MHz may be even poorer. This lower accuracy will adversely affect the precision of the de-imbedded parameters because of the use of saline impedance measurements in the transition calibration procedure. In view of this limitation, the performance of the system, as shown by the comparison to theoretically calculated parameters for saline solutions in Figures 6.13 and 6.14, is therefore very good.

The effect of using the transition/transmission-line standards for the calibration of the analyser for use with the parallel plate electrodes is bound to be detrimental to measurement accuracy. It is not possible to estimate what the extent of the effect will be.

## 7.3 Experimental Results

### 7.3.1 Data for 1-100 MHz Range

Figure 7.5 shows the real and imaginary parts of impedance for a 0.45/1/2 concrete (PTM5) between 10 and 100 MHz at 1 hour and 24 hours after gauging. The impedance values are those acquired before transformation of the raw measurement data (see section 6.2.2).

It can be seen that an abrupt discontinuity occurs in both real and imaginary impedance at frequencies between 40 and 80 MHz. The discontinuity persisted when the raw impedance data was transformed by the calibration procedure, as illustrated in Figure 7.6, indicating that it was not present in the raw data simply as a result of the modified analyser calibration procedure (see section 6.2.2). It was found on de-imbedding of the conductivity and dielectric constant that the discontinuity also affected those parameters in the same frequency range.

The dielectric constant and conductivity of the concrete at 1 hour after gauging are shown in Figure 7.7. These results display traits which are entirely uncharacteristic of dielectric relaxation mechanisms (see chapters 3 and 5), especially the sudden dip to a large negative dielectric constant and the corresponding sharp conductivity peak (both at $\approx$60 MHz). The author concluded that the discontinuity was produced by the electrode hardware and not the electrical properties of the concrete. It was assumed that the discontinuity represented nonlinearities in the electrical characteristics of the electrode system which were severe enough to prevent the de-imbedding procedure from eliminating them. It could be that stray inductive and capacitive reactances not accounted for by the model are resonating at the affected frequencies. This effect should be investigated further.

To verify this conclusion a new electrode system based on the hybrid antenna used at 100-1000 MHz was constructed for use in the range 20-200 MHz. This frequency

range was chosen to provide overlap with both of the other ranges of investigation. The electrode system and results obtained in the 20-200 MHz range are considered in section 7.3.3.

In view of the problems with the parallel plate system it was decided to limit the frequency range for results analysis to 1-30 MHz, which lies sufficiently below the discontinuity to guarantee acceptable data.

**Range of Electrical Parameters - Single Mix**

Figure 7.8 shows the dielectric constant and conductivity for PTM5 at 1 hour and 24 hours after gauging over 1-30 MHz. These results are presented to show that the trend in both parameters between 10 and 30 MHz is essentially a continuation of that in the 1-10 MHz range. Subsequent results for PTM1-5 are therefore presented only for 1-10 MHz.

**Progression of Electrical Parameters - Single Mix**

Figure 7.9 shows the changes in dielectric constant and conductivity for PTM5 over the first 24 hours. The plots presented are for 2, 4, 6, 9.56, 15.15 and 24 hours. The progression in both parameters is typical of all the mixes in this frequency range.

**Comparison of Electrical Parameters - Various Mixes**

Figures 7.10 and 7.11 are a comparison of dielectric constant and conductivity for PTM1-5 at 1 hour and 24 hours respectively, and are presented to show the effect of differences in mix proportions.

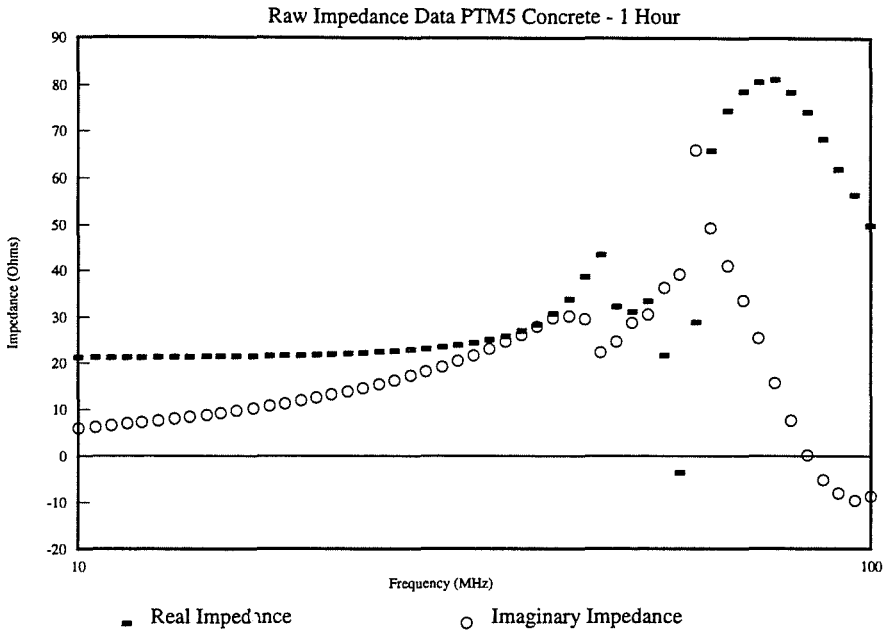


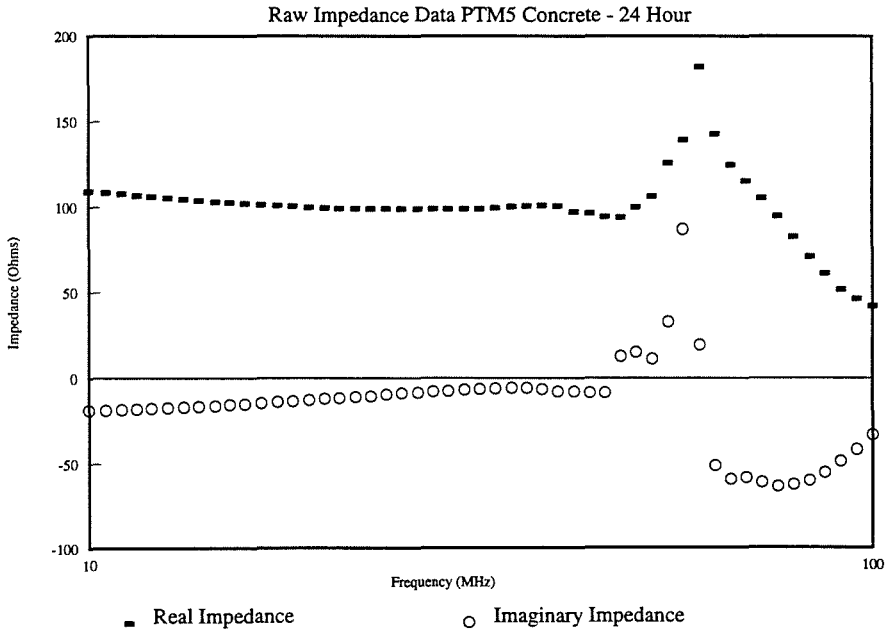


**Figure 7.5 Impedance of PTM5 Concrete at 1 Hour and 24 Hour**

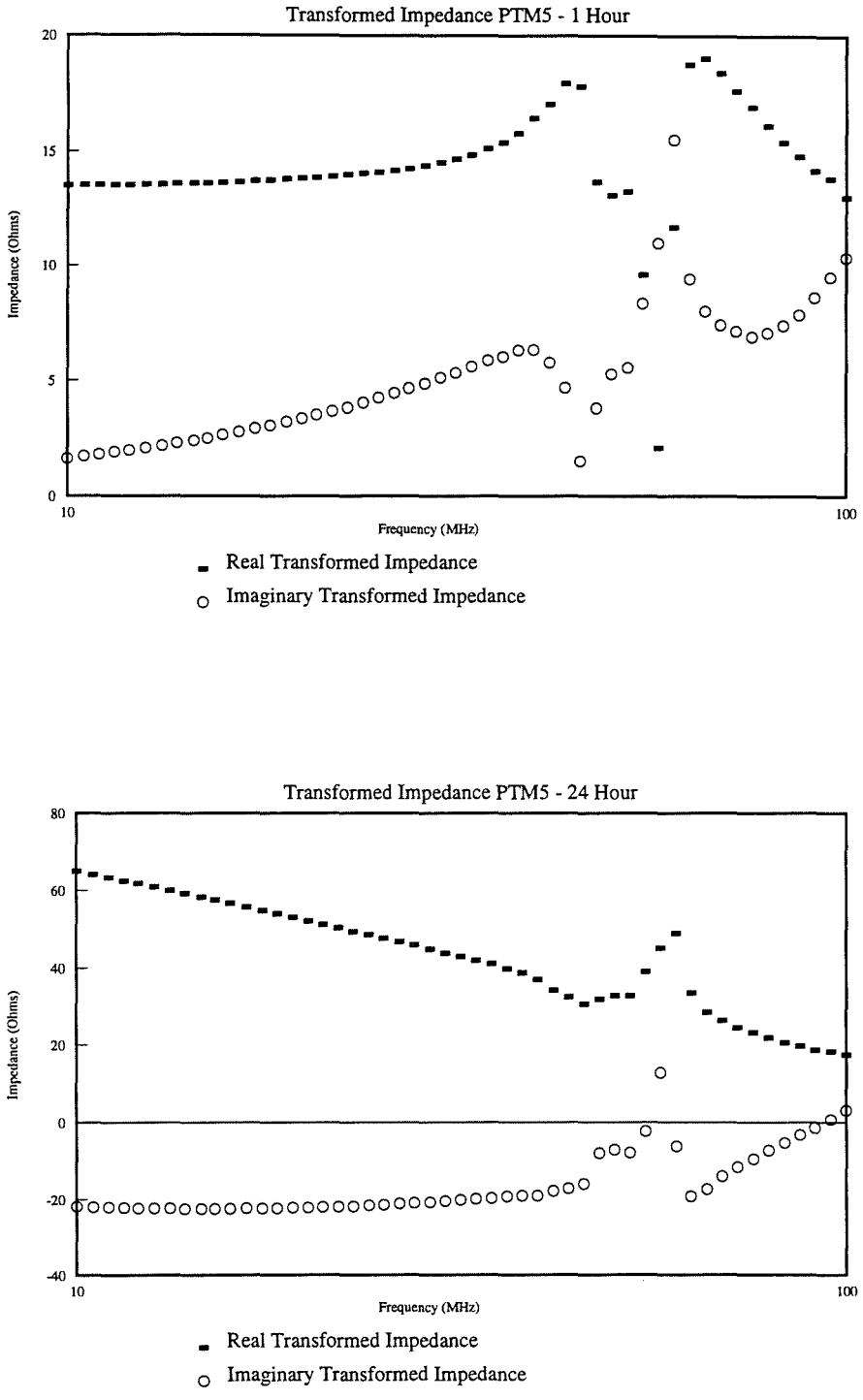


**Figure 7.6 Calibrated Impedance of PTM5 Concrete at 1 Hour and 24 Hour**

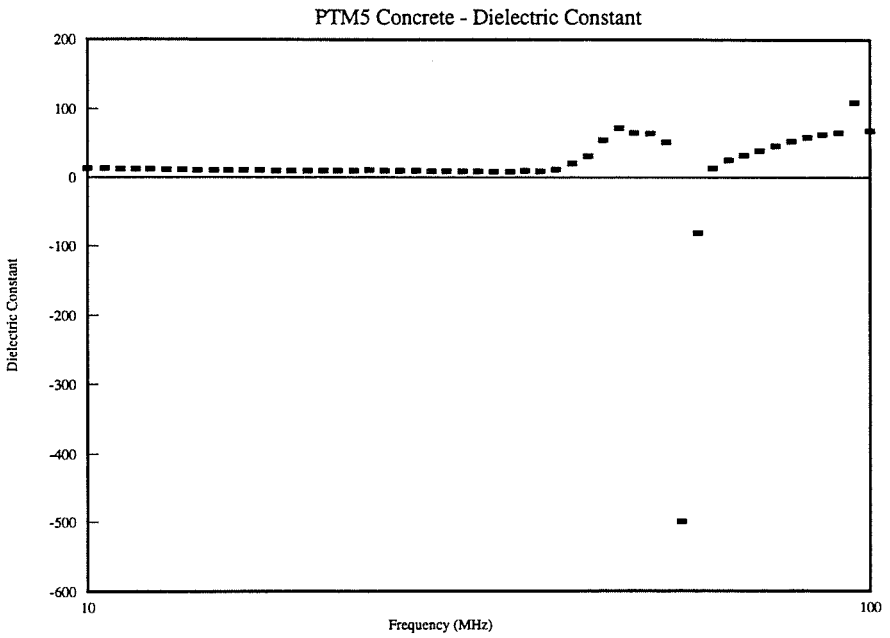


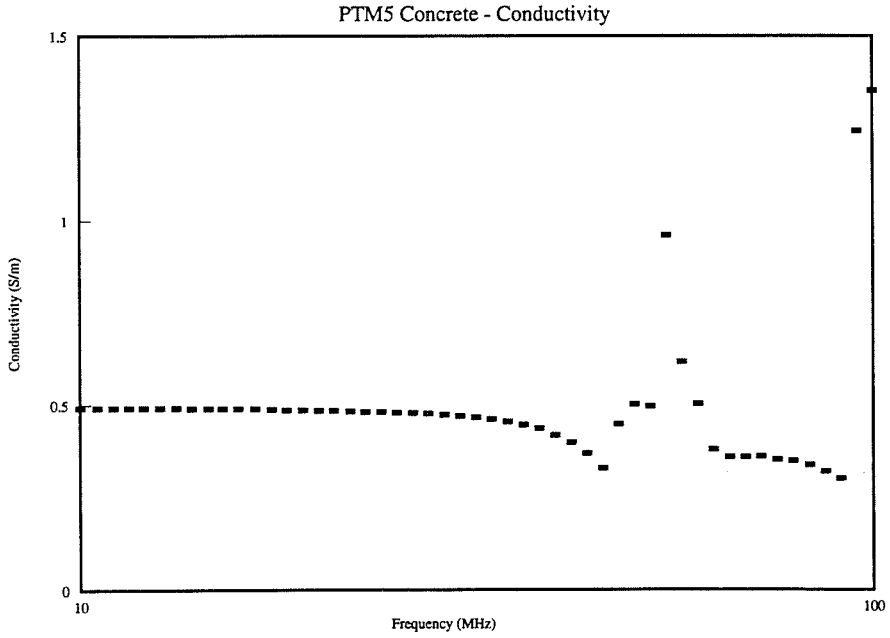


**Figure 7.7 De-imbedded Electrical Parameters of PTM5 Concrete at 1 Hour**

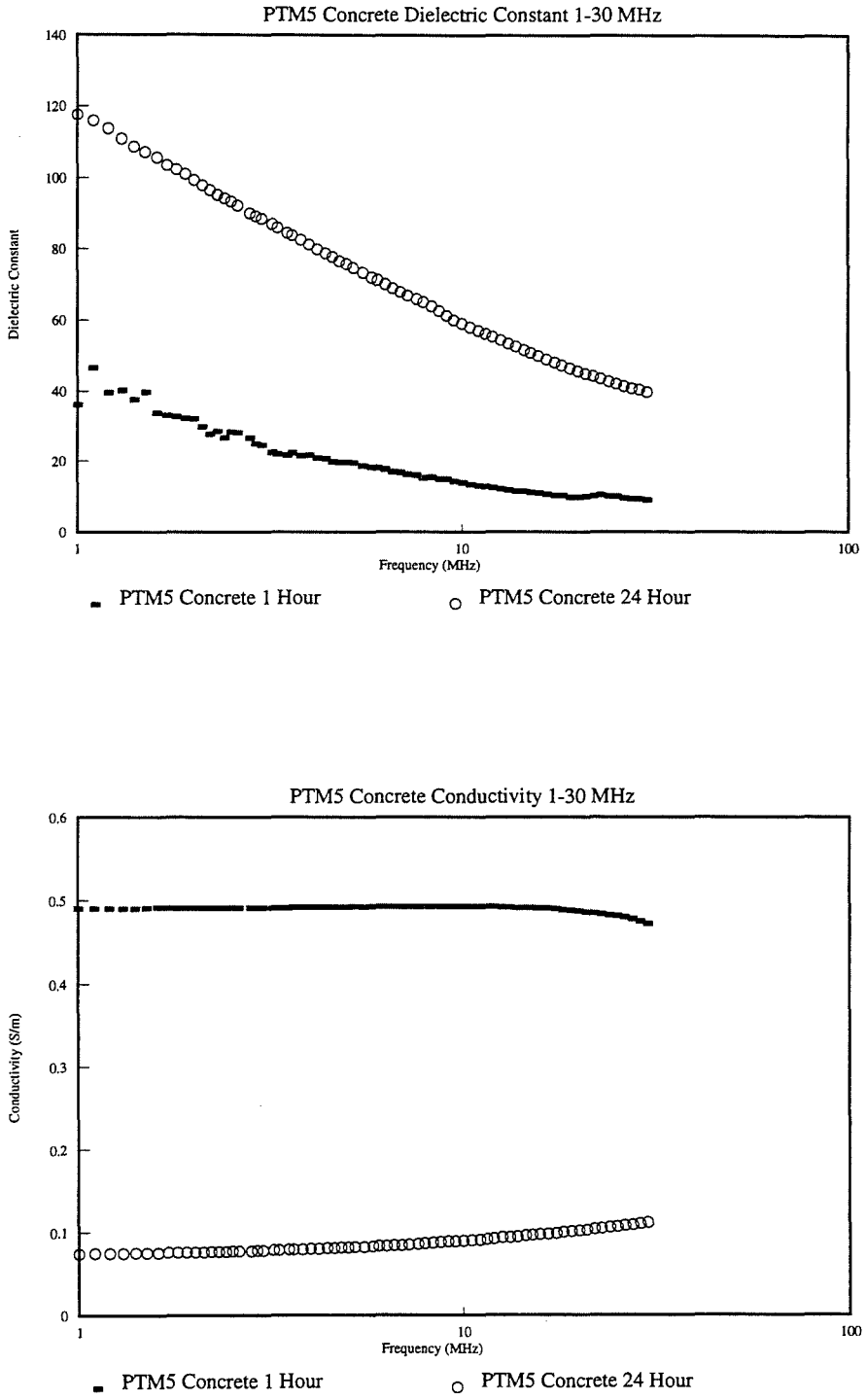


**Figure 7.8 Electrical Parameters for PTM5 at 1 and 24 Hours (1-30 MHz)**

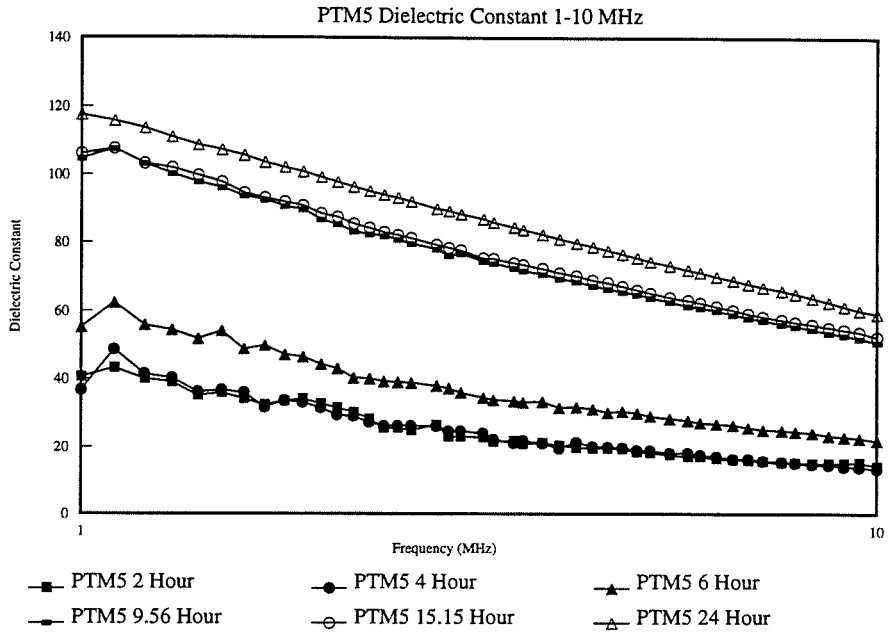


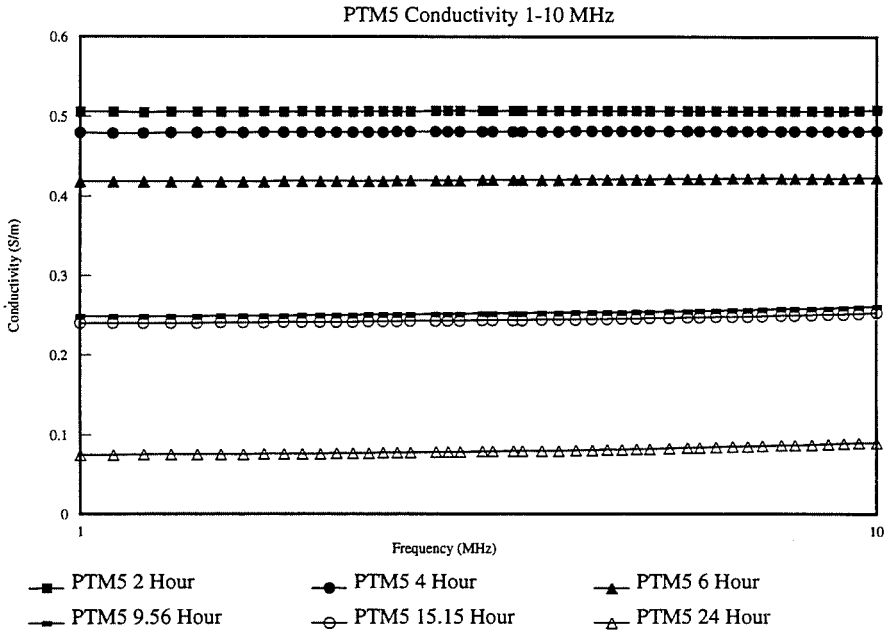


**Figure 7.9 Progression of Electrical Parameters for PTM5 over 24 Hours**

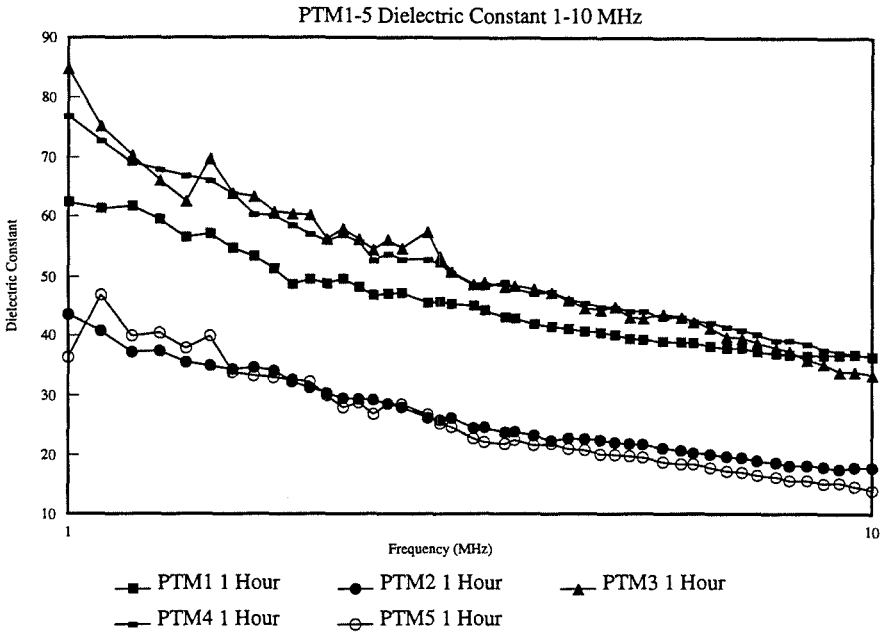


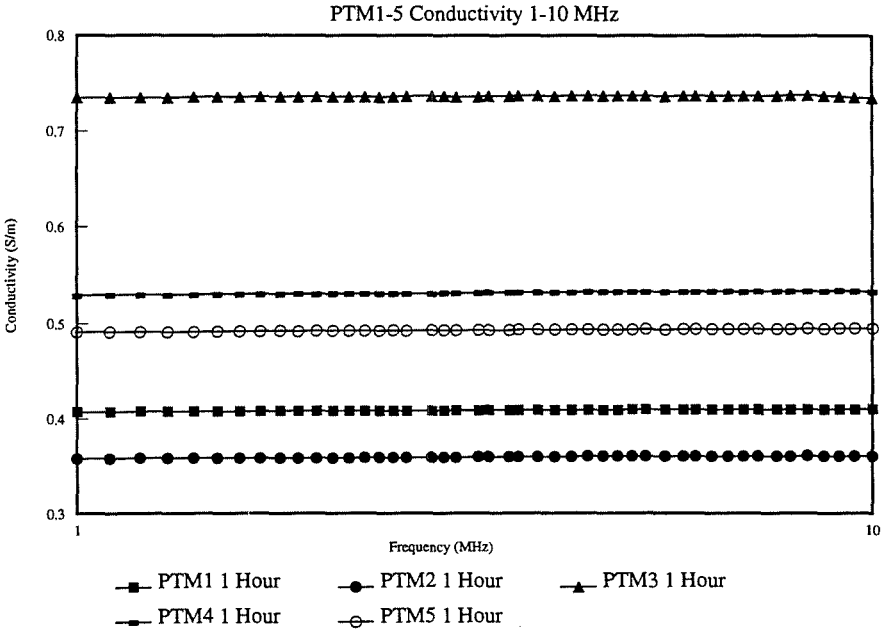


**Figure 7.10 Comparison of Electrical Parameters for PTM1-5 at 1 Hour**

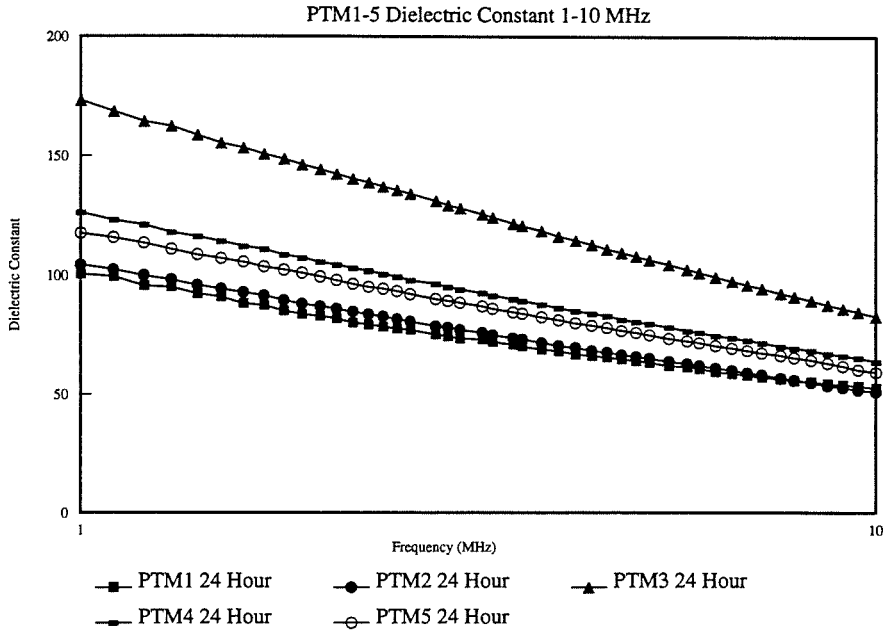


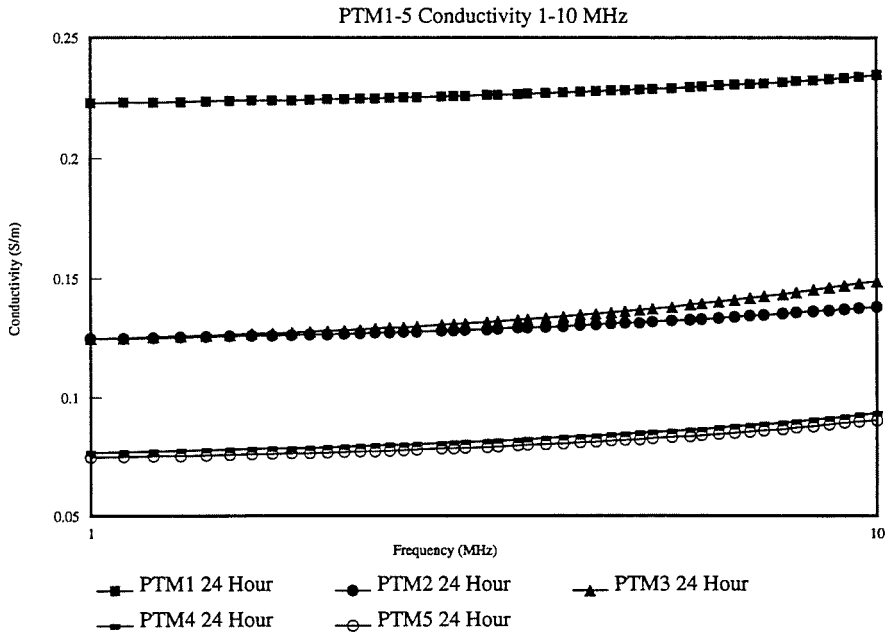


**Figure 7.11 Comparison of Electrical Parameters for PTM1-5 at 24 Hour**

### Compressive Strength Measurements

The cubes from experiments PTM1-5 were tested for compressive strength by crushing to destruction in the Building Engineering department of Napier University. The results are presented in Table 7.2

| Experiment | Mix | Strength |
|---|---|---|
| PTM1 | 0.6/1/2 | 33.973 MPa |
| PTM2 | 0.6/1/3 | 24.182 MPa |
| PTM3 | 0.6/1/1.5 | 38.444 MPa |
| PTM4 | 0.5/1/2 | 47.156 MPa |
| PTM5 | 0.45/1/2 | 50.756 MPa |

**Table 7.2 Compressive Strength of Concrete Mixes for PTM1-5**

While these figures are only a relative guide they can be seen to follow the pattern of decreasing strength for increasing w/c ratio, with constant c/a ratio, and decreasing strength for decreasing c/a ratio, with constant w/c ratio.

## 7.3.2 Data for 100-1000 MHz Range

Figure 6.11 showed a typical impedance plot for measurements acquired using the hybrid antenna probe. No difficulties relating to the electrode hardware were encountered in this frequency range. However, on completion of experiment ATM3 connection problems between the electrode system and the analyser were discovered. The results for ATM3 were therefore invalidated and are not presented here.

**Progression of Electrical Parameters - Single Mix**

Figure 7.12 shows the changes in dielectric constant and conductivity for ATM5 over the first 24 hours. The plots presented are for 2, 4, 6, 9.56, 15.15 and 24 hours. As for the 1-100 MHz case, the progression of both parameters with time is typical of all the mixes in this frequency range.

**Comparison of Electrical Parameters - Various Mixes**

Figures 7.13 and 7.14 are a comparison of dielectric constant and conductivity for ATM1-5 (without ATM3) at 1 hour and 24 hours respectively. Again, these are presented to show the effect of differences in mix proportions.

**Characteristic Comparison - Before/After Setting**

Figure 7.15 shows the characteristics of the dielectric constant for ATM5 before and after stiffening of the cement paste, which occurs at about 7 hours (section 2.1.4). The upper graph shows the plots for 1 - 6 hours and the lower one for 9.56, 15.15 and 24 hours.

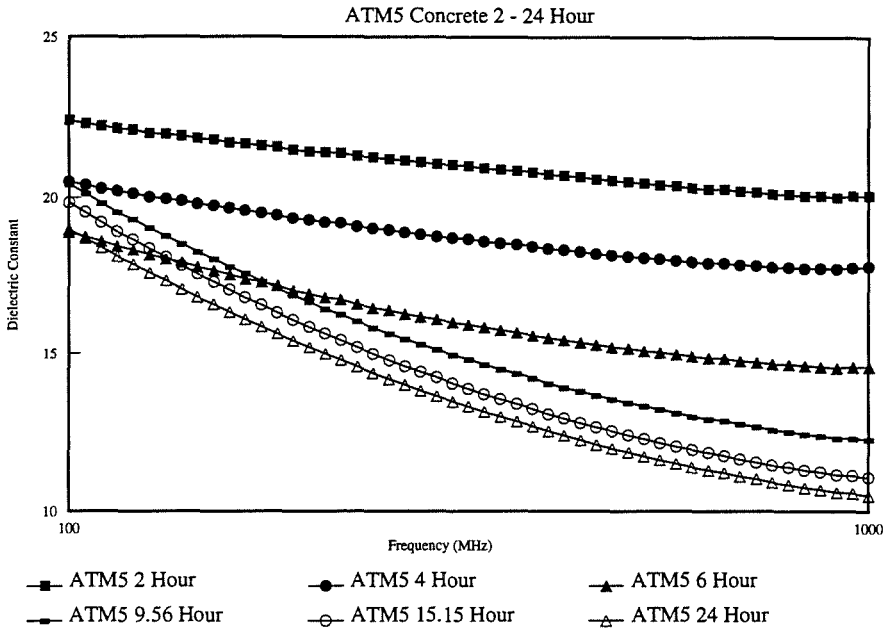


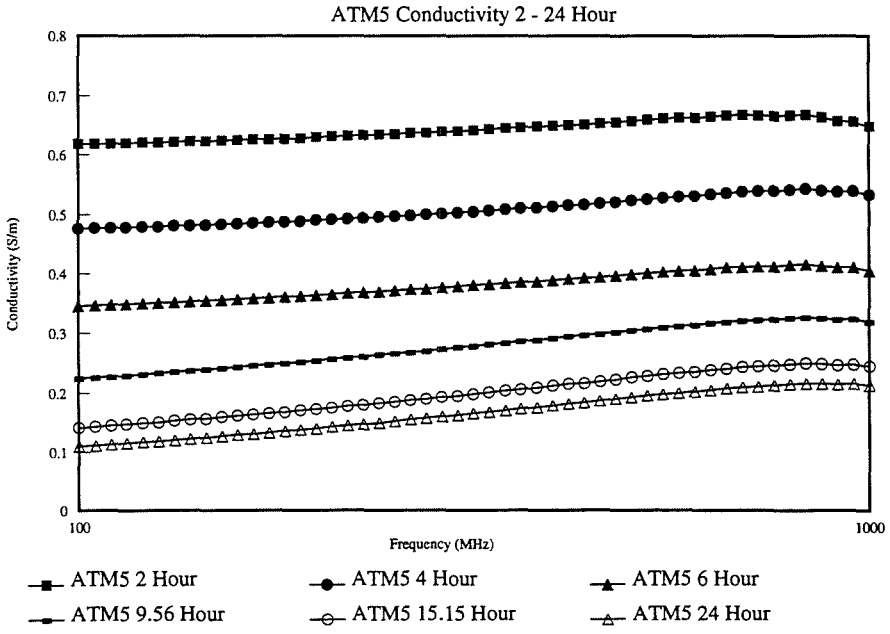


**Figure 7.12 Progression of Electrical Parameters for ATM5 over 24 Hours**

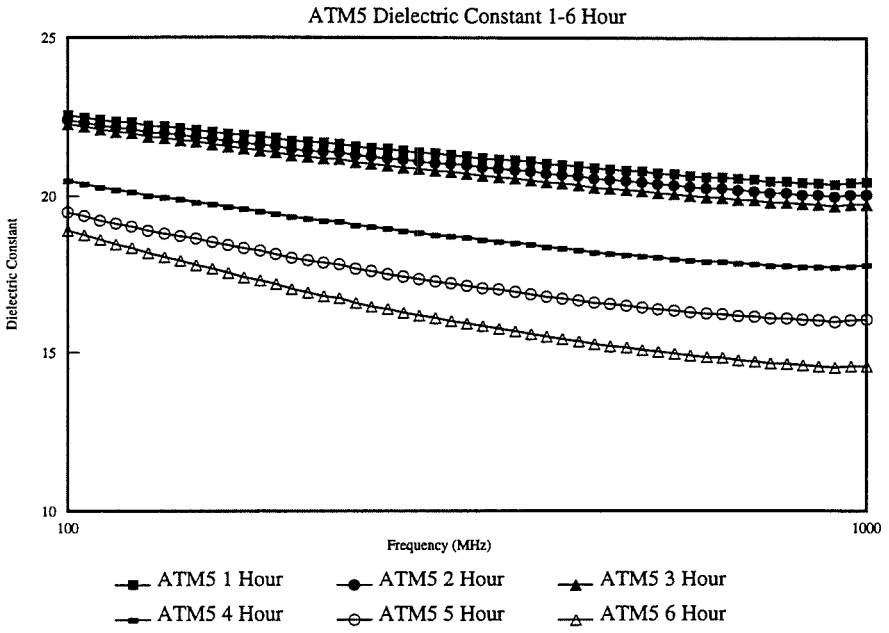


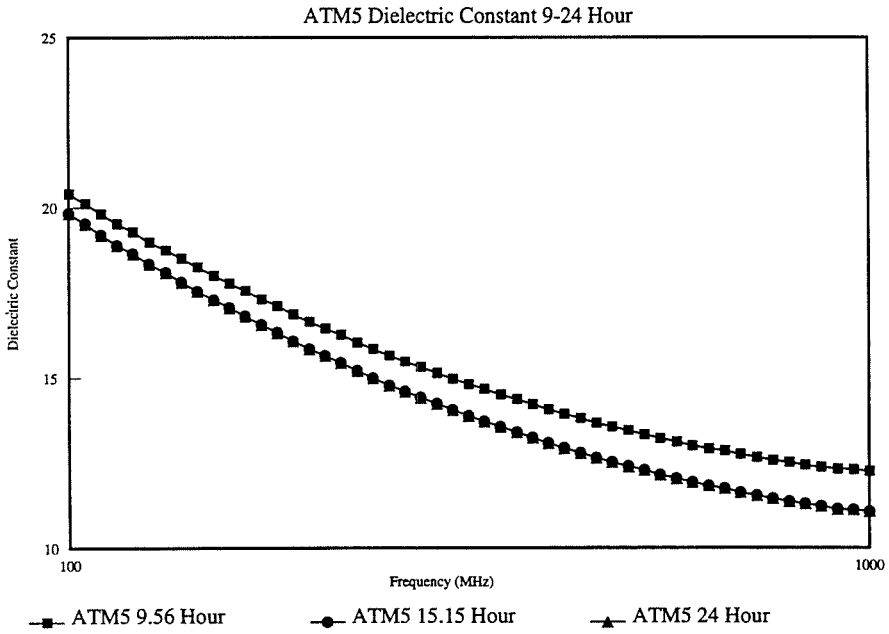


**Figure 7.13 Dielectric Constant for ATM5 Before and After Stiffening**

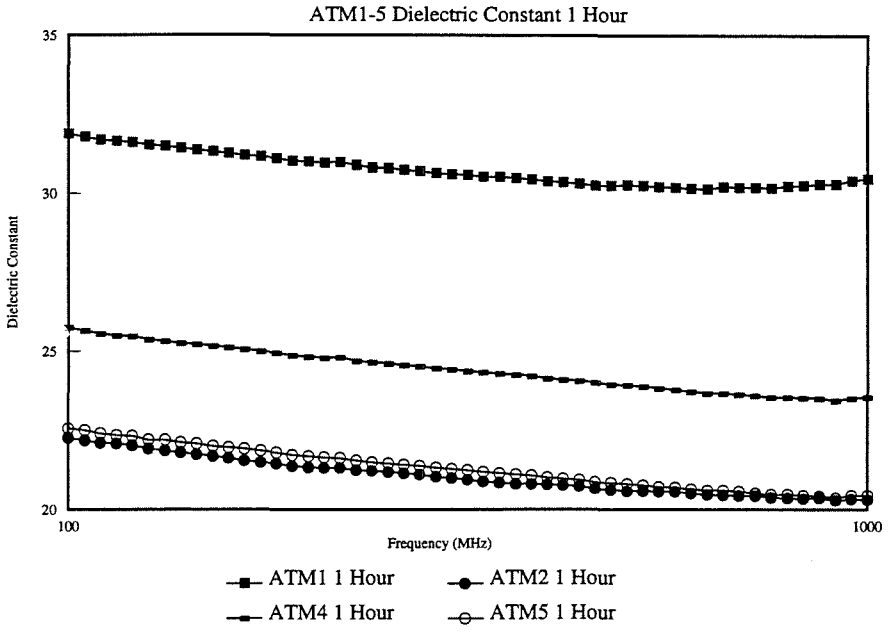


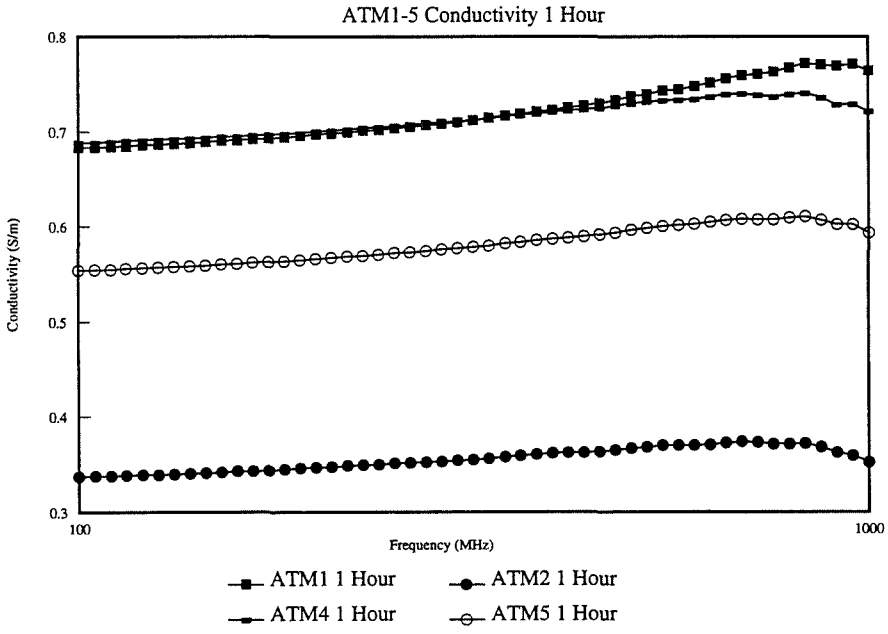


**Figure 7.14 Comparison of Electrical Parameters for ATM1-5 at 1 Hour**

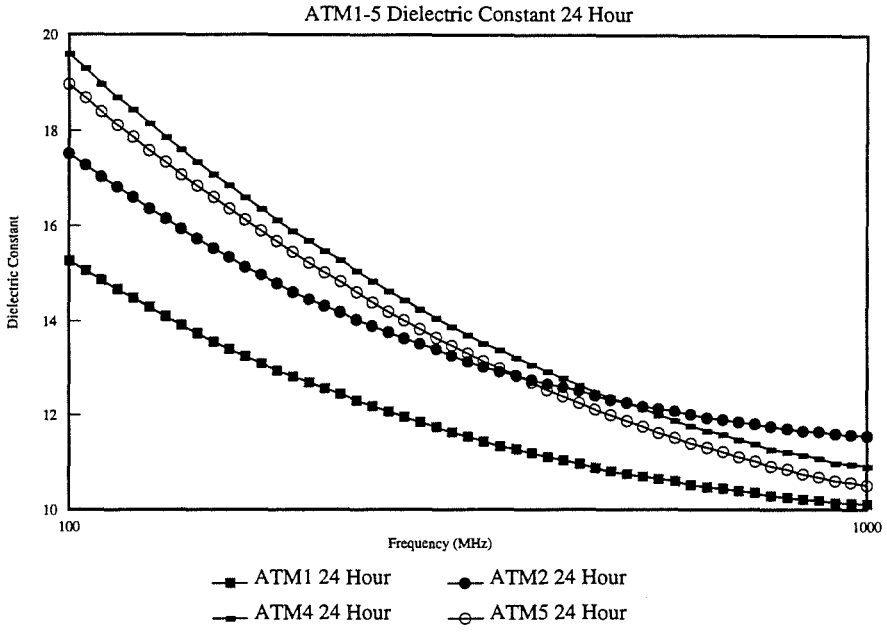


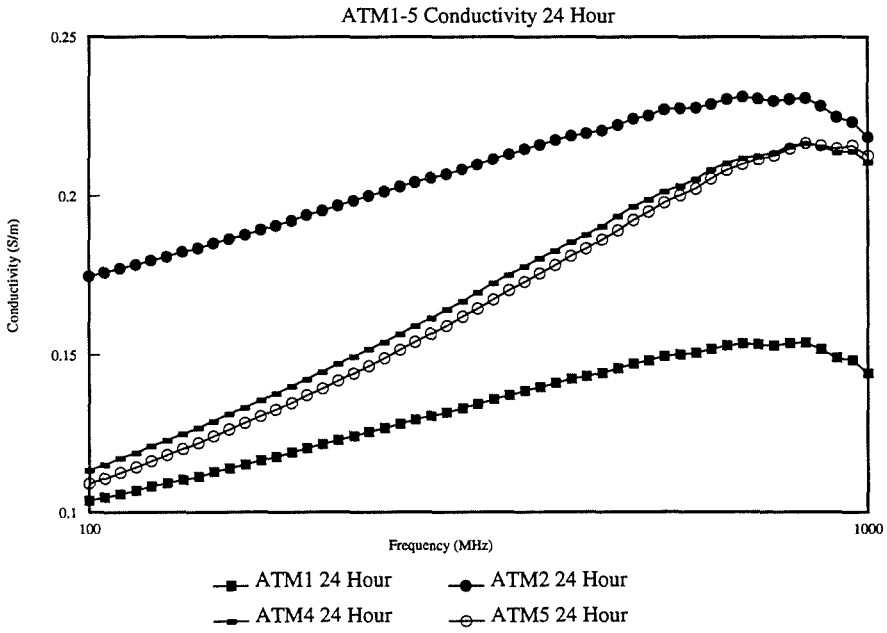


**Figure 7.15 Comparison of Electrical Parameters for ATM1-5 at 24 Hour**

**Measurements on Sand/Saline Mixture**

Measurements were also performed in this frequency range on a sample of Tay sand saturated with saline. The LF conductivity of the saline (≈0.0203 mol.litre$^{-1}$) was measured using a Wayne-Kerr bridge analyser to be 0.2007 Sm$^{-1}$. The sample was prepared in a sealed PVC concrete mould with 150 mm square stainless steel electrodes at opposite faces. The mould was first filled with saline and the oven dried sand was gradually added until the sand level reached the top edge. The mixture was compacted using vibration as in the preparation of the concrete samples. The saline displaced by the sand was collected and its mass measured. The mass was then converted into a volume and this was subtracted from the original volume of saline in the mould to calculate the porosity of the sand/saline mixture. The mass of sand added to the mould was also calculated from the mass of the displaced saline and a measurement of mould/sample mass increase.

The LF conductivity of the sample was measured using the Wayne-Kerr bridge, then the stainless steel electrodes were removed from the mould and the hybrid antenna electrode system fitted. The sample details were as follows :

**i)** Volume of sand 1.95 litres

**ii)** Mass of sand 4.925 Kg

**iii)** Volume of saline 1.425 litre

**iv)** Saline LF conductivity 0.2007 Sm$^{-1}$

**v)** Sand/saline LF conductivity 0.05507 Sm$^{-1}$

The measured dielectric constant and conductivity of the sand/saline sample in the 100-1000 MHz range are shown in Figure 7.16.

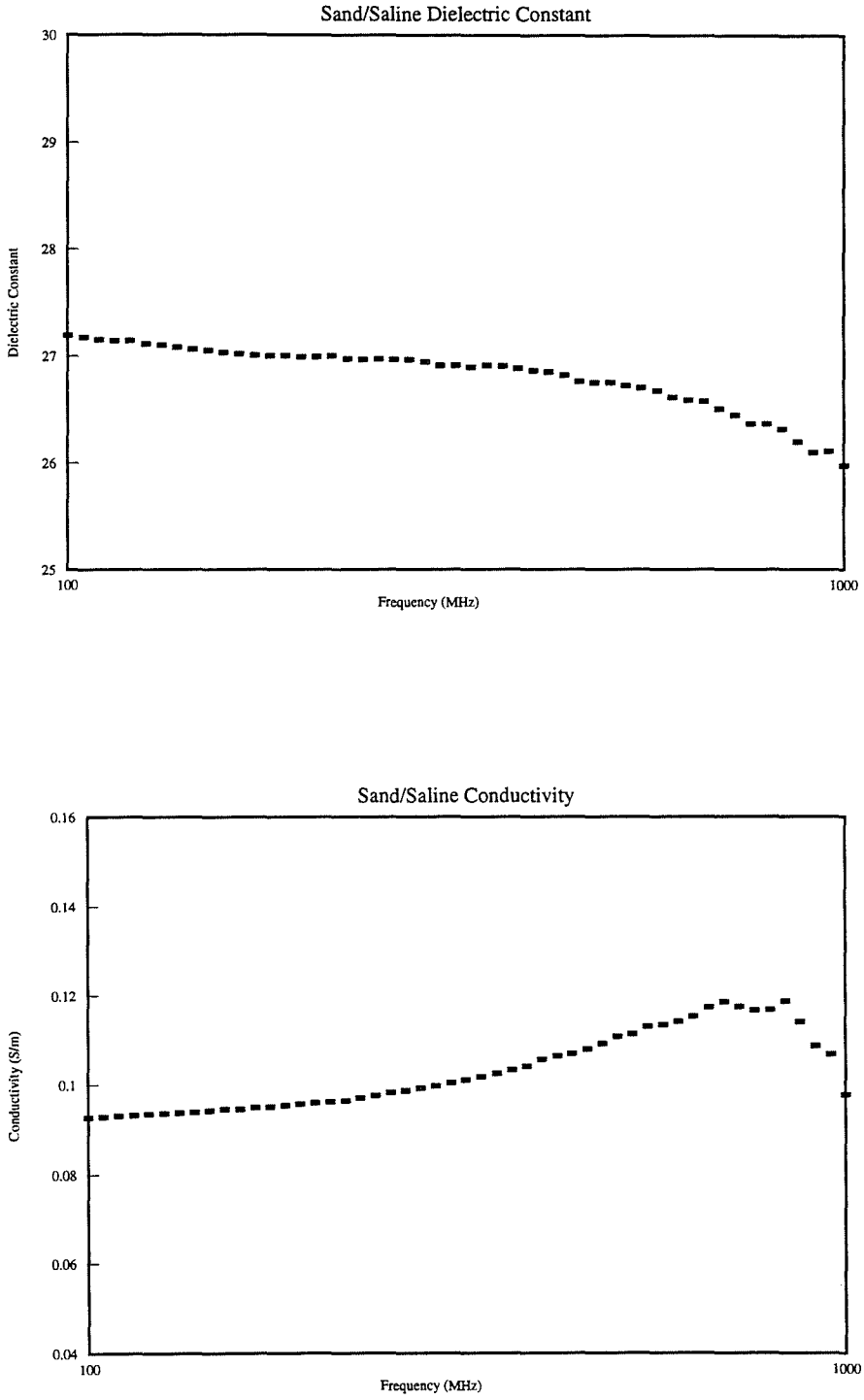


**Figure 7.16 Electrical Parameters of Sand/Saline Sample 100-1000 MHz**

### 7.3.3 Measurements at 20-200 MHz

The results presented in Figures 7.5 to 7.7 demonstrated the apparent inadequacy of the parallel plate electrode system at frequencies above ≈35 MHz. To make sure that the anomalous results were not due to the electrical properties of the sample material it was decided that measurements should be acquired in the affected frequency range using an alternative electrode system. A probe similar to the one used at 100-1000 MHz was therfore constructed for use in the 20-200 MHz band.

An N-type jack receptacle was used in place of the SMA jack of the 100-1000 MHz probe (c.f. Figure 6.9). The central conductor of the N-type jack was extended by soldering on a length of brass rod. The central hole of the ground plane was increased in size to accommodate the N-type jack but the other ground plane dimensions remained unchanged (150 mm square). The probe and aperture dimensions for this electrode system were :

**i)** Inner conductor radius 1.6 mm

**ii)** Outer conductor radius 5mm

**iii)** Recess of coaxial insulation 2mm

**iv)** Length of antenna above ground plane 5 mm

This system was calibrated in the same way as the 100-1000 MHz system with a short circuit of aluminium foil, an open circuit into free space, and a saline solution standard of concentration 0.0927 mol.litre$^{-1}$ with measured LF conductivity of 0.814 Sm$^{-1}$.

Measurements of impedance for a 0.45/1/2 concrete (see Table 7.1) were acquired over the first 24 hours after gauging. Dielectric constant and conductivity were subsequently de-imbedded from these using a modified version of the procedure presented in Appendix I. The results for 4 to 24 hours are presented in Figure 7.17.

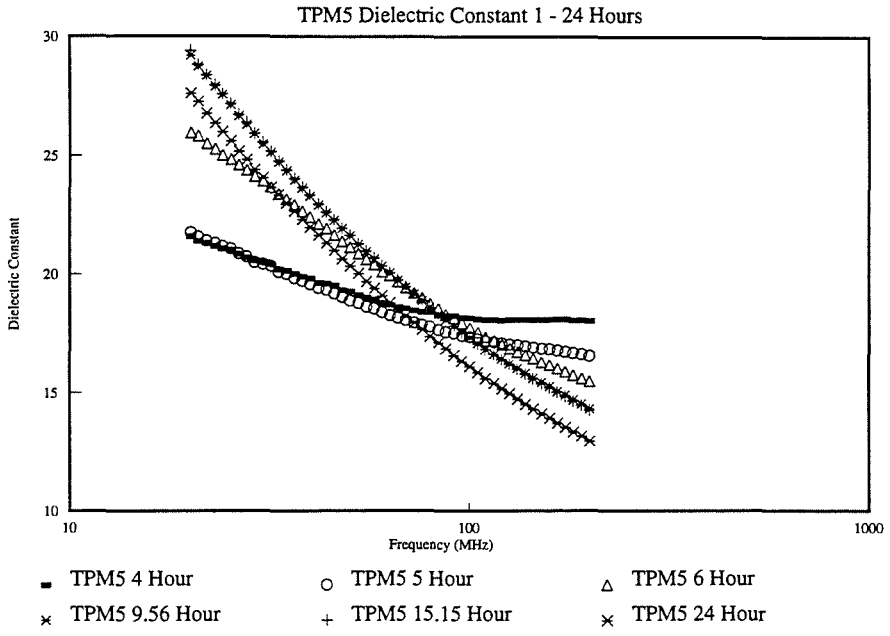


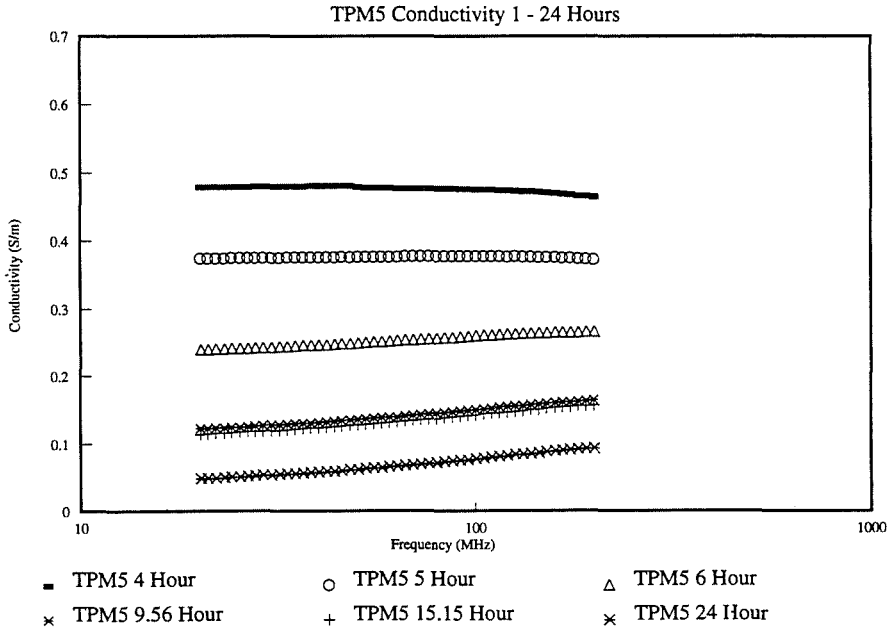


**Figure 7.17 Progression of Electrical Parameters for TPM5 for 4-24 Hours**

## 7.4 Results Analysis

### 7.4.1 Discussion of Results 1-100 MHz

#### Progression of Electrical Parameters - Single Mix

Figure 7.9 shows the dielectric constant and conductivity for PTM5 (0.45/1/2) from 2 to 24 hours after gauging. The general trend in the dielectric constant is for an increase with time. The downward gradient with increasing frequency can be seen to steepen as hydration of the cement proceeds. This is consistent with the theory presented in chapter 5 (sections 5.2 and 5.4) which predicts an increase in polarization in the lower MHz frequency range as the fibrous gel structure develops and conducting ions become increasingly trapped or piled up at barriers, promoting large space charge accumulation.

The relaxation of dielectric constant evident in the early stages of hydration (2 hours) is due to the effects of ionic double layer polarization around hydrating cement grains. Although this is very much a low frequency phenomenon, the induced polarizabilities are so big, and the dispersion so gradual, that the residual effects in the low MHz region are still observed (see sections 5.1.5 and 5.2.1).

The conductivity shows a corresponding trend with a general decrease with time. This is consistent with the increasing tortuosity and constriction of the conduction paths within the cement paste as the structure develops. It is notable that there is an abrupt increase in dielectric constant and decrease in conductivity between 6 and 9 hours. This is the period when the cement paste sets (≈7 hours - section 2.1.4) and the structure becomes more polarizable and less conducting.

These results agree in characteristic with those of Olp et al. [57] and Taylor and Arulanandan [49], and also confirm that concrete does not display negative dielectric constant values at frequencies below 100 MHz (see chapter 1).

### Comparison of Various Mixes - Fresh Concrete

Figure 7.10 shows that the general trend in dielectric constant at 1 hour is the same for all five mixes. This is also the case for conductivity. However, there are some points of note in these graphs. For instance, it could be expected that PTM1 should have a higher early conductivity and dielectric constant than both PTM4 and PTM5 (which have the same aggregate content) because of its higher w/c ratio, but this is not the case. Instead, the conductivity is lower than for both of these mixes and the dielectric constant plot lies between them at the lower end of the range. The dielectric constant of PTM1 does begin to exceed that of PTM4 at ≈10 MHz suggesting that it will be higher at frequencies above this. This is confirmed for 100-1000 MHz by Figure 13, although the comments in section 7.4.2 relating to the ATM1 measurements should be noted. The dielectric constant of PTM4 is higher than might be expected considering the similarity in mix proportions to PTM5 which has a much lower value.

PTM5 and PTM2 have almost equal dielectric constant across the whole range but PTM2 has a substantially lower conductivity than PTM5. The water/solid ratio (w/s - solids being cement plus aggregate) of both these mixes is virtually the same (i.e. ≈0.15) which explains the similarity in dielectric constant at this stage. The conductivity difference is due to the higher proportion of aggregate, which does not contribute conducting ions to the mix, in the solids of PTM2.

As would be expected PTM3 has the highest value of conductivity of all the mixes in the fresh state. The dielectric constant for this mix is also one of the highest at the lower end of the frequency scale but it is not substantially different to that of PTM4 which has lower water and higher aggregate contents. No measurements for ATM3 are available with which to compare the PTM3 results.

### Comparison of Various Mixes - Hardening Concrete

The dielectric constant and conductivity dispersions for hardening concrete (24 hours) are presented in Figure 7.11. At 1 MHz the dielectric constants range from 100 to 173 and at 10 MHz from 50 to 82. The conductivities range from 0.075 to 0.223 $Sm^{-1}$ at 1 MHz and from 0.09 to 0.235 $Sm^{-1}$ at 10 MHz. All the mixes show strong evidence of wide relaxation dispersions in both dielectric constant and conductivity. PTM3 has the highest dielectric constant across the whole range and

also the steepest, which is to be expected given the relatively high w/c ratio and low c/a ratio. Again however, some apparent anomalies are present with respect to the relative position of the plots. The dielectric constants of PTM4 and PTM5 are quite close together, with PTM4 being slightly higher, as might be expected due to its higher w/c ratio, but the plots of PTM1 and PTM2 (w/c 0.6) are both lower than PTM5. The reasons for this are not obvious but the dielectric constants do correspond with the equivalent plots for ATM1-5 at 100-1000 MHz (see Figure 7.14).

Except for PTM3, the conductivity plots fall into a more expected pattern. It is surprising, however, that PTM1 rather than PTM3, of the three mixes with w/c ratio 0.6, should have the highest conductivity. Again, though, there is consistency with the equivalent plots for ATM1-5 in Figure 7.14.

Despite the unexpected relative positions of the plots for both parameters, the general pattern observed for the hardening concrete is consistent with the proposed theory of sections 5.2.2 and 5.4.2.

## 7.4.2 Discussion of Results 100-1000 MHz

### Sand/Saline Mixture

From the porosity of the mixture and the conductivity of the saline a value of LF mixture conductivity may be calculated using Archie's law [44] which is expressed by equation (3.48). This equation is based on an assumption of round sand grains. The porosity was found from the volume of saline (1.425 litre) and the volume of the sample cube (3.375 litre) to be 0.4222. For the measured LF conductivity of saline (0.2007 $Sm^{-1}$) the mixture conductivity given by equation (3.48) for this porosity is 0.05506 $Sm^{-1}$, which is remarkably close to the measured value of 0.05507 $Sm^{-1}$.

The RF dielectric constant and conductivity of the mixture (Figure 7.16) show evidence of a relaxation process in the 100-1000 MHz range. The dielectric constant falls from 27.2 at 100 MHz to 26.0 at 1000 MHz. The conductivity rises from 0.0929 $Sm^{-1}$ at 100 MHz towards $\approx$0.12 $Sm^{-1}$ at $\approx$800 MHz. The conductivity

values shown actually drop between 800 and 1000 MHz but this is probably due to the use of the simplified antenna model (see section 6.2.3) and the peak value was taken as the HF limit.

The dielectric constant at 1000 MHz should be the true mixture value as all space charge relaxation mechanisms, as well as bound water and conductivity effects, can be expected to have dropped out at this frequency (see Figure 5.2). It should therefore be possible to verify the accuracy of dielectric mixture equation (3.47) using this dielectric constant value. From the considerations of section 5.1.2 the dielectric constant of the saline at 1000 MHz is found to be 79.74 at 20°C. From section 5.3 the dielectric constant of sand is 4.5. Using these figures with equation (3.47) gives a porosity of 0.4152. This suggests a saline volume of 1.4012 litre as compared to an actual volume of 1.425 which is a deviation of -1.67%. Assuming that the dielectric constants of the constituents are accurate, as well as the measured volumes, equation (3.47) gives a true dielectric constant for the mixture of 26.5. This gives a deviation in the measured dielectric constant from the theoretical value of 1.89%, which compares well with the measurements on saline presented in Figure 6.13. The accuracy of these results is good and confirms the validity of the results for concrete in this frequency range.

The results for the conductivity of the sand/saline mixture are interesting in that the value at 100 MHz is almost twice the LF measured and calculated values. The enhancement cannot be explained by the increase due to the dipolar effects of the water alone (c.f. Table 5.1). This might suggest that some interfacial relaxation effect is operational in the mixture at frequencies between DC and 100 MHz. The enhancement could be due to ionic surface double layer effects around the sand grains. It may also be caused by the presence of small clay particles which are known to demonstrate both double layer and geometrical polarization effects [80]. These are considered in section 5.2. The important point to make here is that the enhanced conductivity and associated dielectric effects which occur when the sand is in contact with ionic solution may be present in the dispersions demonstrated by fresh concrete. The increase in conductivity across the 100-1000 MHz range is probably due to dipolar relaxation of water molecules (again c.f. Table 5.1) although bound water in small surface imperfections on the sand grains (section 5.1.4) may also be influencing the results.

The measurements on the sand/saline mixture, in conjunction with the measurements on saline presented in section 6.2.3, constitute a useful "proving" trial for the 100-1000 MHz system

**Progression of Electrical Parameters - Single Mix**

The changes in dielectric constant and conductivity over the first 24 hours are shown for ATM5 in Figure 7.12. The general trend over the 100-1000 MHz band is for a fall in both conductivity and dielectric constant with time. This is consistent with the reduction in the amount of free water as hydration proceeds.

At 1000 MHz both parameters essentially reflect the amount of free water in the mix. The conductivity decreases as the products of hydration begin to block the available conduction paths and also as the amount of water for conduction decreases as it is combined in the developing cement paste. The dielectric constant at this frequency is due only to the polarization contributions of the individual constituents. Since water has the largest individual dielectric constant, the overall value decreases as the amount of free water in the mix is reduced.

There is a marked change in the characteristic of the dielectric constant between 6 and 9.56 hours, the period which encompasses the stiffening of the cement paste. The slope on the plots from 9.56 to 24 hours is noticably steeper than that of the plots from 2 to 6 hours. It is also noticable that the dielectric constant at 100 MHz rises between 6 and 9.56 hours before beginning to fall again, and is actually higher at 9.56-24 hours than at 6 hours. This change in slope also occurs with the conductivity plots but is less obvious. Also, the progression in conductivity is the same at all frequencies. Figure 7.13 shows the dielectric constant plots for before and after setting on separate graphs. The major changes are seen to occur between 3 and 9.56 hours with the plots from 4 to 6 hours showing evidence of a gradual steepening.

This change in characteristic could be a useful indicator of the change of state associated with setting having occurred. The more prominent relaxation suggested by the steeper slopes which occur after ≈7 hours is probably due to the presence of bound water in the hardening cement paste. Figure 5.2 shows that the relaxation of bound water is likely to be centered around ≈100 MHz, a point also made by Sen

and Chew [80]. However, there may also be some high frequency residual effects from Maxwell-Wagner relaxation or the geometrical polarization mechanism which is discussed in section 5.2.2 (see Figure 5.7).

**Comparison of Various Mixes - Fresh Concrete**

Figure 7.14 presents a comparison of conductivity and dielectric constant for ATM1, ATM2, ATM4 and ATM5 at 1 hour after gauging. The relative positions of the dielectric constant plots are as expected, with the mix with the largest water/solid ratio (w/s - solids being cement plus aggregate) showing the highest value (ATM1 with w/s≈0.2) and the mix with lowest w/s ratio showing the lowest value (ATM2 with w/s≈0.15). ATM5 has a w/s ratio very similar to that of ATM2 and this is reflected in the proximity of the two respective plots.

Equation (3.37) was used to calculate the theoretical high frequency (1000 MHz) limiting dielectric constants for the four mixes in a two stage process. A value for cement inclusions in water, using equation (5.20) for cement volume fraction, was calculated first. The result was then used to calculate a value for aggregate inclusions in cement paste, using equation (5.24) to obtain aggregate volume fraction. The ionic content and concentration of the mix water, and the resulting conductivity and dielectric constant, were obtained from Tables 5.5 and 5.8.

The theoretical dielectric constants thus calculated are presented with the equivalent measured values in Table 7.3.

| | Dielectric Constant | |
|---|---|---|
| Mix | Calculated | Measured |
| ATM1 | 24.38 | 30 |
| ATM2 | 20.13 | 20.31 |
| ATM4 | 21.9 | 23.54 |
| ATM5 | 20.52 | 20.45 |

**Table 7.3 Calculated and Measured Dielectric Constant (1000 MHz)**

It can be seen that the comparison is very favourable for ATM5 and ATM2, and good for ATM4, but that the measured value for ATM1 is much bigger than the expected theoretical value.

The conductivity plots fall into the same relative positions at 1000 MHz as the dielectric plots. Table 7.4 shows the comparison between calculated conductivities (from equation 3.38) and the measured values. While the trend in the measured values, with respect to w/s ratio, is reflected by that of the theoretical values the absolute correspondence between the two sets is not as good overall as that obtained for dielectric constant. Figure 6.16, however, suggest that less accuracy is to be expected for conductivity. Nevertheless, the results for ATM5 are again particularly good.

| | Conductivity ($Sm^{-1}$) | |
|---|---|---|
| Mix | Calculated | Measured |
| ATM1 | 0.655 | 0.78 |
| ATM2 | 0.512 | 0.38 |
| ATM4 | 0.64 | 0.74 |
| ATM5 | 0.628 | 0.61 |

**Table 7.4 Calculated and Measured Conductivity (1000 MHz)**

The discrepancy between measured and theoretical values could be related to conditions around the aperture of the hybrid antenna electrode system. For instance, extra moisture in the vicinity of the antenna which subsequenly evaporated or was absorbed would contribute to enhanced conductivity and dielectric constant in early measurements, but would promote reduced values in later measurements as a solid/water mixture was gradually replaced by a solid/air mixture. Even very small faults in the vicinity of the tip of the antenna can distort the electric field sufficiently to cause discrepancies [96]. The results for ATM1 could be a reflection of this problem. Some difficulty was encountered fitting the electrode system to the sample for this experiment, although the interface with the concrete seemed acceptable on demoulding.

**Comparison of Various Mixes - Hardening Concrete**

Figure 7.15 presents a comparison of dielectric constant and conductivity for ATM1, ATM2, ATM4 and ATM5 at 24 hours after gauging. The slope of the plots appears to be related to the w/c ratio, with the plots for ATM4 and ATM5 (w/c ratios 0.5 and 0.45) having steeper gradients than those for ATM1 and ATM2 (w/c ratios 0.6). The conductivity plots even suggest a slight difference between the slopes of ATM4 and ATM5 in line with the general trend. All the mixes show strong evidence of a relaxation mechanism operating in this range.

It is interesting to note that the dielectric constant and conductivity plots for ATM1 and ATM2 have reversed their relative positions in the graph in comparison to the results for 1 hour shown in Figure 7.14. This possibly confirms the point made above about the effects of excess water in the vicinity of the antenna. For ATM1 in the fresh state the dielectric constant at 1000 MHz is too high but in the hardening material the value it is probably too low.

An approximate value for the free water content in the capillary pores of the hardening concrete can be calculated from the dielectric constant at 1000 MHz using equation (3.47). If the assumption is made that the cement/aggregate matrix has an effective dielectric constant of 6 (an approximate average of 4.5 for sand, 5.5 for bound water and 7 for cement - sections 5.3, 5.1 and 5.2) and that the free water has a value of 78 (due to the ionic content and the higher temperature at 24 hours - see equation (5.1) and Figure 7.4) then the porosities for ATM1, ATM2 ATM4 and ATM5 will be as presented in Table 7.5. These figures were calculated with water as the host medium which is a necessary condition for maintaining the validity of equation (3.47) [80]. This implies that the material is assumed to have a pore structure which is continuous, an assumption which is validated by Neville [9] who shows that segmentation of the capillaries does not occur until after 7 days for a w/c ratio of >0.45.

| Mix | Calculated Porosity |
|---|---|
| ATM1 | 0.113 |
| ATM2 | 0.146 |
| ATM4 | 0.132 |
| ATM5 | 0.122 |

**Table 7.5 Calculated Porosity of Concrete at 24 Hours**

It is instructive to compare the calculated porosities with the values of compressive strength presented in Table 7.2, although it must be remembered that these are for cubes from different batches. The porosities for ATM2, ATM4 and ATM5 are consistent with the corresponding compressive strength measurements of PTM2, PTM4 and PTM5 [9], but the porosity for ATM1 does not fit the expected pattern, suggesting, again, that the measured value of dielectric constant, and hence porosity, is too low.

### 7.4.3 Discussion of Results 20-200 MHz

Figure 7.17 presents the dielectric constant and conductivity of a 0.45/1/2 concrete mix (TPM5) between 4 and 24 hours after gauging. This set of measurements was taken to confirm that the discontinuities at frequencies greater than 40 MHz in the dispersions presented in Figure 7.7 were due to nonlinearities in the parallel plate electrode system and not the material properties. The results show this to be the case as no abrupt changes are seen to occur across the whole 20-200 MHz band.

These results also confirm that concrete does not display negative dielectric constant values at radio frequencies below 100 MHz (see chapter 1).

The changes in the characteristic of the dielectric constant are similar to those observed at 100-1000 MHz but are more pronounced. The dielectric constant at 20 MHz rises to a peak at about 15 hours and then begins to decrease. This agrees with the findings of Olp et al. [57]. At 200 MHz the dielectric constant falls steadily from 4 to 24 hours, again agreeing with Olp et al. The result is that a relatively flat plot at 4 hours has become steeply sloped at 24 hours. This change reflects the enhancement of low frequency dielectric constant resulting from increased space

charge polarization as hydration proceeds, coupled with the reduction in dielectric constant at 1000 MHz and higher as the free water evaporates or is absorbed into the hydrating paste. It is probable that the relaxation of bound water constitutes the major part of the dispersion at frequencies above ≈60 MHz, while at frequencies lower than this geometrical effects due to gel fibres, double layer effects at solid/liquid interfaces, and possibly Maxwell-Wagner effects in the convoluted pore structure, will predominate.

The shape of the conductivity characteristic shows no obvious changes with time across this frequency range. There is a general reduction in conductivity with time, reflecting the increasing tortuosity of conduction paths as hydration proceeds. This trend exactly matches that seen in both the 1-10 MHz and the 100-1000 MHz ranges. However, while the basic form of the graphs is the same, the absolute values of conductivity are not entirely consistent with the other ranges (c.f. Figures 7.9 and 7.12).

These differences may be a result of variations in the samples, which are from different batches, but it is possible that the electrode system in this band is not as accurate as that used at 100-1000 MHz. The larger outer radius of the coaxial aperture of the probe (section 7.3.3) means that the depth of the recess into the coaxial line (i.e. 2 mm) is reduced in relative terms to less than the difference between the outer and inner radii (i.e. 3.4 mm). As discussed in section 6.1.2, the necessary condition to ensure TEM propagation at the insulation/sample interface is that the recess should be greater than the radii difference (see Figure 6.10). Also, the antenna itself is probably too thick (3.2 mm diameter) for the 7 mm length [101]. The results obtained, however, are reliable enough to provide a guide to the electrical properties of concrete in the 20-100 MHz range.

### 7.4.4 Comparison of Different Ranges

#### Results for Fresh Concrete Compared With Dielectric Model

Figure 7.18 presents the measured dielectric constant and conductivity obtained using the results from PTM5, TPM5 and ATM5 for a 0.45/1/2 concrete at 1 hour after gauging. The model described in sections 5.2.1 and 5.4.1 for fresh concrete (see also Appendix B) was applied to the same mix proportions and the resulting dispersion curves are included in Figure 18 for comparison.

There is good agreement between the model and the measurements. For dielectric constant the agreement is best for the results of TPM5 and ATM5, especially those of ATM5. The dielectric constant results for PTM5 are too low at 10 MHz in comparison to the model and the other measurements, but the basic characteristic of the plot is still in agreement. For conductivity, the plots for PTM5 and ATM5 conform best to the model with PTM5 being slightly too low. The conductivity of TPM5 is relatively high. Again, the agreement between the model and the results for ATM5 is particularly close. These results suggest that the basis of the model, viz. the electrical properties of fresh concrete are determined by double layer polarization around cement grains, interfacial effects between the phases of the mix, and ionic conductivity in the mix water, is correct.

Figure 7.19 shows the dielectric constant and conductivity from the three measurement ranges for the 0.45/1/2 concrete at 4 hours after gauging.
The agreement in the conductivity for these results is very good, considering that three different methods and samples are represented, but measurements of dielectric constant still show some discrepancies between the data in each range. The closer agreement at 4 hours suggests that there might be an optimum value of conductivity or dielectric constant at which the electrode systems used at 1-100 MHz and 20-200 MHz, and/or the associated deimbedding procedures, produce the most accurate results. This assumes that the system used at 100-1000 MHz is accurate across the full range of measured parameter values.

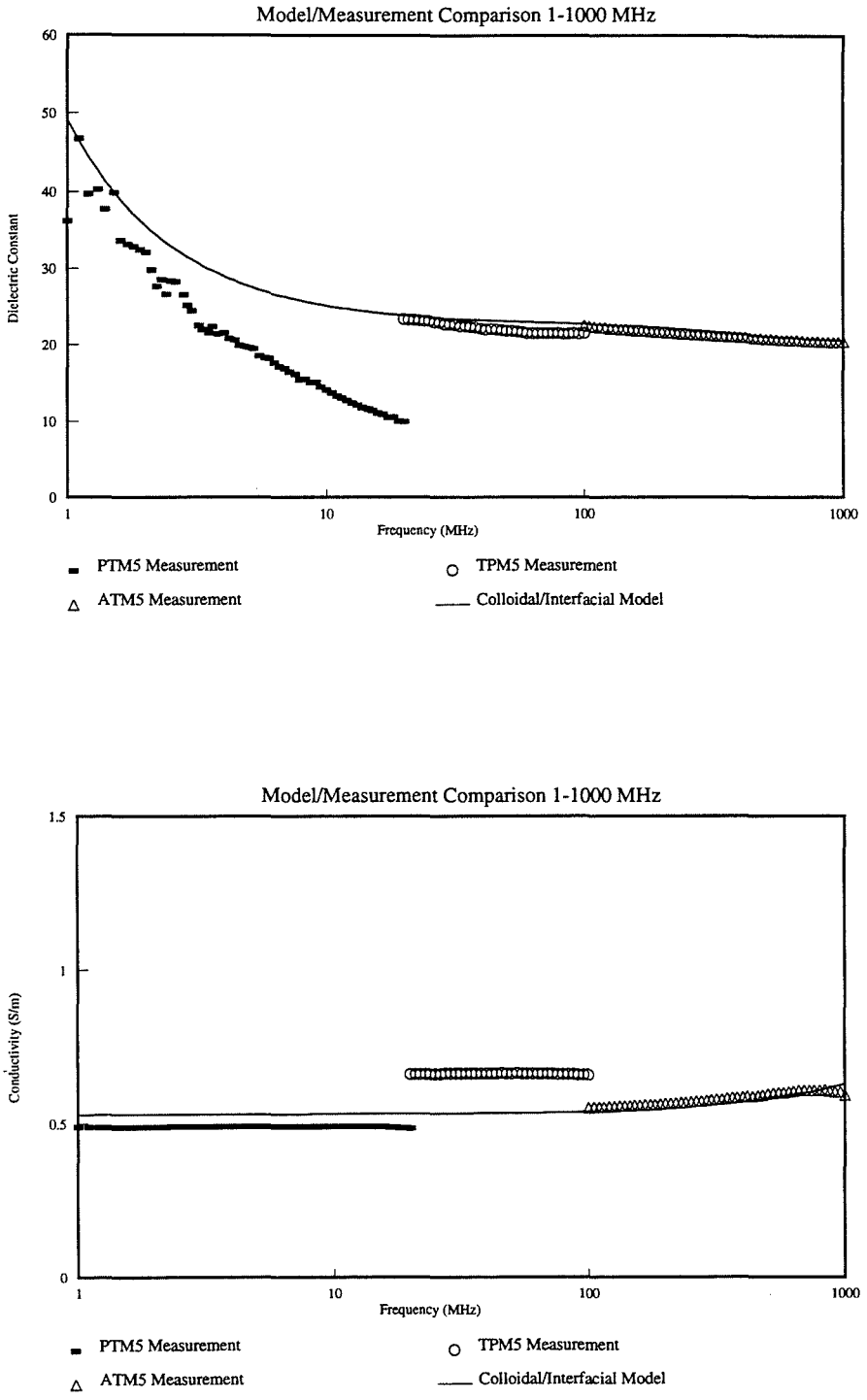


**Figure 7.18 Comparison of Model with Measured Parameters 0.45/1/2 Concrete**

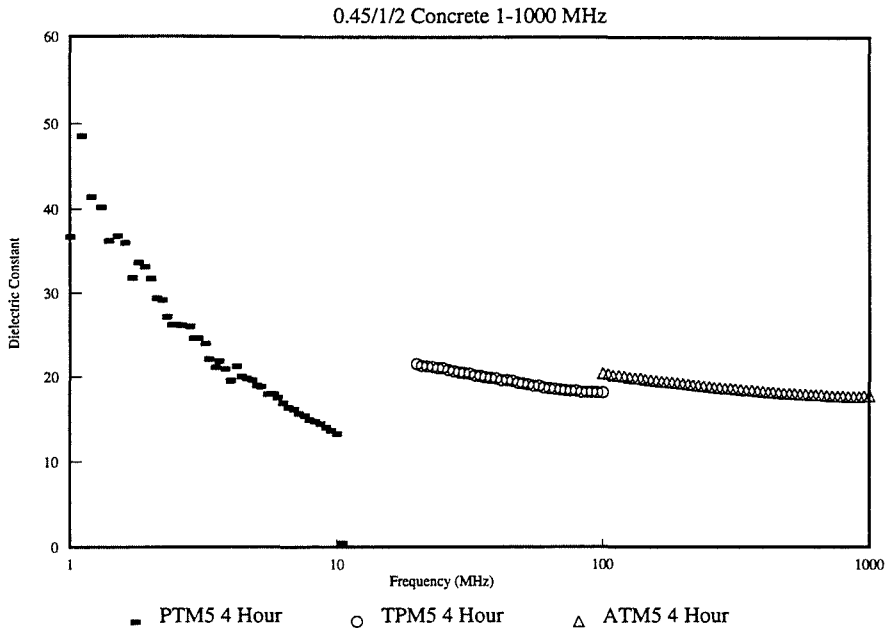


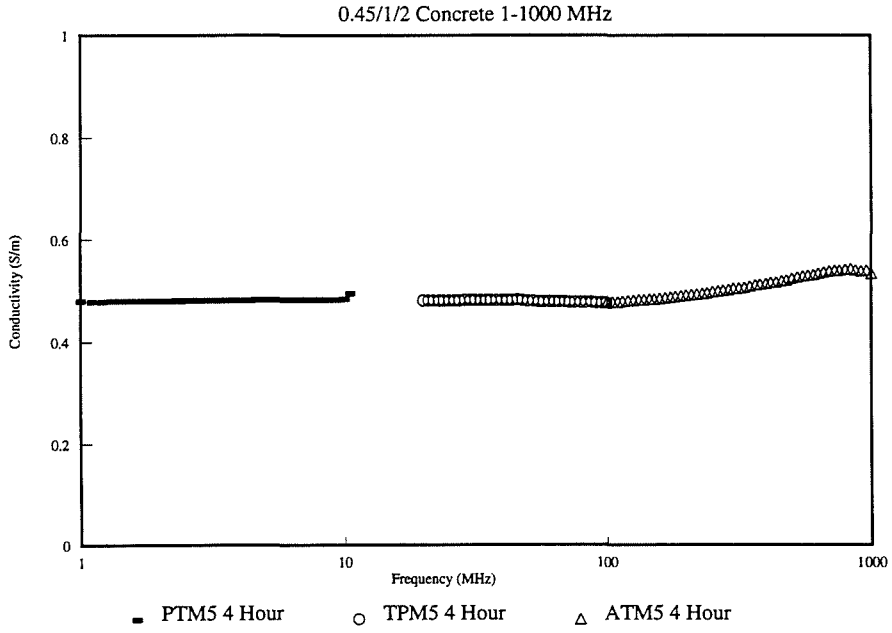


**Figure 7.19 Comparison of Measured Parameters for Concrete at 4 Hours**

**Results for Hardening Concrete**

Figure 7.20 presents the measured dielectric constant and conductivity for a 0.45/1/2 concrete at 24 hours after gauging. The data was obtained from the results of PTM5, TPM5 and ATM5.

From Figure 7.20 it appears that, in comparison to the conductivity of ATM5, the respective values for TPM5 and PTM5 are too low and too high. This is the opposite situation to that of the fresh concrete considered above, and suggests that the "optimum value" hypothesis for these ranges could be correct.

The approximate porosity of this concrete mix at 24 hours, presented in Table 7.5, is 0.122. If Archie's law (equation (3.48)) is applied to the 1 MHz conductivity of the paste water given in Table 5.8 assuming the above porosity then a value of 0.058 $Sm^{-1}$ results. The measured value from PTM5 is 0.075 $Sm^{-1}$ (Figure 7.8). This suggests that the measured PTM5 conductivity should be $\approx$0.02 $Sm^{-1}$ lower.

The dielectric constant of PTM5 may be too high in Figure 7.20. This is suggested by the shape of the accompanying TPM5 dispersion, which itself is slightly too low in comparison to ATM5. Nevertheless, the general trend in the dielectric constant is still clear from the composite graph. The similarity with the gel fibre model of Figure 5.7 is evident, which suggests confirmation of the hypothesis of section 5.2.2.

The results for hardening concrete seems to confirm the hypothesis about optimum measurement values mentioned previously. The range of conductivities apparently measured by the 1-100 MHz parallel plate electrode system is narrower than the true range, while that of the 20-200 MHz hybrid antenna system is wider. Conversely, the apparent dielectric constant range produced by the 1-100 MHz system is wider than it should be, while that of the 20-200 MHz system is narrower. The distortion seems to be dependent on the conductivity rather than the dielectric constant. This problem is not too important for the monitoring of the relative progress with time of the properties of a single sample, but it may have caused inaccuracies in the relative positioning of plots of the properties of different mixes acquired at the same time after gauging.

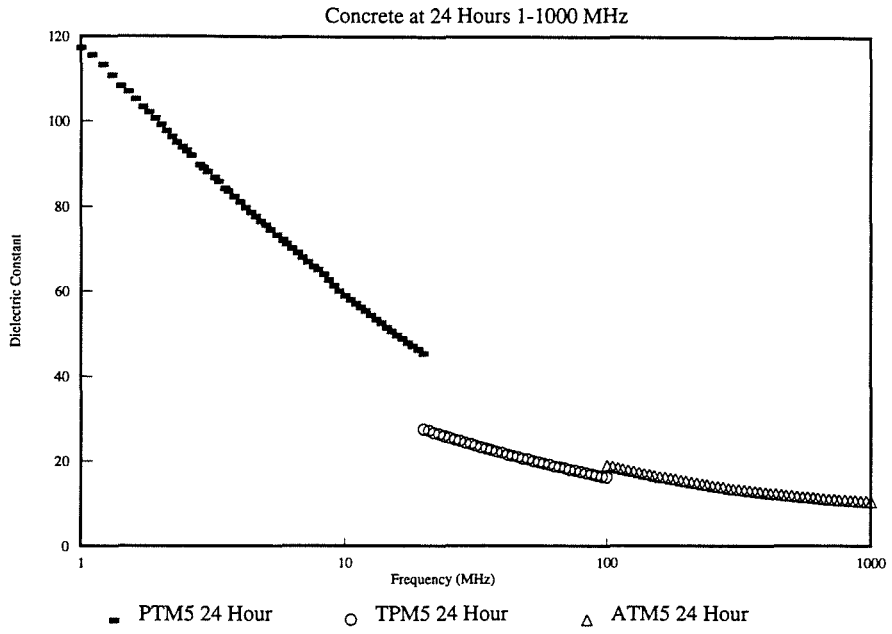


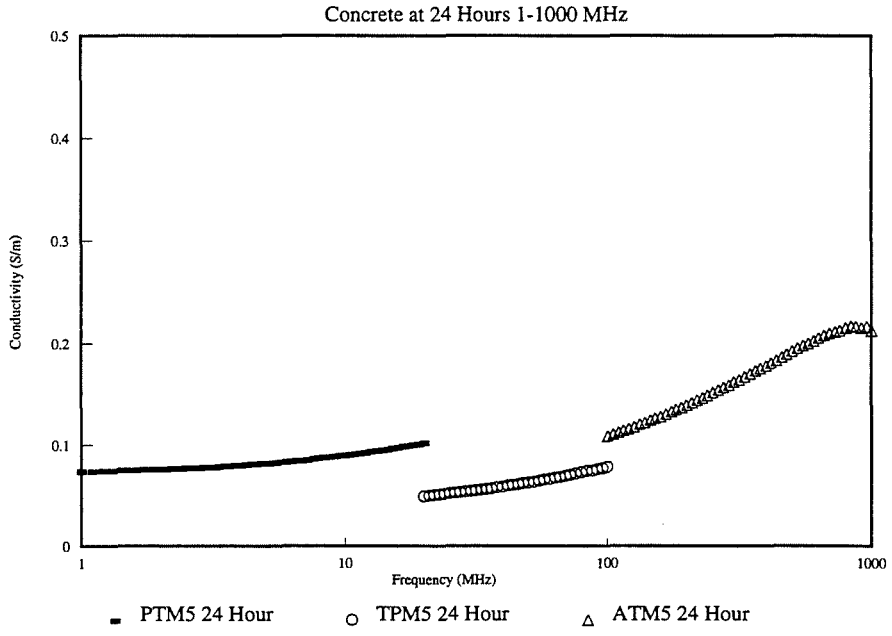


**Figure 7.20 Comparison of Measured Parameters for Hardening Concrete**

### 7.4.5 Considerations for GPR Signals

A brief summary of the use of ground probe radar (GPR) for the investigation of concrete structures was given in section 4.3. The two types of radar signal generally used are a repeating pulse which consists of a damped oscillation of single frequency (pulse radar) [61][58], and a continuous sinusoidal wave which is swept up and down in frequency at a constant rate between fixed limits (frequency modulated continuous wave or FMCW radar) [59]. GPR's generally operate at frequencies between 100 and 1000 MHz [60], although occasionally lower frequencies are used [59].

It is known that there is a shortage of data on the electrical properties of concrete in the normal GPR frequency range [57][61][62], and that such properties are usually assumed by investigators to be constant in the frequency range of operation [58]. However, the results for hardening concrete presented in Figure 7.15 show that the material can manifest significant dielectric dispersion in the 100-1000 MHz range. Ignoring this dispersion during analysis of GPR signals for the purpose of positioning voids, cracks, or reinforcement bars in concrete structures, could lead to significant errors. This problem is potentially more serious for FMCW GPR for which typical frequency sweep ranges are across substantial sections of the 100-1000 MHz range.

The main problem is that the velocity and amplitude of an electromagnetic (EM) wave are directly attributable to the electrical properties of the propagation medium. If the electrical properties vary with frequency then so will propagation of the EM wave. Equations (7.1a) and (7.1b) [59] show the relationship of dielectric constant and conductivity to velocity, $v$, and attenuation, $\alpha$, respectively.

$$v = c\left(\frac{\varepsilon'_r}{2}\left(\sqrt{(1+\delta^2)}+1\right)\right)^{-0.5} \qquad \cdots(7.1a)$$

$$\alpha = \frac{\omega}{c}\left(\frac{\varepsilon'_r}{2}\left(\sqrt{(1+\delta^2)}-1\right)\right)^{0.5} \qquad \cdots(7.1b)$$

where,

$$\delta = \frac{\varepsilon'\omega}{\sigma} \qquad \cdots(7.2)$$

$\delta$ is the *Loss Tangent* of the material, $c$ is the velocity of light *in vacuo*, and $\omega$ is the angular frequency.

Figure 7.21 gives the results for velocity and attenuation obtained by application of equations (7.1a) and (7.1b) to the data for ATM5 at 24 hours. The velocity is given as a normalised quantity (divided by c).

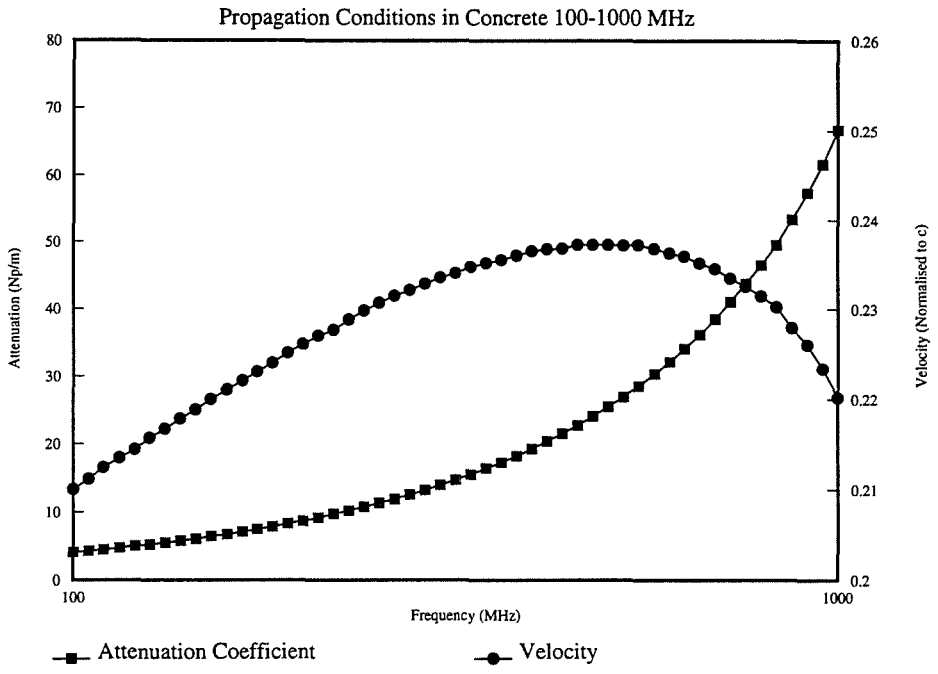


**Figure 7.21 Velocity and Attenuation of an EM Wave in Hardening Concrete**

It can be seen that the effects of dispersion in the hardening concrete will influence the propagation of an EM wave quite differently depending on the frequency. A band of frequencies in this range (100-1000 MHz) would be much more severely attenuated towards the 1000 MHz end, and frequencies at both ends of the range would be progressively delayed relative to those at ≈500 MHz. It is clear that processing of GPR signal data which ignored the above dispersion effects would produce errors.

Further studies on more mature concrete samples in various conditions of moisture retention would be helpful to investigators working with GPR on concrete structures.

## 7.5 Conclusions from Experimental Work

The conclusions which can be drawn from the experimental work may be summarised as follows.

**i)** An electrode system suitable for obtaining reliable impedance data on lossy dielectric materials at high radio frequencies (up to 1000 MHz) has been developed and successfully implemented. The geometry of the system is based on a hybrid design incorporating an electrically short probe extending from the aperture of an open-ended coaxial connector over a finite ground plane.

**ii)** A method for calibrating out the RF effects of the transition network connecting the electrode system to the coaxial line of an impedance analyser has been implemented. The method allows calibration to be effected from measurements carried out on three standard materials of known electrical properties without the need to calculate the electrical properties of the transition network. The known materials were aluminium, air and 0.09126 mol.litre$^{-1}$ sodium chloride solution.

**iii)** Measurements on other saline solutions and on a synthetic soil consisting of sand and saline have been used to prove the system in the 100-1000 MHz range.

**iv)** A parallel plate electrode system has been adapted from earlier work for use in the 1-100 MHz range. The transition effects associated with the connection of this system to the analyser are more severe than for the hybrid system. The same method of calibration used for the hybrid system could not be implemented for this system due to analyser limitations. A new procedure utilising the analyser internal calibration routine with measurements on saline has been used instead. The system was found not to work above 35 MHz, however, due either to non-linearities in the electrical response of the electrodes or to shortcomings in the calibration procedure.

**v)** Another version of the hybrid probe, designed for use at 20-200 MHz, has been used to acquire data in the 30-100 MHz range.

**vi)** The dielectric constant and conductivity of a range of concrete mixes have been successfully charted across a wide band of radio frequencies (1-1000 MHz) using the three separate electrode systems at 1-30 MHz, 20-200 MHz and 100-1000 MHz.

**vii)** To the best of the present author's knowledge, no similar data for the electrical properties of concrete in the frequency range 100-1000 MHz are available in the literature other than the work of Olp et al. [57], which was published after the present investigation was underway. The results of Olp et al. are a useful confirmation of the present work (see section 4.2.7).

**viii)** The experimental work in the frequency range 1-100 MHz was carried out to assess previous work from this project which had produced negative dielectric constants for concrete in this range (section 4.2.6). The results reported here show the previous experimental data to have been inaccurate. No negative dielectric constants were observed, confirming the conclusion of a theoretical investigation presented in chapter 5.

**ix)** The changes in dielectric constant and conductivity of concrete over the first 24 hours after gauging have been observed and found to conform to the theory. It is therefore possible to monitor the stages of hydration of a concrete mix using electrical measurements. A significant shift in the dielectric constant characteristic on setting of the cement paste is observable in the 20-200 MHz and 100-1000 MHz ranges.

**x)** The dielectric constant and conductivity characteristics are shown to be sensitive to differences in mix proportions in the 1-30 MHz and 100-1000 MHz ranges. No mix proportion investigation was implemented in the 20-200 MHz range.

**xi)** Agreement between the results for fresh concrete (less than 2 hours after gauging) and results obtained from a theoretical model is found to be excellent, especially in the 100-1000 MHz range. The model hypothesis is that the electrical properties of fresh concrete are determined by the effects of ionic double layer polarization around hydrating cement grains, Maxwell-Wagner interfacial polarization between the mix constituents, and the electrical properties of the individual constituents including the conductivity of the mix water. The model

requires only the mix proportions as input parameters in order to synthesise the electrical response. While it remains a hypothesis, this is the first model, to the best of the present author's knowledge, which enables quantitative prediction of electrical properties from simple engineering parameters such as w/c and c/a ratio.

**xii)** The results for hardening concrete at 24 hours are shown in general to conform qualitatively to a hypothesis based on consideration of geometrical features in the developing cement paste structure.

**xiii)** The dielectric constant and conductivity of hardening concrete in the 100-1000 MHz range are shown to be highly dispersive. For the propagation of electromagnetic waves in concrete at these frequencies, such as in the use of ground probe radar (GPR) for investigation of concrete structures, the neglect of the dispersive effects could lead to errors in the processing of radar signals. The results reported here should be of interest to those working with GPR on concrete.

## 7.6 Suggestions for Further Work

Despite the general success of the experimental program, a number of problems were also encountered. These concerned the limitations of the range of concrete mixes studied, difficulties with the calibration and subsequent measurements using the parallel plate electrode system, and the impedance limitations of the hybrid antenna system at frequencies towards 1000 MHz. The hybrid system also presented problems when interfacing it with the concrete samples. The following suggestions for further work are therefore made.

**i)** The model used for parallel plate electrode system may have to be re-examined. In particular, it would be worth investigating the true terminating impedance of the line. At present it is assumed to be an open circuit but the validity of this, especially at frequencies above 30 MHz may be in doubt. The effects of capacitance at the discontinuity between the transition network and the parallel plate electrodes could also be considered. These may be partly dependent on the properties of the sample material. A more satisfactory calibration method is required for this electrode system. The effects of the current method using the short and open circuit transition plates along with the saline filled transmission line instead of the standard HP test pieces have not been properly evaluated. A new electrode design or sample configuration may be required in this frequency range.

**ii)** The aperture dimensions of the hybrid antenna used in the 100-1000 MHz range may have to be redesigned to increase the accuracy of the saline based calibration technique. At present the small dimensions promote impedance values when measuring saline solutions which are outside the most accurate measurement range of the analyser at frequencies above ≈500-600 MHz. This is possibly the reason for the drop in conductivity accuracy at higher frequencies shown in Figure 6.14.

**iii)** The present method of fixing the hybrid probe to the top face of the samples is not very satisfactory. Voiding under the ground plane was frequently observed on removing the probe and one preliminary experiment was completely invalidated by voids at the aperture. An arrangement allowing the probe to be mounted on the side of the moulds before the concrete was poured in would be better, but this could cause problems with leakage of mix water into the coaxial connector of the analyser cable. Alternative methods should be explored

**iv)** The model for synthesising the electrical properties of fresh concrete should be further explored. Aspects of the theory need to be examined more thoroughly. A literature search to uncover papers on the chemistry of hydrating OPC which could provide information on zeta potentials and ionic mobilities in electrical double layers is needed to verify the validity of the hypothesis. This is also the case for the geometrical model for hardening cement paste.

**v)** Now that the techniques are available for acquiring the data in the upper RF band, a much wider range of experiments is needed to carefully document the effects of mix proportion variations on the electrical parameters of concrete. The effects of temperature variations, which have not been studied in this work, could also be considered. Studies should also be made of the properties of more mature concrete, especially with respect to the effects of moisture content. Such studies could be carried out in conjunction with investigations involving ground probe radar.

**vi)** A new electrode design for measurements at 100-1000 MHz on concrete structures would be useful. One suggestion is to use an adapted form of microstrip line [91] with larger dimensions than the norm, suitable for lower than microwave frequencies. Bahl and Stuchly [123] have investigated the use of a similar device for the measurement of the electrical properties of lossy materials and have shown the technique to be feasible. The use of a microstrip line would not involve physical penetration of the concrete surface as with the hybrid probe and this could make it more adaptable for measurements *in situ*.

# CHAPTER 8

## Summary of Research

**i)** Concrete is a highly complex material in chemical and microstructural terms. After mixing it remains in a continual state of development for a long time, but the most dramatic and formative changes of state occur within the first 24 hours. The amount of water present at mixing and at later stages is crucial in determining the development of the microstructure of the cement paste, particularly its capillary pore structure. This in turn determines the quality of the concrete for construction applications.

The Civil Engineering and Building industries are in need of an accurate, simple to apply quality assurance test for structural concrete, which can be implemented on the first day after mixing, in order to meet the increasingly tight schedules applied to modern construction projects. In addition, there is growing concern over the number of established concrete structures which have been found to be deteriorating much sooner than expected, suggesting that traditional methods of quality control testing have failed to provide accurate predictive assessment of concrete durability.

Previous investigations suggest that measuring the electrical properties of concrete, which have been found to be influenced by its moisture content, is a promising potential method of assessing its quality. At present, however, there is a lack of scientific understanding of the nature of the relationship between the electrical and physical properties.

**ii)** The electrical properties of any non-magnetic material can be fully specified by the dielectric constant and conductivity which are determined by the movement of bound and free charges respectively. Dielectric theory has been studied with a view to understanding the processes which give rise to the polarization of bound charges within such materials. The dielectric constant and conductivity of heterogeneous materials are strongly correlated to the properties of the individual components and the way in which they are combined. This correlation is manifested in the frequency domain as dispersive behaviour characterised by frequencies of relaxation above

which dielectric constant falls and conductivity rises. Different heterogeneous materials may therefore be identified by their electrical properties, which can be very complicated, if observed across a wide enough band of frequencies.

A range of formulae allowing calculation of the electrical properties of heterogeneous mixtures and their frequency dispersion has been selected as potentially useful for the study of concrete, and typical graphical representations have been presented.

The electrical measurement of materials, such as concrete, containing ionic solutions is problematic at low frequencies because of electrochemical effects at the electrodes which artificially enhance the dielectric constant. The literature on this particular effect has been studied with the conclusion that it is not significant at frequencies above 1 MHz.

**iii)** Previous research into the electrical properties of concrete and cement paste has been studied and a review of the available literature on high frequency properties is presented. Two papers on the low frequency properties have also been reviewed. The results are varied and sometimes confusing. The modelling of the behaviour of concrete is very often arbitrary and empirical, and contradictory points are made. Only one paper was found which presented data for cement paste and mortar in the upper RF range above 100 MHz. One general problem in this frequency range (1-1000 MHz) seems to be a lack of expertise in RF measurement techniques, especially with respect to the calibration of connecting lead distortion, and it is therefore difficult to assess how valid some of the results are. None of the authors have produced a quantitative model which links quality parameters such as strength or w/c ratio to the electrical parameters via the physical structure of the material.

An hypothesis suggesting an explanation for the electrical properties of concrete at 1-1000 MHz which emerged from the previous work of this project has been given particular attention. The basis of the hypothesis is that the dielectric constant characteristic for fresh concrete at 1 MHz is determined by electrode polarization and that at higher frequencies it is controlled by ionic conduction effects which produce negative dielectric constant values. These effects were carefully investigated in the course of the present research.

The use of Ground Probe Radar, which operates in the 100-1000 MHz range, for the integrity testing of concrete has been summarised, and it is suggested that lack of reported data in this range is a hinderence to the successful exploitation of the technique.

**iv)** The properties of concrete as a heterogeneous dielectric are considered. A theoretical investigation into the possible behaviour of concrete and its constituents, drawing upon disciplines such as electrochemistry and geophysics has led to the formulation of a hypothesis for explaining the properties of fresh concrete across a wide band of frequencies. A model which predicts electrical dispersion from simple mix proportions was developed. This produces graphically presented electrical parameters which agree well with the latest published RF data over the 1-300 MHz band. The basis of the model is that fresh cement grains suspended in mix water are surrounded by an electrochemical double layer which is extremely polarizable at low frequencies and manifests residual relaxation effects at frequencies above 1 MHz. The cement grains also interact with the surrounding water by interfacial polarization characterised by the Maxwell-Wagner effect. This model is the first, as far as the present author is aware, to allow the quantitative prediction of electrical properties from knowledge of the mix proportions.

For hardening concrete a hypothesis based on the fibrous structure of the cement gel as it develops in the capillaries is proposed. It is suggested that the gel fibres, along with developing calcium hydroxide crystals, each act as small platelet capacitors which trap ions migrating through the capillary pores, thereby producing a large total polarization. Equations relating the dielectric constant produced by this effect to the aspect ratio and concentration of the platelets, and the conductivity of the pore water, are presented as are graphs of the dispersions at 1-1000 MHz. Bound water is also thought to contribute to dielectric relaxation in the 100-1000 MHz band. Both models were derived from work done in the field of geophysical exploration into porous rocks.

The dielectric effects of ionic conduction are considered in detail. It was found that while there is a negative contribution to dielectric constant from this effect it is so small that it is negligible. The conclusion is that concrete does not have a negative dielectric constant in the RF range. It is also concluded that dielectric enhancement

at 1 MHz is not caused by electrode polarization but by electrochemical double layer polarization around the cement grains in the fresh state and by similar effects plus geometrical aspects of the hydrating structure in the hardening state.

**v)** The requirements and problems of measuring electrical quantities at RF frequencies are considered and the shortcomings of the previous electrode systems used in this project are examined. The effects of distortion at radio frequencies, which arise from the connection between the analyser measurement plane and the required reference plane of the electrode system, have caused major problems to the work of others. Consequently very little hard data has been produced on the electrical behaviour of concrete at lower MHz frequencies and only one very recent study has been published for the 100-1000 MHz range. A previous system of parallel plate transmission line containing a 150 mm cube of concrete has been shown to be inadequate for measurements at 100-1000 MHz, but an updated version allowing a smoother launch of the energising signal from the impedance analser was used at 1-100 MHz. A new electrode structure has been designed for 100-1000 MHz which combines features of the open-ended coaxial probe used in biological and geophysical investigations with those of the monopole antenna radiating over a finite ground plane. The new structure is essentially a hybrid of these two. A range of models for the probe admittance were tried out and the two most accurate used to acquire experimental data on concrete.

Impedance measurements are calibrated to the required reference plane of the probe by a method which utilises measurements on sodium chloride solutions of known electrical properties and measurements on aluminium foil and air. The calibration procedure is based on a model of the transition connection between the probe and the analyser cable which treats it as two port network. This method turns out to be similar to one based on reflection coefficient measurements which has been used in microwave measurements. The system has been proved at 100-1000 MHz by subsequent measurements on saline and on a synthetic soil consisting of a sand/saline mixture. Accuracy is good in comparison to theoretical expectation based on LF conductivity measurement and known concentration. The subsequent measurements on concrete are therefore reliable.

In the lower frequency range the analyser is calibrated directly to the required reference plane of the electrode system by a method which uses the analyser internal routine but replaces the three standard calibration terminations supplied by the manufacturer by short and open circuit terminations identical with the analyser/electrode transition connection, and a measurement on sodium chloride solution. Subsequent measurements are corrected by simple calculation. There are problems with this method at frequencies above 35 MHz which are thought to be due to the shortcomings of the calibration procedure, the electrical model used for the electrode system and possibly with the electrode structure. An alternative method using an electrode system similar to 100-1000 MHz has been therefore been implemented to obtain data between 30 and 100 MHz.

**vi)** A range of concrete mixes were measured over the first 24 hours after gauging and the results are presented graphically. The changes in state of the concrete as hydration proceeds are clearly reflected in the changes in characteristic of the electrical parameters. Differences in mix proportions are also clearly represented. Concrete is characterised by dispersions in the fresh and the hardened state which conform to the electrochemical double layer and gel fibre hypotheses respectively. The dielectric constant and conductivity results for a 0.45/1/2 concrete in the fresh state are compared on a graph with the theoretical dispersion produced by the model. Agreement is excellent especially in the 100-1000 MHz range, suggesting that the theory is valid. The agreement between the results from the three electrode systems is good but there is distortion in the results of the two lower frequency systems.

The results show that previous data from the project has been faulty and that the previous hypothesis explaining the RF properties of concrete is therefore incorrect.

It is noteworthy that the dielectric constant of hardening concrete at 100-1000 MHz has a definite relaxation characteristic. This is thought to be caused by the presence of bound water in the cement paste. Consideration is given to the likely effect of this dispersion on Ground Probe Radar signals and it is confirmed that errors would arise in the processing of such signals if the effects were neglected. The data produced in this work should prove helpful to workers investigating concrete by GPR.

More detailed experiments now need to be performed to establish the effects of differences in w/c ratio and c/a ratio in order to verify theory and provide sufficient data base for the development of a quality test technique. A suggestion is made for a potential electrode structure which could prove adaptable for non-invasive measurements *in situ*.

# APPENDICES

## Appendix A
## Electrophoretic Conduction Effects

In this section expressions are derived for the contribution made to the conductivity and dielectric constant of aqueous ionic solutions by the electrophoretic movement of charged particles.

The differential equation describing the motion of a charged particle in a homogeneous viscous medium is [77] :

$$m\frac{dv}{dt}+R_f v = qE(t) \qquad \cdots(A.1)$$

where,

$v$ is particle velocity ($ms^{-1}$)
$m$ is particle mass (kg)
$R_f$ is coefficient of friction ($kgs^{-1}$)
$q$ is particle charge (C)
$E$ is electric field strength ($Vm^{-1}$)

For a non-varying field equation (A.1) assumes the form :

$$R_f v = qE \qquad \cdots(A.2)$$

The mobility, $\mu$, of an ion is defined as its mean velocity when subjected to an electric field of 1 $Vm^{-1}$. Applying this definition to charged particles in general, $R_f$ may be obtained from equation (A.2) such that :

$$R_f = \frac{q}{\mu} \qquad \cdots(A.3)$$

For a sinusoidally varying field of the form $E_0 e^{j\omega t}$ (where $E_0$ is the peak value of electric field, $\omega$ is the angular frequency and $j$ is the complex operator) equation (A.1) can therefore be expressed as :

$$j\omega m v_0 + \frac{q}{\mu} v_0 = q E_0 \qquad \cdots(A.4)$$

From (A.4) an expression for the frequency dependent velocity of a particle can be derived :

$$v_0 = \frac{\mu E_0}{1 + j\omega\tau} \qquad \cdots(A.5)$$

where :

$$\tau = \frac{m\mu}{q} \qquad \cdots(A.6)$$

is the time constant of the frequency dependent complex velocity. The movement of charged particles, of numerical density $\eta_d$ $m^{-3}$ in aqueous solution, according to the conditions prescribed by (A.5), gives rise to an electrophoretic current density, $J_0$ ($Cs^{-1}m^{-2}$), such that :

$$J_0 = v_0 \eta_d q \qquad \cdots(A.7)$$

and combining (A.5) with (A.7) gives :

$$J_0 = \frac{\mu \eta_d q E_0}{1 + j\omega\tau} \qquad \cdots(A.8)$$

The complex conductivity, $\hat{\sigma}$ ($Sm^{-1}$), of such a conducting solution can be obtained from Ohm's law :

$$J_0 = \hat{\sigma} E_0$$

resulting in :

$$\hat{\sigma} = \frac{\mu \eta_d q}{1 + j\omega\tau} \qquad \cdots(A.9)$$

This can be converted to a complex relative permittivity by using the transform property [119] :

$$\hat{\varepsilon}_r = \frac{\hat{\sigma}}{j\omega\varepsilon_0}$$

Separation of the real and imaginary parts of the resulting expression permits calculation of the contributions made by the electrophoretic movement of charged particles to the conductivity and the dielectric constant of the aqueous medium in which they are suspended. Thus :

$$\hat{\varepsilon}_r = -\left(\frac{\mu\eta_d q\tau}{\varepsilon_0}\cdot\frac{1}{1+(\omega\tau)^2}\right) - j\left(\frac{\mu\eta_d q}{\omega\varepsilon_0}\cdot\frac{1}{1+(\omega\tau)^2}\right) \qquad \cdots(A.10)$$

Which yields the following equations :

$$\varepsilon_r' = -\frac{\mu\eta_d q\tau}{\varepsilon_0}\cdot\frac{1}{1+(\omega\tau)^2} \qquad \cdots(A.11)$$

$$\sigma_d = \mu\eta_d q\cdot\frac{1}{1+(\omega\tau)^2} \qquad \cdots(A.12)$$

In the case of charged particles other than ions (i.e. particles for which a value of $\mu$ is not available) the mobility may be found from Stokes' law [69] if the viscosity of the transport medium is known. Thus, combination of equations (5.5) and (A.2) gives :

$$R_f = 6\pi\eta_v r \qquad \cdots(A.13)$$

where, $\eta_v$ is viscosity ($kgs^{-1}m^{-1}$) and $r$ is particle radius (m).

With reference to equation (A.3) the mobility is found to be :

$$\mu = \frac{q}{R_f} \qquad \cdots(A.14)$$

Also, the time constant, $\tau$, can be calculated from :

$$\tau = \frac{m}{R_f} \qquad \cdots(A.15)$$

Equations (A.14) and (A.15) may then be substituted into equations (A.11) and (A.12) yielding :

$$\varepsilon_r' = -\frac{m\eta_d q^2}{R_f^2 \varepsilon_0} \cdot \frac{1}{1+\left(\omega \frac{m}{R_f}\right)^2} \qquad \cdots(A.16)$$

$$\sigma_d = \frac{\eta_d q^2}{R_f} \cdot \frac{1}{1+\left(\omega \frac{m}{R_f}\right)^2} \qquad \cdots(A.17)$$

# Appendix B
# Electrical Properties of Fresh Concrete - Colloidal Model

This file contains the necessary formulae for the calculation
of dielectric constant, conductivity, and relaxation frequency
of colloidal particles suspended in aqueous ionic solution.
The primary application is for cement paste
- Wednesday 19/1/94

$\varepsilon 0 \equiv 8.854 \cdot 10^{-12}$ $\quad i := \sqrt{-1}$ $\quad$ ORIGIN ≡ 1

Part 1 - The contribution to Dielectric Constant and Conductivity
due to Electrophoretic Movement of Colloidal Particles

$wc := 0.45$ Water/Cement Ratio of Mix

$ca := \frac{1}{2}$ Cement/Aggregate Ratio of Concrete

$q := 1.6020552 \cdot 10^{-19}$ Electron Charge

$z := 50$ Particle Diameter - μm

$r := \frac{z}{2} \cdot 10^{-6}$ Particle Radius - m

$fact := 10^{7}$ Dimensional Correction factor

$sgc := 3.15$ Specific Gravity of OPC

$con := \frac{1}{1 + (sgc \cdot wc)}$

con = Particle Fractional Volume Concentration

$\beta := 0.00102$ Viscosity of Solution - kg/(sm)

$vol := \frac{4}{3} \cdot \pi \cdot r^{3}$ Particle Volume

$m := vol \cdot sgc$ Mass of OPC Grain

$Rf := 6 \cdot \pi \cdot \beta \cdot r$ Frictional Coefficient - kg/s

$$\tau e := \frac{m}{Rf}$$ Electrophoretic Time Constant of Particles

$$N := \frac{con}{vol}$$ Number of Particles per Cubic Metre of Suspension

$$A := 4 \cdot \pi \cdot r^2$$ Surface Area of a Particle

$$Q := A \cdot 0.24$$ Total Surface Charge of a Particle

$$\mu := \frac{Q}{Rf}$$ Mobility of a Particle

$$\varepsilon es := -N \cdot Q^2 \cdot \frac{\tau e}{Rf \cdot \varepsilon 0 \cdot fact}$$ Electrophoretic Static Dielectric Constant of Colloid

$$\sigma e := N \cdot \frac{Q^2}{Rf \cdot fact}$$ Electrophoretic Conductivity of Colloid

$$fr := \frac{1}{2 \cdot \pi \cdot \tau e}$$ Relaxation Frequency of Polarization

$\varepsilon es =$ $fr =$ $\tau e =$

$\sigma e =$ $\mu =$

---

Part 2 - Enhancement to Dielectric Constant and Conductivity of individual Particles due to Double Charge Layer Polarization

$k := 1.38054 \cdot 10^{-23}$ Boltzmann Constant

$T := 293$ Absolute Temperature

$\phi := 82 \cdot 10^{-3}$ Equivalent Zeta Potential for Particle Surface

$v := 1.606$ Equivalent Valence of Ions in Double Layer

$\mu s := 1.246 \cdot 10^{-8}$ Mobility of Ion on Particle Surface (Calcium)

$r =$ Radius

$$t := \tanh\left[\frac{v \cdot q \cdot \phi}{k \cdot T}\right]$$ Calculation Factor - Sen & Chew

$\varepsilon ws := 78.525$ Mix Water Static Dielectric Constant

$$\varepsilon ss := 36 \cdot con \cdot \varepsilon ws \cdot \frac{t^2}{\left[1 - t^2\right]^2}$$ Static Dielectric Constant Due to Surface Polarization (Sen & Chew)

$\varepsilon ss =$

$$\sigma s := \mu s \cdot \frac{Q}{A \cdot r}$$ Particle Surface Conductivity

$$\tau s := q \cdot \frac{r^2}{2 \cdot v \cdot \mu s \cdot k \cdot T}$$ Time Constant of Surface Polarization

$$\varepsilon ss1 := \left[2 \cdot \sigma s \cdot \frac{\tau s}{\varepsilon 0}\right]$$ Static Dielectric Constant Due to Surface Polarization (Schwarz)

---

Part 3 - The Maxwell-Wagner Effect for Colloidal Suspension

fa := READPRN(fr1)  Frequency Vectors  x := 1 ..45

fb := READPRN(fr2)  y := 1 ..50

f3 := READPRN(fr3)  h := 1 ..146

$f1_x := fa_x$  $f2_y := fb_y$

$f1t := f1^T$  $f2t := f2^T$  $f3t := f3^T$

f12t := augment(f1t,f2t)  f123t := augment(f12t,f3t)

$f := f123t^T \cdot 10^6$  Frequency Vector

$\omega := \overline{(f \cdot 2 \cdot \pi)}$  Radian Frequency Vector

$\alpha := 0.004$  Spread Parameter (Particle Size)

$$\varepsilon w_h := 5.5 + \frac{\varepsilon ws - 5.5}{1 + \left[i \cdot \omega_h \cdot 9.2136 \cdot 10^{-12}\right]}$$  Mix Water Relative Permittivity

$\varepsilon h_h := Re[\varepsilon w_h]$  Host Medium Dielectric Constant

σw := 1.3552  Mix Water Ionic Conductivity

$\sigma h_h := \sigma w - Im[\varepsilon w_h] \cdot \varepsilon 0 \cdot \omega_h$  Host Medium Conductivity

εc := 7  Inclusion (Cement) Dielectric Constant

$\sigma i := 6.25 \cdot 10^{-6}$  Inclusion Conductivity

Dielectric Constant of Inclusions
due to Double Layer Enhancement

$$\varepsilon i_h := \varepsilon c + \frac{\varepsilon ss}{\left[1 + \left[i \cdot \omega_h \cdot \tau s + \sqrt{2 \cdot i \cdot \omega_h \cdot \tau s}\right]\right]^{1-\alpha}}$$

$$\sigma s \cdot \frac{\tau s}{\varepsilon 0} =$$

$$\varepsilon ss =$$

$$\tau s =$$

$$\varepsilon e_h := \frac{\varepsilon es - i \cdot \frac{\sigma e}{\omega_h \cdot \varepsilon 0}}{1 + \left[\omega_h \cdot \tau e\right]^2}$$

Electrophoretic Relative Permittivity
Contribution

$$\varepsilon e_1 =$$

$$-\mathrm{Im}\left[\varepsilon e_1\right] \cdot \varepsilon 0 \cdot \omega_1 =$$

---

Part 4 - Total Dielectric Constant and Conductivity Effects of Colloidal Suspension Polarization Mechanisms

$$Eh_h := \sigma h_h + i \cdot \omega_h \cdot \varepsilon 0 \cdot \left[\varepsilon h_h\right]$$

$$Ei_h := \sigma i_h + i \cdot \omega_h \cdot \varepsilon 0 \cdot \left[\varepsilon i_h + \varepsilon e_h\right]$$

$$\varepsilon p_h := \frac{Eh_h}{i \cdot \omega_h \cdot \varepsilon 0} \cdot \frac{2 \cdot Eh_h + Ei_h + 2 \cdot con \cdot \left[Ei_h - Eh_h\right]}{2 \cdot Eh_h + Ei_h - con \cdot \left[Ei_h - Eh_h\right]}$$

$s := 140$

$$\tau m := \varepsilon 0 \cdot \left[\frac{2 \cdot \varepsilon ws + \varepsilon c - con \cdot (\varepsilon c - \varepsilon ws)}{2 \cdot \sigma w + \sigma i - con \cdot (\sigma i - \sigma w)}\right]$$

$$\frac{1}{2 \cdot \pi \cdot \tau m} =$$

$$\sigma p_h := -\mathrm{Im}\left[\varepsilon p_h\right] \cdot \omega_h \cdot \varepsilon 0$$

Conductivity

$\varepsilon pr_h := Re\left[\varepsilon p_h\right]$ Dielectric Constant

$\varepsilon pi_h := -Im\left[\varepsilon p_h\right]$ Loss Factor

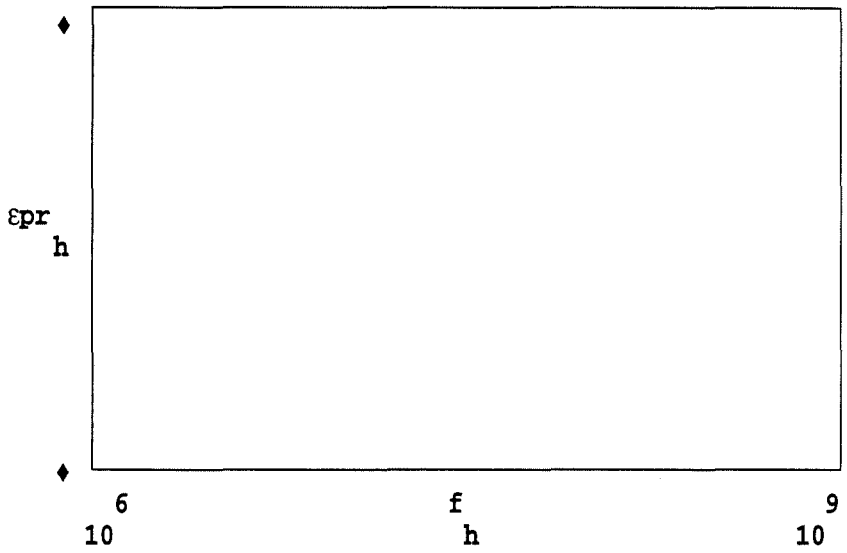


$\varepsilon pr = 96$

$\varepsilon pr = 146$

$\varepsilon pr = 46$

$\sigma p = 120$

$f = 120$

---

Part 5 - The Effects of Introducing Aggregate to the Mix

sga := 2.62  Specific Gravity of Aggregate

$$sgp := \frac{sgc \cdot (1 + wc)}{sgc \cdot wc + 1}$$

Specific Gravity of Cement Paste

ca =

pa := (wc + 1)·ca  Paste/Aggregate Ratio

pa =

sgp =

$$cona := \left[\frac{1}{1 + \frac{sga \cdot pa}{sgp}}\right]$$

Volume Fraction of Aggregate

cona =

εa := 4.5  Dielectric Constant of Aggregate

$\sigma a := 0 \cdot 6.25 \cdot 10^{-6}$  Conductivity of Aggregate

$Ep_h := \sigma p_h + i \cdot \omega \cdot \varepsilon 0 \cdot \varepsilon pr_h$  $Ea_h := \sigma a + i \cdot \omega \cdot \varepsilon 0 \cdot \varepsilon a_h$

$$\varepsilon m_h := \frac{Ep_h}{i \cdot \omega \cdot \varepsilon 0_h} \cdot \frac{2 \cdot Ep_h + Ea_h + 2 \cdot cona \cdot \left[Ea_h - Ep_h\right]}{2 \cdot Ep_h + Ea_h - cona \cdot \left[Ea_h - Ep_h\right]}$$

$$\sigma m_h := -Im\left[\varepsilon m_h\right] \cdot \omega \cdot \varepsilon 0_h$$

$\varepsilon mr_h := Re\left[\varepsilon m_h\right]$  $\varepsilon mi_h := Im\left[\varepsilon m_h\right]$

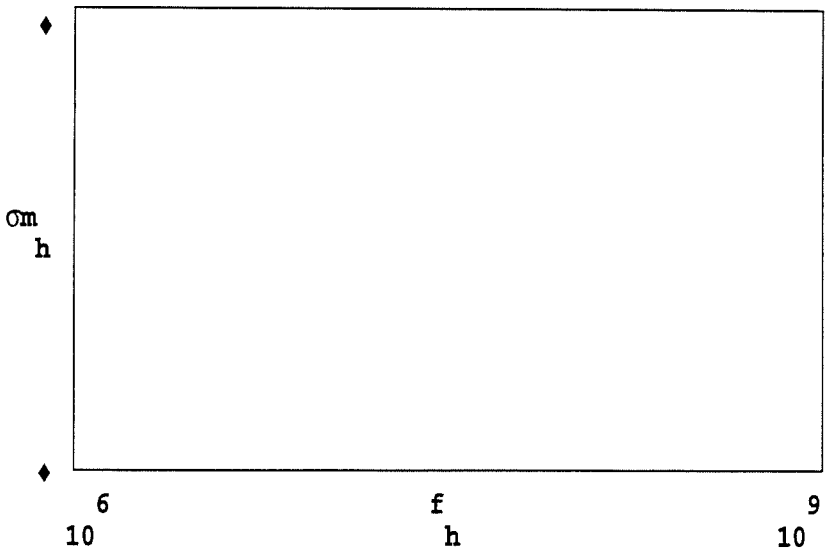


wc =

fpm4 := READPRN(fpm)  Read in Measurement File  c := 1 ..51

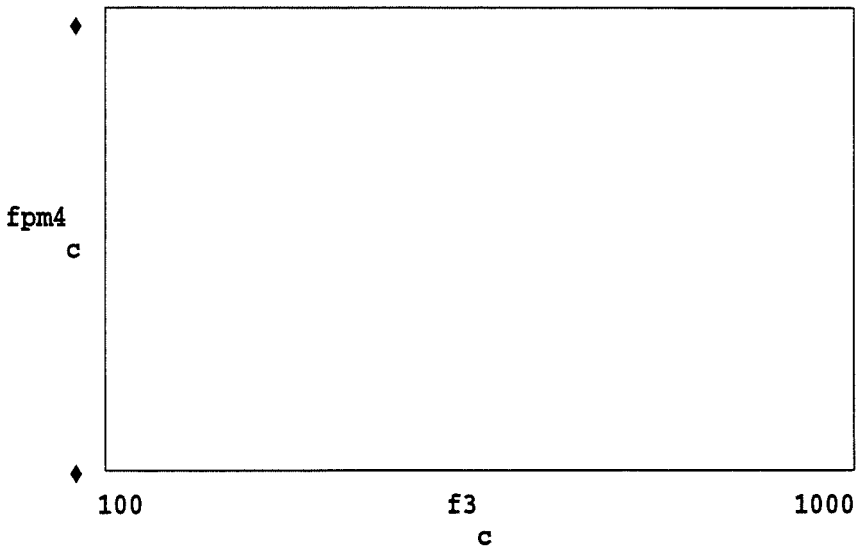


Measured Dielectric Constant of Same Mix

# Appendix C
# Electrical Properties of Hardening Concrete - Gel Fibre Model

This file contains the necessary formulae for the calculation
of dielectric constant, conductivity, and relaxation frequency
of platey particles suspended in aqueous ionic solution.
The primary application is for cement paste
- Tuesday 1/2/94

$\varepsilon 0 \equiv 8.854 \cdot 10^{-12}$ $\quad i := \sqrt{-1}$ $\quad$ ORIGIN ≡ 1

fa := READPRN(fr1) Frequency Vectors x := 1 ..45

fb := READPRN(fr2) y := 1 ..50

f3 := READPRN(fr3) h := 1 ..146

$f1_x := fa_x$ $\quad f2_y := fb_y$

$f1t := f1^T$ $\quad f2t := f2^T$ $\quad f3t := f3^T$

f12t := augment(f1t,f2t) $\quad$ f123t := augment(f12t,f3t)

$f := f123t^T \cdot 10^6$ Frequency Vector

$\omega := \sqrt{(f \cdot 2 \cdot \pi)}$ Radian Frequency Vector

α := 0.2 Spread Parameter (Particle Size)

d := 0.007 Particle Aspect Ratio

$c := 3 \cdot 10^{-3}$ Particle Density

σR := 0.2 Hardened Cement Paste Conductivity (LF) - Olp

εR := 40 Hardened Cement Paste Conductivity (HF) - Olp

εm := 6.3 Matrix Dielectric Constant

$$\varepsilon er := \left[\frac{d - c \cdot d}{d + c - d \cdot c}\right] \cdot \varepsilon R + \left[\frac{c}{(d + c - d \cdot c)^2}\right] \cdot \varepsilon m$$

Effective Static Dielectric Constant

Conductivity

$$\sigma 0 := \left[\frac{d - c \cdot d}{d + c - c \cdot d}\right] \cdot \sigma R$$

Time Constant

$$\tau p := \frac{\varepsilon m \cdot \varepsilon 0}{\sigma R \cdot (d + c - d \cdot c)}$$

$$\varepsilon e_h := \varepsilon R + \frac{\varepsilon er - \varepsilon R}{1 + \left[i \cdot \omega_h \cdot \tau p\right]^{1-\alpha}}$$

Dispersion of Relative Permittivity

$$\sigma 1_h := \mathrm{Im}\left[\varepsilon e_h \cdot \varepsilon 0 \cdot \omega_h\right]$$

Dielectric Conductivity

$$\sigma e_h := \sigma 0 - \sigma 1_h$$

Effective Conductivity

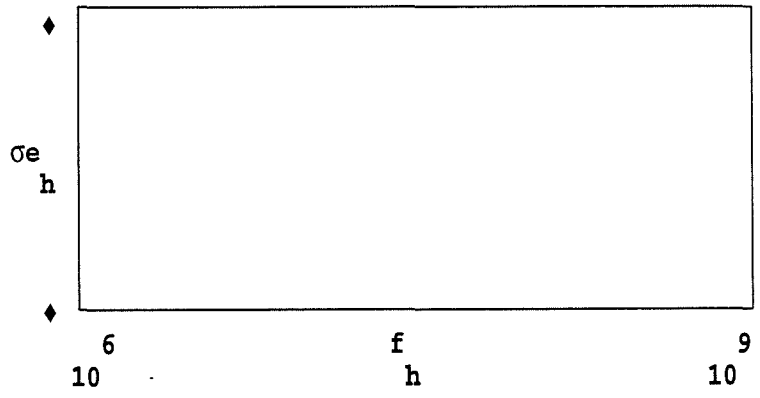


Conductivity

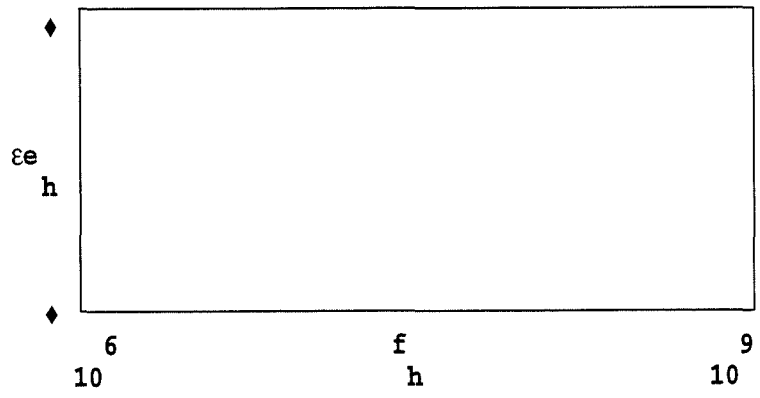


Dielectric Constant

output files - epl and spl

# Appendix D
# Derivation of Transition Network Impedance Relationship

Consider the two-port network represented schematically in Figure D.1.

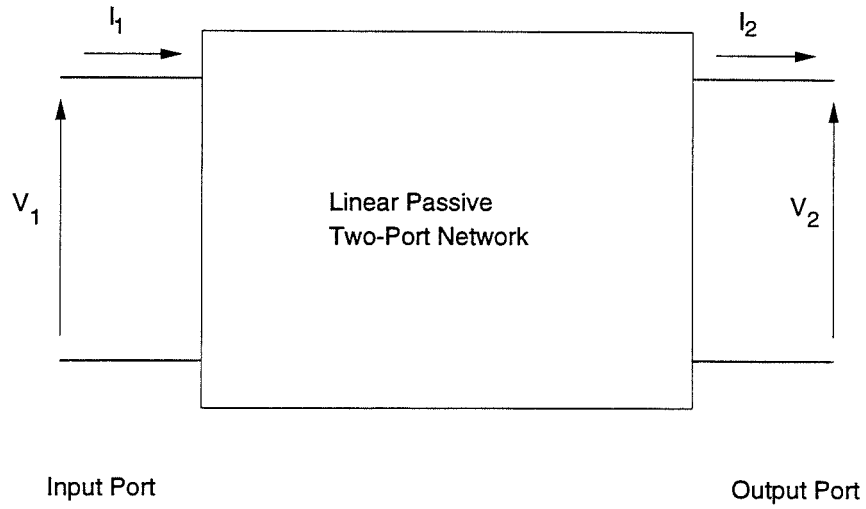


**Figure D.1 Linear Passive Two-Port Network**

The input voltage and current may be given in terms of the output voltage and current such that :

$$V_1 = A V_2 + B I_2 \qquad \ldots(D.1a)$$

$$I_1 = C V_2 + D I_2 \qquad \ldots(D.1b)$$

where, $V_1$, $I_1$, and $V_2$, $I_2$ are the input and output voltages and currents respectively, and $A$, $B$, $C$, and $D$ are the transmission parameters of the network [120].

Dividing expression (D.1a) by (D.1b) gives the input impedance in terms of the output voltage and current :

$$Z_1 = \frac{A V_2 + B I_2}{C V_2 + D I_2} \qquad \ldots(D.2)$$

and dividing the numerator and denominator of the RHS of equation (D.2) by $I_2$ gives the input impedance in terms of the output impedance :

$$Z_1 = \frac{AZ_2 + B}{CZ_2 + D} \qquad \ldots(D.3)$$

Equation (D.3) may be further simplified by dividing the RHS throughout by $D$ to give :

$$Z_1 = \frac{aZ_2 + b}{cZ_2 + 1} \qquad \ldots(D.4)$$

Thus, the input impedance of the linear passive two-port network is expressed in terms of the output impedance and three unknown parameters, *a, b,* and *c*.

In a real network the impedances and the network parameters can be expected to have complex values so that :

$$\hat{Z}_1 = Z_{1r} + jZ_{1i} = \frac{(a_r + ja_i)(Z_{2r} + jZ_{2i}) + (b_r + jb_i)}{(c_r + jc_i)(Z_{2r} + jZ_{2i}) + 1} \qquad \ldots(D.4)$$

where the subscripts *r* and *i* denote real and imaginary quantities respectively.

Multiplying out expression (D.4), and separating the real and imaginary parts in the numerator and denominator gives:

$$\hat{Z}_1 = \frac{P + jQ}{R + jS} \qquad \ldots(D.5)$$

where,

$$P=(a_rZ_{2r}-a_iZ_{2i}+b_r)$$
$$Q=(a_rZ_{2i}+a_iZ_{2r}+b_i)$$
$$R=(c_rZ_{2r}-a_iZ_{2i}+1)$$
$$S=(c_rZ_{2i}+c_iZ_{2r})$$

and by fully separating the real and imaginary parts of equation (D.5) we obtain:

$$\hat{Z}_1 = \left(\frac{PR + QS}{R^2 + S^2}\right) + j\left(\frac{QR - PS}{R^2 + S^2}\right) \qquad \ldots(D.6)$$

This expression was used when programming in HP Basic on the HP9816 Series 200 computer as complex number computations are not possible in this language.

## Appendix E

## Parallel Plate Transmission Line Input Impedance Transformation

The input impedance of a parallel-plate transmission line is given in section 6.1.1 as :

$$Z_l = \frac{Z_0}{\tanh(\gamma d)} \qquad \cdots(E.1)$$

where $Z_0$ and $\gamma$ are as defined for equation (6.2).

Equation (E.1) may be alternatively expressed as an admittance, giving :

$$Y_l = \frac{\tanh(\gamma d)}{Z_0} \qquad \cdots(E.2)$$

Multiplying both sides by the factor $d(R + j\omega L)$ leads to :

$$Y_l d(R + j\omega L) = d\gamma \tanh(\gamma d) \qquad \cdots(E.3)$$

It can be shown that $\tanh(x)$ is equal to $-j\tan(jx)$, which allows equation (E.3) to be expressed as :

$$Y_l d(R + j\omega L) = -jd\gamma \tan(jd\gamma) \qquad \cdots(E.4)$$

If a *conductor impedance*, $B$, is defined for the electrodes (*not* the full transmission line) as shown in equation (E.5) :

$$B = (R + j\omega L) \qquad \cdots(E.5)$$

then equation (E.4) becomes :

$$Y_l B d = -jd\sqrt{B(G + j\omega C)}\tan(jd\sqrt{B(G + j\omega C)}) \qquad \cdots(E.6)$$

As shown by equations (6.7) and (6.8), the specific sample geometry used in this work permits $G$ and $C$ in equation (E.6) to be replaced by $\sigma$ and $\varepsilon_r'\varepsilon_0$. A sample admittivity,

$$\Lambda_s = \sigma + j\omega\varepsilon_r'\varepsilon_0 \qquad \cdots(E.7)$$

may therefore be defined such that equation (E.6) can, by taking the $j$ operator inside the square root signs, be expressed by :

$$-Y_l Bd = d\sqrt{-\Lambda_s B}\tan(d\sqrt{-\Lambda_s B}) \qquad \cdots(E.8)$$

and this can be more conveniently expressed by the equation :

$$z\tan(z) - c = 0 \qquad \cdots(E.9)$$

where,

$$z = d\sqrt{-\Lambda_s B} \qquad \cdots(E.10)$$

$$c = -\frac{Bd}{Z_l} \qquad \cdots(E.11)$$

The value of $c$ at a particular frequency, $\omega$, is easily calculated from a measurement of input impedance, provided $R$ and $L$ are known. $z$ and $c$ are complex and may be expressed in the form :

$$z = x + jy \qquad \cdots(E.12)$$

$$c = a + jb \qquad \cdots(E.13)$$

Solving equation (E.9) for $z$ enables easy calculation of the sample admittivity by way of equation (E.10) leading to conductivity and dielectric constant from equation (E.7).

# Appendix F
# The Anharmonic Ratio of a Bilinear Transformation

Consider the following, after Wylie [121].

Bilinear transformations are the simplest class of conformal transformations. They are defined by the family of functions given by equation (F.1) which map points in the $u$ plane onto corresponding points in the $v$ plane ($u$ and $v$ both arbitrary planes of reference).

$$v = \left.\frac{pu+q}{ru+s}\right|_{ps \neq qr} \qquad \cdots(F.1)$$

where, $p$, $q$, $r$ and $s$ are constants.

This general bilinear transformation depends on *three* essential constants which are the ratios of any three of the coefficients $p$, $q$, $r$ and $s$ to the fourth. Thus, three conditions are necessary to determine the transform, which is unique if three distinct values of $u$ ($u_1$, $u_2$ and $u_3$) have specific distinct mappings in $v$ ($v_1$, $v_2$ and $v_3$).

In general, for the $i^{th}$ and $j^{th}$ mappings of $u$, it is observed that,

$$u_i - u_j = \frac{pv_i+q}{rv_i+s} - \frac{pv_j+q}{rv_j+s} = \frac{(ps-qr)(v_i-v_j)}{(rv_i+s)(rv_j+s)} \qquad \cdots(F.2)$$

Hence the following,

$$\frac{(u_1-u_2)(u_3-u_4)}{(u_1-u_4)(u_3-u_2)} = \frac{\dfrac{(ps-qr)(v_1-v_2)}{(rv_1+s)(rv_2+s)}\dfrac{(ps-qr)(v_3-v_4)}{(rv_3+s)(rv_4+s)}}{\dfrac{(ps-qr)(v_1-v_4)}{(rv_1+s)(rv_4+s)}\dfrac{(ps-qr)(v_3-v_2)}{(rv_3+s)(rv_2+s)}} \qquad \cdots(F.3)$$

$$= \frac{(v_1-v_2)(v_3-v_4)}{(v_1-v_4)(v_3-v_2)} \qquad \cdots(F.4)$$

The fraction expressed by equation (F.4) is known as the *anharmonic ratio* of the points $v_1$, $v_2$, $v_3$ and $v_4$. It can be seen that the anharmonic ratio of the points in the $u$

plane is equal to that of the points in the $v$ plane, which is the same as saying that the anharmonic ratio of any four points is *invariant* under a bilinear transform. Thus, the ratio is a constant. i.e. :

$$\frac{(u_1-u_2)(u_3-u_4)}{(u_1-u_4)(u_3-u_2)}=\frac{(v_1-v_2)(v_3-v_4)}{(v_1-v_4)(v_3-v_2)}=K \qquad \cdots(F.5)$$

A useful characteristic of the invariance property is that if any arbitrary linear transformation is applied to each of the four points in either plane then the anharmonic ratio is unchanged, i.e. :

$$\frac{(u_1-u_2)(u_3-u_4)}{(u_1-u_4)(u_3-u_2)}=\frac{(u'_1-u'_2)(u'_3-u'_4)}{(u'_1-u'_4)(u'_3-u'_2)}\Bigg|_{u'=f(u)} \qquad \cdots(F.6)$$

where $f(u)$ is a linear function of $u$.

It follows from the above that if four points in one plane and three in the image plane are known, then the fourth unknown point in the image plane may be obtained.

If it is assumed that points $v_1$, $v_2$, $v_3$ and $v_4$ as well as $u_2$, $u_3$ and $u_4$ are known, then the value, $K$, of the anharmonic ratio is found from expression (F.4) and the unknown value of $u_1$ is easily calculated from equation (F.7).

$$u_1=\frac{Ku_4(u_2-u_3)-u_2(u_4-u_3)}{(u_3-u_4)-K(u_3-u_2)} \qquad \cdots(F.7)$$

# Appendix G
# Mathcad De-imbedding Algorithm for 1-100 MHz

This file is for the calculation of Dielectric Constant and Conductivity from impedance measurements of an unknown material by means of a parallel plate transmission line model and the Newton-Raphson iterative method - all measurements obtained using a 150mm parallel plate line (plates 150mm wide, 150mm apart and 150mm long) - Friday 15 January 1993

$i \equiv \sqrt{-1}$ $N := 46$ $x := 1..N$ $\varepsilon 0 := 8.854 \cdot 10^{-12}$ ORIGIN ≡ 1

$v_1 := 2.997925 \cdot 10^{8}$ Velocity of Light

Inductance/m of steel $L := 5.94 \cdot 10^{-7}$

$T := 20$ Temperature in Degrees Centigrade

$\varepsilon s := 87.74 - 0.40008 \cdot T + 9.398 \cdot 10^{-4} \cdot T^2 - 1.410 \cdot 10^{-6} \cdot T^3$ Static Dielectric Constant of Water

$\varepsilon s =$

Molar Concentration of Standard Saline :- $co1 := 0.020279335$

$\tau a := 1.1109 \cdot 10^{-10} - 3.824 \cdot 10^{-12} \cdot T + 6.938 \cdot 10^{-14} \cdot T^2 - 5.096 \cdot 10^{-16} \cdot T^3$

$\tau a$ is the temperature dependent relaxation time

$\tau b1 := \tau a - \frac{8 \cdot 10^{-4} \cdot co1}{v_1}$ $\tau b1 =$

$\tau b1$ is the NaCl-concentration-dependent relaxation time

$\tau 1 := \frac{\tau b1}{2 \cdot \pi}$ Relaxation Time of Water Dipoles in Saline $\tau 1 =$

$\varepsilon i := 5.5$ High Frequency Limit of Dielectric Constant of Water

$\varepsilon s1 := \varepsilon s - 5.5 \cdot co1$

$\varepsilon s1 =$ Static Dielectric Constant of Saline1

$f1 := READPRN(freq)$

$\omega_x := f1_x \cdot 2 \cdot \pi \cdot 10^6$

$\sigma s := 0.209$

$$\varepsilon c1 := \left[ \varepsilon i + \frac{\varepsilon s1 - \varepsilon i}{1 + i \cdot \omega \cdot \tau 1} - i \cdot \frac{\sigma s}{\omega \cdot \varepsilon 0} \right]$$

Dispersion Curve of Saline

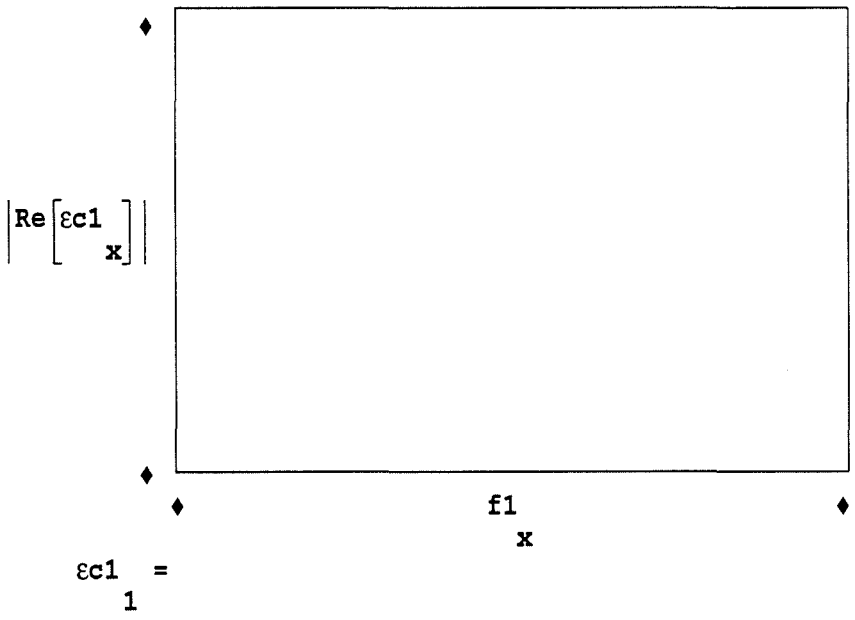


Dielectric Constant of Saline

$\varepsilon c1_1 =$

$f := f1 \cdot 10^{6}$ Frequency in Hertz

$R_x := 6.5359 \cdot 10^{-5} \cdot \sqrt{f_x}$ Resistance/m of steel plates

$d := 0.15$ Length of TX Line

$B := \sqrt{\sqrt{R + i \cdot \omega \cdot L}}$ "Impedance" Factor of Tx-Line conductors

$$\frac{\mathrm{Re}\left[\varepsilon c1_N\right]}{\sqrt{\left[\mathrm{Im}\left[\left[\varepsilon c1_N\right]\right] \cdot (-\varepsilon 0) \cdot \omega_N\right]}} =$$

$Zmr := READPRN(zcr)$ Raw Data Files

$Zmi := READPRN(zci)$ $Zm_x := Zmr_x + i \cdot Zmi_x$

$Zmr_N =$ $Zmr_1 =$

$Zmi_N =$ $Zmi_1 =$

Impedance of a Parallel-Plate Line containing Saline

$$Zs := \frac{\sqrt{\frac{\sqrt{\frac{-}{B}}}{\sqrt{\frac{-}{-}}\sqrt{\frac{-}{i\cdot\omega\cdot\varepsilon 0\cdot\varepsilon c1}}}}}{\tanh\left(d\cdot\left(\frac{-}{B}\cdot\sqrt{\frac{-}{-}\sqrt{\frac{-}{i\cdot\omega\cdot\varepsilon c1\cdot\varepsilon 0}}}\right)\right)}$$

Conversion of Concrete Impedance Measurement into Parallel-Plate Equivalent

$$Zl := \sqrt{\frac{-}{-}}\sqrt{\frac{-}{Zm\cdot\frac{Zs}{50}}}$$

Calibration Conversion

Transformed Impedance

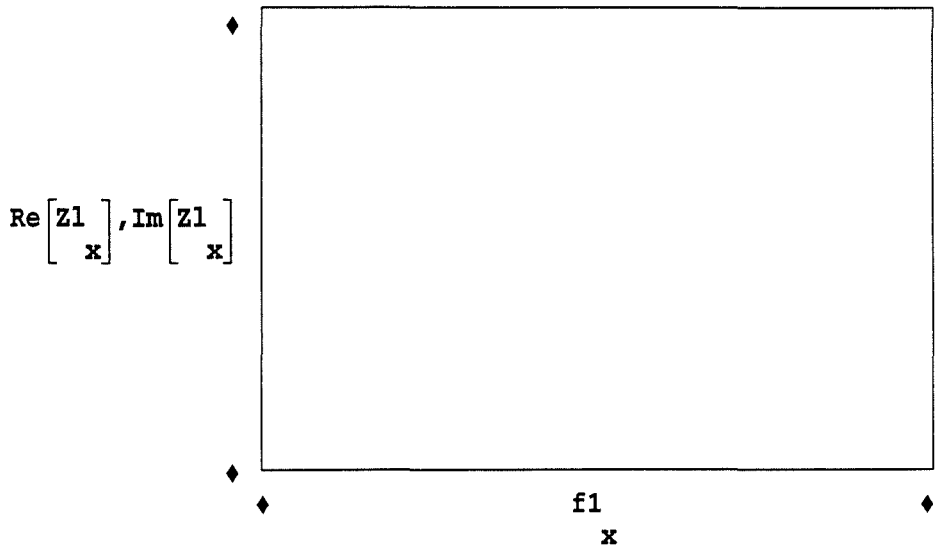


impr and impi

Output Data Files

Parameters for use in Newton-Raphson Iteration

K := 15 Number of required iterations

n := 1 ..K

$$c := \left[\left[\frac{2}{B}\right] \cdot \frac{d}{\overline{-Zl}}\right]$$

Transformed Admittance Measurement

a := Re(c)

b := Im(c)

|c| =

Starting estimate
for first root
(Vaillancourt)

$$z^{\langle 1\rangle} := \left[\operatorname{atan}\left(\left|\frac{\sqrt{}}{c}\right|\right) + i\cdot\left[\frac{\sqrt{b + 3\cdot b^{3}}}{\left[\sqrt{1 + \left|\frac{}{c}\right|^{2}}\right]\cdot\left[\sqrt{1 + 2\cdot\left|\frac{}{c}\right|^{2}}\right]}\right]\right]$$

$$\left[z^{\langle 1\rangle}\right]_{1} =$$

Newton-Raphson Method of Iteration

$$z^{\langle n+1\rangle} := \left[\left|\frac{}{z}\right|^{\langle n\rangle} - \frac{\left[\left|\frac{}{z}\right|^{\langle n\rangle}\cdot\tan\left(\left|\frac{\sqrt{}}{\left|\frac{}{z}\right|^{\langle n\rangle}}\right|\right) - c\right]}{\left[\frac{\left|\frac{}{z}\right|^{\langle n\rangle}}{2} + \tan\left(\left|\frac{\sqrt{}}{\left|\frac{}{z}\right|^{\langle n\rangle}}\right|\right)\right]\cdot\left[\frac{1}{\left[\cos\left(\left|\frac{\sqrt{}}{\left|\frac{}{z}\right|^{\langle n\rangle}}\right|\right)\right]^{2}}\right]}\right]$$

Solution to y*

$$ys := \overline{\left[\frac{\left[\overline{\left[z\right]}\right]^{\langle K \rangle}}{B \cdot d}\right]} \qquad yss := -\overline{\left[ys^{2}\right]}$$

Computed values of Conductivity and Dielectric Constant

$$\varepsilon t := READPRN(et)$$

$$\sigma e := \overline{\left[Re\left[\overline{(yss)}\right]\right]} \qquad \varepsilon e := \overline{\left[Im\left[\overline{\left[\frac{yss}{\varepsilon 0 \cdot \omega}\right]}\right]\right]}$$

k := 1 ..46

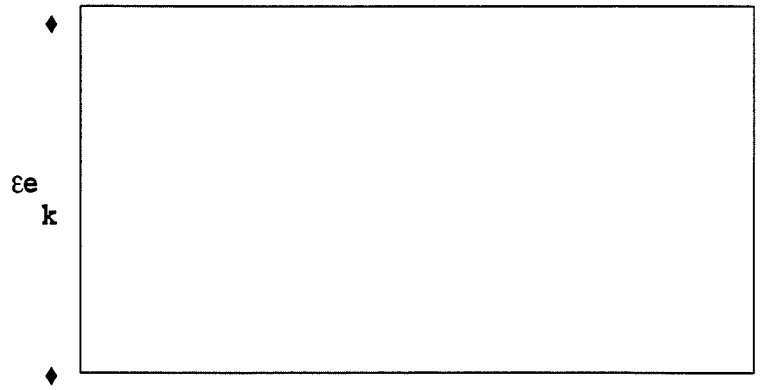


εe = 46

εt = 46

f1 = 31

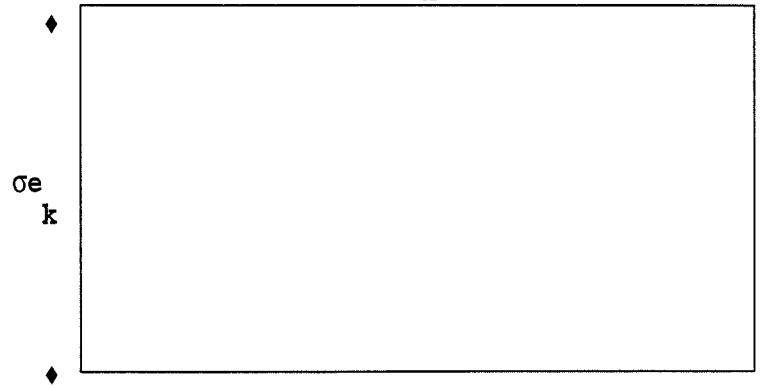


σe = 25

σe = 01

WRITEPRN(dout) := $\varepsilon e_k$ WRITEPRN(cout) := $\sigma e_k$ Data Output

$$Zrl := \frac{\left[\frac{\left[\frac{-}{B}\right]}{\left[\sqrt{yss}\right]}\right]}{\left[\tanh\left[d \cdot \left[\frac{-}{B} \cdot \left[\sqrt{yss}\right]\right]\right]\right]}$$

Recomputed Transmission Line Impedance

Percentage Convergance Accuracy of the Newton-Raphson Method

$$\frac{\left[\left|\left[\begin{matrix} Zr1 \\ x \end{matrix}\right]\right| - \left|\left[\begin{matrix} Z1 \\ x \end{matrix}\right]\right|\right]}{\left|\left[\begin{matrix} Z1 \\ x \end{matrix}\right]\right|} \cdot 100$$

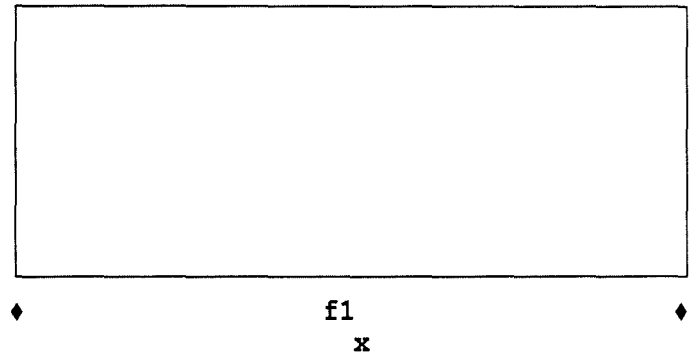

# Appendix H
# Mathcad De-imbedding Algorithm for 100-1000 MHz - Model II

This file is for the calculation of Dielectric Constant and Conductivity from measurements of three known standards and an unknown material, by means of the Anharmonic Cross Ratio properties of Bilinear transforms and the Newton-Raphson iterative method - all measurements obtained using a 3mm monopole probe (Marsland & Evans Model) - Tuesday 5th January 1993

$i \equiv \sqrt{-1}$ $x := 1..51$ $\varepsilon 0 := 8.854 \cdot 10^{-12}$ ORIGIN ≡ 1

$T := 18.06$ Water Temperature in Degrees Centigrade

$v_1 := 2.997925 \cdot 10^{8}$ Velocity of Light

$\varepsilon s := 87.74 - 0.40008 \cdot T + 9.398 \cdot 10^{-4} \cdot T^2 - 1.410 \cdot 10^{-6} \cdot T^3$ Static Dielectric Constant of Water

$\varepsilon s =$

Molar Concentrations of Standard Salines :-

LSC HSC VSC ESC

$coL := 0.0050698$ $coH := 0.060838$ $coV := 0.091257$ $coE := 0.1889$

$\tau a := 1.1109 \cdot 10^{-10} - 3.824 \cdot 10^{-12} \cdot T + 6.938 \cdot 10^{-14} \cdot T^2 - 5.096 \cdot 10^{-16} \cdot T^3$

$\tau a$ is the temperature dependent relaxation time

$$\tau bL := \left[ \tau a - 8 \cdot 10^{-4} \cdot \left[ \frac{coL}{v_1} \right] \right] \qquad \tau bH := \left[ \tau a - 8 \cdot 10^{-4} \cdot \left[ \frac{coH}{v_1} \right] \right]$$

$$\tau bV := \left[ \tau a - 8 \cdot 10^{-4} \cdot \left[ \frac{coV}{v_1} \right] \right] \qquad \tau bE := \left[ \tau a - 8 \cdot 10^{-4} \cdot \left[ \frac{coE}{v_1} \right] \right]$$

$\tau bL$, $\tau bH$, $\tau bV$, $\tau bE$ are the NaCl-concentration-dependent relaxation times

$\tau L := \frac{\tau bL}{2 \cdot \pi}$ $\tau H := \frac{\tau bH}{2 \cdot \pi}$ $\tau V := \frac{\tau bV}{2 \cdot \pi}$ $\tau E := \frac{\tau bE}{2 \cdot \pi}$ Relaxation Time of Water Dipoles in Salines

$\varepsilon i := 5.5$ High Frequency Limit of Dielectric Constant of Water

$\varepsilon sL := \varepsilon s - 5.5 \cdot coL$

$\varepsilon sL =$ Static Dielectric Constant of Saline LSC

$\varepsilon sH := \varepsilon s - 5.5 \cdot coH$

$\varepsilon sH =$ Static Dielectric Constant of Saline HSC

$\varepsilon sV := \varepsilon s - 5.5 \cdot coV$

$\varepsilon sV =$ Static Dielectric Constant of Saline VSC

$\varepsilon sE := \varepsilon s - 5.5 \cdot coE$

$\varepsilon sE =$ Static Dielectric Constant of Saline ESC

$f1 := READPRN(freq)$

$$\omega 1 := \left[ f1 \cdot 2 \cdot \pi \cdot 10^{6} \right]$$

$\sigma L := 0.05128$

$$\varepsilon cL := \left[ \varepsilon i + \frac{\varepsilon sL - \varepsilon i}{1 + i \cdot \omega 1 \cdot \tau L} - i \cdot \frac{\sigma L}{\omega 1 \cdot \varepsilon 0} \right]$$

$\sigma H := 0.565$

$$\varepsilon cH := \left[ \varepsilon i + \frac{\varepsilon sH - \varepsilon i}{1 + i \cdot \omega 1 \cdot \tau H} - i \cdot \frac{\sigma H}{\omega 1 \cdot \varepsilon 0} \right]$$

$\sigma V := 0.834$

$$\varepsilon cV := \left[ \varepsilon i + \frac{\varepsilon sV - \varepsilon i}{1 + i \cdot \omega 1 \cdot \tau V} - i \cdot \frac{\sigma V}{\omega 1 \cdot \varepsilon 0} \right]$$

$\sigma E := 1.71$

$$\varepsilon cE := \left[ \varepsilon i + \frac{\varepsilon sE - \varepsilon i}{1 + i \cdot \omega 1 \cdot \tau E} - i \cdot \frac{\sigma E}{\omega 1 \cdot \varepsilon 0} \right]$$

(The conductivities above are obtained by MEASUREMENT using the Wayne-Kerr Bridge Analyser in conjunction with 150mm square stainless steel electrodes)

WRITEPRN(VSCr) := Re(εcV)

WRITEPRN(VSCi) := Im(εcV)

Output εcV to file for use in FINAL1 analysis

These are the Dispersions for the respective Salines (L, H, V, & E)

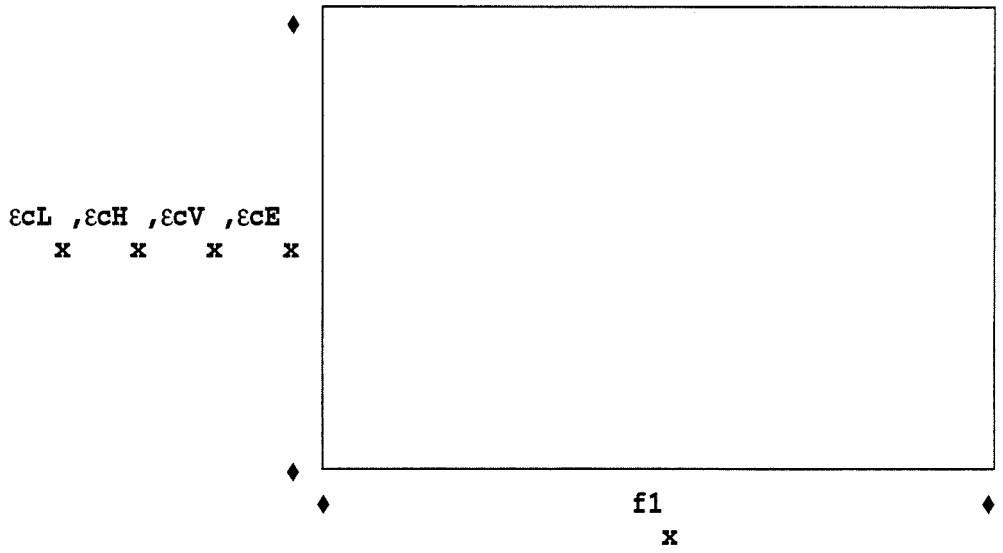


N := 20  For selecting which frequency

εa := 0

$\sigma a := 3.27 \cdot 10^{7}$  These are for Aluminium

$$\varepsilon cA := \sqrt{\left[\varepsilon a - \sigma a \cdot \frac{i}{\varepsilon 0 \cdot \omega 1}\right]}$$

εfs := 1

σfs := 0  These are for Free-Space

$$\varepsilon cF := \sqrt{\left[\varepsilon fs - \sigma fs \cdot \frac{i}{\varepsilon 0 \cdot \omega 1}\right]}$$

Measured Impedances for Respective Standards

zmAr := READPRN(zar) ALF zmFr := READPRN(zfr) AFS

zmAi := READPRN(zai) zmFi := READPRN(zfi)

zmA := zmAr + i·zmAi zmF := zmFr + i·zmFi

zmLr := READPRN(zlr) LSC zmVr := READPRN(zvr) VSC

zmLi := READPRN(zli) zmVi := READPRN(zvi)

zmL := zmLr + i·zmLi zmV := zmVr + i·zmVi

zmEr := READPRN(zer) ESC zmHr := READPRN(zhr) HSC

zmEi := READPRN(zei) zmHi := READPRN(zhi)

zmE := zmEr + i·zmEi zmH := zmHr + zmHi·i

Differences From Standards

DVA := zmV - zmA DFL := zmF - zmL DAF := zmA - zmF

DVF := zmV - zmF DVL := zmV - zmL DLA := zmL - zmA

DFV := zmF - zmV

εrA := εcA εrL := εcL εrE := εcE The Dielectric Constants of

εrV := εcV εrH := εcH εrF := εcF the Standards

expo := 2.5 The exponent for the Admittance Model

For the calculation of G a Quadratic expression is formed

$$aa1 := \left[\varepsilon rV^{expo} \cdot \left[\varepsilon rA^{expo} + \varepsilon rL^{expo} + \varepsilon rF^{expo}\right]\right]$$

$$aa2 := \left[\varepsilon rF^{expo} \cdot \left[\varepsilon rL^{expo} + \varepsilon rA^{expo}\right]\right]$$

$$aa := \left\lfloor aa1 + aa2 + (\varepsilon rL \cdot \varepsilon rA)^{expo} \right\rfloor$$

$$bb1 := \left\lfloor DVA \cdot DFL \cdot \left\lfloor \varepsilon rV^{expo} \cdot \varepsilon rA + \varepsilon rA^{expo} \cdot \varepsilon rV + \varepsilon rF^{expo} \cdot \varepsilon rL + \varepsilon rL^{expo} + \varepsilon rF \right\rfloor \right\rfloor$$

$$bb2 := \left\lfloor DVL \cdot DAF \cdot \left\lfloor \varepsilon rV^{expo} \cdot \varepsilon rL + \varepsilon rL^{expo} \cdot \varepsilon rV + \varepsilon rA^{expo} \cdot \varepsilon rF + \varepsilon rF^{expo} + \varepsilon rA \right\rfloor \right\rfloor$$

$$bb3 := \left\lfloor DVF \cdot DLA \cdot \left\lfloor \varepsilon rV^{expo} \cdot \varepsilon rF + \varepsilon rF^{expo} \cdot \varepsilon rV + \varepsilon rL^{expo} \cdot \varepsilon rA + \varepsilon rA^{expo} + \varepsilon rL \right\rfloor \right\rfloor$$

$$bb := (bb1 + bb2 + bb3)$$

$$cc1 := (DVA \cdot DFL \cdot (\varepsilon rV \cdot \varepsilon rA + \varepsilon rF \cdot \varepsilon rL))$$

$$cc2 := (DVL \cdot DAF \cdot (\varepsilon rV \cdot \varepsilon rL + \varepsilon rA \cdot \varepsilon rF))$$

$$cc3 := (DVF \cdot DLA \cdot (\varepsilon rV \cdot \varepsilon rF + \varepsilon rL \cdot \varepsilon rA))$$

$$cc := (cc1 + cc2 + cc3)$$

$$G := \left[ \frac{-bb + \sqrt{bb^2 - 4 \cdot aa \cdot cc}}{2 \cdot aa} \right]$$ Root of Quadratic in G

G =
51

WRITEPRN(geor) := Re(G) Output to file for use in FINAL1

WRITEPRN(geoi) := Im(G)

G is the Probe Geometrical Radiation/Fringing Constant

$$yA := \left[ \varepsilon rA + G \cdot \varepsilon rA^{expo} \right]$$ Marsland and Evans Model for Short Probe

$$yF := \left[ \varepsilon cF + G \cdot \varepsilon cF^{expo} \right] \qquad yL := \left[ \varepsilon rL + G \cdot \varepsilon rL^{expo} \right]$$

$$yE := \left[ \varepsilon rE + G \cdot \varepsilon rE^{expo} \right] \qquad yV := \left[ \varepsilon rV + G \cdot \varepsilon rV^{expo} \right]$$

$$yH := \left[ \varepsilon rH + G \cdot \varepsilon rH^{expo} \right]$$

DyFL := yF - yL DyAF := yA - yF

Model Difference Parameters

Measured Impedances for Respective Unknowns

zmHr := READPRN(zhr)  Saline HSC

zmHi := READPRN(zhi)  zmH := zmHr + zmHi·i

zmUr := READPRN(zur)  Concrete

zmUi := READPRN(zui)  zmU := zmUr + i·zmUi

zmSSr := READPRN(zssr)  Sand/Saline

zmSSi := READPRN(zssi)  zmSS := zmSSr + i·zmSSi

DUA := zmSS - zmA  Differences for Measurements of the Unknown Material

DUL := zmSS - zmL

DUF := zmSS - zmF

$$Km := \left[\frac{DUA}{DUL} \cdot \frac{DFL}{DAF}\right]$$

Bilinear Transform Method

Km =
N

yA =
N

yF =
N

yL =
N

yE =
N

$yV_N =$

$yH_N =$

$$yU := \left[\frac{Km \cdot yL \cdot DyAF - yA \cdot DyFL}{Km \cdot DyAF - DyFL}\right]$$

$yU_N =$

Output of Transformed Admittance data to file for use in FINAL1

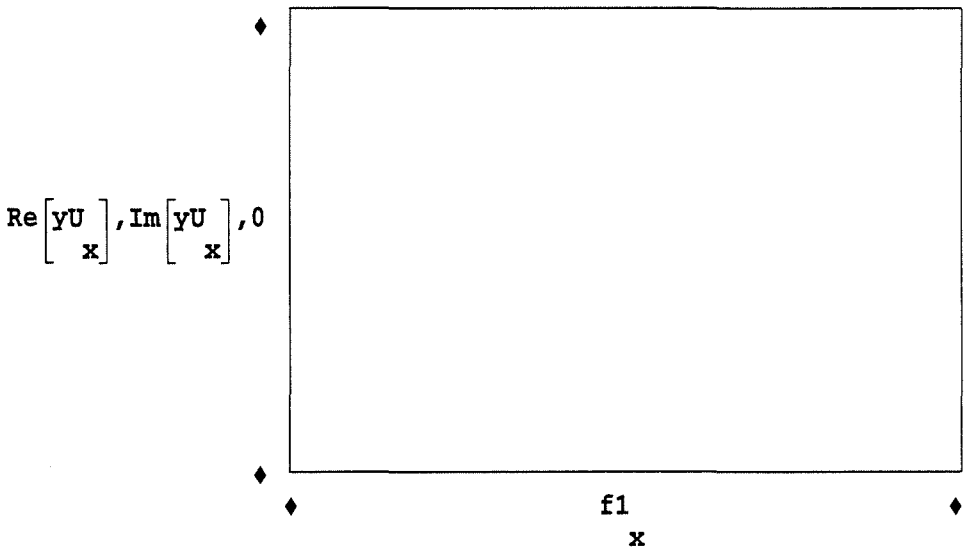


This must be solved by iteration for Complex Relative Permittivity

Output Amittance to File

WRITEPRN(admitr) := $Re\left[yU_x\right]$ WRITEPRN(admiti) := $Im\left[yU_x\right]$

This file is for the calculation of values of Dielectric Constant and Conductivity from computed values of transformed Admittance (based on the Marsland and Evans Model of a short monopole probe) using the Newton-Raphson iterative technique - 7/1/92

$i \equiv \sqrt{-1}$ $\quad x := 1..51$ $\quad \varepsilon 0 := 8.854 \cdot 10^{-12}$ $\quad ORIGIN \equiv 1$

$yUr := READPRN(admitr)$ $\quad startr := READPRN(vscr)$

$yUi := READPRN(admiti)$ $\quad starti := READPRN(vsci)$

$yU := yUr + i \cdot yUi$ $\quad start := startr + i \cdot starti$

$Gr := READPRN(geor)$ $\quad f1 := READPRN(freq)$

$Gi := READPRN(geoi)$ $\quad \omega 1 := 2 \cdot \pi \cdot 10^{6} \cdot f1$

$G := Gr + i \cdot Gi$

$n := 1..8$ The number of iterations

Starting estimate $start = 1$

$\varepsilon r^{\langle 1 \rangle} := start$ $\quad expo := 2.5$ Newton-Raphson Iteration

$$\varepsilon r^{\langle n+1 \rangle} := \left[ \varepsilon r^{\langle n \rangle} + \frac{\overline{yU - \varepsilon r^{\langle n \rangle} - G \cdot \left[ \varepsilon r^{\langle n \rangle} \right]^{expo}}}{1 + expo \cdot G \cdot \left[ \varepsilon r^{\langle n \rangle} \right]^{-expo-1}} \right]$$

These are the final solutions for the unknown material

$\varepsilon_r := \varepsilon r^{\langle 8 \rangle}$ $\quad \sigma V_x := -starti_x \cdot \varepsilon 0 \cdot \omega 1_x$ $\quad \varepsilon V_x := startr_x$

$\varepsilon f := Re\left[\varepsilon_r\right]$ $\quad \sigma f_x := -Im\left[\varepsilon_{r_x}\right] \cdot \varepsilon 0 \cdot \omega 1_x$

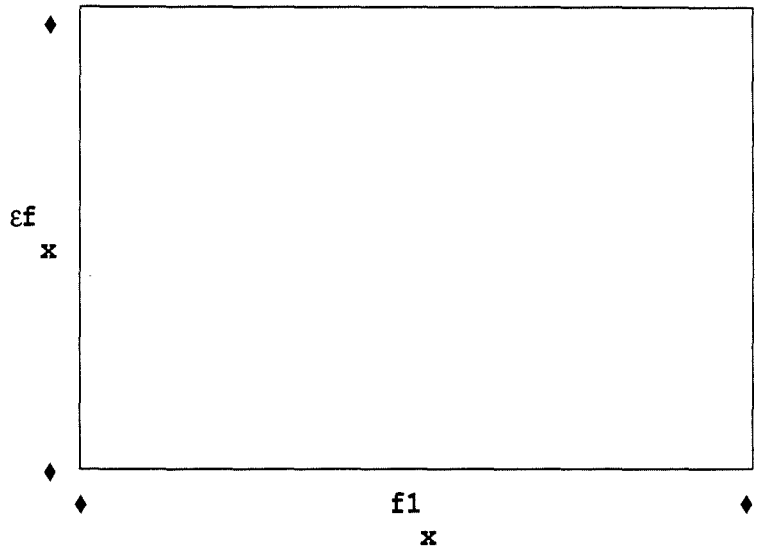


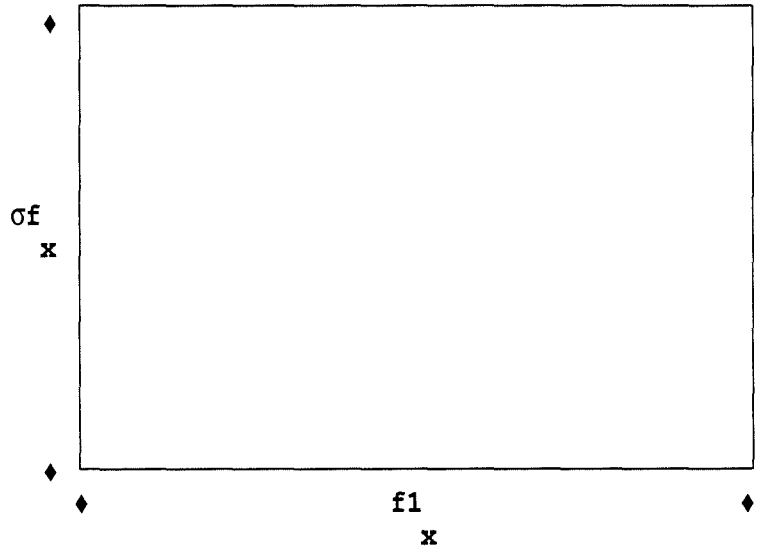


Plots of Dielectric Constant and Conductivity

# Appendix I
# Mathcad De-imbedding Algorithm for 100-1000 MHz - Model VI

This file is for the calculation of Dielectric Constant and Conductivity from measurements of three known standards (including a short circuit made up from aluminium foil) and an unknown material, by means of the Anharmonic Cross Ratio properties of a Bilinear transform - all measurements obtained using a 3mm monopole probe
(Simplified Lumped Element Model) - Thursday 28th January 1993

$i \equiv \sqrt{-1}$ $x := 1..51$ $\varepsilon 0 := 8.854 \cdot 10^{-12}$ ORIGIN ≡ 1

$T := 18.06$ Water Temperature in Degrees Centigrade

$v_1 := 2.997925 \cdot 10^{8}$ Velocity of Light

$\varepsilon s := 87.74 - 0.40008 \cdot T + 9.398 \cdot 10^{-4} \cdot T^2 - 1.410 \cdot 10^{-6} \cdot T^3$ Static Dielectric Constant of Water

$\varepsilon s =$

Molar Concentrations of Standard Salines :-

LSC HSC VSC ESC

$coL := 0.0050698$ $coH := 0.060838$ $coV := 0.091257$ $coE := 0.1889$

$\tau a := 1.1109 \cdot 10^{-10} - 3.824 \cdot 10^{-12} \cdot T + 6.938 \cdot 10^{-14} \cdot T^2 - 5.096 \cdot 10^{-16} \cdot T^3$

$\tau a$ is the temperature dependent relaxation time

$$\tau bL := \left[ \tau a - 8 \cdot 10^{-4} \cdot \left[ \frac{coL}{v_1} \right] \right] \qquad \tau bH := \left[ \tau a - 8 \cdot 10^{-4} \cdot \left[ \frac{coH}{v_1} \right] \right]$$

$$\tau bV := \left[ \tau a - 8 \cdot 10^{-4} \cdot \left[ \frac{coV}{v_1} \right] \right] \qquad \tau bE := \left[ \tau a - 8 \cdot 10^{-4} \cdot \left[ \frac{coE}{v_1} \right] \right]$$

$\tau bL$, $\tau bH$, $\tau bV$, $\tau bE$ are the NaCl-concentration-dependent relaxation times

$\tau L := \frac{\tau bL}{2 \cdot \pi}$ $\tau H := \frac{\tau bH}{2 \cdot \pi}$ $\tau V := \frac{\tau bV}{2 \cdot \pi}$ $\tau E := \frac{\tau bE}{2 \cdot \pi}$ Relaxation Time of Water Dipoles in Salines

$\varepsilon i := 5.5$ High Frequency Limit of Dielectric Constant of Water

$\varepsilon sL := \varepsilon s - 5.5 \cdot coL$

$\varepsilon sL =$ Static Dielectric Constant of Saline LSC

$\varepsilon sH := \varepsilon s - 5.5 \cdot coH$

$\varepsilon sH =$ Static Dielectric Constant of Saline HSC

$\varepsilon sV := \varepsilon s - 5.5 \cdot coV$

$\varepsilon sV =$ Static Dielectric Constant of Saline VSC

$\varepsilon sE := \varepsilon s - 5.5 \cdot coE$

$\varepsilon sE =$ Static Dielectric Constant of Saline ESC

$f1 := READPRN(freq)$ Read Frequency File

$$\omega 1 := \left[ f1 \cdot 2 \cdot \pi \cdot 10^{6} \right]$$

$\sigma L := 0.05128$

$$\varepsilon cL := \left[ \varepsilon i + \frac{\varepsilon sL - \varepsilon i}{1 + i \cdot \omega 1 \cdot \tau L} - i \cdot \frac{\sigma L}{\omega 1 \cdot \varepsilon 0} \right]$$

$\sigma H := 0.565$

$$\varepsilon cH := \left[ \varepsilon i + \frac{\varepsilon sH - \varepsilon i}{1 + i \cdot \omega 1 \cdot \tau H} - i \cdot \frac{\sigma H}{\omega 1 \cdot \varepsilon 0} \right]$$

$\sigma V := 0.834$

$$\varepsilon cV := \left[ \varepsilon i + \frac{\varepsilon sV - \varepsilon i}{1 + i \cdot \omega 1 \cdot \tau V} - i \cdot \frac{\sigma V}{\omega 1 \cdot \varepsilon 0} \right]$$

$\sigma E := 1.71$

$$\varepsilon cE := \left[\varepsilon i + \frac{\varepsilon sE - \varepsilon i}{1 + i \cdot \omega 1 \cdot \tau E} - i \cdot \frac{\sigma E}{\omega 1 \cdot \varepsilon 0}\right]$$

(The conductivities above are obtained by MEASUREMENT using the Wayne-Kerr Bridge Analyser in conjunction with 150mm square stainless steel electrodes)

These are the Dispersions for the respective Salines (L, H, V, & E)

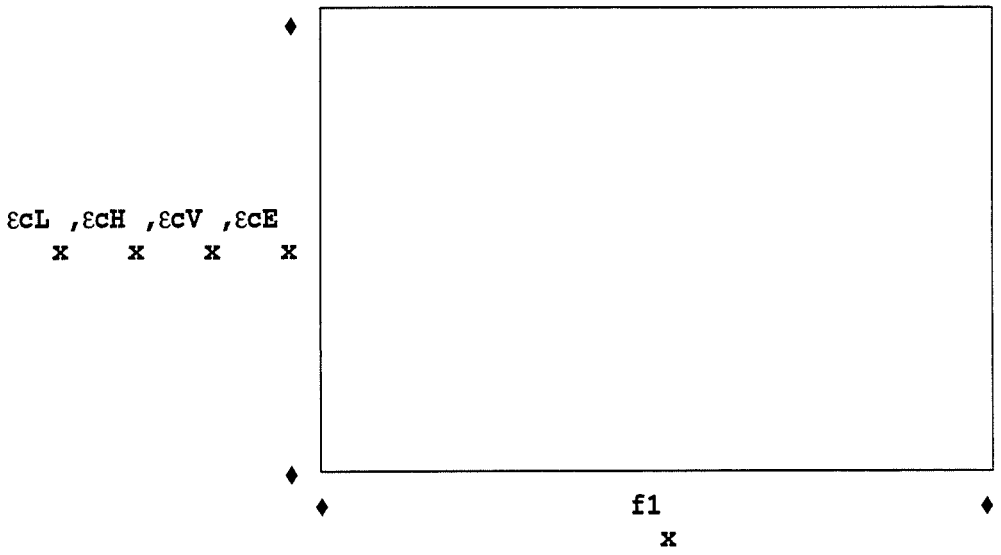


$N := 1$ · For selecting which frequency

$\varepsilon a := 0$

$\sigma a := 3.27 \cdot 10^{7}$ These are for Aluminium

$$\varepsilon cA := \left[\varepsilon a - \sigma a \cdot \frac{i}{\varepsilon 0 \cdot \omega 1}\right]$$

$\varepsilon f := 1$

$\sigma f := 0$ These are for Free-Space

$$\varepsilon cF := \left[\varepsilon f - \sigma f \cdot \frac{i}{\varepsilon 0 \cdot \omega 1}\right]$$

Measured Impedances for Respective Standards

zmAr := READPRN(zar) ALF zmFr := READPRN(zfr) FSP

zmAi := READPRN(zai) zmFi := READPRN(zfi)

zmA := zmAr + i·zmAi zmF := zmFr + i·zmFi

zmLr := READPRN(zlr) LSC zmVr := READPRN(zvr) VSC

zmLi := READPRN(zli) zmVi := READPRN(zvi)

zmL := zmLr + i·zmLi zmV := zmVr + i·zmVi

zmEr := READPRN(zer) ESC zmHr := READPRN(zhr) HSC

zmEi := READPRN(zei) zmHi := READPRN(zhi)

zmE := zmEr + i·zmEi zmH := zmHr + zmHi·i

Differences From Standards

DVA := zmV - zmA DVF := zmV - zmF DVA := zmV - zmA

DVE := zmV - zmE DVF := zmV - zmF DFA := zmF - zmA

εrA := εcA εrL := εcL εrE := εcE The Dielectric Constants of

εrV := εcV εrH := εcH εrF := εcF the Standards

DyVF := εrV - εrF DyVA := εrV - εrA Model Difference Parameters

Measured Impedances for Respective Unknowns

zmTr := READPRN(ztr) Tap Water

zmTi := READPRN(zti) zmT := zmTr + zmTi·i

zmHr := READPRN(zhr) Saline HSC

zmHi := READPRN(zhi) zmH := zmHr + zmHi·i

zmUr := READPRN(zur) Concrete

zmUi := READPRN(zui) zmU := zmUr + i·zmUi

zmSSr := READPRN(zssr)  Sand/Saline

zmSSi := READPRN(zssi)  zmSS := zmSSr + i·zmSSi

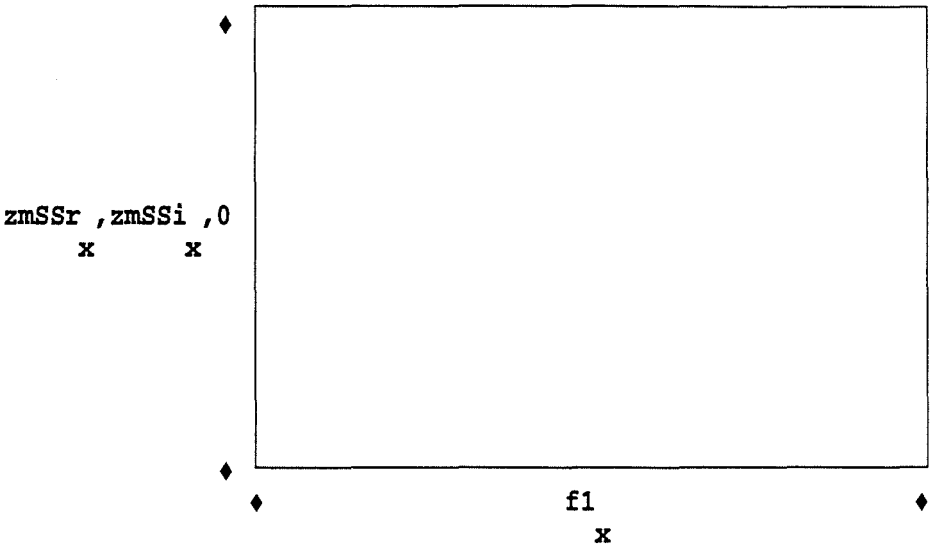


Measured Impedance

DUA := zmSS - zmA  Differences for Measurements of the Unknown Material

DUF := zmSS - zmF

DUV := zmSS - zmV

$$Km := \overline{\left[\frac{DUA}{DUF}\cdot\frac{DVF}{DVA}\right]}$$

Bilinear Transform Method

Km = N  Anharmonic Ratio

Computed Transform of Unknown Admittance

$$\varepsilon U := \overline{\left[\frac{Km\cdot\varepsilon rF\cdot DyVA - \varepsilon rA\cdot DyVF}{Km\cdot DyVA - DyVF}\right]}$$

$\varepsilon U_N$ = Calculated Relative Permittivity

$\varepsilon rL_N$ = Standard for Comparison

$\varepsilon := Re(\varepsilon U)$

$\sigma_x := -Im(\varepsilon U_x) \cdot \varepsilon 0 \cdot \omega 1_x$

$\varepsilon 1_x := Re(\varepsilon rL_x)$

$\sigma 1_x := -Im(\varepsilon rL_x) \cdot \varepsilon 0 \cdot \omega 1_x$

Plots of the Dielectric Constant and Conductivity

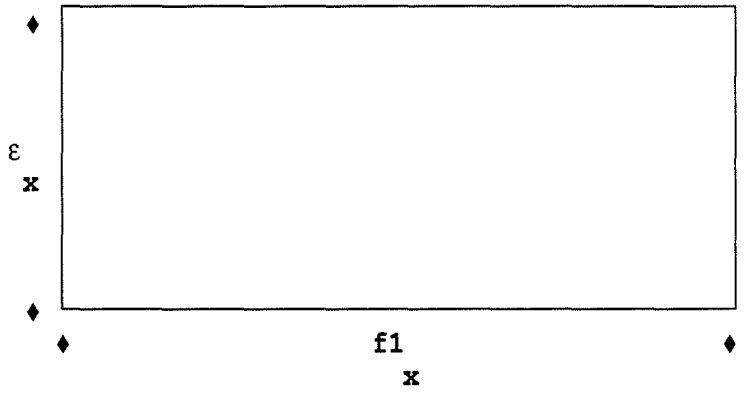


Dielectric Constant

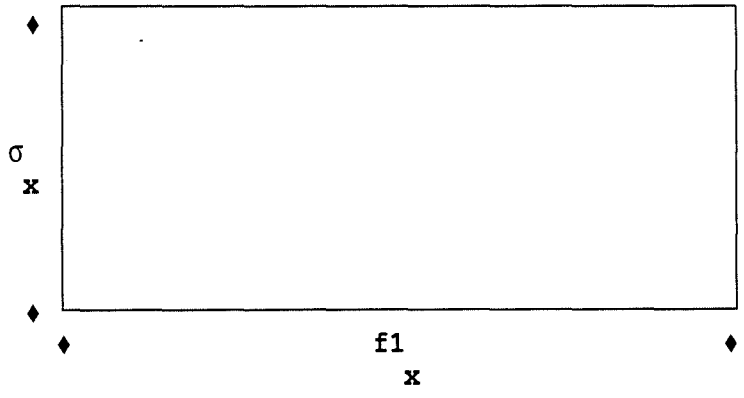


Conductivity

# List of References


1. **Beeby, A.W.** : "Empiricism versus Understanding, in the Successful Use of Materials in a Changing World", Editorial Comment, Magazine of Concrete Research, Vol 43, No 156, 1991, pp 141-142

2. **Wilson, J.G.** : "The Electrical Properties of Concrete", PhD Thesis (Unpublished), University of Edinburgh, 1986

3. **Wilson, J.G., Whittington, H.W.** : "Low Frequency Electrical Characteristics of Fresh Concrete", IEE Proceedings-A, Vol 133, Part A, No 5, July 1986, pp 265-271

4. **Wilson, J.G., Whittington, H.W.** : "Measurement of the Electrical Properties of Concrete", Proceedings of the 2nd International Conference on Computer Applications in Concrete, Nanyang Technology Institute, Singapore, C-84, 1988

5. **Wilson, J.G., Whittington, H.W.** : "Variations in the Electrical Properties of Concrete with Change in Frequency", IEE Proceedings-A, Vol 137, Part A, No 5, September 1990, pp 246-254

6. **Hippel, A.R. von** : "Dielectrics and Waves", 3rd Edition, John Wiley and Sons, New York, 1962

7. **Kittel, C.** : "Introduction to Solid State Physics", 5th Edition, Wiley, USA, 1976, pp 286, 304-305, 329

8. **Bate, S.C.C.** : "Lessons from the Past - Achievements and Failures", Chapter 2 in "Handbook of Structural Concrete", Pitman Books Limited, London, 1983, pp 2_1 to 2_56

9. **Neville, A.M.** : "Properties of Concrete", 3rd Edition, Longman Scientific & Technical, 1988

10. **Lea, F.M.** : "The Chemistry of Cement and Concrete", 3rd Edition, Edward Arnold (Publishers) Ltd, London, 1970

11. **Berner, U.R.** : "Modelling Pore-Water Chemistry in Hydrated Portland Cement", Materials Research Society, Symposium Proceedings, Vol 84, 1987, pp 319-330

12. **Orchard, D.F.** : "Concrete Technology", Vol 1 - "Properties of Materials", 3rd Edition, Applied Science Publishers Ltd, England, 1973

13. **Chong, C.V.Y.** : "Properties of Materials", MacDonald & Evans Limited, Plymouth, 1977, pp 24-29

14. **Advertisement Feature** : "Quality Assured Repairs Using Micro Silica Technology", Concrete, July 1990, p 39

15. **Ben-Bassat, M., Nixon, P.J., Hardcastle, J.** : "The Effect of Differences in the Composition of Portland Cement on the Properties of Hardened Concrete", Magazine of Concrete Research, Vol 42, No 151, June 1990, pp 59-66

16. **Bogue, R.H.** : "Chemistry of Portland Cement", Reinhold, New York, 1955

17. **Henderson, E., Bailey, J.E.** : "Sheet-like Structure of Calcium Silicate Hydrates", Journal of Materials Science, Vol 23, February 1988, pp 501-508

18. **Double, D.D.** : "New Developments in Understanding The Chemistry of Cement Hydration", Philosophical Transactions of the Royal Society of London, Series A, Vol 310, 1983, pp53-66

19. **Double, D.D., Hellawell, A., Perry, S.J.** : "The Hydration of Portland Cement", Proceedings of the Royal Society of London, Vol A359, 1978, pp 435-451.

20. **Birchall, J.D., Howard, A.J., Bailey, J.E.** : "On the Hydration of Portland Cement", Proceedings of the Royal Society of London, Vol A360, 1978, pp 445-453.

21. **Gross, J.M., Wiseall, B.** : "Principles of Physical Chemistry", M&E Handbooks, Macdonald & Evans Ltd., Plymouth, 1972, pp 322-323

22. **Penttala, E.V.** : "Nature of Compression Strength in Concrete", Magazine of Concrete Research, Vol 44, No 159, June 1992, pp 87-106

23. **Darley, J.C.** : "Testing and Investigation of Concrete Structures", Promotional Document, Frank Saynor and Associates Limited (Consulting Engineers), Glasgow, 1990

24. **Bungey, J.H.** : "Testing of Concrete in Structures", 2nd Edition, Surrey University Press, London, 1989

25. **Price, W.F.** : "Moisture Measurement Techniques for Fresh Concrete", Measurement and Control, Vol 24, April 1992, pp 74-77

26. **Hippel, A.R. von** : "Dielectric Materials and Applications", The M.I.T. Press, Cambridge, USA, 1966

27. **Bottcher, C.J.F.** : "Theory of Electric Polarisation", Elsevier Publishing Company, London, 1952

28. **Cole, K.S., Cole, R.H.** : "Dispersion and Absorption in Dielectrics. I. Alternating Current Characteristics", Journal of Chemical Physics, Vol 9, April 1941, pp 341-351

29. **van Beek, L.K.H.** : "Dielectric Behaviour of Heterogeneous Systems", Progress in Dielectrics, Vol 7, 1967, pp 69-114

30. **Debye, P.J.W.** : "Polar Molecules", Chemical Catalog Company, New York, 1929

31. **Maxwell, J.C.** : "Electricity and Magnetism", Vol 1, Clarendon Press, Oxford, 1892

32. **Wagner, K.W.** : "Die Isolierstoffe der Elektrotechnik", Edited by Schering, H., Springer, Berlin, 1924

33. **Fricke, H.** : "The Maxwell-Wagner Dispersion in a Suspension of Ellipsoids", Journal of Physical Chemistry, Vol 57, December 1953, pp 934-937

34. **Nikkannen, P.** : "On The Electrical Properties of Concrete and Their Application", Valtion Teknillinen Tutkimuslaitos, Tiedotus, Sarja III, Rakennus 60, 1962, pp 175 (in Finnish)

35. **Koryta, J.** : "Ions, Electrodes and Membranes", J. Wiley & Sons Ltd, New York, USA, 1982

36. **Sylvan, K.** : "RF Electrolytic Conductivity Transducers", PhD Thesis (Unpublished), University of Edinburgh, December 1987

37. **Onaral, B., Schwan, H.P.** : "Linear and Nonlinear Properties of Platinum Electrode Polarisation. Part 1 : Frequency Dependence at Very Low Frequencies", Medical & Biological Engineering & Computing, Vol 20, May 1982, pp 299-306

38. **Terry, E.M.** : "Advanced Laboratory Practice in Electricity and Magnetism", 2nd Edition, McGraw-Hill, New York, 1929, p 197

39. **McCarter, W.J., Brousseau, R.** : "The A.C. Response of Hardened Cement Paste", Cement and Concrete Research, Vol 20, 1990, USA, pp 891-900

40. **Giri, M.G., Carla, M., Gambi, C.M.C., Senatra, D., Chittofrati, A., Sanguineti, A.** : "Dielectric Permittivity Measurements on Highly Conductive Perfluoropolyether Microemulsions at Frequencies up to 100 MHz", Measurement Science and Technology, Vol 4, No 5, May 1993, pp 627-631

41. **Scott, J.H., Carroll, R.D., Cunningham, D.R.** : "Dielectric Constant and Electrical Conductivity Measurements of Moist Rock: A New Laboratory Method", Journal of Geophysical Research, Vol 72, No 20, October 1967, pp 5101-5115

42. **Subedi, P., Chatterjee, I.** : "Dielectric Mixture Model for Asphalt-Aggregate Mixtures", Journal of Microwave Power and Electromagnetic Energy, Vol 28, No 2, 1993, pp 68-72

43. **Whittington, H.W., M$^{c}$Carter, W.J., Forde, M.C.** : "The Conduction of Electricity Through Concrete", Magazine of Concrete Research, Vol 33, N° 114, March 1981, pp 48-60

44. **Archie, G.E.** : "The Electrical Resistivity Log as an Aid in Determining Some Reservoir Characteristics", Transactions of The American Institute of Mining and Metallurgical Engineers, Vol 146, 1942, pp 54-62

45. **Spencer, R.W.** : "Measurement of The Moisture Content of Concrete", Journal of The American Concrete Institute, Proceedings, Vol 34, Sept-Oct 1937, pp 45-61

46. **Buenfeld, N.R., Newman, J.B.** : "The Permeability of Concrete in a Marine Environment", Magazine of Concrete Research, Vol 36, No 127, June 1984, pp 67-80

47. **McCarter, W.J., Curran, P.N.** : "The Electrical Response Characteristics of Setting Cement Paste", Magazine of Concrete Research, Vol 36, No 126, March 1984,pp 42-49

48. **Wilson, J.G., Whittington, H.W.** : Letter on "The Electrical Response Characteristics of Setting Cement Paste" by M$^{c}$Carter and Curran, Magazine of Concrete Research, Vol 37, No 130, March 1985, pp 52-53

49. **Taylor, M.A., Arulanandan, K.** : "Relationships Between Electrical and Physical Properties of Cement Pastes", Cement and Concrete Research, Vol 4, No 6, 1974, pp 881-897

50. **Arulanandan, K., Smith, S.S.** : "Electrical Dispersion in Relation to Soil Structure", Journal of the Soil Mechanics and Foundations Division, ASCE, Vol 99, No SM12, Proc Paper 10235, December 1973, pp1113-1133

51. **Sachs, S.B., Speigler, K.S.** : "Radio Frequency Measurements of Porous Conductive Plugs. Ion-Exchange Resin-Solution Systems", The Journal of Physical Chemistry, Vol 68, 1964, pp 1214-1222

52. **Kim, H.C., Yoon, S.S.** : "Dynamic Dielectric Analysis During Early Stage Hydration of Ordinary Portland Cement", Journal of Physics D: Applied Physics, Vol 21, 1988, pp 1215-1220

53. **McCarter, W.J., Garvin, S.** : "Dependence of Electrical Impedance of Cement Based Materials on Their Moisture Condition", Journal of Physics D: Applied Physics, Vol 22, 1989, pp 1773-1776

54. **Wilson, J.G., Whittington, H.W., Forde, M.C.** : "Dielectric Properties of Concrete at Different Frequencies", Proceedings from Fourth International Conference on Dielectric Materials (Measurements and Applications), Lancaster, England, September 1984, pp 157-160

55. **McCarter, W.J., Afshar, A.B.** : "Monitoring the Early Hydration Mechanisms of Hydraulic Cement", Journal of Materials Science, Vol 23, 1988, pp 488-496

56. **McCarter, W.J., Afshar, A.B.** : "Some Aspects of the Electrical Properties of Cement Paste", Journal of Materials Science Letters, Vol 3, 1984, pp 1083-1086

57. **Olp, K., Otto, G., Chew, W.C., Young, J.F.** : "Electromagnetic Properties of Mortars Over a Broad Frequency Range and Different Curing Times", Journal of Materials Science, Vol 26, 1991, pp 2978-2984

58. **Alongi, A.V., Cantor, T.R., Kneeter, C.P., Alongi, A.,Jr** : "Concrete Evaluation by Radar Theoretical Analysis", Transportation Research Record 853, Transportation Research Board, Washington D.C., USA, 1982, pp 31-37

59. **Daniels, D.J., Gunton, D.G., Scott, H.F.** : "Introduction to Subsurface Radar", IEE Proceedings-F, Vol 135, No 4, August 1988, pp 278-320

60. **Glover, J.** : "Radar Roots Out Concrete Features", Concrete, February 1989, pp 21-22

61. **Millard, S.G., Bungey, J.H., Shaw, M.** : "The Assessment of Concrete Quality Using Pulsed Radar Reflection and Transmission Techniques", Conference Proceedings of The British Institute of Non-Destructive Testing International Conference - NDT in Civil Engineering, Held at The University of Liverpool, 14-16 April 1993, pp 161-185

62. **Laine, E.F., Dines, K.A., Okada, J.T., Lytle, R.J.** : "Probing Concrete with Radio Waves", Journal of The Geotechnical Engineering Division, July 1980, pp 759-766

63. **von Hippel, A.R.** : "The Dielectric Relaxation Spectra of Water, Ice, and Aqueous Solutions, and their Interpretation", IEEE Transactions on Electrical Insulation, Vol 23, No 5, October 1988, pp 801-816

64. **Hastead, J.B.** : "Aqueous Dielectrics", Chapman & Hall Ltd, London, 1973

65. **Malmberg, C.G., Maryott, A.A.** : "Dielectric Constant of Water from 0° to 100° C", Journal of Research of The National Bureau of Standards, 2641, Vol 56, No 1, Research Paper, January 1956, pp 1-8

66. **Grant, E.,Buchanan, T., Cook, H.** : "Dielectric Behaviour of Water at Microwave Frequencies", Journal of Chemical Physics, Vol 26, 1957, p 156

67. **Pottel, R.** : "Dielectric Properties", in "Water : A Comprehensive Treatise", Vol 3 ("Aqueous Solutions of Simple Electrolytes"), Ed. Felix Franks, Plenum Press, New York-London, 1974, Ch 8, pp 401-431

68. **Denaro, A.R.** : "Elementary Electrochemistry", 2nd Edition, Butterworth & Co (Publishers) Ltd, London, 1971

69. **Davies, C.W.** : "Electrochemistry", George Newnes Ltd, London, 1967, p 21

70. **Collie, C.H., Ritson, D.M., Hastead, J.B.** : "_____", Journal of Chemical Physics, Vol 16, No 1, 1948

71. **Cooper, R.** : "The Electrical Properties of Salt Water Solutions Over the Frequency Range 1-4000 Mc/s", Journal of IEE, Part III, Vol 93, 1946, pp 69-75

72. **Glasstone, S.** : "An Introduction to Electrochemistry", van Nostrand, Princeton, 1942

73. **Palmer, L.S., Cunliffe, A., Hough, J.M.** : "_____", Nature, Vol 170, 1952, p 796

74. **Thompson, F.** : "Moisture Measurement Using Microwaves", Measurement and Control, Vol 22, September 1989, pp 210-215

75. **de Loor, G.P.** : "The Dielectric Properties of Wet Materials", IEEE Transactios on Geoscience and Remote Sensing, Vol GE-21, No 3,July 1983, pp 364-369

76. **Clifford, J.** : "Properties of Water in Capillaries and Thin Films", in "Water : A Comprehensive Treatise", Vol 5 ("Water in Disperse Systems"), Ed. Felix Franks, Plenum Press, New York-London, 1975, Ch 2, pp 75-132

77. **Schwan, H.P., Schwarz, G., Maczuk, J., Pauly, H.** : "On the Low-Frequency Dielectric Dispersion of Colloidal Particles in Electrolyte Solution", Journal of Physical Chemistry, Vol 66, December 1962, pp 2626-2635

78. **Schwarz, G.** : "A Theory of the Low-Frequency Dielectric Dispersion of Colloidal Particles in Electrolyte Solution", Journal of Physical Chemistry, Vol 66, December 1962, pp 2636-2642

79. **Bolt, G.H.** : "_____", Journal of Physical Chemistry, Vol 61, 1957, p 1166

80. **Sen, P.N., Chew, W.C.** : "The Frequency Dependent Dielectric and Conductivity Response of Sedimentary Rocks", Journal of Microwave Power, Vol 18, Part 1, 1983, pp 95-105

81. **Chew, W.C., Sen, P.N.** : "Dielectric Enhancement due to Electrochemical Double Layer: Thin Double Layer Approximation", Journal of Chemical Physics, Vol 77, No 9, November 1982, pp 4683-4693

82. **Poley, J.P., Nooteboom, J.J., de Waal, P.J.** : "Use of VHF Dielectric Measurements for Borehole Formation Analysis", The Log Analyst, Vol XIX, May-June 1978, pp 8-30

83. **Sen, P.N.** : "Relation of Certain Geometrical Features to the Dielectric Anomaly of Rocks", Geophysics, Vol 46, No 12, December 1981, pp 1714-1720

84. **Parkhomenko, E.I.** : "Electrical Properties of Rocks", Plenum Press, New York, 1967 (Translated from Russian to English by Keller, G.V.)

85. **Monfore, G.E.** : "The Electrical Resistivity of Concrete", Journal of the PCA Research and Development Laboratories, Vol 10, Part 2, May 1968, pp 35-48

86. **Xie Ping, Beaudoin, J.J., Brousseau, R.** : "Flat Aggregate-Portland Cement Paste Interfaces, I. Electrical Conductivity Models", Cement and Concrete Research, Vol 21, No 4, USA, pp 515-522

87. **Morris, N.M.** : "Electrical Circuit Analysis and Design", The Macmillan Press Ltd., London, 1993, Chapter 8

88. **British Standards Institution** : "Methods of Testing Concrete", BS1881, Parts 3 and 4, 1970 (and Ammendments)

89. **Connor, F.R.** : "Wave Transmission", 1st Edition, Edward Arnold (Publishers) Ltd., London, 1980

90. **Sharp, J.** : Private communication, Department of Electronic, Electrical and Computer Engineering, Napier University, Edinburgh, April 1992

91. **Ramo, S., Whinnery, J.R., van Duzer, T.** : "Fields and Waves in Communication Electronics", 2nd Edition, John Wiley & Sons Inc, Canada, 1984

92. **Wheeler, H.A.** : "Transmission-Line Properties of Parallel Wide Strips by a Conformal Mapping Approximation", IEEE Transactions on Microwave Theory and Techniques, Vol 12, May 1964, pp 280-289

93. **Wei, Y.Z., Sridhar, S.** : "Technique for Measuring the Frequency Dependent Complex Dielectric Constants of Liquids up to 20 GHz", Review of Scientific Instrumentation, Vol 60, No 9, September 1989, pp 3041-3046

94. **Staebell, K.F., Misra, D.** : "An Experimental Technique for *In Vivo* Permittivity Measurement of Materials at Microwave Frequencies", IEEE Transactions on Microwave Theory and Techniques, Vol 38, No 3, March 1990, pp 337-339

95. **Burdette, E.C., Cain, F.L., Seals, J.** : "*In Vivo* Probe Measurement Technique for Determining Dielectric Properties at VHF Through Microwave Frequencies", IEEE Transactions on Microwave Theory and Techniques, Vol MTT-28, No 4, April 1980, pp 414-427

96. **Marsland, T.P., Evans, S.** : "Dielectric Measurements With an Open-Ended Coaxial Probe", IEE Proceedings, Vol 134-H, No 4, August 1987, pp 341-349

97. **Athey, W.T., Stuchly, M.A., Stuchly, S.S.** : "Measurement of Radio Frequency Permittivity of Biological Tissues with an Open-Ended Coaxial Line: Part I", IEEE Transactions on Microwave Theory and Techniques, Vol MTT-30, No 1, January 1982, pp 82-92

98. **Stuchly, M.A., Stuchly, S.S.** : "Coaxial Line Reflection Methods for Measuring Dielectric Properties of Biological Substantces at Radio and Microwave Frequencies - A Review", IEEE Transactions on Instrumentation and Measurement, Vol IM-29, No 3, September 1980, pp 176-183

99. **Iskander, M.F., DuBow, J.B.** : "Time and Frequency Domain Techniques for Measuring the Dielectric Properties of Rocks: A Review", Journal of Microwave Power, Vol 18, No 1, 1983, pp 55-74

100. **Bahl, I.J., Stuchly, S.S.** : "Effect of Finite Size of Ground Plane on the Impedance of a Monopole Immersed in a Lossy Medium", Electronics Letters, Vol 15, No 22, 25th October 1979, pp 728-729

101. **King, R.W.P., Smith, G.S., (contributions by Owens, M. and Wu, T.T.)** : "Antennas in Matter - Fundamentals, Theory, and Applications", M.I.T. Press, London, 1981

102. **Deschamps, G.A.** : "Impedance of an Antenna in a Conducting Medium", IEEE Transactions on Antennas and Propagation, Vol AP-10, 1962, pp 648-650

103. **Smith, G.S., Nordgard, J.D.** : "Measurement of the Electrical Constituent Parameters of Materials Using Antennas", IEEE Transactions on Antennas and Propagation, Vol AP-33, No 7, July 1985, pp 783-792

104. **Smith, G.S., King, W.P.** : "The Resonant Linear Antenna as a Probe for Measuring the *In Situ* Electrical Properties of Geological Media", Journal of Geophysical Research, Vol 79, No 17, June 10th 1974, pp 2623-2628

105. **Kadaba, K.P.** : "Penetration of 0.1 GHz to 1.5 GHz Electromagnetic Waves into the Earth Surface for Remote Sensing Applications", Proceedings of the IEEE S.E. Region Third Conference, 1976, pp 48-50

106. **Fu, W., Metaxas, A.** : "A Mathematical Derivation of Power Penetration Depth for Thin Lossy Materials", Journal of Microwave Power and Electromagnetic Energy, Vol 27, No 4, 1992, pp 217-222

107. **Misra, D.K.** : "A Quasi-Static Analysis of Open-Ended Coaxial Lines", IEEE Transactions on Microwave Theory and Techniques, Vol MTT-35, No 10, October 1987, pp 925-928

108. **Wei, Y.Z., Sridhar, S.** : "Radiation-Corrected Open-Ended Coax Line Technique for Dielectric Measurements of Liquids up to 20 GHz", IEEE Transactions on Microwave Theory and Techniques, Vol 39, No 3, March 1991, pp 526-531

109. **Potter, M.C., Goldberg, J.** : "Mathematical Methods", 2nd Edition, Prentice Hall International Inc., New Jersey, USA, 1987, p 491

110. **Ralston, A., Rabinowitz, P.** : "A First Course in Numerical Analysis", 2nd Edition, McGraw-Hill Inc., New York, USA, section 8.8

111. **Starrs, G., Wilson, J.G., Whittington H.W.** : "Measurement and Applications of the Electrical Properties of Concrete", Final Report for S.E.R.C. Grant No GR/F/01482, Napier Polytechnic of Edinburgh, October 1991

112. **Tanguay, L., Vaillancourt, R.** : "Numerical Solution of the Dielectric Equation for a Coaxial Line", IEEE Transactions on Instrumentation and Measurement, Vol IM-33, No 2, June 1984, pp 88-90

113. **Hofstadter, D.R.** : "Strange Attractors: Mathematical Patterns Delicately Poised Between Order and Chaos", Scientific American, Vol 245, 1981, pp 22-43

114. **Roberts, D.E.** : Private Communication, Department of Mathematics, Napier University, Edinburgh, March 1991

115. **Misra, D., Chabbra, M., Epstein, B.R., Mirotznik, M., Foster, K.R.** : "Noninvasive Electrical Characterization of Materials at Microwave Frequencies Using an Open-Ended Coaxial Line: Test of an Improved Calibration Technique", IEEE Transactions on Microwave Theory and Techniques, Vol 38, No 1, January 1990, pp 8-14

116. **Hewlett Packard, Operation and Service Manual**, Model 4191A RF Impedance Analyser, Part No 04191-90012, Yokogawa-Hewlett-Packard Ltd, Tokyo, August 1981, p 3-47

117. **Murphy, P.** : "Additional Mathematics - Made Simple", W.H. Allen & Co Ltd, London, 1974, p 21

118. **British Standards Institution** : BS882, 1994

119. **Pohl, A.H.** : "Dielectrophoresis", Cambridge University Press, 1978, Chapter 2

120. **Connor, F.R.** : "Networks", Edward Arnold (Publishers) Ltd., London, 1982

121. **Wylie, C.R.** : "Advanced Engineering Mathematics", International Student Edition, McGraw-Hill Kogkusha Ltd, Tokyo, 1975, Section 18.3

122. **Sen, P.N., Scala, C., Cohan, M.H.** : "A Self-Similar Model for Sedimentary Rocks with Application to the Dielectric Constant of Fused Glass Beads", Geophysics, Vol46, No 5, May 1981, pp 781-795

123. **Bahl, I.J., Stuchly, S.S.** : "Analysis of a Microstrip Covered with a Lossy Dielectric", IEEE Transactions on Microwave Theory and Techniques, Vol MTT-28, No 2, February 1980, pp 104-109